SYNTHESIS OF (R)-1-METHYL-4-(1-METHYLETHENYL) CYCLOHEXENE MULTIFUNCTIONAL DERIVATIVES AND THEIR EFFECTS ON *JATROPHA CURCAS* AND ALGAE BIOFUEL BLENDS

JOHN M. KAHINDO (MSc.)

I84/23199/2010

A THESIS SUBMITTED IN FULFILMENT OF THE REQUIREMENTS FOR THE AWARD OF THE DEGREE OF DOCTOR OF PHILOSOPHY IN CHEMISTRY IN THE SCHOOL OF PURE AND APPLIED SCIENCE, KENYATTA UNIVERSITY

OCTOBER, 2020

DECLARATION

This thesis is my original work and has not been presented for degree or any other award in any other University.

Signature…… Date……..

John M. Kahindo - I84/23199/2010

Department of Chemistry

SUPERVISORS

We confirm that the work reported in this thesis was carried out by candidate under our supervision as university supervisors.

Signature…… Date……..

Prof. Sumesh C. Chhabra

Department of Chemistry

Kenyatta University

Signature…… Date……..

Dr. Richard M. Musau

Department of Chemistry

Kenyatta University

Signature…… Date……..

Prof. Josiah O. Odalo

Department of Pure and Applied Sciences

Technical University of Mombasa

Signature…… Date……..

Prof. Thomas F. N. Thoruwa

Department of Physics and Technology

Pwani University

DEDICATION

I dedicate this thesis to my mother Margaret W. Kahindo and late father Peter Kahindo Mariwa who modelled and made me who I am. To my wife Miriam Wangari for being a true companion and helper.

ACKNOWLEDGEMENTS

First I wish to acknowledge the almighty God for giving me strength and divine health then express my special gratitude, appreciation and thanks to my first supervisor Prof. Sumesh C. Chhabra for guiding and supervising this research with a lot of dedication. To my other supervisors; Dr. Richard M. Musau, Prof. Josiah O. Odalo and Prof. Thomas F. N. Thoruwa great thanks for your continuous guidance, encouragement and positive criticism during experimental work and thesis preparation.

Special thanks to all who supported me during experimental work, technologists Mr. Kennedy Agoi, Mr. Nobert Atego and Ms Joan Chelagat of the Pharmacy and Microbiology laboratory of Technical University of Mombasa (TUM), Mr. Pius Makau and Ms Monica Koinange of Analytical chemistry laboratory of TUM. To Mr. Kennedy Oketch of SGS Kenya Pipeline Laboratories Mombasa and Ms Felister Wanjiru of Intertek Laboratories Mombasa, I salute you for your support during my work on physicochemical and fuel properties tests, Mr. Preston Akenga of Jomo Kenyatta University of Agriculture and Technology (JKUAT), Mr George Musyoki and Mr George Nzai of Government Chemist Mombasa for their support in my GC-MS and FTIR work. Also Mr Elias Maina Chief Technician, Chemistry Department of Kenyatta University for your help in extractions and purification of samples.

Special thanks to my mum Margaret, wife Miriam, my children Samuel, Solomon, Emmanuel and Grace Rose, to my sister Millicent, brothers Eston, Charles and Benson for their immense encouragement, moral support and prayers during the entire course of my PhD study.

Thanks to Kenyatta University fraternity for providing conducive environment for studies and research work. Finally to the National Council of Science and Technology (NACOSTI) for the award of research grant which made my research work possible.

TABLE OF CONTENTS

LIST OF TABLES

LIST OF FIGURES

LIST OF PLATES

ABBREVIATIONS AND ACRONYMS

AO	Algae oil
AO FAEE	Algae oil fatty acid ethyl ester
ASTM D 6751	American Standard test methods for biofuels
ATCC	American Type Culture Collection strain number
CTO	Citrus oil
B100	Biodiesel 100
DIN EN 14214	Deutsches Institute für Normung - German Standard test methods for biofuels
EB-Diesel	Ethanol - biodiesel - diesel microemulsions
EN 14214	European Standard test methods for biofuels
FAEE	Fatty acid ethyl ester
FTIR	Fourier transform Infra-red spectrophotometer
GC-MS	Gas chromatography – mass spectrometer
^{1}H NMR	Proton Nuclear Magnetic Resonance
IR	Infra-red spectrophotometer
JAB	*Jatropha curcas* and Algae Biodiesel blend
JABLA	JAB blend with limonene derivatives as additives
JO	*Jatropha curcas* oil
JO FAEE	*Jatropha curcas* oil fatty acid ethyl ester
JOFA	*Jatropha curcas* oil from field A
JOFB	*Jatropha curcas* oil from field B
JOFC	*Jatropha curcas* oil from field C
JOFD	*Jatropha curcas* oil from field D
JOFE	*Jatropha curcas* oil from field E

KMFRI	Kenya Marine and Fisheries Research Institute
Pd/Al_2O_3	Palladium alumina catalyst
Pd/HT	Palladium hydrotalcite catalyst
$scCO_2$	Supercritical carbon dioxide
STATA	Statistical analysis software
YPD	Yeast extract, peptone and dextrose
XRF	X-Ray fluorescence

ABSTRACT

There is a growing increase in biofuel consumption around the world. Currently there is a desire to enhance biodiesel and biodiesel blends properties by use of multifunctional additives. This project sought to evaluate the miscibility of fatty acid ethyl ester blends from algae and *Jatropha curcas* L. oils and also synthesise hydrogenated and oxygenated derivatives of *d*-limonene as potential additives. Sampling of citrus peels was done from Milly Fruit Processors and Kongowea Mombasa. Algae were from Shimoni in Kwale, Shelly beach Mombasa, Jamvi la Wageni Mtongwe Likoni, English point Mombasa. *J. curcas* seeds were from contracted farmers in Shimba hills, Kwale County. Extraction of citrus oil containing *d*-limonene was done by use of hexane and liquid / Sc CO_2. Catalytic synthesis of hydrogenated and oxygenated limonene derivatives was done using palladium on alumina Pd/Al_2O_3 and palladium on hydrotalcite Pd/HT respectively. Algae and jatropha seeds were dried, blended and extracted using hexane. The algae and citrus biomass were saccharified then fermented to obtain bioethanol.The algae and jatropha oils were transesterified using bioethanol, blended to form JAB then 2 – 10 % limonene and derivatives added to 20% JAB to form JABLA. GC-MS and FTIR spectrophotometers were used for characterisation. Determination of physicochemical and fuel properties was done using standard methods. Antimicrobial assay of JAB20 and JABLA was done using paper disc diffusion method. The properties of JAB and JABLA were then compared with those of diesel fuel and standard B100 biodiesel. The yield of orange oil was 5.748±0.719 $\%^{w}/_{w}$ using hexane. Pd composition of Pd/Al_2O_3 and Pd/HT was confirmed using XRF spectrometry to be 5% and 4.74% respectively. Characterisation showed that the oxidation products were mainly endo- and exo-epoxides, dihydrocarveol, carveol and carvone and hydrogenated products *p*-menthene, *cis*-*p*-menthane, *trans*-*p*-menthane, (S)-1-methylene-4-(1-methylethyl)cyclohexane and (R)-1-methylene-4-(1-methylethyl)cyclohexane. Bioethanol from citrus biomass was 9.42±1.031 $\%^{v}/_{w.}$ Algae oil produced 57-62% FAEE and *J. curcas* oil 63-70% FAEE. Characterisation of the ethyl esters showed mainly dodecanoic acid, tetradecanoic acid, pentadecanoic acid and hexadecanoic acid ethyl esters from algae oil and hexadecanoic acid, octadecanoic acid and 9z-octadecenoic acid ethyl esters from jatropha oil. JAB 5-20% was miscible, physicochemical and fuel characteristics showed that there was significant effect on the *J. curcas* FAEE calorific value, kinematic viscosity, pour point and cloud point with $p < 0.05$. The 2-8 % *d*-limonene additive showed effect on properties of JAB20 density, calorific value, kinematic viscosity, flash point, cetane index, pour point and cloud point with $p< 0.05$ except for CFPP with a $p = 0.215$. For 2-8 % hydrogenated *d*-limonene additive showed effect on density, calorific value, kinematic viscosity, flash point, cetane index, pour point and cloud point $p< 0.05$. The 2-8 % oxygenated *d*-limonene additive had effect on density, cetane index and pour point $p < 0.05$ according to data obtained using STATA/SE 13.0 and Xlstat at 95% confidence level two -tailed. JABLA showed no significant difference in fuel properties with petroleum diesel and standard B100 biodiesel p=0.110. The 8% oxygenated *d*-limonene also showed *Pseudomonas aeroginosa* growth inhibition of 23.20 ± 0.80 mm and *Candida albicans* growth inhibition of 25.30± 0.30 mm. From the findings the additives have beneficial effect on physicochemical and fuel properties of *J. curcas* and *R. grande* biofuel blend for increased sustainability and longer shelf life hence potential additives to the biofuels.

CHAPTER ONE

1 INTRODUCTION

1.1 Background Information

Chemicals and transport fuels when derived from fossil resources are major emitters of carbon dioxide. The use of petroleum fuels at current levels is unsustainable. An alternative sustainable supply based on renewable biomass and efficient carbon dioxide scrubbers is necessary (Eviana, 2008). Vegetable oils from crops of high oil content such as soya bean, sunflower and coconut would provide an alternative source. Alkyl esters prepared by transesterification of the oils from these plants have been tested and evaluated (Sahoo and Das, 2009).

There are various current issues with biofuel products and use discussed in popular media and scientific journals such as food versus fuel debate (Kazinform, 2008; Qui *et al*., 2008). Hence the need for non-food crops biomass such as *Jatropha curcas* L. and carbon dioxide scrubbers such as algae. It is estimated that algae can produce up to 30 times more energy per acre than land crops such as soyabean hence more sustainable (Eviana, 2008). *J. curcas.* constitute 53–57% non–edible oils (Jumat and Rozaini, 2008).

There is a growing increase in biofuel consumption mainly ethanol and biodiesel as well as their blends with petroleum diesel so as to reduce cost while retaining the advantages of biofuels such as increasing lubricity and reduction of exhaust emissions (Núbia *et al*., 2007). However there are hardly any records of biomass based blends such as algae and *J. curcas* fatty acid esters that have saturated derivatives of terpenes as additives.

Currently there is a desire to extend or enhance diesel and diesel blended properties by use of additives (Núbia *et al.*, 2007). Fuel additives have become indispensable

tools not only to decrease fuel drawbacks but also to produce specified products that meet international and regional standards such as EN 14214, ASTM D 6751, and DIN EN 14214 (Suppes *et al*., 2001; Keith, 2007). Additives improve ignition and combustion efficiency, stabilize fuel mixtures, protect the motor from abrasion and wax deposition, and reduce pollutant emissions, among other features. Several additives' compositions may be used as long as they keep the basic chemical functions that are active (Núbia *et al.*, 2007).

Multifunctional diesel fuel additives from triglycerides have been synthesized (Suppes *et al*., 2001), and evaluated for ignition related properties and lubricity (Ambadas *et al.*, 2010). However no plant based hydrocarbon additives have been synthesized and evaluated on biofuels. *d*-Limonene is a cyclic terpene and has been considered as biofuel (Green Car Congress, 2007). Citrus oil containing d-Limonene produced from citrus juice industry is more than 60,000 tonnes per year (Lange, 2015). Currently there are no reports of its use or its saturated derivatives as additives in biofuels. Hydrogenated oils can be blended with diesel in all proportions which shows high miscibility. These oils have several advantages including good performance at low temperatures, no storage stability problems and no susceptibility to microbial attack (Evans, 2008).

In Kenya, the Ministry of Energy is promoting the development of bioethanol and biodiesel. Through biofuel production, the Ministry aims to reduce the number of households using fuel wood by 25% by 2015, and those using kerosene by 50% by 2050 (Birdlife International, 2012).

This work sought to evaluate the miscibility of the fatty acid ester blends from algae and *J. curcas* oils and synthesise hydrogenated and oxygenated derivatives of *d*-

limonene as additives to the biofuel blends to enhance their ignition-related properties, miscibility and thermochemical properties.

1.2 Problem Statement

There are various natural resources that have been explored as potential biofuel options within the continent of Africa. Some have met various levels of success, while others have met environmental, economic failure and food competition (Kurnia *et al*., 2016).

Biofuel from food based sources is discouraged and there is need for non-food sources. *J. curcas* L. has high quantity of oil but still non sustainable (Jumat and Rozaini, 2008). Transesterification of triglycerides has been done using mainly methanol which is synthetic. Ethanol from plant materials can also be used which is more sustainable in presence of additives.

Biofuels have several disadvantages including poor performance at low temperatures, storage stability problems, lower energy content than petrodiesel and susceptibility to microbial attack. No record of plant based oxygenated and hydrogenated *d*-limonene derivatives have been synthesized and evaluated as additives for the improvement of biofuels.

1.3 Justification

The projected global supply of biofuels is expected to be around 30% by 2030 and petroleum oil is expected to continue being the slowest-growing source of energy 20 years from now (B.P, 2012). Biofuels are providing new opportunities for both energy growth and economic growth in Africa considering their renewable and easily accessible sources. A biofuel blend of *J. curcas* with algae fatty acid alkyl esters would improve sustainability since it is readily available and easily produced. The

main renewable feedstock that has the potential to replace petroleum diesel completely without adversely affecting food supply chain and other crop products is algal oil (Demirbas and Demirbas, 2011, Ehimen *et al*., 2010, Pienkos and Darzins, 2009). Ethanol if obtained from plant materials can also be useful in esterification reaction of oils from non food feedstock which is more sustainable and add value to the plants. *d*-Limonene is abundantly available from citrus peelings (Smith *et al*., 2001) which provides the starting material for synthesis of oxygenated and hydrogenated derivatives. Biofuels have several disadvantages including poor performance at low temperatures, storage stability problems and susceptibility to microbial attack among others which may be improved by additives (Evans, 2008).

1.4 Hypothesis

d-Limonene and its hydrogenated and oxygenated derivatives as additives enhance physicochemical and ignition–related properties, miscibility, thermochemical and fuel properties of biofuel blends from algae and *J. curcas* oils.

1.5 Objectives

1.5.1 General Objective

The general objective of this research project was to prepare and investigate physicochemical and fuel properties of biofuel blends from *J. curcas* and algae oils transesterified using bioethanol with *d*-limonene [(R)-1-methyl-4-(1-methylethenyl) cyclohexene] and its oxygenated and hydrogenated derivatives as additives in comparison to petroleum diesel fuels and standard B100 biodiesel.

1.5.2 Specific Objectives

The specific objectives of this research project were to:

i. Prepare, purify and characterise bioethanol from algae and citrus peelings biomass;

ii. Synthesize oxygenated and hydrogenated derivatives of *d*-limonene extracted from citrus peelings using liquid CO_2 and hexane followed by determination of their physicochemical properties;

iii. Transesterify and blend *J. curcas* and algae oils with bioethanol from algae and evaluate their miscibility, density, calorific value, kinematic viscosity, flash point, cetane index, pour point, cold filter plugging point and cloud point;

iv. Evaluate the physicochemical, fuel properties and antimicrobial activity of the fatty acid ethyl ester blends with *d*-limonene and its oxygenated and hydrogenated derivatives as additives in comparison to petroleum diesel fuels and standard B100 biodiesel.

1.6 Scope of the Study

The research was carried out both in the field and in the laboratory. Probability and purposeful sampling methods were both used to collect ten marine macro-algae species from the Indian ocean by hand picking. *Rhizoclonium grande* was found to contain the largest amount of algae oil for transesterification. Three species of citrus fruits for peelings were bought from Kongowea Mombasa county and Milly fruit processors Kilifi County used for citrus oil extraction. *Citrus senensis* was found to contain largest quantity of *d*-limonene for catalytic synthesis of hydrogenated and oxygenated *d*-limonene derivatives. The two residual biomass from *Rhizoclonium grande* and *Citrus senensis* were used for bioethanol production. *J. curcas* L.seeds were bought from five contracted farmers within Shimba hills in Kwale County for

Jatropha curcas oil extraction and transesterification. The research was conducted using a randomized block design comprising of three blocks. Oils from *Citrus sinensis, Rhizoclonium grande* and *Jatropha curcas*, ethyl esters (JOEE and AOEE) from the *J. curcas* and *R. grande* oils and their blends (JAB), and ethyl ester JAB blend with d-limonene derivatives catalytically synthesised from *C. sinensis* peeling oil (JABLA). Each sample from a block was subjected to several treatments with three replication measurements per treatment.

CHAPTER TWO

2 LITERATURE REVIEW

2.1 Supercritical and Liquid Carbon Dioxide

At pressures above ambient, carbon dioxide can exist as a liquid or supercritical fluid. Carbon dioxide is a liquid under relatively mild temperatures and pressures, in the ranges of -56.6 to 31.0 °C and 520 to 7380 kPa. Supercritical carbon dioxide ($scCO_2$) is produced at temperatures higher than the critical temperature of 31.0 °C and between the critical pressure 7380 kPa and extremely high pressures of approximately 10400 kPa (McKenzie *et al.*, 2004).

Supercritical fluids have no distinct liquid or vapour phase but retain properties of each. $ScCO_2$ is especially beneficial when used as a solvent in selective extraction processes. The gas-like properties, such as very low surface tension and viscosity, allow the solvent to penetrate into the substrate, while the liquid-like properties solubilise compounds and remove them from the substrate.

Small changes in pressure or temperature alter the bulk density of the fluid leading to increased or decreased solubility of various compounds. In this way, the use of supercritical fluids can allow for control of separations of materials. Through manipulation of temperature and pressure conditions within accessible ranges, both the phase and properties of CO_2 can be easily controlled. During the past two decades, technical advances have been made in the industrial use of supercritical and liquid carbon dioxide in place of organic solvents (Beckman, 2002, 2003).

2.2 Applications of CO_2 as an Alternative Solvent

The tuneable solubility properties, low toxicity, and ease of removal of CO_2 have led to well established $scCO_2$ technology for the extraction of various food products, including essential oils and hops, and for the decaffeination of coffee and tea. The

mild conditions necessary for extraction and absence of residual solvent result in superior products and have motivated an industrial shift to CO_2 from hazardous solvent extractions or steam distillations (Tanchoux and Leitner, 2002).

The oil products from $scCO_2$ extraction processes are of higher purity and contain no thermal degradation products. The ability to influence solubility of compounds through variations in temperature and pressure has resulted in enhanced extraction of desired compounds from natural products and in the ability to enrich oils during post-extraction treatment with $scCO_2$. It has also been used in other processes including analytical extractions and chromatography, metal degreasing, and textile dyeing (Tanchoux and Leitner, 2002; Chafer *et al*., 2001).

A commitment to replacing hazardous solvents and improving environmental footprints has led to many new green methods of materials synthesis and processing with CO_2 (Beckman, 2002, 2003; Tanchoux and Leitner, 2002). Carbon dioxide is relatively inert, is resistant to oxidation, cannot serve as a chain transfer agent, and provides for tuneable miscibility. These chemical advantages have led to an increasing number of industrial-scale reactions which use $scCO_2$.

Although most industrial applications use supercritical CO_2, liquid phase carbon dioxide has also proven effective. The wide range of lower temperatures and pressures offers flexibility in the design of processes using liquid CO_2. The mild conditions prevent degradation of products. As with $scCO_2$, ideal density, viscosity, and surface tension can be obtained through manipulation of pressure and temperature. Liquid CO_2 has been employed extensively as an industrial solvent for the extraction of essential oils and in new greener methods of dry cleaning (Beckman, 2003).

2.3 Extraction of Citrus Oil Containing *d*-limonene from Orange Peels

Dry ice sublimes at atmospheric pressure and temperatures above -78 °C. If the CO_2 is sealed in a vessel during sublimation, the internal pressure in the vessel increases. After the temperature and pressure have increased sufficiently, liquid carbon dioxide forms. Due to this accessible phase change, carbon dioxide can be used for bench top extraction processes.

Approximately two and a half grams of grated orange peel and a wire and filter paper or metal screen solid trap are placed in a 15 mL polypropylene centrifuge tube with plug seal cap (Mukhopadhyay**,** 2000). The centrifuge tube is completely filled with crushed dry ice, capped tightly, and dropped into a plastic cylinder or polycarbonate bottle which is half-filled with warm (40–50 °C) water. As pressure builds in the tube, gas escapes slowly through the threading of the cap (Polak *et al*., 1989).

After approximately fifteen seconds, the solid begins to melt, and liquid CO_2 appears in the tube. Solid, liquid, and gas phases are visible in the tube for a short period of time. The liquid boils, and gas escapes for almost three minutes. During this time, the liquid CO_2 moves through the solid, extracts the citrus oil (CTO) from the orange peels , and collects in the bottom of the tube. The solid trap successfully prevents the orange peels from moving into the tip of the tube during extraction because the wire coils are supported by the sides of the centrifuge tube at the point where it narrows (McKenzie *et al.*, 2004).

After the extraction solvent completely evaporates, the isolated product remains at the tip of the tube. Once the liquid has stopped bubbling and gas is no longer escaping, the centrifuge tube is removed from the cylinder with tweezers, and the extraction process is repeated by refilling the tube containing the orange peels and solid trap with dry ice, recapping it, and replacing it in the cylinder. Two or three extraction

cycles result in isolation of approximately 0.1 mL of pale yellow oil. The extracted product is predominantly *d*-limonene [(R-1-methyl-4-(1-methylethenyl) cyclohexene)] **(1)** (Smith *et al.*, 2001) as indicated by ^{1}H NMR, IR and GC-MS (97%) (McKenzie *et al*., 2004).

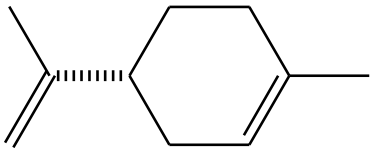

1

2.4 Oxygenated Limonene Derivatives from Orange Oil

The production of several oxygenated derivatives of limonene has been previously carried out by using orange oil and molecular oxygen as the sole initial reactants under solvent-free conditions (Monteiro and Veloso, 2004). Palladium–copper supported on carbon and hydrotalcite-like compounds were found to display good catalytic properties to accelerate autoxidation reactions of limonene yielding a mixture of the different oxygenated derivatives, mainly 1,2- limonene epoxide **(2)**, 8,9-limonene epoxide **(3)**, 1,2,8,9- diepoxylimonene **(4)**, carveol **(5)** and carvone **(6)**.

Vacuum distillation of the final product mixture allow easy separation of the 1,2-limonene epoxide **(2)** and 8,9-limonene epoxide **(3)**. The other compounds, mainly carveol **(5)** and carvone **(6)**, were not completely separated and remained together with the other oxygenated products, such as the di-epoxylimonene isomers (Beatriz *et al*., 2007).

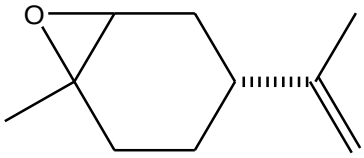

2

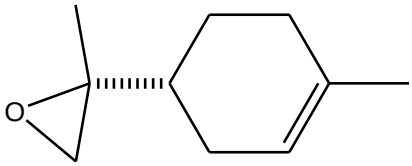

3

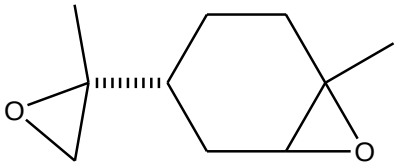

4

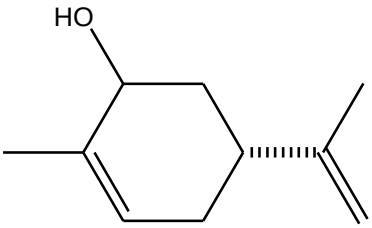

5

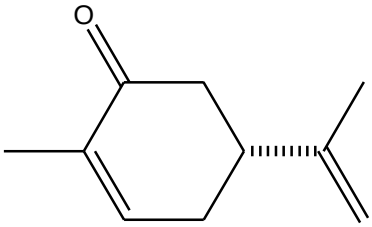

6

Palladium supported on copper–magnesium–aluminium hydrotalcite display the best properties due to its higher catalytic activity and lifetime. The pelletized form of these catalysts can be easily recovered and reused. The amount of palladium in the catalysts can be verified using elemental analysis by energy dispersive X-ray (ED XRF) (Katleen *et al.*, 2007). XRF analyzers determine the chemistry of a sample by measuring the fluorescent (or secondary) x-ray emitted from a sample when it is excited by a primary x-ray source. Each of the elements present in a sample produces a set of characteristic fluorescent x-rays ("a fingerprint") that is unique for that specific element, that is why XRF spectroscopy is an excellent technology for qualitative and quantitative analysis of material composition.

2.5 Hydrogenated Monoterpenes Additives in Petrodiesel

Catalytic hydrogenation of both myrcene (7-methyl-3-methyleneocta-1,6-diene) **(7)** and limonene **(1)** have been reported in the literature (Speziali *et al.* 2005; Swift, 2004;

Gusevskaya *et al***.** 2000; Grau *et al.* 1999). However, these studies are not necessarily interested in the completely hydrogenated species that would be useful as biofuel additives. Instead, the partially hydrogenated olefinic products of myrcene and limonene are studied for use as precursor molecules for scents, flavorings (Speziali *et al.* 2005, Grau *et al.* 1999, Gusevskaya *et al.* 2000 and Robles-Dutenhefner *et al.* 2005), or other chemical precursors (Mathers *et al.* 2006). For example, Speziali *et al.* (2005) used various palladium, ruthenium, chromium, iridium, and rhodium catalysts, with the goal of selecting the mono-olefinic species. They found the reaction to be highly selective, with the rhodium catalysts being the most selective. Such a catalyst, however, was relatively unselective for the paraffinic product, with production ranging from a trace to 4%.

From a fuel perspective, the multiple, highly reactive, unsaturated bonds present in terpenes would be problematic if these species were added directly to a diesel fuel. As a result, these species need to be fully hydrogenated to eliminate double-bond reactivity. With this in mind, (Tracy *et al.* 2009) considered the total hydrogenation of myrcene and limonene to 2,6-dimethyloctane **(8)** and 1-isopropyl-4-methylcyclohexane **(9)** (commonly known as *p*-menthane) respectively, and use of these molecules as possible additives to diesel fuels. These terpene-based fuel additives are totally renewable because they come from plant tissues (Robles-Dutenhefner *et al.* 2004; Finn and Sharpless, 1991; Robert *et al.* 1988).

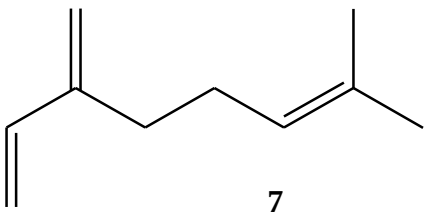

7

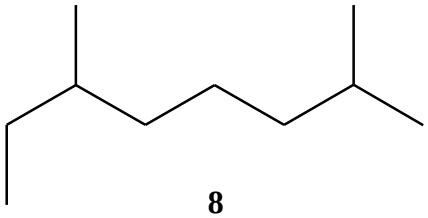

8

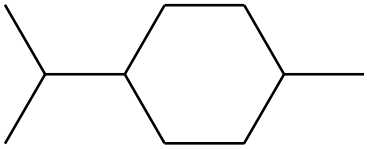

9

The hydrogenated products were found to decrease the cloud point of consumer grade diesel fuel by 1 °C when mixed into the fuel at 5–10%. All fuel mixtures met ASTM D975 minimum standards for viscosity. The viscosity increase as the level of hydrogenated myrcene increased in the diesel fuel, but decreased with the addition of the hydrogenated limonene. Adding 10% hydrogenated myrcene produced the greatest viscosity, 3.899 mm^2/s, which was near the ASTM D975 limit of 4.1 mm^2/s. However, the viscosity decreased to 2.3 mm^2/s by adding 10% hydrogenated limonene. Too great a viscosity causes the fuel to atomize poorly, resulting in a loss of power in the engine (Jones and Pujado, 2006). The amount of soot emitted from diesel engines increases with viscosity and cetane number (Zannis et *al*., 2007). This suggests that a 10% hydrogenated limonene blend would be preferable to 5 or 10% 2,6-dimethyloctane mixture because it would produce less soot due to its lower viscosity.

The hydrogenated limonene blend should produce less soot during combustion, compared to the unblended retail diesel. However, the 2,6-dimethyloctane **(8)** would likely increase soot emissions due to the increased viscosity of the blends compared to the retail diesel. Therefore, hydrogenated forms of myrcene, and preferentially limonene, can be used as blending agents in diesel fuels without significant

detrimental effects on the properties of the fuels. This would represents a potential usefulness of terpenes which are bio-derived hydrocarbons as renewable fuel supplements.

2.6 Algae Harvesting

Gathering algae consists of separating algae from the growing medium, drying, and processing it to obtain the desired product. Separating algae from its medium is known as harvesting. Harvesting methods depends primarily on the type of algae. The high water content of algae must be removed to enable harvesting. The most common harvesting processes are flocculation, microscreening and centrifugation. Macroalgae harvesting employs manpower whereas, microalgae are usually harvested using microscreens, centrifugation, flocculation (Divakaran and Sivasankara, 2002) or by froth flotation.

A highly efficient froth flotation procedure can be developed for harvesting algae from dilute suspensions. Harvesting is carried out in a long column containing the feed solution which is aerated from below. A stable column of foam is produced and harvested from a side arm near the top of the column.

2.7 Ethanol and Oil from Algae

The algae oil contains 7.44% palmitic acid **(10)**, 2.78% palmitoleic acid **(11)**, 6.58% stearic acid **(12)**, 68.10% oleic acid **(13)**, 10.07% 9,12-octadecadienoic acid **(14)**, 4.02% 9,12,15-octadecatrienoic acid **(15)**, giving a total unsaturated fatty acid esters content around 85% (Meng *et al*., 2009). Additionally it contains 0.01-0.02% moisture and 0.45-1.75 % free fatty acid (FFA) (Pokoo-Aikins *et al.*, 2009). Notably, FFA is always below 2% (Sanford *et al*., 2009). Based on these data, it is assumed that triolein and oleic acid represent the bulk of the algae oil (Gunstone and Harwood, 2007).

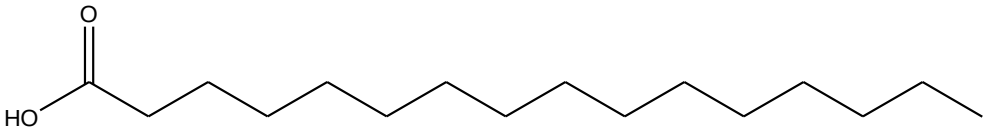

10

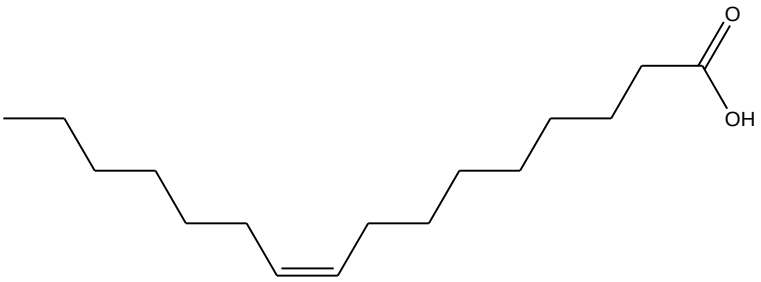

11

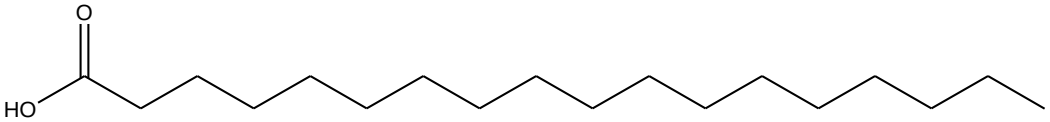

12

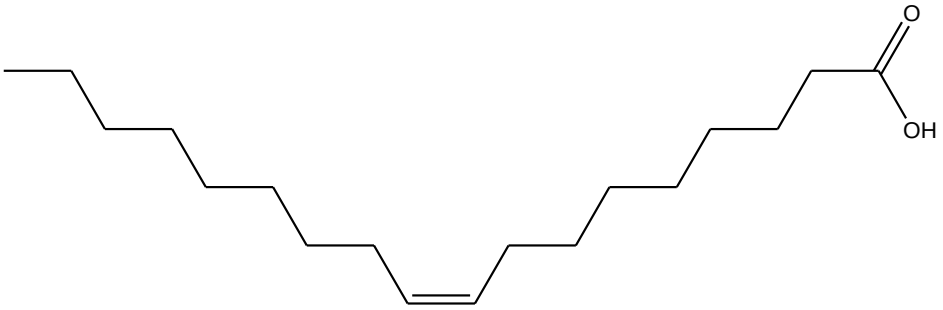

13

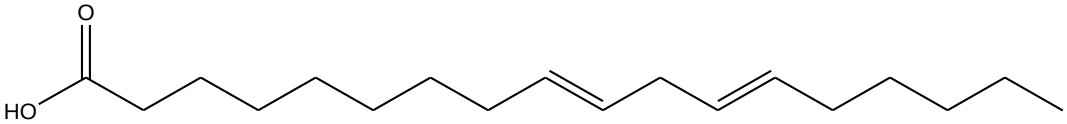

14

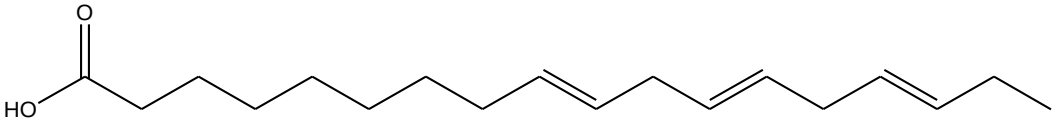

15

Algae have a tendency to have a much different makeup than does most feedstocks used in ethanol production such as corn and sugar cane. Ethanol production from algae is possible from the starch and cellulose components. Lipids in algae oil (AO) can be

made into biodiesel, while the carbohydrates can be converted to ethanol. Algae are the optimal source for second generation bioethanol due to the fact that they are high in carbohydrates and have thin cellulose walls (Svein, 2009). Some prominent strains of algae that have high carbohydrate content and hence are promising candidates for ethanol production are *Sargassum*, *Glacilaria*, *Prymnesium parvum* and *Euglena gracilis* among others.

Fermentation process to produce ethanol include growing starch-accumulating, filament-forming, or colony-forming algae in an aqua culture environment; harvesting the grown algae to form a biomass; initiating decay of the biomass using a suitable saccharising agent such as *Aspergilus niger*; mixing the decaying biomass with a yeast capable of fermenting it to form a fermentation solution; and separating the resulting ethanol from the fermentation solution. Initiating decay means that the biomass is treated in such a way that the cellular structure of the biomass begins to decay with cell wall rupture to release the carbohydrates and free sugars. Initiating decay can be accomplished mechanically or non-mechanically. The yeasts used are typically brewers' yeasts (*Saccharomyces cerevisiae* and *Saccharomyces uvarum*). It has been reported that besides yeast, genetically altered bacteria are useful for fermentation (Glass, 2010).

2.8 Biodiesel Stability and Additives

The oxidation and thermal instability of biodiesel is a serious concern. It is caused by the presence of some highly polar and unsaturated species in a biodiesel persisting even after its purification. During the storage of biodiesel, one may observe increase in water content due to the hygroscopic nature of biodiesel; build up of auto-oxidation products of biodiesel; and sedimentation and gum formation by impurities in biodiesel. It is therefore important to improve the stability of biodiesel. For this, the

concentration of impurities in biodiesel should be effectively reduced first by adopting elaborate purification procedures and addition of an antioxidant (or a mixture of antioxidants) to the purified biodiesel. The natural antioxidants such as α-tocopherol **(16)** present in vegetable oils are usually denatured or decomposed during various stages of production, storage and use of biodiesel at high temperatures. The common antioxidants added to biodiesel include 4-butyl -2-hydroxy toluene (BHT) **(17)**, propyl-3, 4, 5-trihydroxybenzoate (propyl gallate, PG) **(18)**, N,N-diphenyl-*p*-phenylenediamine (DPD)**(19)**, maize flour contaminated by mycotoxins, tert-butyl-hydroquinone (TBHQ) **(20)** and α-tocopherol **(16)** (Xin *et al*., 2008; Enferadi *et al*., 2006).

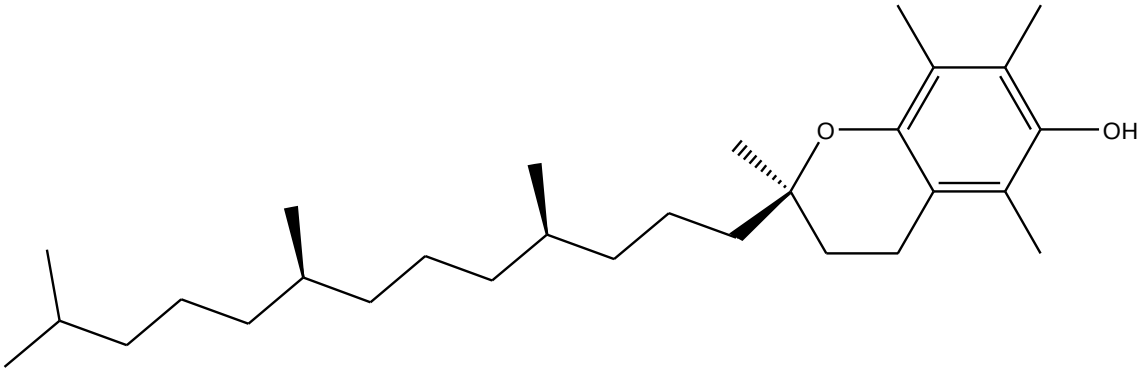

16

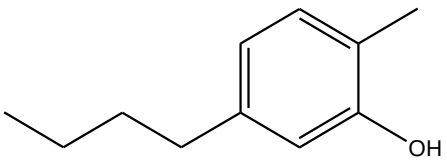

17

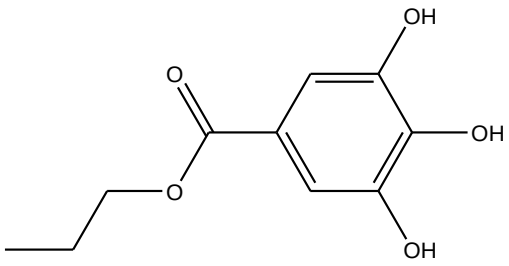

18

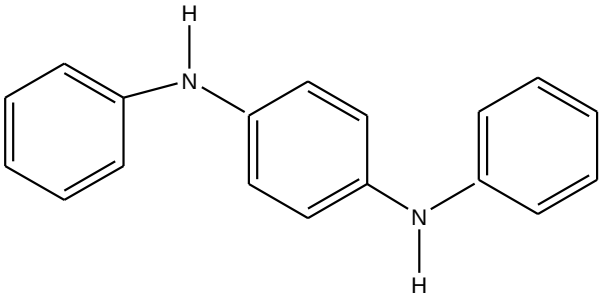

19

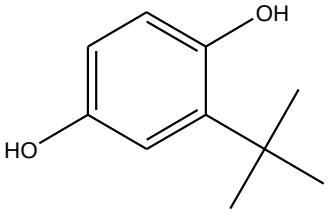

20

The advantages of biodiesel are that it is biodegradable and is less flammable than most fuels with high flash point. Biodiesel is biodegradable because it is oxidatively unstable naturally (Waynick, 2005). That means that when exposed to air, biodiesel immediately starts to break into smaller molecules that are more easily digested by microbes in the environment.

The primary feature in any biodiesel fuel additive is the ability to provide oxidation inhibition (Prankl and Schindlbauer, 1998). The amount needed is generally 10-50 times more oxidation inhibitor than what is needed for ultra-low sulfur diesel refined from petroleum. Oxidation inhibitor should be added before the biodiesel is sold or stored even if it meets the minimum Rancimat Oxidation Stability requirement. The reason for this is that oxidation starts as soon as the biodiesel is exposed to air. These additives do not reverse oxidation, they can only inhibit further oxidation, so adding them early means getting maximum benefit from the inhibitor additive.

In addition, the products of oxidation catalyze more oxidation, so the older the fuel is, the less effective the chemical inhibitor. The products of oxidation cause filter plugging, fuel injector fouling, corrosion and sludge formation in the engine lubricating oil. Biodiesel is much less volatile, and therefore less flammable than petroleum diesel. This property makes biodiesel safer to use, transport and store. However, low volatility, also means that "fuel blow by" accumulates in the lubricating

oil crank case and does not easily evaporate from the crankcase as it does with petroleum diesel. To combat this problem the use of a fuel additive that contains a detergent component capable of cleaning fuel injectors and keeping them clean should be considered. Proper fuel injection minimizes the chance of "fuel blow by" because if the fuel/air mixture is more efficient, the fuel burn more completely and there is less unburned fuel to get exhausted into the crankcase (Núbia *et al.*, 2007).

The other alternative is to use quality detergent lube oil that promises to keep the piston oil and fire rings clean. This means that these rings do not build up deposits and are able to flex properly. This minimises wear on the cylinder liners which again means less "fuel blow by" into the lube oil crankcase. According to research findings in this area, changing lube oil often on biodiesel powered vehicles is recommended (McCormick, 2009).

2.9 Phase Miscibility in Oil Mixtures by FTIR and Thermomechanical Analysis

Quantitative infrared analysis in the carbonyl region with a simple curve-fitting procedure and thermomechanical measurements were used to analyse critical behaviours in naturally aged oil/resin mixtures covering a wide range of composition. The results were discussed on the basis of a comparative study performed with fresh mixtures of the same composition, used as standards, and a phase miscibility analysis (Pagés *et al*. 1996).

Thermomechanical measurements give macroscopic evidence for phase segregation in naturally aged mixtures with a resin component content strictly below 50%, while above this threshold the basic components are totally involved in the formation of a stable mixed oil/resin phase. At the molecular scale, infrared measurements appear to

be sensitive to the subsequent oil/resin interaction in aged mixtures which appears to develop at the first stage of the mixing.

Oxygenated diesel fuel blends have advantages over regular diesel. Oxygenation significantly reduces particulate matter (PM) and reduces toxic gases such as carbon oxides (CO_x), sulfur oxides (SO*x*), and, at times, nitrogen oxides (NO*x*) from tailpipe emissions. Ethanol, which is oxygenated in Ethanol-diesel blend, is a renewable fuel that reduces the dependency of non-oil-producing countries on foreign petroleum. However, a major drawback with ethanol-diesel is that ethanol is immiscible in diesel over a wide range of temperatures (Fernando and Hanna, 2004).

Ternary phase diagrams are widely used to depict the phase behaviour of three-component systems (Svein, 2009; Robert et *al*., 1988). Phase boundaries can be determined using the titration method (Robert *et al*., 1988). Initially, a mixture of 5% ethanol and 95% diesel (5% E-diesel) is titrated with biodiesel to get a clear endpoint. Similarly, mixtures of E-diesel concentrations ranging from 5% to 95% in 5% increments are titrated with biodiesel to develop the phase diagram (Stloukal *et al*. 1997).

Studies have revealed that biodiesel, which is another renewable fuel, can be used successfully as an amphiphile (a surface-active agent) to stabilize ethanol and diesel. Research also has revealed that ethanol-biodiesel-diesel (EB-diesel) fuel blend microemulsions are stable well below sub-zero temperatures and have shown equal or superior fuel properties to regular diesel fuel. Microemulsions of certain component concentrations have shown substantially increased lubricity without compromising the cetane numbers and energy values (Svein, 2009).

Despite ethanol having a considerably lower energy value, cetane number and lubricity value than biodiesel or diesel fuel alone, the heat of combustion and cetane numbers of the EB-diesel blends remain steady, without significant reduction.

2.10 Biodiesel Synthesis

Biodiesel is a product designed from the transesterification reaction between vegetable triglycerides and alcohol. It has more favourable combustion emission profile than fossil- based fuel (Zhang *et al*., 2003a and Zhang *et al*., 2003b). Transesterification is the most common method used to synthesise biodiesel carried out under atmospheric condition catalysed by both homogeneous and heterogeneous catalysts. Potassium and sodium hydroxide are the most used homogenous alkali catalysts in the transesterification of oil with very low fatty acid content. Alkali metal catalysts are found to be more effective than acidic catalyst (Barnwal and Sharma, 2005).

Generally, the mechanism of the base-catalysed transesterification of vegetable oils involves four steps. The first step is the reaction of the base with the alcohol, producing an alkoxide and the protonated catalyst. The second step is the nucleophilic attack of the alkoxide at the carbonyl group of the triglyceride generating a tetrahedral intermediate (Meher *et al.*, 2006).

The third step involves the formation of the alkyl ester and the corresponding anion of diglyceride. The final step involves deprotonating the catalyst, thus regenerating the active species, which is now able to react with a second molecule of the alcohol, starting another catalytic cycle. Diglycerides and monoglycerides are converted by the same mechanism to a mixture of alkyl esters and glycerol. The above steps are summarized in **Scheme 1 (**Aransiola *et al*., 2014).

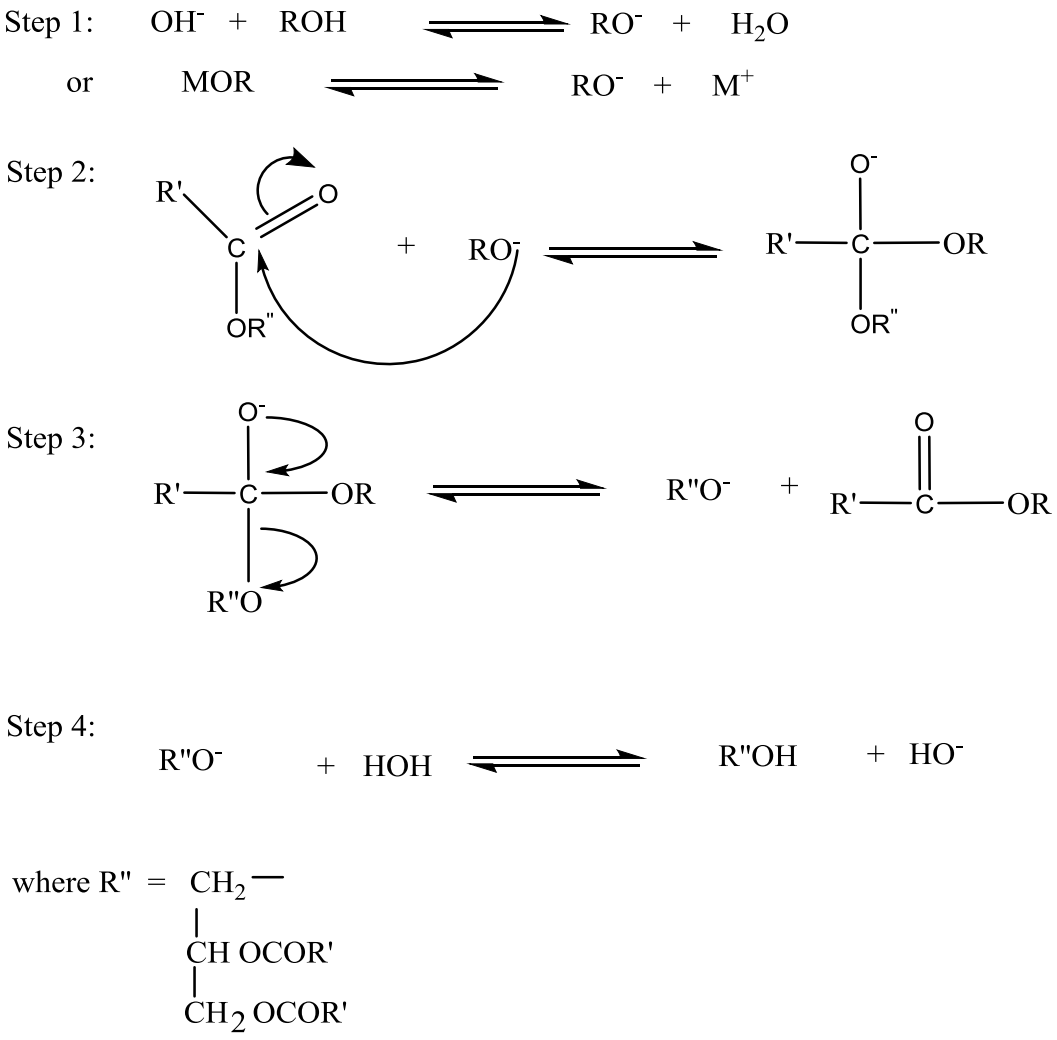

where R" = CH_2—
CH OCOR'
CH_2 OCOR'

R′ = Carbon chain of fatty acid, R = Alkyl group of alcohol

Scheme 1. Mechanism for base catalysed transesterification process.

The base-catalyzed transesterification of vegetable oils are reported to proceed faster than the acid- catalyzed reactions and since they are less corrosive than acidic compounds, industrial processes usually favour base catalysts, such as alkaline metal alkoxides and hydroxides (Gryglewiez, 2000) as well as sodium or potassium carbonates (Hirano and Tsuto 2000). Alkaline metal alkoxides are the most active catalysts. They give yields greater than 98% in a relatively short reaction time of 30 min. even at low molar concentrations of about 0.5 mol%, but the requirement of the

absence of water makes them inappropriate for typical industrial processes in which water cannot be avoided completely.

Alkaline metal hydroxides such as KOH and NaOH are cheaper than metal alkoxides, but less active. Nevertheless, they are a good alternative since they can give the same high conversions of vegetable oils just by increasing the catalyst concentration to 1 or 2 mol%. However, even if water-free alcohol/oil mixture is used, some water is produced in the system by the reaction of the hydroxide and the alcohol (Ejikeme *et al.,* 2010).

2.11 Methanol and Ethanol in Transesterification

The use of methanol as the alcohol in the transesterification reaction is more common than ethanol because of its low cost. However, several researchers prefer using ethanol derived from sugarcane in the transesterification reaction (Zagonel *et al.,* 2004). Methanol is also preferred because the base catalyzed formation of fatty acid methyl esters (FAME) is simple compared to the formation of fatty acid ethyl esters. Specifically, the formation of a stable emulsion during transesterification using ethanol is a problem. Methanol and ethanol are not miscible with triglycerides at ambient temperature, and the reaction mixtures are usually mechanically stirred to enhance mass transfer. During the course of the reaction, emulsions usually form. In the case of transesterification using methanol, these emulsions quickly and easily break down to form a glycerol phase at the bottom and a FAME phase at the top. In transesterifications using ethanol, these emulsions are more stable and severely complicate the separation and purification of fatty acid ethyl ester (Zhou *et al*., 2003). The molar ratio of triglyceride to alcohol is one of the most important variables affecting the yield of FAME (Tomasevic and Marinkovic, 2003; Anastopoulos *et al*., 2009). The stoichiometric ratio for transesterification requires one mole of triglyceride

and three moles of alcohol to yield three moles of FAME and one mole of glycerol. However, transesterification is an equilibrium reaction in which a large excess of alcohol is required to drive the reaction to products. For the optimal conversion of triglyceride to FAME, a 1 : 6 molar ratio of oil– alcohol should be used. However, the high molar ratio of alcohol to vegetable oil interferes with the separation of glycerine because there is an increase in solubility. When glycerine remains in solution, it helps to reverse the equilibrium back to the reactant, lowering the yield of esters. The transesterification of 1,2,3-propanetriyloctadec-9z-enoate (triolein) **(21)** as a substrate is a good single-component model for vegetable oil with methanol, and has been studied at different molar ratios. Transesterification occur using potassium or sodium hydroxide as a base catalyst, in a microwave apparatus in sealed tubes at 50 ^{o}C.

Optimal reaction conditions involved using a 1:6 triolein–methanol ratio (1:2 stoichiometric ratio), 5 wt% KOH, heating the reaction mixture to 50 ^{o}C, and holding at this temperature for 1 min. These conditions yielded a 98% conversion of the triolein to methyl oleate. An increased triolein– methanol ratio, reaction time, and reaction temperature or KOH loading did not increase the yield. The 1:6 molar ratio of oil–methanol used under microwave conditions is lower than that reported when conventional heating is applied. Under conventional heating a ratio varying from 1:9 up to 1:30 is more common (Leadbeater and Stencel, 2006).

21

2.12 Biodiesel Processing

Once the reaction is complete, two major products exist: glycerol and biodiesel. Each has a substantial amount of excess alcohol that is used in the reaction. The reacted mixture is sometimes neutralized at this step if needed. The glycerol phase is much denser than biodiesel phase and the two can be gravity separated by drawing off glycerol at the bottom of the settling vessel. In some cases, a centrifuge is used to separate the two materials faster (Zagonel *et al*., 2004). Once the glycerol and biodiesel phase have been separated, the excess alcohol in each phase is removed with a flash evaporation process or by distillation. In other systems, the alcohol is removed and the mixture neutralized before the glycerol and esters have been separated. In either case, the alcohol is recovered using distillation equipment and is re-used. Care is taken to ensure no water accumulates in the recovered alcohol stream.

The glycerol by-product contains unused catalyst and soap that are neutralized with an acid and sent to storage as crude glycerol. In some cases the salt formed during this phase is recovered for use as a fertilizer. Water and alcohol are removed to produce 80-88% pure glycerol that is ready to be sold as crude glycerine. In more sophisticated operations,

the glycerol is distilled to 99% or higher purity and sold into the cosmetic and pharmaceutical markets (Keith, 2007).

Once separated from the glycerol, the biodiesel can be purified by washing gently with warm water to remove residual catalyst, soap, remnant glycerol and excess alcohol. The use of warm water (40 to 60°C) prevents precipitation of unsaturated fatty acid esters and retards the formation of emulsions with the use of gentle washing action. The following are the main washing methods as described by Keith (2007).

2.12.1 Mist washing

Mist washing was developed as a way to address emulsification issues. This system uses a very fine mist head, suspended over a container of biodiesel, with a way to drain the water after it falls through the fuel. The mist stirs up the fuel less than in bubble washing, and removes soaps gradually. The gentler agitation gives less opportunity for the soap and many mono and diglycerides to form emulsion (Keith, 2007).

2.12.2 Bubble washing

Bubble washing involves gently adding water to biodiesel in a 1:2 ratio respectively, adding an aquarium air stone and air pump set up to the water portion where water sinks to the bottom and biodiesel float on top and bubbling air through the water. The air bubbles allow an indirect agitation of the two fluids such that they pick up a tiny amount of water and gently carry it through the biodiesel also picking up soap and other contaminants. When the bubble bursts at the surface it drops the water which picks up more of the soap and contaminants on its way back down. After about 6 hours of this washing, the air is stopped, water is drained, more fresh water is added, and the process repeated about 3 times on average- until the water measures the same pH as the

tap water, and is perfectly clear (Keith, 2007).

2.12.3 Stir Washing

This method involves mixing the biodiesel with water and stirring to a homogeneous state by use of a motor driven impeller. The mixture is then allowed to settle for an hour in a settling tank. The biodiesel separates and forms a clear layer on top of the water and is siphoned or decanted out. This process is repeated at least twice. Compared to other methods it is quick and more effective and there is no masking of poor reaction or oxidation since biodiesel is actively agitated.

2.12.4 Biodiesel Drying

A dry fuel is clear referring to lack of haze as a sign. The water content in biodiesel can be reduced by any of the following methods:

2.12.4.1 Vacuum driers

In vacuum driers the biodiesel is subjected to highly reduced pressure. This allows the water in the biodiesel to evaporate at low temperature. Vacuum driers can be either batch or continuous (Keith, 2007).

2.12.4.2 Falling film evaporator

In a falling evaporator, a thin film of the biodiesel runs down a heated surface of the evaporator. The direct contact with the heated wall evaporates the water rapidly. Falling film evaporates allow for rather high heating and evaporation rates. In this process caution is taken in avoiding high temperatures that lead to darkening of the biodiesel, which is a sign of polymerizing of the poly-unsaturated methyl ester (Keith, 2007).

2.12.4.3 Bubble-drying

Bubble drying uses the same principle as bubble washing discussed above, the exception is that here water is not used. Air is bubbled through the biodiesel,

enhancing the evaporation of water in the biodiesel. It has the same disadvantage of oxidizing and polymerizing the biodiesel as occurs in bubble washing (Keith, 2007).

2.12.4.4 Evaporation

Biodiesel when exposed to an open place for a day or longer it clears on its own. This process can be accelerated by heating the biodiesel at 40-50˚C, and allowing it to cool in a vented container.

2.13 Biodiesel Quality Testing

Biodiesel characteristics vary slightly depending on the feedstock used. This does not however compromise the final quality of the processed biodiesel. To ensure safe running of biodiesel in the diesel engine it is essential to test for quality (Keith, 2007). Free glycerol, incomplete conversion of oils/fats and sodium or potassium arising from the addition of catalyst are contaminants which have severe impact on the fuel system of a diesel engine. Several standards for testing biodiesel have been developed where biodiesel is commercially in use. Biodiesel standards such as of European EN 14214, Germany's DIN 51606 and America's US ASTM D-6751-02 have been used to test the quality. However, for quality checks where standard tests are not available, the following tests were proposed that can be used to check quality of biodiesel (Keith, 2007).

2.13.1 Wash test

In a half litre glass jar 150ml of unwashed biodiesel is mixed with 150ml of water, the lid is then screwed tightly and the jar shaken violently for ten seconds or more, until a homogeneous mixture was formed. The mixture was then left to settle. For a good quality biodiesel, the biodiesel is supposed to separate from the water in half an hour or less, with amber biodiesel on top and milky water below. If it turns into something like mayonnaise and does not separate, or separates slowly with a white

creamy layer sand-witched between water and biodiesel, the fuel is of poor quality.

2.13.2 Reprocessing test

A small amount of the finished biodiesel is reprocessed again as if were neat vegetable oil. If more glycerol drops out, then the fuel is not of good quality.

2.13.3 Methanol test

In a measuring glass 25ml of biodiesel is dissolved with 225ml of methanol. The biodiesel should be fully soluble in the methanol, forming a clear bright phase. If not, there is contamination of the biodiesel. This method gives indication of impurities in the biodiesel. It is valid only for biodiesel made from vegetable oils and animal fats and is not valid for biodiesel made from oils with a very wide fatty acid patterns, such as fish oils.

2.14 Microbial Attack on Biofuels and Petroleum Blends

One of biodiesel's positive features is that it is biodegradable. However, in a poor environment, this can also be one of biodiesel's negative features. In this case, microorganisms in the environment that feed on straight chain fatty acids have a chemical protocol that starts by trying to feed on straight-chain hydrocarbons that they modify from the petroleum hydrocarbon to a fatty acid. If these molecules are not available, they proceed to the next molecule to try and convert it into a fatty acid. Biodiesel and its blends can provide an easier pathway for the microorganism as the fatty acid methyl ester molecule is in the final stage prior to breaking down the fuel for energy (Chesneau, 2008). Some biofuels are degraded by microorganisms at a rate comparable to that of sugar (Blin *et al.*, 2007). Such degradation might lead to undesired fuel properties such as acid formation, and particle formation in the biofuel. Biofuels are hygroscopic in nature and therefore contain more water than what is usually found in petrochemical fuels. Increased water content in the fuel matrix will

lead to increased growth of microorganisms in the fuel-water interphase. An increase in microbiological growth and activity is known to speed up corrosion rates, a phenomenon known as Microbiologically Influenced Corrosion (MIC) in the fuel handling infrastructure. With the switch towards increased proportions of sustainable fuels, MIC caused by biofilm formation will be a major challenge to storage and distribution facilities. Furthermore, biofuels promote corrosion more directly through increased presence of water or the adhesion of precipitates. Several strains of microorganisms have been identified in biodiesel and blends with petroleum diesel (DeMello *et al*., 2007). Some important microbial species with this potential belong to the genera *Arthrobacter, Halomonas, Pseudomonas, Bacillus, Klebsiella, Proteus, Aspergillus, Neurospora, Rhizopus, Mucor and Trichoderma.* Microbial species differ in their biodegradation capabilities (Varjani *et al*., 2013).

Various biocides have been suggested to prevent the growth of microorganisms in petroleum products. The chemical biocide such as methylene-bis-oxazolidine (MBO) selected must be rapidly effective against large number of microbes in the presence of substantial organic fouling. It must be safe to use, and with acceptable environmental impact (Zimmer *et al*., 2013).

2.15 Methods for Analysis of Physicochemical Parameters for Oils

2.15.1 Gas-Chromatography (GC-MS) Analytical Method

The structure of sample components that dictate polarity and their boiling points are the major factors determining the retention time (Van Gerpen *et al.,* 2004). Usually, larger molecules have longer retention times in GC. When a material eluting from the column at a certain retention time is detected, this is shown by a peak in the chromatogram. The integrated value of the peak amplitude over time is proportional to the amount of material causing them (Younis *et al.,* 2009). This constitutes the usefulness of GC in

quantifying the amounts of components in a mixture. Compounds with known retention times are used as standards to indicate when a compound of a specific nature can be expected to elute. They are therefore very useful in establishing the nature of the compounds in a mixture (Younis *et al*., 2009, Mittelbach *et al*., 1996).

The structural identity of a component is established through the use of hyphenated method. The most common method is combination with mass spectrometry (GC-MS). The spectra in MS record how a compound is broken up into fragments by beam of electrons energy. The way a compound splits into fragments is characteristic of its structure (Van Gerpen *et al*., 2004).

2.15.2 Infra-red spectroscopic analysis

Infrared Spectroscopy (IR) is a technology that uses the property of organic materials to absorb infrared light. This enables analysis for composition and functional properties. Infrared light has wavelengths in the range next to and longer than visible light. Specific features of the absorption of the infrared light by the organic materials are used in the calibration process. Calibration involves developing a mathematical model between the spectral features of a set of samples and chemical or other conventional analytical data on the same samples. Once IR instruments are calibrated, they accurately predict the quantities of up to 30 constituents or functional properties of new samples simultaneously in seconds. Little or no sample preparation is required.

Near Infrared spectroscopy has been shown to be useful in monitoring the transesterification reaction used to convert vegetable oils, animal fats, or waste oils into biodiesel (Meher *et al*., 2006). Standards for biodiesel set by the American Standard for Testing Materials (ASTM) address the presence of materials such as free and total glycerol, water, free fatty acid, and residual alcohol. These materials need to be minimised in biodiesel so that it does not deteriorate during storage and it is safe for use

in engines. Near infra red (NIR) spectroscopy is used to monitor the trans-esterification reaction (Knothe, 1999). The basis for quantization of the turn over from triglyceride feedstock to alkyl ester product is different in the NIR spectra of these classes of compounds. Ethyl esters could be distinguished in a similar fashion (Knothe, 1999). The mid-range IR spectra of triglycerides and methyl esters of fatty acids are almost identical and offer no possibility for distinguishing. Monitoring such a reaction would be difficult due to the broad peaks presented by the alcohol. In a subsequent study, NIR was used to quantitatively monitor the transesterification reaction by correlating the NIR data with ^{1}H nuclear magnetic resonance spectroscopy (NMR) results (Knothe, 2000).

2.15.3 Thin layer chromatography

Thin layer chromatography (TLC) is performed on a sheet of glass, plastic, or aluminum foil, which has been coated with a thin layer of adsorbent material, usually silica gel, aluminium oxide, or cellulose blotter paper. This layer of adsorbent is known as the stationary phase. TLC is usually used as a qualitative technique for the identification of components within a mixture since it is hard to quantitatively deposit known quantities of the mixture on the plate (Stashenko *et al*, 2004; Spangenberg *et al*., 2010).

The esterification reaction and biodiesel conversion can be monitored by TLC, and performed on glass plates coated with silica gel. The eluent used is a mixture of hexane and diethyl ether (80:20 v/v), and iodine vapor is used for visualization. In one of the methods raw material and biodiesel are separately spotted on a TLC plate. The solvent mixture of petroleum ether and ethyl acetate 9:1 was used as the mobile phase and iodine used for the visualization of spots.

TLC analyses has also been used to qualitatively determine composition of essential oils from plant extracts (Háznagy-Radnal *et al*., 2007) performed on two kinds of plates: TLC Sil G F_{254} and HPTLC Sil G F_{254} precoated plates. The TLC plate is conditioned with methanol and dried at 110°C for 3 h before use. The samples were applied with a Linomat 5 device as 5 mm bands, 20 µL for plant extracts and 7 µL for standards. In the case of HPTLC plates the applied volume was decreased at 10 µL for extracts and at 5 µL for standards. A mixture of toluene-ethyl acetate (93:7, v/v) was used as mobile phase. The developed plates were sprayed with anisaldehyde and then heated 3 min at 110°C when red-bluish bands appear. The plates were inspected in daylight and also at 366 nm in UV range (Háznagy-Radnal *et al*., 2007).

2.16 Analytical Methods of Fuel Parameters

2.16.1 Water Content (ASTM-D95)

This test method covers water in the range from 0 to 25 % volume in petroleum products, tars, and other bituminous materials by the distillation method using Dean and Stark apparatus. The fuel sample to be tested is heated under reflux with petroleum ether, which co-distills with the water in the sample (ASTM, 1999b).

2.16.2 Density (ASTM D1298)

This test method covers petroleum products normally handled as liquids using a glass hydrometer. The hydrometer cylinder and its contents are placed in a constant temperature bath to avoid excessive temperature variation during the test. The values are measured on a hydrometer at either the reference temperature or at another convenient temperature. Accurate determination of the density is necessary for the conversion of measured volumes to volumes or masses, or both, at the standard reference temperatures by means of the petroleum measurement tables (ASTM, 2006).

2.16.3 Flash Point (ASTM -D93)

The flash point measures the temperature at which the test specimen forms a flammable mixture with air under controlled laboratory conditions. It is one of the properties which must be considered in assessing the overall flammability hazard of a fuel (ASTM, 2007).

2.16.4 Copper Corrosion (ASTM-D130)

This test method covers the detection of the corrosiveness to copper of a fuel. A polished copper strip is immersed in a given quantity of sample and heated at a temperature of boiling water for 3 h. At the end of this period the copper strip is removed, washed, and compared with the ASTM copper strip corrosion standards which are presented in increasing degree of tarnish and corrosion (ASTM, 1994).

2.16.5 Color (ASTM-D1500)

This test method covers the visual determination of the color of a wide variety of petroleum products. The property is used mainly for manufacturing control purposes and is an important quality characteristic since color is readily observed by the user of the product. In some cases the color may serve as an indication of the degree of refinement of the material. When the color range of a particular product is known, a variation outside the established range may indicate possible contamination with another product. The ASTM color standard ranges in value from 0.5 to 8.0 units (ASTM, 2002a).

2.16.6 Kinematic Viscosity (ASTM-D445)

The viscosity of petroleum fuels is important for the estimation of optimum storage, handling, and operational conditions (Knothe *et al*., 2005). Thus, the accurate determination of viscosity is essential to many product specifications (ASTM, 2004a).

ASTM D445 specifies a procedure for the determination of the kinematic viscosity of liquid petroleum products, both transparent and opaque, by measuring the time for a given volume of liquid to flow under gravity through a calibrated glass capillary viscometer. The measurements are recorded and the average used in the calculation of the kinematic viscosity from the measured flow time and the viscometer constant using equation 2.1.

$$V = Ct \quad \text{..... 2.1}$$

where;

V = Kinematic viscosity (mm^2/s),

C = calibration constant of the viscometer ($(mm^2/s)/s$)

t = time in seconds

2.16.7 Ash Content (ASTM-D482)

Knowledge of the amount of ash-forming material present in a product provides information as to whether or not the product is suitable for use in a given application. Ash can result from oil or water-soluble metallic compounds or from extraneous solids such as dirt and rust (ASTM, 2000a).

The test method covers determination of ash in the range 0.001-0.180% mass from petroleum products, in which any ash-forming materials present are normally considered to be undesirable impurities or contaminants. The sample, contained in a suitable vessel is ignited and allowed to burn until only ash and carbon remain. The carbonaceous residue is reduced to an ash by heating in a muffle furnace at 775°C, cooled and weighed.

2.16.8 Distillation at Atmospheric Pressure (ASTM-D86)

Besides its importance for quality control, boiling point at atmospheric pressure is also the basis for the prediction of temperature-dependent properties such as vapor

pressure, density, latent heat of vaporization, viscosity, and surface tension of fuels therefore the distillation characteristics are critically important for both automotive and aviation gasoline affecting starting, warm-up, and tendency to vapor lock at high operating temperature and high altitude. The presence of high boiling point components in biofuels can significantly affect the degree of formation of solid combustion deposits (Yuan *et al*., 2005). The test method ASTM-D86 covers the atmospheric distillation of petroleum products using a laboratory batch distillation unit to determine quantitatively, the boiling range characteristics of petroleum liquid fuels (ASTM, 2000b).

2.16.9 Cetane Index (ASTM D-4737)

One of the most important properties of a diesel fuel is its readiness to auto- ignite at the temperatures and pressures present in the cylinder when the fuel is injected. The laboratory test that is used to predict this tendency is the calculated cetane index (Knothe *et al*., 2003). Fuels with a high cetane index have short ignition delays and a small amount of premixed combustion since little time is available to prepare the fuel for combustion.

Calculated cetane index CCI is worked out as shown in equation 2.2 as a correlation in SI units between the density at 15 ^{o}C and 10 %, 50 %, and 90 % recovery temperatures of the fuel as follows:

$$CCI = 45.2 + (0.0892)(T_{10N}) + [0.131+(90.901)B][T_{50N}]+[0.0523-(0.420)(B)][T_{90N}] +[0.00049] [(T_{10N})^2 -(T_{10N})^2] + (107)(B) + (60)B^2 \quad \text{..... 2.2}$$

Where CCI = Calculated Cetane Index

$B=[e^{(-3.5)(DN)}]-1$ where DN=(Density at 15^{o}C-0.85)

$T_{10N}= T_{10}-125$ where T_{10} = 10% recovery temperature determined by test method ASTM D86.

T_{50N}= T_{50}-260 where T_{50} = 50% recovery temperature determined by test method ASTM D86.

T_{90N}= T_{90}-310 where T_{90} = 90% recovery temperature determined by test method ASTM D86.

The calculated cetane index by four variable equation (ASTM D-4737) is useful for estimating ASTM cetane number when a test engine is not available for determining this property directly and when cetane improver is not used. It may be conveniently employed for estimating cetane number when the quantity of sample available is too small for an engine rating (ASTM, 2009).

2.16.10 Cold filter plugging point (CFPP) (ASTM D6371)

This test is a more complicated procedure involving using a vacuum to draw a 20 cc fuel sample through a 45 micron screen within 60 seconds. The lowest temperature at which the volume of biodiesel completely flows under vacuum through the 45 micron screen within 60 s is recorded as the cold filter plugging point (ASTM, 1999a). The CFPP test employs rapid cooling conditions. The CFPP is generally considered to be a more reliable indicator of low-temperature operability than cloud point or pour point, since the fuels contain solids of sufficient size to render the engine inoperable due to fuel filter plugging once the CFPP is reached (Park *et al.*, 2008). The test simulates the performance of an average or typical vehicle and is not protective of the most challenging fuel system designs from a low temperature operability standpoint, which make up roughly one-third of heavy-duty vehicles or one-fifth of light-duty vehicles.

2.16.11 Cloud Point (ASTM D2500)

This test determines the point where wax becomes visible in a fuel sample. This wax first appears as a floating cloudiness in a transparent fuel. It is recorded as the

temperature at which crystal growth is large enough (diameter ≥ 0.5 μm) to be observed using the naked eye (ASTM, 2002b). At temperature below cloud point, large crystals fuse together and form agglomerations that eventually become extensive enough to prevent pouring of the fluid. Below the cloud point, these crystals might plug filters or could drop to the bottom of a storage tank. However, fuels can usually be pumped at temperatures below cloud point (Park *et al*., 2008).

2.16.12 Pour point (ASTM D97)

Pour point (PP), measures the lowest temperature at which the oil is observed to flow. It defines the lowest temperature at which the fuel can still be moved, before it has gelled. Fuels with high pour points are more difficult to use in areas with lower temperatures because the fuel must be kept warm by some method, such as installation of electric heaters with insulated tanks. Distributors and blenders use pour point as an indicator of whether the fuel can be pumped (Knothe *et al*., 2005).

2.16.13 Calorific value (ASTM D4809)

Calorific value is the amount of heat produced by the combustion of a fuel mass, and is typically expressed in joules per kilogram. All elements considered to be fuels have a calorific value. The two calorific values for fuels are higher and lower values. Higher value assumes that water vapor is totally condensed and the heat produced is recovered. Lower value assumes that the water vapor is retained but not the heat. The heat of combustion is determined by burning a weighed sample in an oxygen-bomb calorimeter under controlled conditions. The temperature increase is measured by a temperature reading instrument which allows the precision of the method to be met. The heat of combustion is calculated from temperature observations before, during, and after combustion, with proper allowance for thermo-chemical and heat-transfer corrections. Either isoperibol or adiabatic calorimeters may be used.

The gross heat released is calculated from equation 2.3.

$$H = \frac{(Cv\Delta T - 0.01260)}{M} \quad \text{.....} \quad 2.3$$

where, H =Calorific value,

Cv = Heat capacity of apparatus (10.380 J/

°C) and 0.12600 J = Constant heat gain

ΔT = Rise in temperature

M = mean weight of sample

The heat of combustion is a measure of the energy available from a fuel. A knowledge of this value is essential when considering the thermal efficiency of equipment for producing either power or heat. The mass heat of combustion, that is, the heat of combustion per unit mass of fuel, is measured by this procedure (ASTM D4809). Its magnitude is particularly important to weight limited vehicles such as airplanes, surface effect vehicles, and hydrofoils as the distance such crafts can travel on a given weight of fuel is a direct function of the mass, heat of combustion and density of the fuel (ASTM, 2013).

CHAPTER THREE

3 MATERIALS AND METHODS

This chapter describes materials and methods used in collection and preparation of samples, extraction of oils from citrus peelings, *R. grande* and *J. curcas*. Catalytic synthesis of oxygenated and hydrogenated *d*-limonene from *C. sinensis* citrus oil. Synthesis of bioethanol from algae *R. grande* and citrus biomass by saccharification followed by fermentation.

Base catalytic conversion of algae *R. grande* and *J. curcas* oil to fatty acid ethyl esters using bioethanol and blending. Identification of constituent compounds in citrus oil, oxygenated and hydrogenated *d*-limonene, fatty acid ethyl esters from algae *R. grande* and *J. curcas* by FTIR and GC-MS spectroscopy.

Determination of miscibility, physicochemical and fuel properties of the extracted oils, fatty acid ethyl ester blends from algae *R. grande* and *J. curcas* oil (JAB) and those with d-limonene, oxygenated and hydrogenated derivatives as additives (JABLA).

Statistical assessment of the effect of *d*-limonene, oxygenated and hydrogenated derivatives additives to JAB on microbial attack, physicochemical and fuel properties and comparison to fossil diesel ASTM D975 standards and biofuel ASTM 6751-08 standards.

3.1 Research Design

The research was carried out both in the field and in the laboratory. Probability and purposeful sampling methods were both used to collect marine macro-algae species from the Indian ocean by hand picking, citrus fruit peels from Kongowea Mombasa county and Milly fruit processors Kilifi county and *J. curcas* L. from Shimba hills in Kwale County. The research was conducted using a randomized block design

comprising of three blocks. Oils from *Citrus sinensis*, *Rhizoclonium grande* and *Jatropha curcas*, ethyl esters (JOEE and AOEE) from the *J. curcas* and *R. grande* oils and their blends (JAB), and ethyl ester JAB blend with d-limonene derivatives catalytically synthesised from *C. sinensis* peeling oil (JABLA). Each sample from a block was subjected to several treatments with three replication measurements per treatment. The oil extractions was done using oil press, carbon dioxide and hexane solvent. Catalytic synthesis of oxygenated and hydrogenated *d*-limonene was carried out using palladium catalysts (Pd/HT and Pd/Al_2O_3) from the citrus oil containing mainly *d*-limonene. Base transesterifications were carried out on *R. grande* and *J. curcas* oils to produce fatty acid ethyl esters. Blending was done by adding *d*-limonene, oxygenated *d*-limonene and hydrogenated *d*-limonene to the fatty acid blends followed by analysis of composition, physicochemical and fuel properties.

3.2 Sampling and Treatments

3.2.1 Collections and Treatment of Citrus Peelings

3.2.1.1 Sampling site

Citrus fruits were bought from traders in Kongowea market which were originally obtained from farmers in Malindi region, Shimba hills region in Kenya and Muheza - Tanga region in Tanzania, 5° 10' 23.300" S 38° 47' 13.725" E according to the wholesale traders. Kongowea Market, $4^0 3' 25.934'' S\ 39^0 40' 23.775'' E$, is in the North Coast 5 Km from Mombasa City. Another sampling site where ready citrus peelings were obtained from is Milly Fruit Processors, $4^0\ 2' 36.518'' S\ 39^0\ 40' 5.543'' E$, in Mtwapa about 16 Km to the North East of Mombasa city on the Mombasa-Malindi Road. This fruit processing firm buys citrus fruits from the same farmers producing a lot of peels as byproduct.

3.2.1.2 Collection and treatment

Citrus fruits obtained from Kongowea market in Mombasa were confirmed by a taxonomist as lemons *C. lemoni* L, oranges *C. sinensis* L. and tangerines *C. tangerine* L. The fruits were sampled using probabilitive and purposeful sampling from the traders. 120 fruits of each kind were randomly picked and bought from the traders. The sample size was dependent on the fruit availability and size of the fruit and worked out using Cochran formula (Lehmann *et al*., 2013). From a population of 1000 fruits of each kind, sample proportion of 10% assuming a margin of error of 5% and confidence level of 95%. The fruits were brought to Technical University of Mombasa (TUM), Chemistry laboratory for pretreatment and oil extractions.

The samples were stored in a refrigerator set at 4^{o}C. Each fruit was cleaned using distilled water and weighed by Ohaus Scout analytical balance, model AdventurerPro AV264, Switzerland. Four fruits closest in mass were put together as a sample, each was cut into four using a sharp knife. The citrus fleshy part was then separated from the peels by hand. The peels (plate 3.1) were cleaned using distilled water. The white part of the peels containing pectin was peeled out using a scalpel to expose the oil sacs. The clean citrus peels free from pectin from each fruit were weighed and ground using Sanford blender model SF 5525BR, Sri Lanka. Fresh citrus peels were also obtained from citrus processing firm Milly fruit processors Mombasa and stored in a refrigerator set at 4 ^{o}C.

Plate 3.1: *Citrus sp* peels

3.2.2 Collection and Treatment of Algae

3.2.2.1 Sampling sites

Macroscopic and filamentous algae were collected from five sites during low tide from Shimoni shores, 4° 38′49.786″S 39° 22′ 49.488″E, in Kwale South Coast, Shelly beach, 4° 4′ 59.854″S 39° 40′ 19.685″E, in Likoni South Coast, Jamvi la Wageni, 4° 4′ 59.854″S 39° 40′ 19.685″E, in Likoni South Coast, English point, 4° 2′ 36.518″S 39° 40′ 5.543″E near Kenya Marine and Fisheries Research Institute (KMFRI) Mombasa North coast and Tudor Creek, 4° 1′ 35.698″S 39° 39′ 15.829″E, near Kenya Meat Commission on Makupa Causeway.

3.2.2.2 Collection and treatment

Macroscopic and filamentous marine algae species from the different sampling sites were randomly sampled and separated from the growing medium (Appendix I). Ten macroalgae and filamentous species (*Enteromorpha kylinii , Rhizoclonium africanum,* (*Trichodesmium* sp.) Blue green, *Rhizoclonium grande, Galaxaura subvertillata, Ulva reticulate, Ulva pertusa, Rhizoclonium viparium, Enteromorpha muscoides* and *Chaetomorpha viellardi*) were separately collected and put in polythene sample bags. The samples were kept in cold boxes and transported to Technical University Laboratories for further treatment. The ten species were identified by a taxonomist

from Kenya Marine and Fisheries Research Institute (KMFRI). The algae species were dried under a shade for three days. Each species was ground to powder using Hamilton Beach commercial blender HBB250SR, USA.

The high water content of microscopic algae was removed to enable harvesting by microscreening and centrifugation using centrifuge Model Neofuge 15R, China. Collection of microscopic algae was abandoned due to the small quantities obtained.

3.2.2.3 Lipid distribution in different algae species by differential staining using Sudan IV dye

Umarah *et al.,* (2011) method was used with some modifications where 5 g of Sudan IV ($C_{24}H_{20}N_4O$) obtained from Sigma - Aldrich, Germany was weighed and dissolved in a total of 100 mL 70% ethanol (Umarah *et al.*, 2011). From each of the dry algae species such as in plate 3.2, 0.02g tissue was weighed using Ohaus Scout analytical balance model AdventurerPro AV264, Switzerland and transferred to a microscope slide (Appendix II). Two drops of the dye solution were added and allowed to stand for 5 minutes. The slides were observed under a light microscope magnification X400. The number of lipid globules that took up the red dye in the field was then counted for each species. The species with the largest number of globules per field was selected for oil extraction.

Plate 3.2: Dry *Rhizoclonium grande* algal tissue

3.2.3 Collections and Treatment of *Jatropha curcas L.* Seeds

Kwale County is one of the major Jatropha growing area (Appendix III). *J. curcas* seeds were collected from Shimba hills 4^0 10′ 28″S 39^0 27′ 37″E (Appendix IV). The out grower scheme Energy Africa in Shimba hills, Kwale county in South Coast was selected for collection of the seeds from contracted farmers. The farmers were non probabilitively sampled by snow balling (Sheteni, 2016) and the seeds were bought in 50 kilogram gunny polypropene bags. The husked seeds (plate 3.3a) were transported to Technical University of Mombasa where they were dehusked using a locally fabricated dehusker (Appendix V). The dehusked seeds (plate 3.3b) were weighed and preserved in polythene bags in an air conditioned room at temperature 25 ^oC ready for extraction.

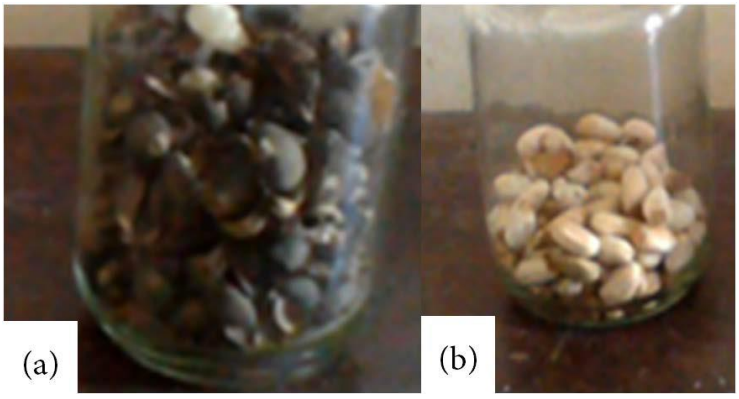

Plate 3.3: *Jatropha curcas* seeds

3.2.4 Collection of Petroleum Diesel

Diesel fuel samples measuring 1.0 L were collected from service stations in different areas of Mombasa County from the north, south, east, west and the Central Business District. The diesel samples were obtained from the various sampling sites in dark Winchesster glass bottles as shown in **Table 3.1.**

Table 3.1: Sampling sites for petrodiesel

Specific Area	Geographical coordinates
Shell Petrol Station - Likoni	4º5′6″S 39º39′17″E
National Oil Petrol Station - Mombasa island	4º3′36″S 39º40′19″E
Engen Nyali - Kisauni	4º2′25″S 39º40′42″ E
National Oil Petrol Station - Bamburi	4º3′24″S 39º40′12″E
Total Petrol Station - Jomvu	4º0′28″S 39º36′1″E

A representative sample was drawn directly from the pump into the bottle and well corked in order to prevent loss of light hydrocarbons that may affect the test results. The bottles were labelled immediately after the samples were obtained.

The diesel samples were then transported to chemistry laboratory, Jomo Kenyatta University of Agriculture and Technology (JKUAT) where a small quantity of each sample was transferred into a smaller glass bottle and stored in a cool dry place awaiting GC-MS and FTIR analysis whereas the remainder of the sample was transported to the Kenya Pipeline Limited, Changamwe for analysis.

The chemical and physical parameters analysed were based on the standardized analytical methods, American Standards for Test and Materials (ASTM) chemical methods such as the distillation (ASTM D 86), density (ASTM D 1298), kinematic viscosity (ASTM D 445), cetane index (ASTM D 4737) and flash point (ASTM D 93) were carried out (ASTM, 2013). FTIR spectroscopy and GC-MS analysis were carried out to obtain the fingerprint functional group identification.

3.3 Extractions, Analysis of Oils and Fermentation of Biomass

3.3.1 Liquid Extraction of Citrus Oil Containing *d*-limonene From Citrus Peelings

3.3.1.1 Extraction Using Hexane

The ground peelings from each sample (100-180 g) of the three types of citrus fruits were separately placed in 1 litre Erlenmeyer flasks then was added 250 mL of hexane boiling point range 63-70 ^{o}C obtained from Rankem Chemicals, India. The mixture was kept in a cupboard in Chemistry laboratory at Technical University of Mombasa for three days. The mixture was then filtered by vacuum filtration method into a 500 mL Buchner flask. The solvent was recovered using a vacuum evaporator model ROVA-3L at 45^{o}C with a negative pressure 450 mmHg (Appendix XI). The citrus oils obtained were kept open for a further three hours to evaporate all the solvent in a fume cupboard then measured using 10 mL measuring cylinder and 1000 µL

micropipettes and their mass recorded. The citrus oils were transferred into glass sample bottles and labelled (Appendix VI).

The composition of the citrus oils was analysed using GC-MS to establish the composition of the oils according to the method of Frizzo *et al.(*2004). The biomass after extractions were separately placed in polythene bags, labelled and preserved in a refrigerator for production of bioethanol.

3.3.1.2 Extraction using liquid CO_2

The extraction of *d*-limonene from citrus peeling was carried out as described by McKenzie *et al*. (2004). A modified form of the method was developed to accommodate larger quantities of the ground peelings at 20 g in an autoclave model LTKBS-50LV for safety purposes. A solid trap was constructed by bending copper wire into coils and a handle, metal screen placed between the wire coils. For extraction, the ground peelings were placed in a stainless steel percolator (Appendix VII), filled with 50 g of crushed dry ice and then sealed with a cap. The prepared peelings in the percolator was placed in water at 40-50 ^{o}C. The pressure in the autoclave increased considerably to a maximum of 0.2068 MPa (30 psi) and as pressure built in the container, gas escaped slowly through the safety valve of the autoclave, the liquefaction of CO_2 and extraction of the citrus oil was allowed to occur over a five minutes period. The citrus oils obtained were measured using 10 mL measuring cylinder and 1000 µL micropipettes. The citrus oils were transferred into glass sample bottles and labelled. The composition of the citrus oils was analysed using GC-MS to establish the percentage of limonene in the oils according to the method of Frizzo *et al.* (2004). The biomass after extractions were separately placed in labelled polythene bags and stored in refrigerator.

3.3.2 Extraction of Algae Oil

3.3.2.1 Liquid extraction of lipids from algae using hexane

Ground marine algae *Rhizoclonium grande* (350 g) was weighed and placed in 1litre Erlenmeyers flask and then added 700 mL of hexane with boiling point range 63-70 ^{o}C obtained from Ranchem Chemicals, India. The mixture was kept in a cupboard in Chemistry laboratory at Technical University of Mombasa for three days to allow proper soaking of the solvent. The mixture was then filtered by vacuum filtration method into a 500 mL Buchner flask. The solvent was recovered using a vacuum evaporator model ROVA-3L at 50 ^{o}C with a negative pressure 450 mmHg (Appendix VIII). The algae oil obtained was kept open for a further three hours to evaporate all the solvent in a fume cupboard then measured using 10 mL and 100 mL measuring cylinders. Traces of chlorophyll were removed from algae oil using activated charcoal over a filter paper by vacuum filtration. The algae oils were transferred into glass sample bottles and labelled. The biomass after extractions were separately placed in polythene bags and labelled.

3.3.2.2 Liquid carbon dioxide (CO_2) extraction of lipids from algae

A modified method by Polak *et al*. (1989) was adopted where liquid and supercritical CO_2 (sc CO_2) extraction of lipids (AO) from dried algae *R. grande* between 17 and 31 MPa at 40°-50^{o}C was carried out. Extracted lipids (AO) were then analyzed with gas chromatography. Macroalgae with higher number of globules from the pretest using sudan IV dye was expected to give higher amounts of lipids. Only little amount of chlorophyll in the algae was extracted by supercritical CO_2 (Polak *et al.,* 1989). The other nine algae samples were therefore ignored. The oil (AO) was then analysed for oil physicochemical properties using standard methods from the Association of

Official Analytical Chemists (AOAC, 2000), official methods and ASTM procedures and GC-MS for composition.

3.3.3 Extraction and Analysis of Jatropha Oil

3.3.3.1 Extraction of oil from *Jatropha curcas* seeds

J. curcas oil (JO) was extracted using fabricated cold oil press (Appendix IX) and *n*-hexane as the solvent after grinding using an industrial blender. The oil was allowed to settle then filtered using vacuum filtration. For the solvent extracted oil from the cake the solvent was recovered by vacuum evaporator model ROVA-3L at 50 ^{o}C with a negative pressure 450 mmHg and reused. The amount of oil in both cases was measured using a 100 mL measuring cylinder, transferred into glass containers (Appendix X) and kept in a refrigerator at 4 ^{o}C to be later analysed for oil physicochemical properties using standard methods from the Association of Official Analytical Chemists (AOAC) 17th edition, 2000, official methods and ASTM procedures and GC-MS for composition.

3.3.4 Saccharification and Fermentation of Citrus and Algae Biomass

The algal (*R. grande*) biomass and orange peelings (*C. Sinensis*) biomass after extraction of oil were separately collected in sterile containers and oven dried at 80 ^{o}C in the laboratory to remove excess hexane. Two fungal cultures *Aspergillus niger* for saccharification obtained from Microbiology Laboratory Kenyatta University and *Saccharomyces cerevisiae* for fermentation were obtained from Agrochemical and Food Company Limited, Kisumu. The fungi *A. niger* was cultured and maintained on potato dextrose agar medium at 30 ^{o}C. The yeast *S. cerevisiae* was cultured and maintained on yeast extract, peptone and dextrose (YPD) agar media at 30 ^{o}C. The ground and dried *C. sinensis* and *R. grande* biomass were sieved through sieve of

mesh number 18 equivalent to 1 mm pore. The separate fine powder obtained were used for saccharification and fermentation experiments.

3.3.4.1 Saccharification of the citrus and algae biomass

De-oiled and dried fine powder (150 g) of marine algae *R. grande* and orange *C. sinensis* peelings were separately weighed and formed the biomass for ethanol production. Mycelial mat of *A. niger* (0.85 g) was weighed on analytical balance and added to the biomass, 75 mL of distilled water was added and homogenised using a sterile blender and then transferred into stainless steel trays (Appendix XI). The biomass was allowed to start decaying to rapture the thin cell walls and release fermentable carbohydrates by *A. niger*. The saccharification was carried out for a period of six days at 30 ^{o}C and the amount of reducing sugars released was analysed every day.

3.3.4.2 Spectrophotometric analysis of reducing sugars produced during saccharification

The reducing sugar level was followed by use of UV-Visible spectrophotometry Miller's dinitrosalicylic method (Gusakov *et al*., 2011). The process was monitored every 24 h for sugars released by *Millers* method of glucose estimation using standard calibration graph. Glucose (100 mg) in distilled water (100 mL) was prepared as the reducing sugar standard stock solution. Other concentrations 0.2, 0.4, 0.6, 0.8 and 1 mL in 10 mL of solution in distilled water were further prepared and used as the standard solutions for calibration. Similarly sample solutions were prepared by 2.5 g of sample in 1000 mL distilled water followed by filtration.

3.3.4.3 Fermentation of saccharised algae biomass

After 6 days of saccharification 10% of brewers' yeast (*Saccharomyces cerevisiae)* in distilled water was added to the fermentable sugars in distilled water which contained

150g of biomass/L. The mixture was allowed to ferment for 4 days at room temperature 30 ^{o}C.

3.3.4.4 Separation of algae bioethanol by fractional distillation

The bioethanol produced was then separated from the fermentation solution by fractional distillation method (Harwood *et al*., 1999) (Appendix XII). Ethanol boils at 78.4 °C while water boils at 100 °C. When the mixture was heated, ethanol which is the most volatile component concentrated to a greater degree in the vapor phase and left the liquid. The distillate formed an azeotrope, comprising of mainly 96 % bioethanol and 4 % water at 78.2 °C and the mixture is more volatile than pure ethanol. For this reason, ethanol was further purified by dehydration using anhydrous sodium sulphate.

3.3.4.5 Drying of bioethanol using anhydrous magnesium sulphate

Ethanol obtained was dried using 10 g of anhydrous magnesium sulphate drying agent for every 100 mL of bioethanol in a beaker. The magnesium sulphate crystals formed larger clumps when they absorbed water after standing for 15 minutes which were then removed by filtration to obtain dry bioethanol (Han *et al*., 2014).

3.4 Synthesis and Analysis

3.4.1 Synthesis and Analysis of Oxygenated and Hydrogenated Derivatives of *d*- Limonene

Extracted *d*-limonene from citrus (*C. sinensis*) peelings was hydrogenated to give a mixture of *d*-limonene derivatives (Mathers *et al*., 2006). Oxygenated derivatives of limonene were also catalytically synthesized concurrently (Beatriz, 2007, Andres *et al*., 2012).

Citrus oils contain 93-97 % limonene. The low percentage content of other terpenic compounds allowed synthetic reactions of *d*-limonene to be performed directly from

citrus oil. The amount of *d*-limonene was highest in orange peels oil coupled by the availability of oranges which allowed the use of orange peel oil in all the synthesis. Oils from lemon and tangerine peelings contain larger quantities of *l*-limonene (Dugo and Mondello, 2010).

Physicochemical and fuel properties were investigated using calorimetry, viscometry, flash point and cetane index using standard ASTM procedures and composition using GC-MC and FTIR.

3.4.1.1 Hydrogenation of d-limonene using palladium catalysts

A modified catalytic reactor (Figure 3.1) was set up to carry out hydrogenation of d-limonene (Beatriz *et al*., 2007, Milewska *et al*., 2005) (Appendix XIII). The reactor comprised of cuboid water bath vessel made of glass equipped with a mechanical stirring device to facilitate mass transfer between catalyst and the liquid reactant. Palladium catalyst (3.8 g) containing Pd/Al_2O_3 (5 % Pd) was used as cylindrical pellets placed in the stainless steel meshed basket (Grau *et al*., 1999). The Pd composition was confirmed by XRF using Bruker AXS spectrometer, model S8 TIGER with rhodium lamp. The catalyst sample was fused with lithium tetraborate for the formation of fused beads. Pure hydrogen gas was allowed to flow continuously in the reactor containing 50 mL of orange oil constituting mainly *d*-limonene. Heating was provided by a waterbath set at 50 ^oC, pressure 101.3 kPa and flow rate of the gas at 60 cm^3/min. The stirrer was set at 200 rpm for 60 minutes.

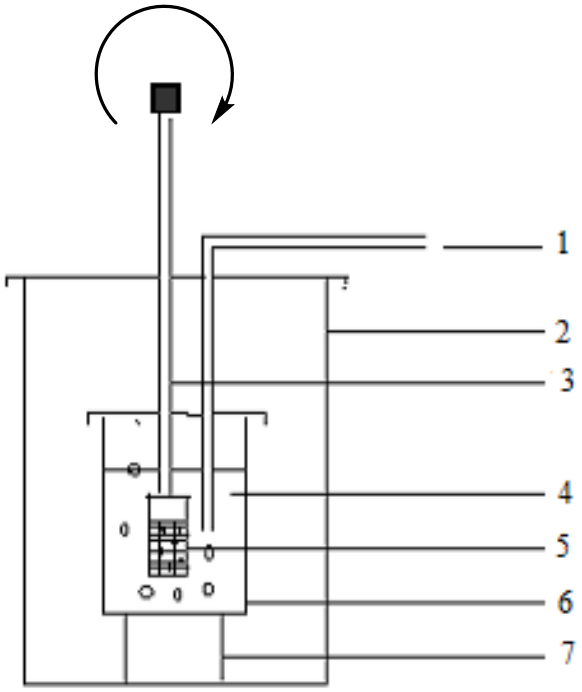

Figure 3.1: Catalytic reactor assembly

1. Gas supply inlet (molecular hydrogen or oxygen)
2. Thermostated waterbath with transparent windows
3. Electromechanical stirrer (wisemix homogeniser HG-15D)
4. d-limonenesample (orange oil)
5. Catalyst in stainless steel meshed basket
6. Glass sample container
7. Stainless steel stand

3.4.1.2 Catalytic Oxidation of *d*-limonene Using Oxygen

A modified catalytic reactor was set up (Figure 3.1) to carry out oxidation of *d*-limonene (Beatriz *et al.*, 2007). The reactor comprised of a vessel made of glass equipped with a electromechanical stirring device to facilitate mass transfer between hydrotalcite derived copper magnesium aluminium metal oxide system doped with Palladium as catalyst (4.74 % Pd) (3.8 g) and the liquid reactant orange oil (50 mL).

The palladium catalyst was used as cylindrical pellets placed in a stainless steel meshed basket. The Pd composition was confirmed by XRF using Bruker AXS spectrometer, model S8 TIGER with rhodium lamp. The catalyst sample was fused with lithium tetraborate for the formation of fused beads. Pure oxygen gas from a gas cylinder was allowed to flow continuously in the reactor through 50 mL of orange oil containing *d*-limonene. Heating was provided by a water bath set at 80 ^{o}C, pressure 101.3 kPa and flow rate of gas at 60 cm^3/min. The stirrer was set at 200 rpm for 60 minutes. The catalyst pellets were rinsed with acetone after each test to remove surface deposits.

3.4.1.3 Analysis of Orange Oil Containing *d*-limonene and Derivatives

The crude *Citrus sinensis* oil containing *d*-limonene, oxygenated and hydrogenated limonene products were analysed by GC-MS (Frizzo *et al.*, 2004) and FTIR (Mahamuni and Adewuyi, 2009; Moussa and Hamed, 2007) to ascertain composition.

3.4.1.3.1 GC-MS analysis

Analysis of the essentials oils and derivatives was performed using GC-MS a Finnigan GC 8000 series interfaced with a Voyager EI-MS mass selective detector and a Rtx-5 MS capillary column (20 m x 0.25 mm, film thickness 0.25 μm). For GC-MS detection, an electron ionization system with an ionization energy of 70 eV was used. Helium at a pressure of 25kpa was used as carrier gas. Injector and MS transfer line temperatures were set at 220 and 240 °C, respectively. Oven temperatures program was initial temperature of 60 ^{o}C held for 2 minutes then ramped at a rate of 15 ^{o}C to 240 ^{o}C which was maintained for 5 minutes. The scanning range was from 40-550 m/z. Database hits were retrieved by National Institute of Standards and Technology (NIST) materials and measurement library. Diluted samples (1/10 acetone, v/v) of 0.2 μL were injected automatically in the split mode (split ratio 1/44).

The components were identified by comparing their relative retention times and mass spectra (Appendix XIV) with those of standards for the main components, NIST library data of the GC-MS system, retention time and literature data. All the tests were performed in triplicates.

3.4.1.3.2 FTIR Analysis

The FTIR spectroscopy machine (Bruker alpha model) was warmed for 1 hour then a background spectrum of an empty liquid cell was run and saved with air as the blank. Each of the water free samples (2µL) was transferred with the use of a syringe pipette onto the two well-polished and acetone cleaned KBr disks, it was then spread creating a thin film and analyzed between a range of 400 cm^{-1} to 4000 cm^{-1}. A normal resolution of 16 cm^{-1} was used. Then each spectrum was printed out (Appendix XV).

3.4.1.3.3 Physicochemical and thermodynamic properties analysis

The crude products citrus oil containing *d*-limonene, oxygenated *d*-limonene, hydrogenated *d*-limonene and the oils extracted from *Rhizoclonium grande* and *Jatropha curcas* were analysed for physicochemical and thermodynamic properties using AOCS, AOAC and ASTM standard test methods which include: Density kg/dm^3 ASTM D1298 at 20^oC, Calorific Value (KJ/Kg) ASTM D4809, Kinematic Viscosity at 40^oC (cSt) ASTM D445, Flash point (^oC) ASTM D93, Cetane Index ASTM D4737, Pour Point (^oC) ASTM D97, Cold Filter Plugging Point (CFPP) (^oC) ASTM D6371/ IP 309 and Cloud Point (^oC) ASTM D2500 (ASTM, 2002b). Others were Refractive index, Acid value, Iodine value and Saponification value (AOAC, 2000).

3.4.2 Transesterification of Oil from Algae

Dry ethanol prepared from marine algae *Rhizoclonium grande* and *Citrus sinensis* biomass was used for transesterification (Svein, 2009). Dry potassium hydroxide was

reacted with the bioethanol in a ratio of 1: 10 respectively to produce the ethoxide ions mixture. The mixture was added to *R. grande* oil in a ratio of 3:10 bioethanol to oil preheated at 65 ^{o}C with constant stirring using a mechanical stirrer at 200 rpm for two hours to produce fatty acid ethyl ester biofuels. The ethyl esters were then separated from the glycerol by centrifugation using centrifuge Model Neofuge 15R at 10,000 rpm for 15 minutes followed by decantation, washing with distilled water in a separating funnel. The ethyl esters obtained were dried using 10 g of anhydrous magnesium sulphate drying agent for every 100 mL of the ethyl esters in a beaker (Han *et al*., 2014) followed by vacuum filtration.

3.4.3 Transesterification of Oil from *J. curcas L.* Seeds

Dry bioethanol prepared from marine algae *R. grande* and *C. sinensis* biomass was used for transesterification (Svein, 2009). Dry potassium hydroxide was reacted with the ethanol to produce the ethoxide ions mixture in a ratio of 1: 10. The mixture was added to *J. curcas* oil in a ratio of 3:10 bioethanol to oil preheated at 65 ^{o}C with constant stirring using a mechanical stirrer at 200 rpm for two hours to produce fatty acid ethyl ester biofuels. The ethyl esters were then separated from the glycerol by centrifugation using centrifuge Model Neofuge 15R at 10,000 rpm for 15 minutes followed by decantation, washing with distilled water (Appendix XVI). The ethyl esters obtained were dried using 10 g of anhydrous magnesium sulphate drying agent for every 100 mL of the ethyl esters in a beaker (Han *et al*., 2014) followed by vacuum filtration.

3.4.4 Analysis of Ethyl Esters from Algae and *J. curcas L* oils

The Ethyl Esters from algae and *J. curcas L.* were analysed by GC-MS analysis to ascertain composition. The components were identified by comparing their relative retention times and mass spectra (Appendix XVII). They were also analysed by FTIR

to confirm presence particular functional groups from the FTIR spectra (Appendix XVIII). The crude ethyl esters were then analysed for physicochemical and thermodynamic properties using ASTM standard test methods as per sections 3.4.1.3.1, 3. 4.1.3.2 and 3.4.1.3.3.

3.5 Blending and Analysis of the *Rhizoclonium grande* and *Jatropha curcas* Fatty Acid Ethyl Esters

Each of the fatty acid ethyl esters (FAEE) from *R. grande* and *J.curcas* was analysed for fuel properties separately before blending. Different proportions from 5, 10, 15, 20 and 25 % of FAEE from *R. grande* oil were blend with 95, 90, 85, 80 and 75 % of FAEE from *J. curcas* oil respectively. Again analysis of the JAB blends was carried out to determine the miscibility and fuel properties according to procedures based on ASTM D4682 and D6751.

3.6 Addition of *d*-limonene and Derivatives to the Fatty Acid Ethyl Ester Blends

d-Limonene, the oxygenated and hydrogenated *d*-limonene derivatives were each separately added to *J. curcas* and *R. grande* fatty acid ethyl ester blends (JAB) biofuel blends in small quantities of 2, 4, 6, 8 and 10 per cent to form JAB with limonene additives (JABLA) blend samples.

3.7 Evaluation of Thermochemical and Fuel Properties of JABLA

The analysis of the biofuels blends with multifunctional additives for thermochemical and fuel properties were done using standard procedures ASTM D6751-10 on all the JABLA proportions. Comparison of thermochemical and fuel properties of JABLA with JAB biodiesel, petroleum fuels and B-100 standard FAME was also carried out. The thermochemical and fuel properties of biofuel blends with additives from *d*-limonene multifunctional derivatives JABLA (2-10% additives) obtained were compared with those of biofuel blends without additives JAB (20% algae FAEE and

80% Jatropha FAEE) and petroleum fuels collected from five different vendors in Mombasa city and its environs.

3.7.1 Miscibility Test

3.7.1.1 Phase miscibility and stability of the blends of biodiesel (JAB) with limonene and limonene derivatives (JABLA)

The experiments on miscibility and phase stability were performed in two stages: Firstly, JAB blends with 5, 10, 15, 20 and 25 % v/v of algae FAEE with 95, 90, 85, 80 and 75 % v/v of Jatropha FAEE respectively, which were named as JAB5, JAB10, JAB15, JAB20 and JAB25. Secondly, 2, 4, 6,8 and 10 % v/v of limonene, hydrogenated limonene derivatives and oxygenated limonene derivatives as additives with 98, 96, 94, 92 and 90 % v/v of JAB20 respectively in each case which were named as JABLA2, JABLA4, JABLA6, JABLA8 and JABLA10. The fuels with the predetermined volume were mixed into a homogeneous mixture by a magnetic stirrer for five minutes. Then, the final blends were kept in a graduated measuring cylinder for observation of the solubility and phase stability. This was confirmed by ASTM D4682-87 standard method, FTIR and thermomechanical distillation method (Moussa and Hamed, 2007; Pages *et al*., 1996).

3.7.1.2 ASTM D4682-87 miscibility test procedures

The analysis of the biofuels blends with additives for miscibility according to ASTM D4682-87 test procedures was separately done on all the JAB (5, 10, 15, 20 and 25 % v/v of algae FAEE) and JABLA (2, 4, 6, 8 and 10 % v/v of limonene, hydrogenated limonene and oxygenated limonene additives) proportions (ASTM, 2002c).

3.7.1.3 Distillation test

A 100 mL of each sample was distilled in a laboratory batch autodistillation unit (Figure 3.2 and Appendix XIX A) at ambient pressure under conditions that are

designed to provide approximately one theoretical plate fractionation. Systematic observations of temperature readings and volumes of condensate were made and the observed temperatures were corrected for barometric pressure. The volumes of the residue and the losses were also recorded (ASTM, 2004). Test results were expressed as percentage evaporated versus corresponding temperature and presented as a plot of the distillation curve.

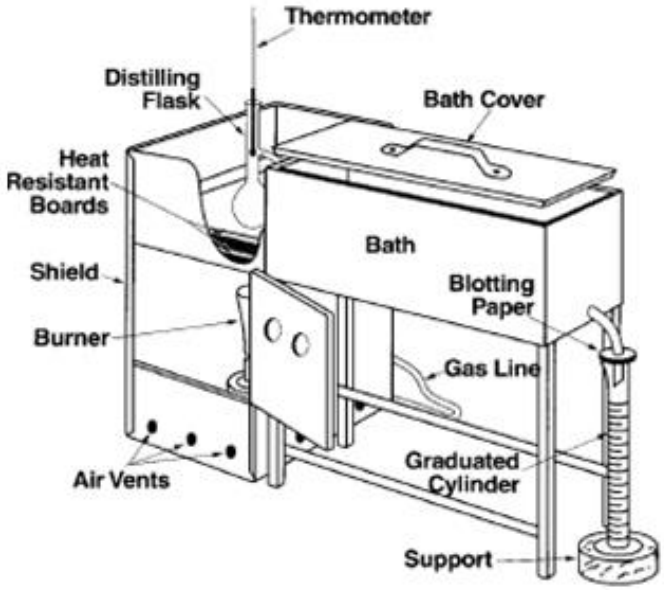

Figure 3.2: Distillation unit ASTM D 86

3.7.1.4 FTIR test method

FTIR spectrometry is a rapid and precise method for quantification of biofuel blends using the methodology specified by ASTM D7371. Infrared spectra of biodiesel blends exhibit nonlinear behavior (peak shifts) with respect to concentration, due to interactions between the mixture components. It is therefore impossible to have a single, simple linear model spanning the full range of possible blends. In ASTM D7371, this issue is addressed by the use of three separate chemometric partial-least-squares (PLS) model such as 0–10, 10–30, and 30–100% v/v FAEE. ASTM D7371

specifies an attenuated total reflectance (ATR) measurement on neat fuel blend and a chemometric partial-least-squares (PLS) model (ASTM, 2008).

A background spectrum of an empty liquid cell was run and saved. Each sample (2μL) was transferred with the use of a syringe on to the two well-polished KBr disks, it was then spread creating a thin film. A normal resolution of 16 cm^{-1} was used. The spectrum for each sample was printed out. The spectra were used to explain the interactions between mixture components.

3.7.2 Density Test Method

Density test method, ASTM D1298 (ASTM, 2006) was used in determination of densities using glass hydrometers. The 250 ml sample was brought to prescribed 25^{o}C temperature and transferred to a cylinder at approximately the same temperature. The appropriate hydrometer (600-1100 g/cm^3) was then lowered slowly into the sample and allowed to settle. At least 5 minutes were allowed for the hydrometer to come to rest, and for all air bubbles to come to the surface. After temperature equilibrium had been reached, the hydrometer scale was read and the temperature of each sample noted. The observed hydrometer reading was reduced to the reference temperature of 20^{o}C and 15^{o}C using the density table provided in the standard procedure.

3.7.3 Calorific Value

The gross calorific value using ASTM D4809 method was determined using bomb calorimeter model Gallenkamp autobomb (Figure 3.3). Approximately 0.8 g biofuel sample was weighed in a bomb crucible. The bomb cup was placed on its stand provided with the outfit. Firing nickel wire piece was stretched between the electrodes of the bomb (ASTM, 2013). A wicking cotton thread, 9 cm long was tied to the stretched wire and the end dipped inside the sample in the crucible. The crucible

then was placed on the support ring.

Exactly 1 mL of distilled water was pipetted out into the body of the bomb and then charged with gas upto a pressure of 3.0×10^6 N/m^2. Calorimeter can was filled with distilled water until a weight of 3 kg (water plus the can) was obtained to submerge the bomb completely. The bomb was placed on the supports in the calorimeter vessel and checked for leakage. Cooling water was adjusted to flow at rate of 300 mL per minute. Cover of the water jacket with thermometers and stirrer was lowered and circuit completeness tested by firing circuit test plug.

The temperature of the calorimeter vessel was allowed to stabilize and the initial temperature taken ±0.001°C, the fire switch was then pressed for 2 seconds to ignite the sample. The final temperature of the apparatus was taken after 10 minutes ±0.001°C. Readings were taken after sequential 3 minutes until the reading was found to be within a range of ±0.002°C. The final temperature was recorded. Rise in temperature was calculated as a difference from initial to final temperature reading. Each sample was tested three times and the average values of weight of sample and temperature rise taken for the final determination of total heat released from the sample. The gross heat released is calculated from equation 2.3.

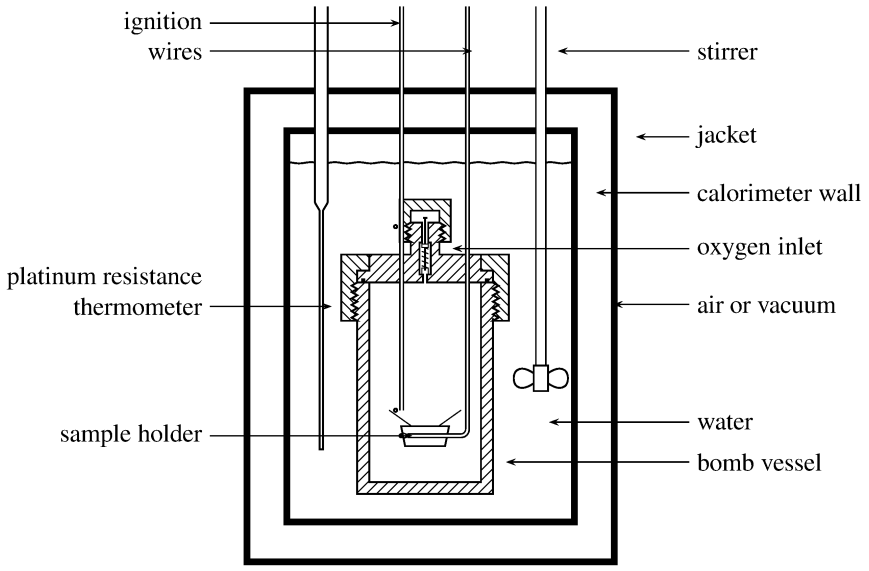

Figure 3.3: Bomb calorimeter

3.7.4 Kinematic Viscosity

Kinematic viscosity standard method ASTM D445 (ASTM, 2004) procedure was followed. Calibrated Ubbelohde type viscometer (Ubbelohde Viscometer series 1B No. H315) with a narrow capillary tube was selected for each fuel sample (Figure 3.4). The Ubbelohde viscometer is a U-shaped piece of glassware with a reservoir on one side and a measuring bulb with a capillary on the other. A liquid was introduced into the reservoir then sucked through the capillary and measuring bulb. The liquid was allowed to travel back through the measuring bulb and the time it took for the liquid to pass through two calibrated marks was taken as a measure for viscosity.

The third arm extending from the end of the capillary and open to the atmosphere allows the pressure head to depend only on a fixed height and no longer on the total volume of liquid. Viscometers holders were used to mount the calibrated glass capillary viscometer vertically in a water bath (Viscosity bath TXVB 40/150) maintained at 40°C. The viscometer was charged with the test sample to the mark and allowed to remain in the bath for 30 minutes to reach the test temperature.

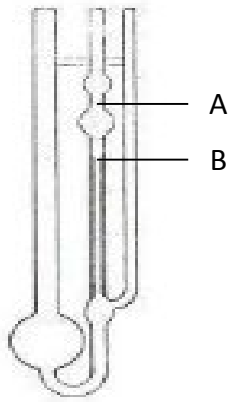

Figure 3.4 : Ubbelohde viscometer

The volume of the sample was adjusted to the mark after temperature equilibrium was reached. Pressure was applied to adjust the head level of the sample to a position in the capillary arm of the instrument about 7 mm above the first timing mark. With the sample flowing freely, the time required for the meniscus to pass from the first (A) to the second timing mark (B) was taken in seconds ±0.1. The procedure was repeated three times for each sample to make three measurements of flow time. The measurements were recorded and the average used in the calculation of the kinematic viscosity from the measured flow time and the viscometer constant using equation 2.1 .

3.7.5 Flash Point

The test method ASTM D93, using semi-automated Pensky-Martens closed-cup apparatus (HERZOG Gmmb) was followed (ASTM, 2007a). The 75 ml sample was filled to the mark inside of the test cup. Temperatures of the cup and test sample were set at 18 °C below the expected minimum flash point (100 °C for esters).

The cup was then covered and the assembly placed into the apparatus (Appendix XIX B). The locking device was properly engaged and the thermometer inserted into its holder. The test flame was lit, and adjusted to a diameter of 3.2-4.8 mm. Heat was applied and controlled to increase at a rate of 5-6 °C per minute. The stirring device was set at 100 rpm, stirring in a downward direction.

When the temperature of the test sample reached 23±5 °C below the expected flash point (100 °C), the ignition source was directed into the test cup at 5 minutes intervals with simultaneous interruption of the stirring until a flash was detected. The reading on the temperature measuring device at the time of flash detection was recorded as the observed flash point. Each fuel was tested three times and the average reported as the flash point of the test sample.

3.7.6 Cetane Index

The calculated cetane index was determined following ASTM D4737 (ASTM, 2004) procedures which incorporates density at 15 °C and distillation temperatures from ASTM D86 (ASTM, 2006). Four variables equation (equation 2.2) was used to estimate the cetane index of distillate fuels. Density of each fuel was determined at 15 °C as described in test method D1298, recovery temperatures of the fuel at 10%, 50%, and 90% was recorded as described in test method D86 (ASTM, 2006).

Calculated cetane index CCI was then calculated as a correlation in SI units between the density at 15 ^{o}C and 10 %, 5 0%, and 90 % recovery temperatures of the fuel using equation 2.2.

3.7.7 Pour Point

Pour point (PP) ASTM D97, (ASTM, 2005) measures the lowest temperature at which the 45 mL sample oil is observed to flow. The sample was poured into the test jar to the level mark and closed with the cork carrying the thermometer. The position of the cork and thermometer was adjusted so that the cork fitted tightly.

The thermometer and the test jar are coaxial, and the thermometer bulb is immersed so that the capillary is 3 mm below the surface of the sample (Figure 3.5). The test jar was transferred to a water bath maintained at 24°C and observations for pour point commenced.

The disk was placed in the bottom of the jacket and the gasket around the test jar, 25 mm from the bottom. The test jar was inserted in the jacket. After the sample had cooled to allow the formation of paraffin wax crystals, great care was taken not to disturb the mass of sample nor permit the thermometer to shift in the sample which may lead to low and erroneous results.

The appearance of the sample was examined when the temperature of the sample was 9°C above the expected pour point (estimated as a multiple of 3°C). At each test thermometer reading that is a multiple of 3°C below the starting temperature the test jar was removed from the jacket. To remove condensed moisture that limits visibility the surface was wiped with a clean cloth moistened in ethanol. The jar was tilted just enough to ascertain whether there is a movement of the sample in the test jar and immediately returned. Since most samples had not ceased to flow when temperature

reached +9°C, the test jar was transferred to the next lower temperature bath -18ºC in accordance with the standard method.

As soon as the sample in the jar stopped to flow when tilted, the jar was held in a horizontal position for 5 s, as noted by an accurate timing device and observed carefully. The observed reading of the test thermometer was recorded. 3°C were added to the temperature recorded and reported as the Pour Point, ASTM D 97(ASTM, 2005).

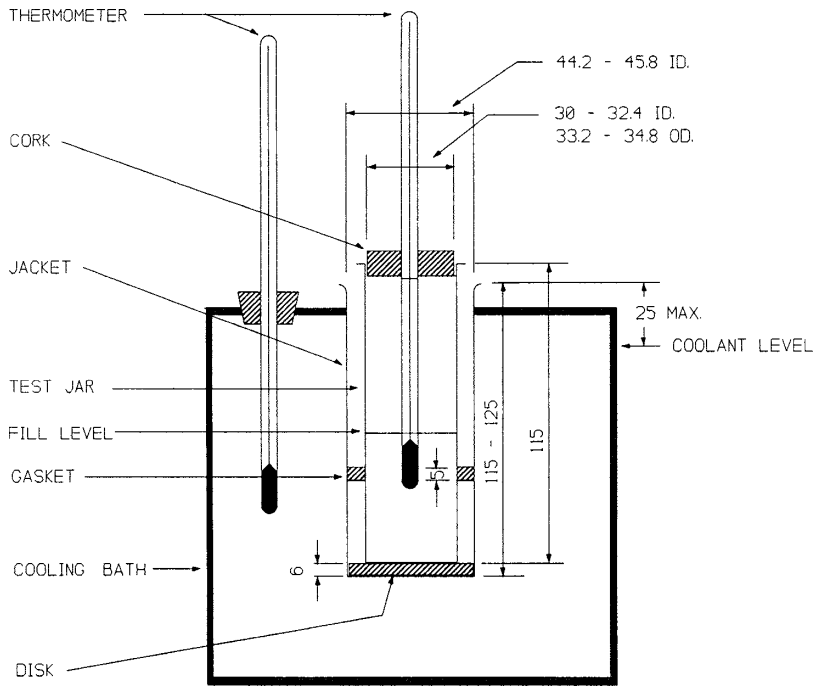

Figure 3.5: Apparatus for pour point test

3.7.8 Cold Filter Plugging Point

Cold Filter Plug Point (CFPP) ASTM D6371 test method is a procedure involving a vacuum to draw a 20 mL sample through a 45 micron screen within 60 s from a flat bottomed test jar 45 mL. The biofuel sample was cooled under specified conditions of cooling bath. At intervals of 1ºC, the sample was drawn into a pipet under a controlled vacuum through a standardized 45 micron screen.

The procedure was repeated, as the sample continued to cool, for each 1°C below the first test temperature. Testing was continued until the amount of wax crystals that separated out of solution was sufficient to stop or slow down the flow so that the time taken to fill the pipet exceeded 60 s or the fuel failed to return completely to the test jar before the fuel was cooled by a further 1°C. The lowest temperature at which the volume of biodiesel completely flowed under vacuum through the 45 micron screen within 60 s was recorded as cold filter plugging point CFPP.

3.7.9 Cloud Point (CP)

The cloud point (CP) ASTM D2500 method was used. The sample to be tested was brought to a temperature at least 14°C above the expected cloud point. Any moisture present was removed by filtration through dry lintless filter paper until the sample was perfectly clear. The sample was poured into the test jar to the level mark (45mL). The test jar was closed tightly by the cork carrying the test thermometer. The low cloud and pour thermometer was used since the expected cloud point is below −36°C. The position of the cork and the thermometer was adjusted so that the cork fitted tightly, the thermometer (with ice point 0±10°C) and the jar are coaxial, and the thermometer bulb resting on the bottom of the jar.

After confirming that the disk, gasket, and the inside of the jacket were clean and dry the disk was placed in the bottom of the jacket. The disk and jacket had been placed in the cooling medium 10 min before the test jar was inserted. The gasket around the test jar was placed, 25 mm from the bottom. the test jar was then inserted in the jacket (Appendix XIX C) care taken never to place the jar directly into the cooling medium. The temperature of the cooling bath was maintained at 0±1.5°C. At each test thermometer reading, the test jar was removed from the jacket quickly but without

disturbing the sample, inspected for cloud, and replaced in the jacket. The sample did not show a cloud when it had been cooled to 9°C, so the test jar was transferred to a jacket in a second bath maintained at a temperature of −18 ± 1.5°C (according to the standard) without transferring the jacket. When the sample showed signs of a cloud observed at the bottom of the test jar, which was confirmed by continued cooling the temperature was reported as cloud point, to the nearest 1°C (ASTM, 2002b).

3.7.10 Microbial analysis

3.7.10.1 Inoculation of the test isolates

Test strain of bacteria *Pseudomonas aeroginosa* (ATCC 25923) was separately inoculated in nutrient broth then incubated at 37 ^{o}C for 24 h aerobically in the Astra incubator. The nutrient broth turned turbid. *Candida albicans* (ATCC 70231) isolate were inoculated on Sabouroud dextrose agar at 25 ^{o}C for 48 h with growth observation done after every 24 h.

3.7.10.2 Agar disc diffusion tests

Fresh cultures of the test isolate were used for susceptibility test which was 24 h old culture for *Pseudomonas aeroginosa* and 48 h for *Candida albicans*. Mueller Hinton agar was prepared and dispensed on plate ready for inoculation with a uniform distribution by smear method of the micro-organisms (Varjani *et al*., 2013). Six (6) mm filter discs were prepared by using a paper punch to make small circular discs from filter paper, then they were wrapped in aluminum paper foil and sterilized at 121^{o}C in an autoclave model wiseclave. Permanent markers were used to mark the petri-dishes.

A dilute suspension of *P. aeroginosa* bacteria was prepared by suspending two microbial colonies in 2 mL of nutrient broth and inoculated on test plates by use of sterile swab and allowed to dry for five minutes. Then the sterile filter paper discs

were inoculated with the three JABLA samples gently placed and pressed against the agar surface to ensure good contact with media. Incubation of the plate was done for 24 h. Antibacterial activity of the limonene and derivatives were determined by measuring the diameter of the inhibition zones. For *Candida albicans* the test was run on Mueller Hinton agar and incubated aerobically for 48 h.

Negative control was set by inoculating filter disk with JAB. The antimicrobial assay for each of the test samples against all microorganisms tested was performed in triplicates. Quality control was performed by incubating a blank media.

3.8 Statistical Analysis

Each experiment was conducted as a completely randomized design with three treatments. Exploratory data analysis and standard statistical analyses were done using the statistical software package STATA, version SE 13 (STATA/SE13 © 1985-2013 StataCorp LP). The General Linear Models (GLM) procedure was used to analyze the effect of the experimental synthesised derivatives of limonene on fuel properties of ethyl ester blends obtained from jatropha and algae oils. When the means of the GLM were statistically different, these means were further compared between the control and the experimental groups using pairwise comparisons, t-tests and ANOVA. Significance was based on $P < 0.05$. The data was presented as means and standard deviation (SD). This statistical design was put forward to allow for unequivocal hypothesis testing. Data obtained was analysed statistically, graphs and curve fittings given to demonstrate the relationship. Experimental data interpretations were done and additional experiments proposed for further understanding and interpretation where necessary.

CHAPTER FOUR

4 RESULTS AND DISCUSSION

4.1 General Overview

The present study investigated physicochemical and fuel properties of biofuel blends prepared from *J. curcas* and algae oils with d-limonene [(R)-1-methyl-4-(1-methylethenyl) cyclohexene] and its oxygenated and hydrogenated derivatives as additives. Data collected and analysis undertaken was under the following:

i. Preparation, purification and characterisation of bioethanol from algae and citrus peelings biomass;
ii. Synthesis of oxygenated and hydrogenated derivatives of d-limonene extracted from citrus peelings followed by determination of their physicochemical properties;
iii. Transesterification and blending of *J. curcas* and algae oils with the bioethanol from biomass and evaluation of their fuel properties and miscibility;
iv. Addition of *d*-limonene and its oxygenated and hydrogenated derivatives to the fatty acid ethyl ester blends and evaluation of the physicochemical and fuel properties in comparison to petroleum fuels and standard B100 FAME.

The research findings and discussions are presented as follows:

4.2 Bioethanol from Citrus Peelings and Algae Biomass

4.2.1 Mass of Citrus Peelings from Different Citrus Fruits

The peels, after removing pectin by scrapping out using a knive, from each *Citrus sinensis* fruit samples were weighed in triplicate and percentage peelings per fruit calculated. Each sample data comprised mean ± SD (Appendix XX). The results were

further summarised and presented as mean ± SD per sampling site (growing areas) as shown in Table 4.1 and Figure 4.1

Malindi recorded the heaviest oranges and peelings with a mean 210.318±26.590 g and 26.821±2.969 g respectively per fruit. Muhenza recorded the lightest with a mean of 199.619±19.403 g and 26.285±3.471 g respectively per fruit (Table 4.1).

Table 4.1: % Peelings from *Citrus sinensis* Obtained from Kongowea Market

Sample Site	Mass of Whole Fruit (Grams±SD)	Mass of Peelings Per fruit (Grams±SD)	% Peelings per fruit (mean ± SD)
Malindi	210.318±26.590	26.821±2.969	12.811±1.004
Muheza	199.619±19.403	26.285±3.471	13.152±0.923
Shimba hills	206.415±19.721	27.062±2.957	13.109±0.698

The highest percentage of orange peelings per fruit was observed in Muhenza followed by Shimba hills. Malindi recorded the largest variation in amount of orange peelings (Figure 4.1).

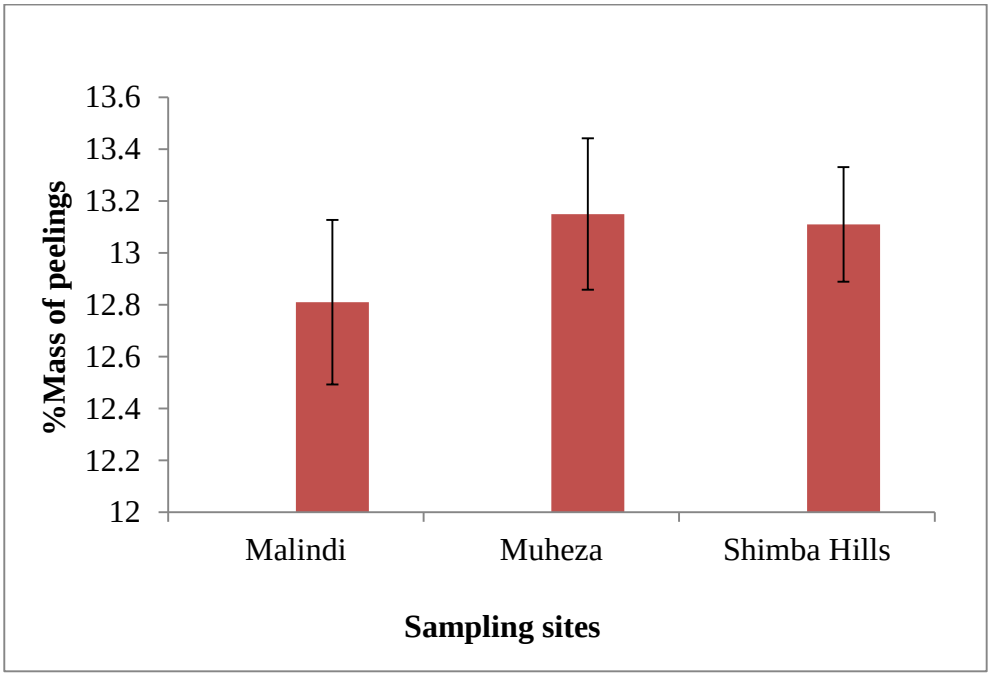

Figure 4.1: Percentage Orange peelings per fruit

Malindi recorded the heaviest lemons and peelings with a mean 171.472±18.539g and 60.886±10.961g (35.330±3.189 %) respectively per fruit. Muheza recorded the lightest with a mean of 160.416±6.419g and 56.178±5.835 (34.951±2.535%) respectively per fruit (Table 4.2).

Table 4.2: % Peelings from *Citrus limoni* Obtained from Kongowea Market

Sample Site	Mass of Whole Fruit (Grams±SD)	Mass of Peelings Per fruit (Grams±SD)	% Peelings per fruit (mean ± SD)
Malindi	171.472±18.539	60.886±10.961	35.330±3.189
Muheza	160.416±6.419	56.178±5.835	34.951±2.535
Shimba hills	170.107±18.073	59.800±9.939	35.040±3.102

The highest percentage of lemon peelings per fruit was observed in Malindi followed by Shimba hills. Malindi recorded the largest variation in amount of lemon peelings (Figure 4.2).

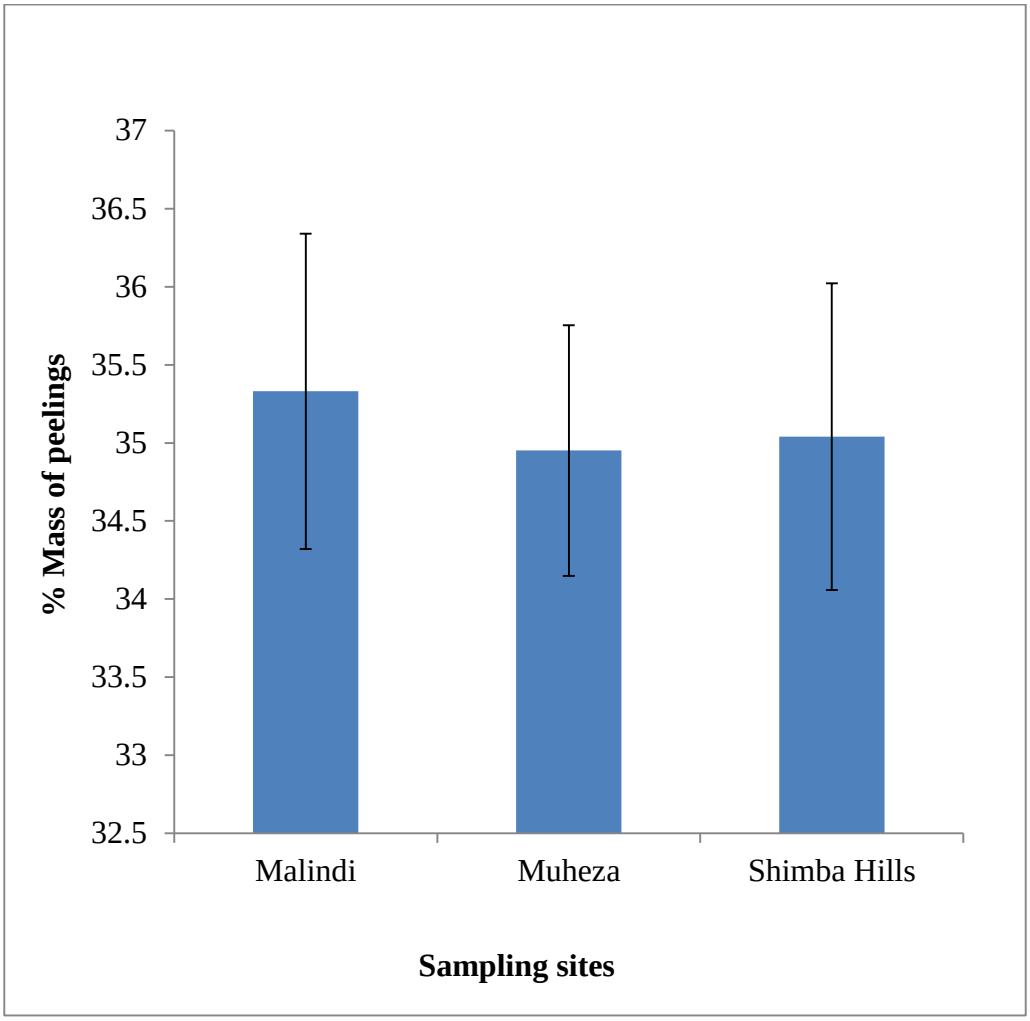

Figure 4.2: Percentage Lemon Peelings Per Fruit

Muheza recorded the heaviest tangerines and peelings with a mean 89.753±11.382 g and 20.851±3.393 g (23.174±1.670 %) respectively per fruit. Shimba Hills recorded the lightest tangerine fruits with a mean of 72.199±8.472 g and Malindi the lightest % peelings 18.872±3.107 g (21.606±1.542 %) per fruit (Table 4.3).

Table 4.3: % Peelings from *Citrus tangerina* Obtained from Kongowea Market

Sample Site	Mass of Whole Fruit (Grams±SD)	Mass of Peelings Per fruit (Grams±SD)	% Peelings per fruit (mean ± SD)
Malindi	87.035±10.551	18.872±3.107	21.606±1.542
Muheza	89.753±11.382	20.851±3.393	23.174±1.670
Shimba hills	72.199±8.472	16.743±3.776	22.970±2.915

The highest percentage of tangerine peelings per fruit was observed in Muheza followed by Shimba hills. Shimba Hills recorded the largest variation in amount of tangerine peelings (Figure 4.3).

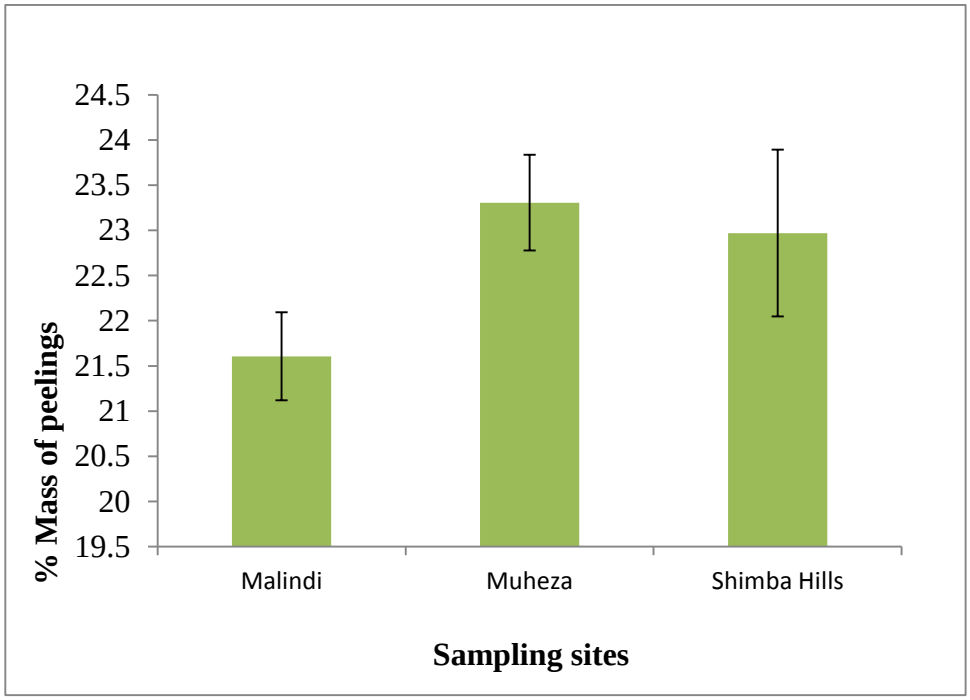

Figure 4.3: Percentage Tangerine Peelings per Fruit

Various citrus fruits are known to have % peelings ranging from 21.5 – 45 %. Lemon peelings have the highest and oranges the lowest percentages of peelings (Ahmad *et al*., 2006). The difference could be attributed to the variation in climate, adaptations of particular variety to the climate and soil conditions causing variation in ratio of flavedo and albedo (Ahmad *et al*., 2016).

4.2.2 Citrus Oil Yields from Selected Citrus Fruits Peelings

4.2.2.1 Citrus Oil Yields from Selected Citrus Fruits Peelings using Hexane

Table 4.4 shows mass of orange oil (Appendix XXI) extracted from peelings using hexane from different sampling sites**.** The % w/w of orange oil per gram of Peelings (%±SD) using hexane was highest in Malindi (6.683±1.499) and lowest in Muheza (5.748±0.719) (Table 4.4).

Table 4.4: Mass of orange oil extracted from the citrus peelings using hexane

No. of Samples	Sample Site/Source	Mass of Peelings per fruit (Grams±SD)	Mass of Orange Oil Extracted (Grams±SD)	% w/w of Orange Oil Per Gram of Peelings (%±SD)
30	Malindi	26.821±2.969	1.781±0.359	6.683±1.499
30	Muheza	26.285±3.471	1.502±0.208	5.748±0.719
30	Shimba hills	27.062±2.957	1.604±0.202	5.969±0.866

The highest percentage of orange oil per gram of peelings using hexane was observed in Malindi followed by Shimba hills. Malindi also recorded the largest variation in amount of orange oil while Muheza the lowest variation (figure 4.4). The values compare well with those obtained by Vashist *et al*. (2014) through hydrodistillation of *citrus sinensis* peelings where 3.3% w/w or 4.3% v/w was obtained (Vashist *et al.*, 2014). The higher yield can be attributed to the fact that both the citrus oil and hexane are organic so the solvent is expected to extract more of the oil.

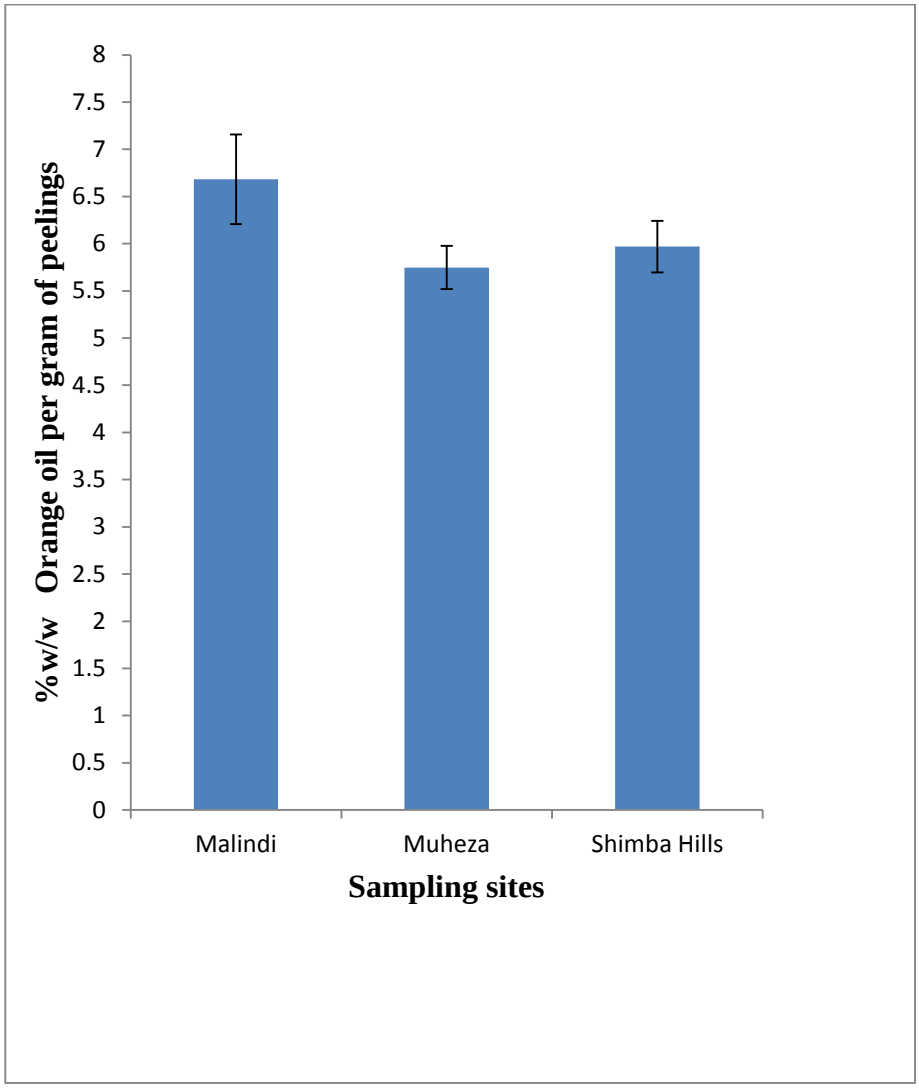

Figure 4.4: Percentage (% w/w) orange oil per gram of peelings using hexane

From table 4.5 the % w/w of lemon Oil Per Gram of Peelings (% ± SD) using hexane was highest in Malindi (3.281 ± 1.127) and lowest in Muheza (2.944 ± 0.321).

Table 4.5: Mass of lemon oil extracted from the citrus peelings using hexane

No. of Samples	Sample Site/Source	Mass of PeelingsPer fruit (Grams±SD)	Mass of Lemon Oil Extracted (Grams±SD)	% w/w of Lemon Oil Per Gram of Peelings (%±SD)
30	Malindi	60.886±10.961	1.876±0.313	3.281±1.127
30	Muheza	56.178±5.835	1.628±0.303	2.944±0.321
30	Shimba hills	59.800±9.939	1.840±0.243	3.122±0.529

The highest percentage of lemon oil per gram of peelings using hexane was observed in Malindi followed by Shimba hills. Malindi also recorded the largest variation in amount of lemon oil while Muheza the lowest variation (Figure 4.5). The values compare well with those obtained by Vashist *et al* 2014 through hydrodistillation of *Citrus lemon* peelings who obtained 2.3% w/w or 3% v/w (Vashist *et al.*, 2014). The higher yield can be attributed to the fact that the citrus oil is organic so hexane an organic solvent is expected to extract more of the oil.

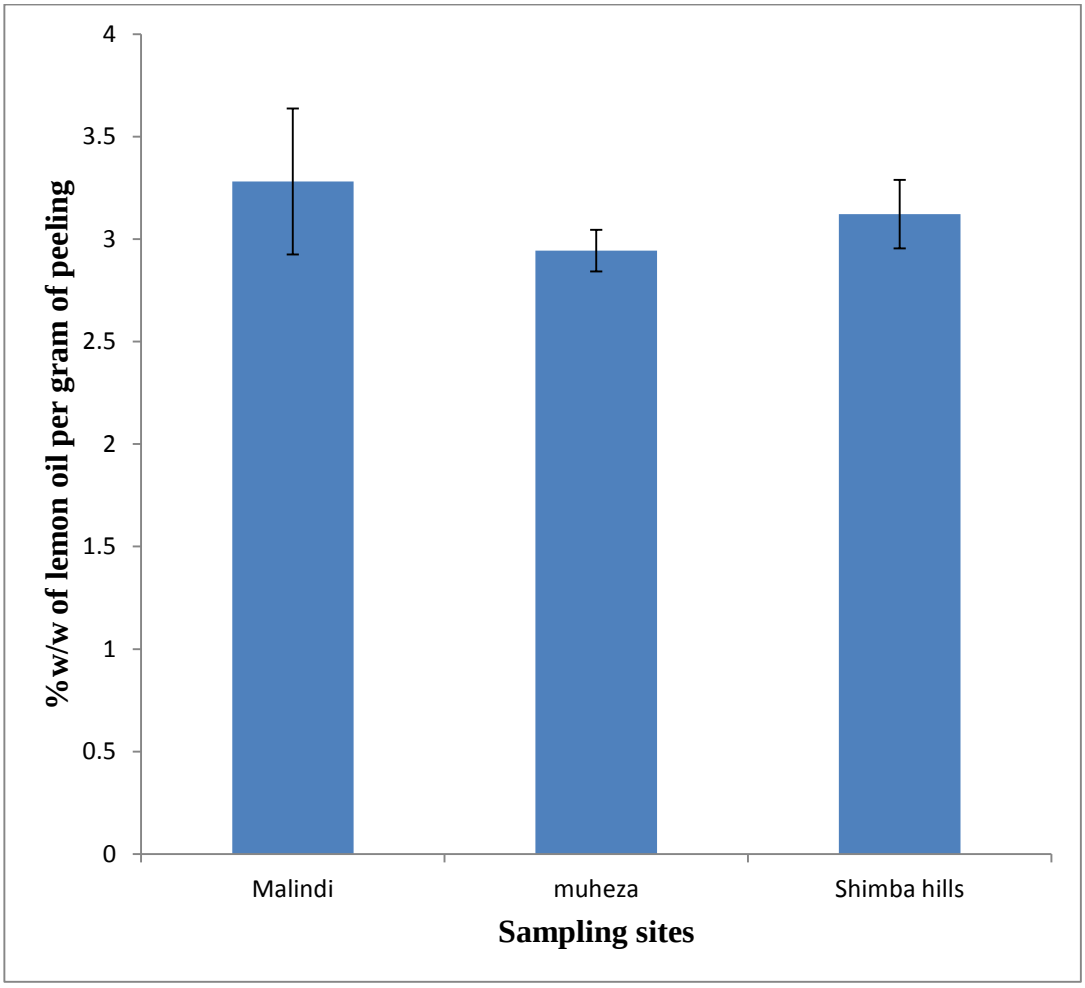

Figure 4.5: Percentage (% w/w) Lemon oil per gram of peelings using hexane

From Table 4.6 the % w/w of tangerine oil per gram of peelings (% ± SD) using hexane was highest in Shimba Hills (4.500 ± 0.465) and lowest in Muheza (3.914 ± 0.760).

Table 4.6: Mass of tangerine oil extracted from the citrus peelings using hexane

No. of Samples	Sample Site/Source	Mass of PeelingsPer fruit (Grams±SD)	Mass of Tangerine Oil Extracted (Grams±SD)	% w/w of Tangerine Oil Per Gram of Peelings (%±SD)
30	Malindi	18.872±3.107	0.831±0.242	4.432±1.284
30	Muheza	20.851±3.393	0.801±0.089	3.914±0.760
30	Shimba hills	16.743±3.776	0.742±0.122	4.500±0.465

The highest percentage of tangerine oil per gram of peelings using hexane was observed in Shimba hills. Malindi recorded the largest variation in amount of tangerine oil while Shimba Hills the lowest variation (Figure 4.6). These values are higher than those obtained using cold expression by Ahmad *et al*. (2006) yielding 0.2 to 2.0%. The difference could be attributed to loss of oil in the biomass during extraction by cold pressing.

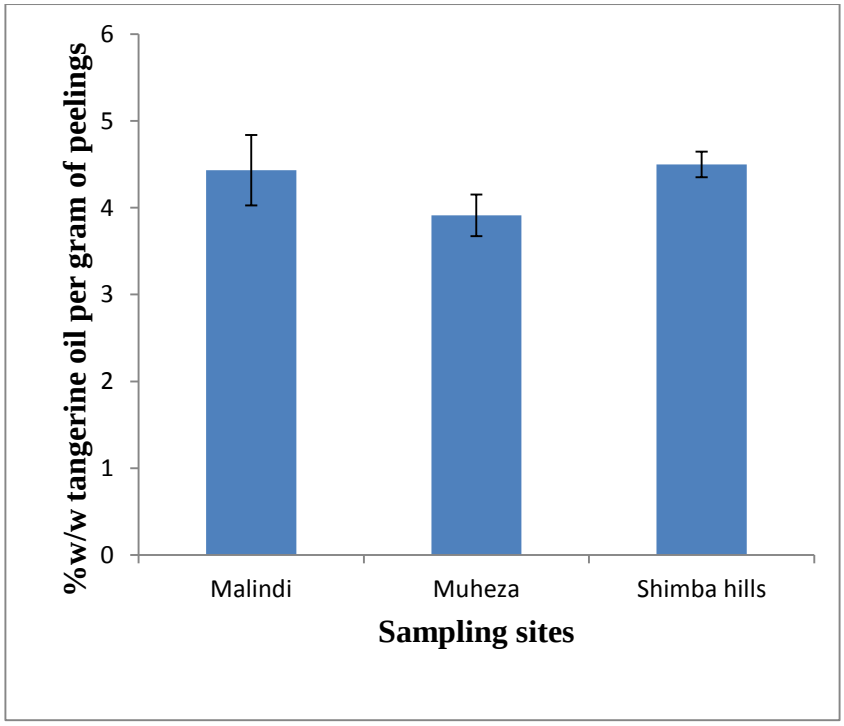

Figure 4.6: Percentage (%w/w) Tangerine oil per gram of peelings using hexane

4.2.2.2 Yields of citrus oil containing d-limonene from orange peelings using liquid and Sc CO2

Table 4.7 below shows the amount of oil extracted using liquid and Sc CO_2 using modified method by Mckenzi *et al*. (2004). From the Table 4.7 the first batch of solvent extracts most of the orange oil (0.405 ± 0.003 mL) and the third batch the least (0.105±0.003). The total amount of 3.56% per gram of orange peelings is low compared to that from hexane extraction of 6.683 ± 1.499% in Table 4.4.

Table 4.7: *d*-Limonene extraction from orange peelings using liquid and Sc CO_2

No. of extractions Solvent portion 50g	Orange peelings (g)	Volume of oil (ml)	%v/w of oil from orange peelings
1^{ST}	20	0.405±0.003	2.03±0.015
2^{ND}	20	0.202±0.002	1.01±0.010
3^{RD}	20	0.105±0.003	0.53±0.015
Total	20	0.712±0.003	3.56±0.015

According to Mckenzi *et al.* (2004) 0.75g of orange peels produces about 0.1ml of orange oil (13%v/w). This yield was hard to reach due to the difficulty experienced in obtaining liquid CO_2.

4.2.3 Macro Algae Distribution in the Sampling Sites and Lipid Distribution

Ten macroscopic and filamentous marine algae species collected from the different sampling sites and their lipid distribution which was determined by the sudan IV dye are recorded in Table 4.8. The species with the largest number of globules per field, was chosen for lipid extraction and algae biomass.

Blue green algae (*Trichodesmium* sp.) and *Galaxaura subvertillata* showed negligible lipid content while (*Rhizoclonium grande)*, showed the highest number of lipid globules per gram view ranging from 6000 to 9000 from Shelly beach and Jamvi la

Wageni respectively and was chosen for lipid extraction. The same method was used by Umarah *et al*., (2011) that showed two algae species *Pithophora* sp. (Chlorophyte) and *Botrydiopsis arhiza* Borzi (Xanthophyte) contained more lipids than the rest of the samples.

Table 4.8: Macro algae distribution in the sampling sites and lipid distribution

Sampling site	No. of macro algae species	Scientific names of macro algae	No. of lipid globules in 0.002g sample (mean ±SD)	No. of lipid globules per gram view (mean)
English point	3	*Chaetomorpha viellardi*	4 ±1.0	2000
		Ulva pertusa	10±1.5	5000
		(*Trichodesmium* sp.) Blue green	negligible	negligible
Tudor Creek	3	*Enteromorpha muscoides*	8±1.0	4000
		Rhizoclonium grande	16±1.0	8000
		Rhizoclonium viparium	5± 1.5	2500
Shimoni shores	3	*Rhizoclonium grande*	17± 2.0	8500
		Ulva pertusa	11±1.0	5500
		Ulva reticulata	6±1.0	3000
Shelly beach	4	*Ulva reticulata*	7±1.5	3500
		Rhizoclonium grande	12±1.0	6000
		Galaxaura subvertillata	negligible	negligible
		(*Trichodesmium* sp.) Blue green	negligible	negligible
Jamvi la Wageni	3	*Rhizoclonium grande*	18±1.5	9000
		Rhizoclonium africanum	12±1.0	6000
		Enteromorpha kylinii	7±0.0	3500

Plate 4.1 shows the lipid globules of *Rhizoclonium grande* taking up sudan IV dye (reddish brown) as seen under a light microscope during lipid detection of the algae species.

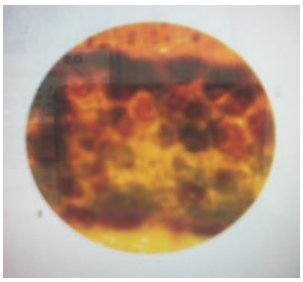

Plate 4.1: *Rhizoclonium grande* lipid globules showing Sudan IV dye stain

4.2.4 Yield of Algae oil Extracted from *Rhizoclonium grande*

Table 4.9 shows the volume of algae oil extracted using hexane from four sampling sites, Tudor Creek, Shimoni shores, Shell beach and Jamvi la wageni.

Table 4.9: Volume of algae oil extracted using hexane

Sample site	Algae biomass (g)	Vol. of hexane (ml)	Vol. of algae oil (ml)	yield %v/w
Tudor creek	350	700	28.9±0.395	8.26±0.114
Shimoni shores	350	700	30.36±0.319	8.68±0.084
Shelly beach	350	700	23.5±0.481	6.72±0.130
Jamvi la wageni	350	700	36.61±1.276	10.46±0.365

From Table 4.9 Jamvi la Wageni recorded the highest yield of algae oil 36.61 ± 1.276 mL (10.46±0.365 % v/w) and Shelly beach recorded the lowest 23.5±0.481mL (6.72 ± 0.130 % v/w). The higher oil yield of *R. grande* from Jamvi la Wageni sampling site can be attributed to the low depth of the ocean water and higher nutrients from the sediments in the area. The yields are comparable to those obtained from other filamentous algae such as *Rhizoclonium sp.* and *Cladophora sp.* from waste water where 3 – 11.5% of dry weight was extracted using hexane (Grayburn *et al*., 2013).

4.2.5 Reducing sugars and bioethanol from *Rhizoclonium grande* algae and *Citrus sinensis* Biomass after oil extraction

Table 4.10 shows the spectrophotometric analysis data of the reducing sugar obtained by dinitrosalicylic acid (DNS) method (Qui, 2008; Svein, 2009) during saccharification of orange and algae biomass left after oil extractions.

Table 4.10: Spectrophotometric analysis data of reducing sugars produced during saccharification of orange and algae biomass

Day	Absorbance of 2.5g/l biomass		Concentration of reducing sugars (mg/l) from 2.5g/l biomass		Amount of reducing sugars per 100gram biomass		% conversion to reducing sugars	
	Algae	orange	Algae	orange	Algae	orange	Algae	orange
0	0.284	0.394	720.25 ±0.19	1442.35 ±0.26	28.81	57.69	-	-
1	0.402	0.512	1174.54 ±0.28	1934.45 ±0.24	46.96	77.36	18.17	19.68
2	0.403	0.513	1176.23 ±0.22	1935.20 ±0.23	47.04	77.40	18.24	19.71
3	0.406	0.528	1178.04 ±0.21	1936.21 ±0.27	47.12	77.44	18.31	19.75
4	0.406	0.527	1178.38 ±0.29	1936.78 ±0.25	47.13	77.47	18.33	19.78
5	0.409	0.526	1195.03 ±0.19	1937.58 ±0.24	47.80	77.50	18.99	19.81
6	0.409	0.527	1195.58 ±0.26	1937.62 ±0.23	47.82	77.50	19.01	19.81

Aspergillus niger is cellulolytic and amylolytic in nature as it produces cellulases and amylases. These enzymes hydrolyze the cellulose and starch present in the biomass and release free sugars (Slidevi *et al*., 2008; Shihui *et al*., 2016). From Table 4.10 after 6 days the amount of reducing sugar present was higher in orange biomass (77.50 g/100 g) than in algae biomass(47.82 g/100 g). Generally the conversion level (19.01%) for algae biomass is similar to that reported for spirogyra biomass a similar filamentous green algae. The amount of carbohydrates in some algae can be 40-60% (Devedra and Rakesh, 2013).

After fermentation for four days, separation and drying processes (Appendix IX), the yields of the bioethanol produced are as shown in Table 4.11.

Table 4.11: Amount of bioethanol produced after fermentation

Sample	Biomass (g)	Bioethanol (ml)	% v/w yield of bioethanol
Algae - Jamvi	150	7.50	5.00
Algae - Tudor	150	8.10	5.40
Algae - Shelly	150	8.75	5.83
Algae - Shimoni	150	7.80	5.20
Mean ± SD		8.04±0.534	5.36±0.355
Orange - Malindi	150	12.00	8.00
Orange - Muheza	150	15.50	10.33
Orange – Shimba	150	14.00	9.33
Mean ± SD		14.13±1.548	9.42±1.031

From Table 4.11 Shelly beach algae recorded the highest bioethanol production 5.83 % and Jamvi la Wageni the lowest 5.00 %. For orange biomass Muheza recorded the highest bioethanol 10.33 % and Malindi the lowest 8.00 %.The mean bioethanol recorded for orange biomass (9.42±1.031 %) was more than for algae biomass (5.36±0.355 %). Devedra and Rackesh (2013) recorded 6 g/100 g biomass from algae biomass. The difference may be attributed to the higher reducing sugar level and higher conversion rate in orange biomass than in algae.

4.2.6 GC-MS spectra of bioethanol produced from *Rhizoclonium grande* algae and *Citrus senensis* peelings biomass

Bioethanol from fermentation of *Rhizoclonium grande* algae and *Citrus senensis* peelings biomass produced different GC-MS spectra.

4.2.6.1 GC-MS spectra of bioethanol produced from *Rhizoclonium grande*

Figure 4.7 shows the GC-MS spectrum of bioethanol obtained from *R. grande* biomass.

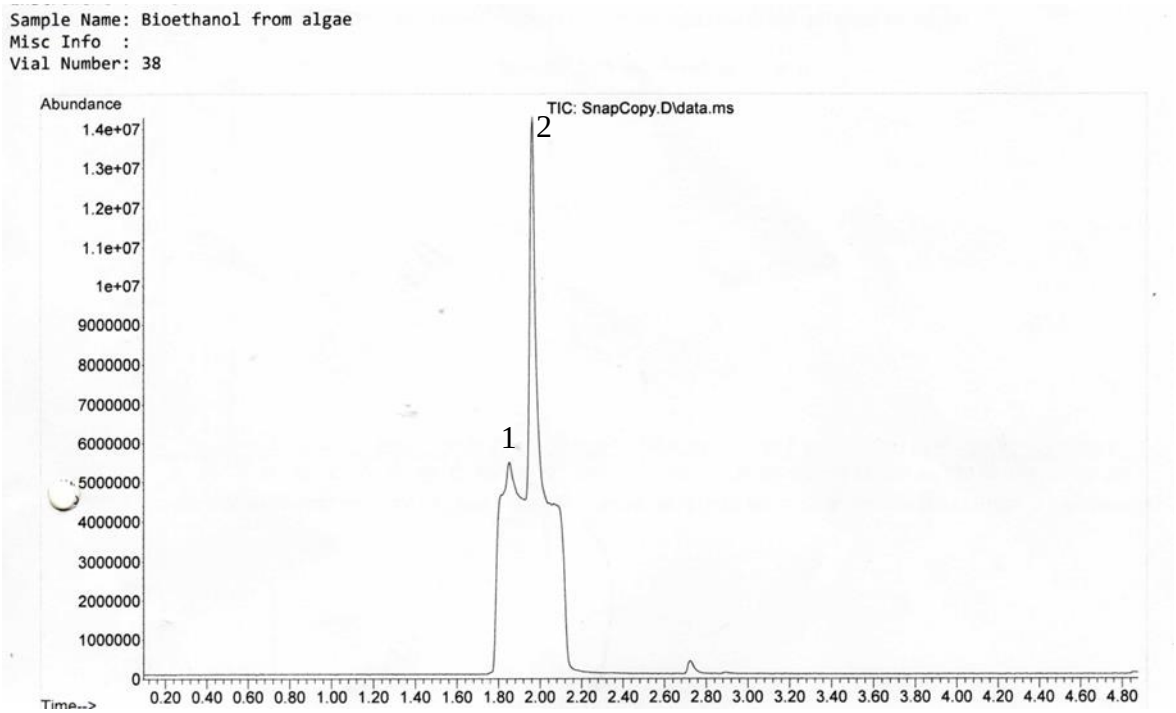

Figure 4.7: GC-MS Spectra for Bioethanol from *Rhizoclonium Grande* Biomass

It can be depicted that the main component in the mixture after drying is (2) ethanol (71.42 %), also present in low quantities is (1) methanol (25 %) and others (3.58 %). The composition was obtained from peak areas. The small quantities of other alcohols apart from ethanol can be attributed to presence of enzymes during sacharification that catalyse the formation of the same in the biomass.

4.2.6.2 GC-MS spectra of bioethanol produced from *Citrus senensis*

Figure 4.8 shows the GC-MS spectrum of bioethanol obtained from *Citrus senensis* peelings biomass.

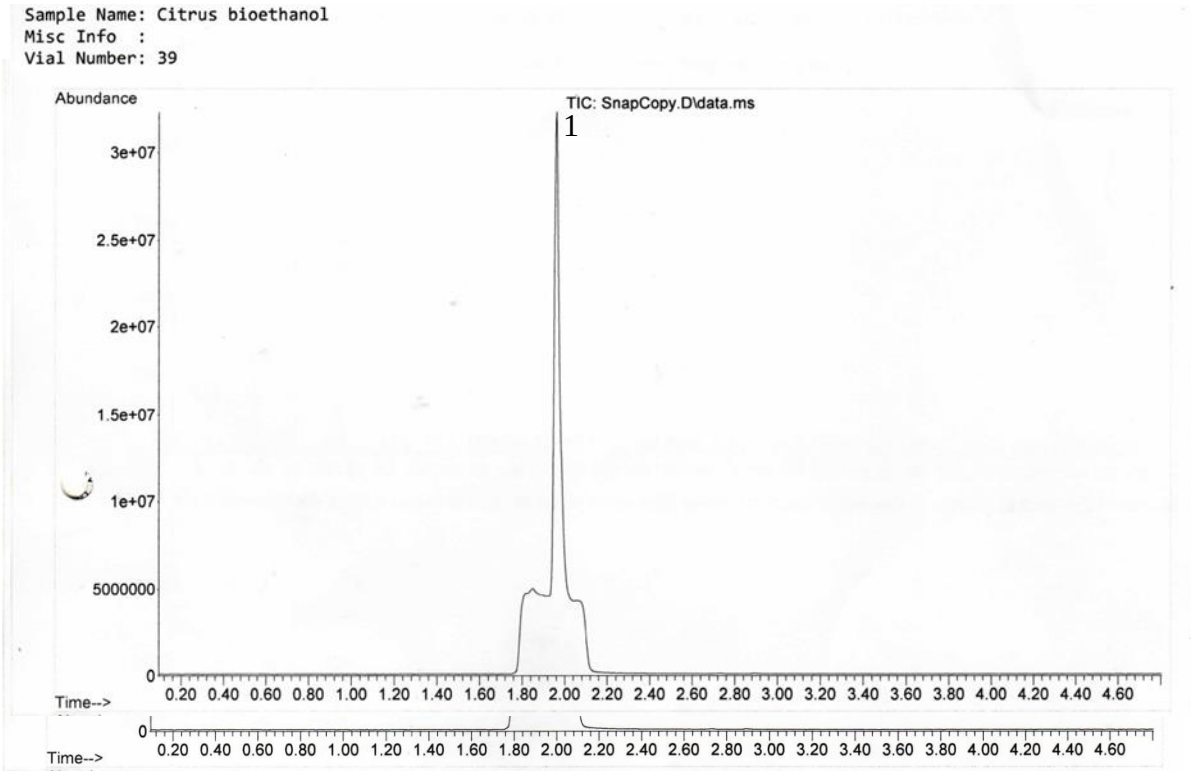

Figure 4.8: GC-MS Spectra for Bioethanol from *Citrus senensis* Biomass

The main alcohol present is (1) ethanol (88.23 %) and others (11.77 %). The peak enhancement may be attributed to presence of other alcohols such as methanol though in lower concentrations than those from *R. grande*.

4.3 *d*-Limonene from *Citrus senensis* Oil, Synthesis Products and their Physicochemical Properties

Synthesis products, oxygenated and hydrogenated derivatives from *d*-limonene in the oil extracted from *Citrus senensis* and physicochemical analysis results are presented in this section.

4.3.1 GC-MS spectra of *Citrus senensis* oil

Figure 4.9 shows GC-MS spectra of *C. senensis* oil blend from Malindi, Shimba and Muheza. sampling regions.

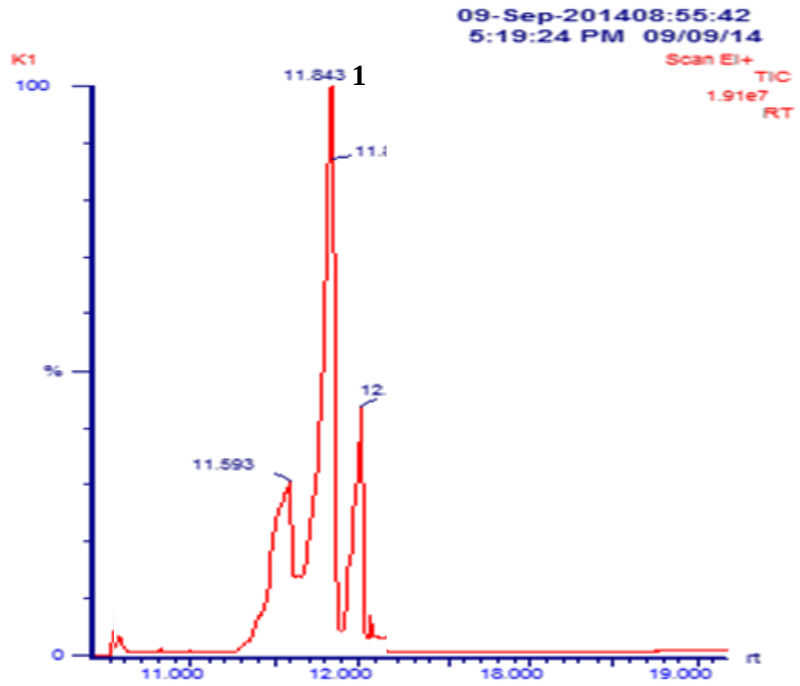

Figure 4.9: GC-MS spectrum of orange (*Citrus sinensis* L.*)* oil

From Figure 4.9 the crude *C. senensis* oil contain a variety of compounds as shown by various peaks. The main compound (1) with a retention time Rt = 11.843 is *d*-limonene m/z 41, 55, 69, 81, 95, 107, 135 (Appendix XIV A). The other peaks are relatively showing lower concentrations of components in the orange oil. The orange oil contain mainly *d*-limonene. *C. lemon* and *C. tangerina* contain *d*-limonene however they also contain *l*-limonene in considerable amounts.

4.3.2 FTIR spectra of *Citrus sinensis* L oil

Figure 4.9 shows spectral peaks of *C.senensis* peel oil blend from Malindi, Shimba Hills and Muheza sampling regions.

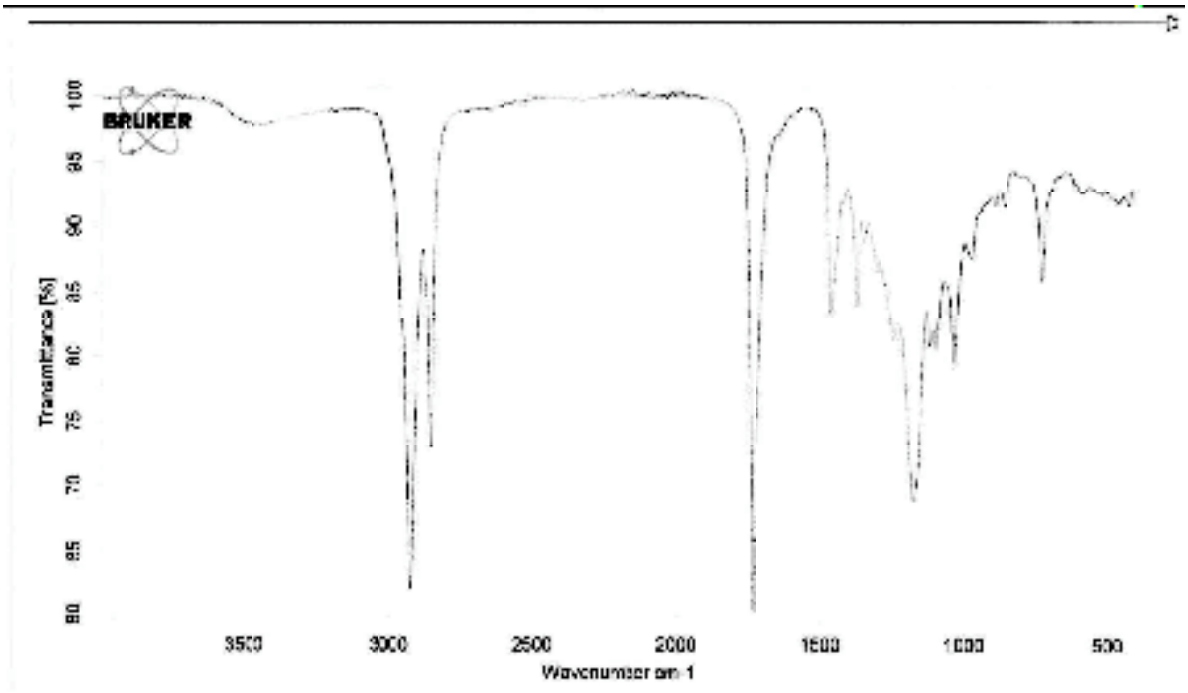

Figure 4.10: FTIR Spectra of Orange (*Citrus sinensis* L*)* Oil

From figure 4.10 the functional groups of the crude *C. senensis* peel oil components were identified as CH_3, CH_2, C-H, CH_3C-H, =C-H and =CH_2 others were C-OH, =C-O- C, C-O, C=O and H-C=O. These functional groups were identified according to the absorption frequency of the infra red waves in wave number cm^{-1}. The absorption frequencies are a characteristic of each of the functional groups as shown in Table 4.12.

Table 4.12: Functional groups and mode of vibration from FTIR spectra of *Citrus senensis* peel oil

S. NO.	Peak(s) position on FTIR spectra (cm^{-1})	Class of Compounds	Functional groups	Intensity	Mode of vibration
1	880-995	Alkenes	C-H	Medium to Strong	Out of plane and bend
2	970-1250	Alcohols	C-O	Medium to Strong	Stretch
3	1230-1280	Ethers/epoxide	C-O-C	Medium to Strong	Asymmetric Stretch
4	1350-1470	Alkanes and Alkyls	CH_3C-H	Medium	Bend
5	1395-1440	Alcohols	C-O-H	Medium	Bend
6	1710-1740	Ketones	C=O	Strong	Stretch
		Aldehydes	C=O		
		esters	O-C=O		
7	2690-2840	Aldehydes	H-C=O	Medium	Stretch
8	2850-3000	Alkanes and Alkyls	C-H	Strong	Stretch
9	3020-3100	Alkenes	=C-H and $=CH_2$	Weak to medium	Stretch
10	3580-3650	alcohol	O-H	Weak to medium	Stretch

4.3.3 Hydrogenated Derivatives of *d*-Limonene Obtained Using 5% Palladium Catalysts

4.3.3.1 GC-MS spectrum hydrogenated d-limonene crude products

Figure 4.11 shows the GC-MS of hydrogenated derivatives of *d*-limonene obtained from synthesis.

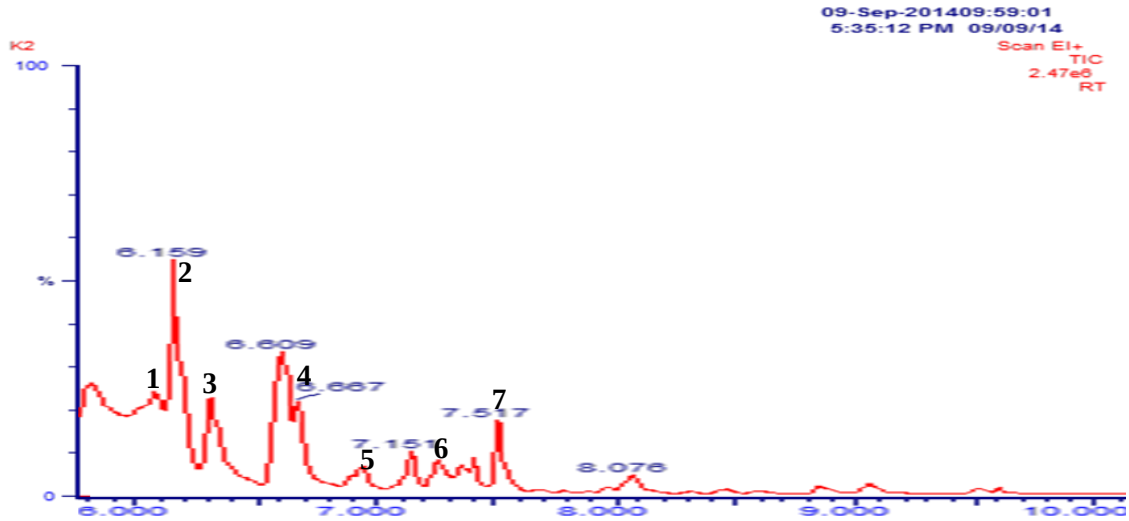

Figure 4.11: GC-MS spectrum hydrogenated d-limonene crude products

From Figures 4.11 of GC-MS, m/z values in appendix XIV B and NIST library, it is confirmed that the main hydrogenated limonene derivatives formed during catalytic hydrogenation labelled 1 to 4 are (S)-1-methyl-4-isopropyl-cyclohexane or *cis*-p-menthane (**22**), (*R)*-1-methyl-4-isopropyl-cyclohexane or *trans*-p-menthane (**23**), (S)-1-methylene -4-(1-methylethyl)cyclohexane (**24**), (R)-1-methylene -4-(1-methylethyl)cyclohexane (**25)** which represent 60 % of the whole amount of hydrogenated products formed. In addition other compounds labelled 5 to 7 were present though in lower quantities with retention times 7.142, 7.251 and 7.517. The compounds identified at Rt 7.142 is Octahydro-7-methyl-3-methylene-4-(1-methylethyl)-1H-cyclopenta[1.3]cyclopropa[1.2] benzene (**26**), Rt 7. 251 is R-1,2,3,5,6,7,8,8a-octahydro-1,8a-dimethyl-7-(1-methylethenyl)naphthalene or valencene (**27)** and at Rt 7.517 is R- 1,2,3,4,4a,5-hexahydro-1,6-dimethyl-4-(1-methylethyl)naphthalene (**28**) (Appendix XIV B).

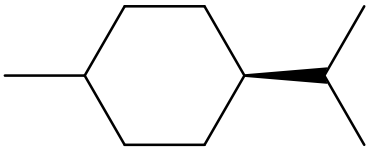

22

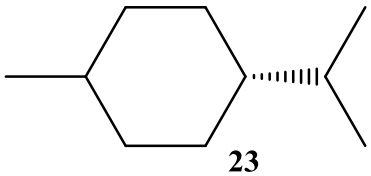

23

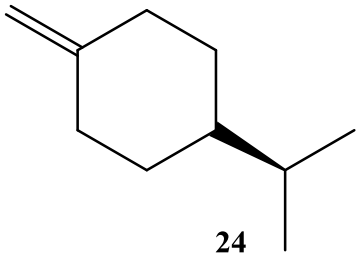

24

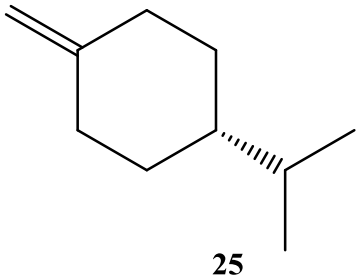

25

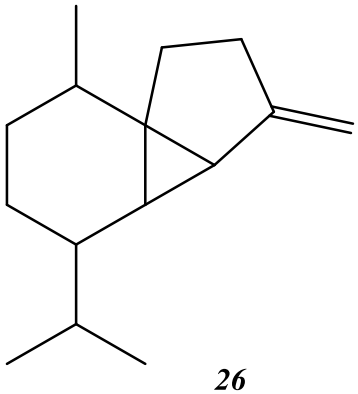

26

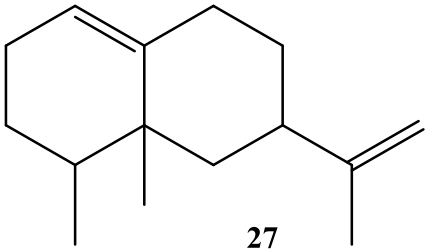

27

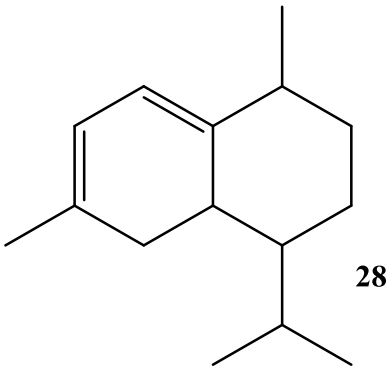

28

The relative composition of the hydrogenated *d*-limonene derivatives are shown in the Table 4.13.

Table 4.13: Relative composition % of hydrogenated derivatives

S No.	Rt	Compound	R. composition %	Structure No.
1	6.075	S-1-methyl -4-(1-methylethyl)cyclohexane	7.160	22
2	6.159	R-1-methyl -4-(1-methylethyl)cyclohexane	30.758	23
3	6.317	S-1-methylene -4-(1-methylethyl)cyclohexane	11.951	24
4	6.667	R-1-methylene -4-(1-methylethyl)cyclohexane	13.758	25
5	7.142	Octahydro-7-methyl-3-methylene-4-(1-methylethyl) -1H-cyclopenta [1.3]cyclopropa[1.2]benzene	5.686	26
6	7.251	R-1,2,3,5,6,7,8,8a-octahydro-1,8a-dimethyl-7-(1-methyethenyl)naphthalene	4.188	27
7	7.517	R-1,2,3,4,4a,5-hexahydro-1,6-dimethyl-4-(1-methylethyl)naphthalene	11.061	28

From figure 4.11 and table 4.13 R-1-methyl-4-(1-methylethyl)cyclohexane (**23**) high relative composition (30.758%) can be attributed to ability of palladium catalyst supported on alumina to convert the two C=C bonds in *d*-limonene into C-C saturated bonds by molecular hydrogen (Tracy *et al*., 2009). The presence of S- stereoisomers indicate that extensive isomerisation may have preceeded hydrogenation.

4.3.3.2 FTIR spectrum of hydrogenated *d*-limonene crude products

Figure 4.12 shows the FTIR spectra of hydrogenated derivatives of *d*-limonene after synthesis in the *C. senensis* peel oil.

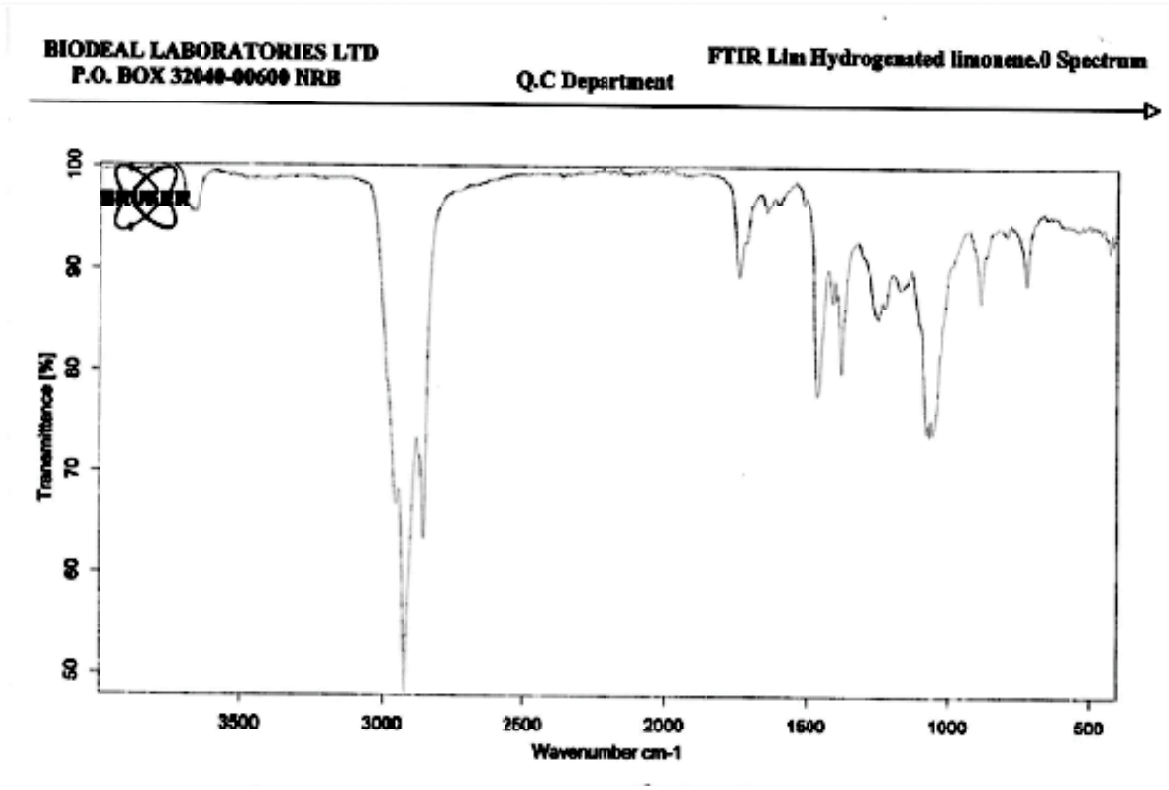

Figure 4.12: FTIR spectrum of hydrogenated d-limonene crude products

From Figure 4.12 FTIR spectra the $=CH_2$ bend at 900 cm^{-1}, CH_3 symmetric bend at 1375cm^{-1}, internal C=C medium stretch at 1640 cm^{-1}, C-H stretch at 2850-3000 cm^{-1} and aromatic C-H weak stretch at 3480 cm^{-1} can be attributed to presence of the functional groups present in the mixture. This agrees with the findings of Grau *et al*. (1999).

4.3.4 Oxygenated Derivatives of *d*-limonene Using Oxygen

4.3.4.1 GC-MS spectra of oxygenated derivatives of *d*-limonene after synthesis

Figure 4.13 shows GC-MS spectra of oxygenated derivatives of *d*-limonene after synthesis in the *C. senensis* peel oil.

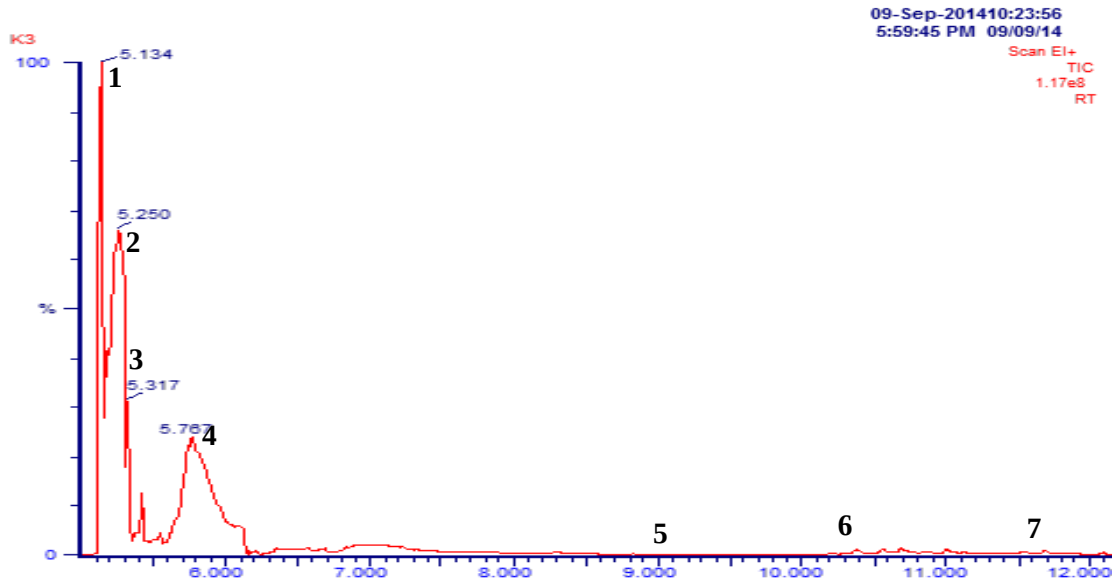

Figure 4.13: GC-MS spectra of oxygenated *d*-limonene crude products

From Figure 4.13 of GC-MS spectra, m/z values in appendix XIV C and NIST library it is confirmed that oxygenated limonene derivatives formed during catalytic oxidation were mainly the 1,2- limonene epoxide (2), 8,9-limonene epoxides (**3**), 1,2,8,9- diepoxylimonene (**4**), carveol (**5**) and carvone (**6**) which represent 78.402 % of the whole amount of products formed at retention times 5.134, 5.250, 5.317, 5.767 and 10.201 (Appendix XIV C) . This agrees with the findings of Pena *et al*, (2012) of 45–60 % considering that the *C. senensis* peel oil was in crude form . Also at retention times 9.043 and 11.685 *cis*-p-menth-2,8-dienol (**29**) and *trans* – carveyl ethanoate (**30**) were observed.

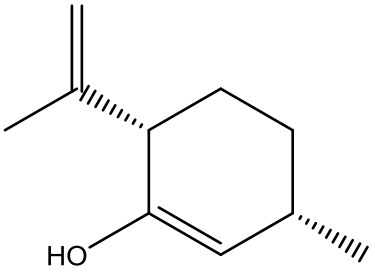

29

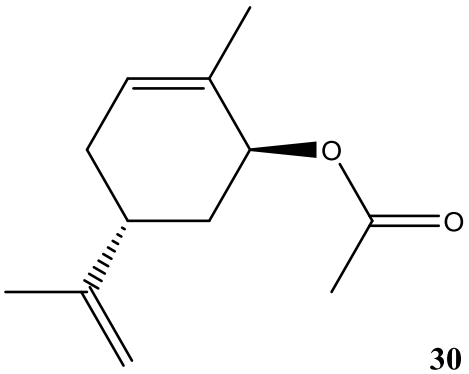

30

The relative composition of oxygenated derivatives labelled 1 to 7 in figure 4.13 are shown in Table 4.14 below.

Table 4.14: Relative composition % of oxygenated derivatives

S No.	Rt	Compound	Relative composition %	Structure No.
1	5.134	1,2- limonene epoxide	33.042	2
2	5.250	8,9-limonene epoxide		3
3	5.317	1,2,8,9- diepoxylimonene		4
4	5.767	carvone	34.428	6
5	9.043	*cis*-p-menth-2,8-dienol	0.988	29
6	10.201	Carveol	10.932	5
7	11.685	*trans*-carveyl ethanoate	3.436	30

From Figure 4.13 and Table 4.14 the high yield of 1,2-limonene epoxide is attributed to the selective electrophilic attack on the C=C at position 1-2 in presence PdHT/O_2 (Bussi *et al*., 2003). The high yield of carvone (34.428%) can be attributed to the formation of carveol by allylic oxidation over PdHT catalyst. Carveol is then converted to carvone by oxidation on the external surface of PdHT catalyst due to steric limitation influence (Wroblewska, 2014). The presence of *trans*-carveyl ethanoate indicate presence of carveol before it is converted to carvone. This may reduce the biodegradation of the biofuels by offering microorganisms alternative esters.

4.3.4.2 FTIR spectra of oxygenated derivatives of *d*-limonene after synthesis

Figure 4.14 shows FTIR spectra of oxygenated derivatives of *d*-limonene after synthesis in the *C. senesis* peel oil.

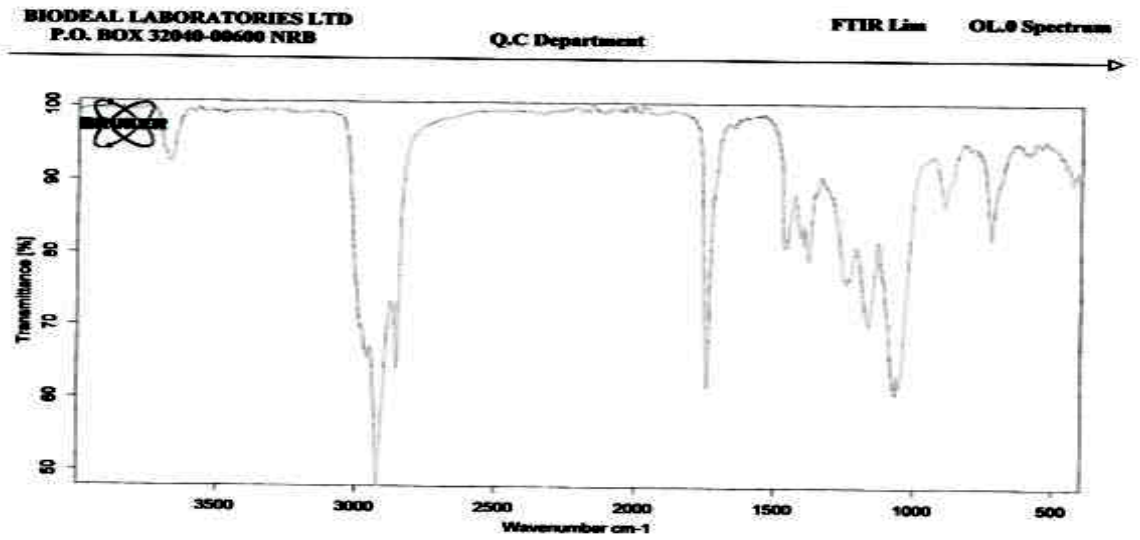

Figure 4.14: FTIR spectrum of oxygenated *d*-limonene crude products

From Figure 4.14 of FTIR spectra it is confirmed that for epoxides the ring-stretch weak band near 1280-1230 cm^{-1}, asymmetric ring deformation strong band near 950-815 cm^{-1}; symmetric ring deformation strong band near 880-750 cm^{-1}. Monosububstituted epoxides absorb near the higher end. Disubstituted epoxides absorb near the lower end. $=CH_2$ bend at 900 cm^{-1}, C=O stretch at 1700 cm^{-1}, CH_3 symmetric bend at 1375 cm^{-1} , C-O-C stretch at 1250 cm^{-1}, C-O-H medium bend at 1400 cm^{-1} and C-H stretch around 2850-3000 cm^{-1}.

4.3.5 Physicochemical and Thermodynamic Properties of *d*-limonene and Derivatives from Orange Peel Oil

Table 4.15 shows the analysis results of the crude synthetic products (Appendix XIII). These are the physicochemical and thermodynamic properties using American Oil Chemists' Society (AOCS), Association of Official Analytical Chemists (AOAC) and

American Society for Testing and Materials (ASTM) standard test methods as described in section 3.4.1.3.3.

Table 4.15: Physicochemical and thermodynamic properties of *d*-limonene and derivatives from orange oil

Sample No.	Limonene and Derivatives	Physicochemical and Thermodynamic Properties (mean values from replicates)							
		Density kg/dm^3	Calorific Value (MJ/Kg)	Kinematic Viscosity at 40^{o}C (cSt)	Flash point (^{o}C)	Cetane Index	Pour Point (^{o}C)	CFPP (^{o}C)	Cloud Point (^{o}C)
Malindi	*d*-limonene (95%)	772	34.38	0.946	74	46	-18	-6	-10
Muheza	*d*-limonene (95%)	768	34.60	0.947	73	46	-18	-6	-10
Shimba hills	*d*-limonene (95%)	758	34.65	0.947	73	46	-18	-6	-10
	Mean±SD	766±	34.543	0.947	73.333	46±	-18±	-6±	-10±
		7.211	±0.1436	±0.001	±0.577	0.000	0.000	0.000	0.000
Malindi	Oxygenated derivatives	865	33.20	0.984	77	48	-14	-5	-8
Muheza	Oxygenated derivatives	863	33.45	0.984	75	48	-14	-5	-8
Shimba hills	Oxygenated derivatives	855	33.80	0.985	77	50	-14	-5	-8
	Mean±SD	861±	33.483	0.984±	76.333	48.666	-14±	-5±	-8±
		5.292	±0.303	0.001	±1.155	±1.155	0.000	0.000	0.000
Malindi	Hydrogenated derivatives	864	34.80	0.997	75	47	-14	-5	-7
Muheza	Hydrogenated derivatives	861	34.78	0.997	74	47	-14	-5	-7
Shimba hills	Hydrogenated derivatives	844	34.85	0.996	74	49	-14	-5	-7
	Mean±SD	856±	34.81	0.997	74.333	47.667	-14±	-5±	-7±
		10.786	±0.036	±0.001	±0.577	±1.155	0.000	0.000	0.000

From Table 4.15 it is shown that oxygenated limonene derivatives have the highest density (861±5.292 kg/dm^3) and limonene has the lowest (766±7.211 kg/dm^3) comparable to relative density of 844kg/dm^3 obtained by Jobard (Jobard, 2010). The higher densities of oxygenated and hydrogenated limonene derivatives than *d*-limonene attributable to presence compounds with higher densities such as the epoxides and *p*-menthane respectively. Hydrogenated limonene derivatives have the highest calorific value (34.810±0.036 MJ/Kg) and oxygenated the lowest (33.483±0.303 MJ/Kg). The high calorific value of hydrogenated limonene can be attributed to the high hydrogen content in the composite compounds which are the major determinants of calorific value (Thangarasu and Anand, 2019). Hydrogenated limonene derivatives have the highest kinematic viscosity (0.997±0.001 cSt) and limonene the lowest (0.947±0.001 cSt). The high kinetic viscosity of hydrogenated limonene derivatives can be attributed to the reduction in fluidity with hydrogenation of essential oils (Bart *et al*., 2013) Oxygenated limonene derivatives have the highest flash point (76.333±1.155 ^{o}C) and limonene the lowest (73.333±0.577 ^{o}C). The high flash point of oxygenated limonene derivatives can be attributed to presence of low volatile compounds (Fingas, 2011) such as carvone. Oxygenated limonene derivatives have the highest cetane index (48.666±1.155) and d-limonene the lowest (46.000±0.000). Cetane index is an indicator of octane number. The high octane index of oxygenated limonene derivatives can be attributed to the presence of oxygen atom in the components which enables complete combustion (Bello *et al*., 2012). Limonene has the lowest pour point (-6.000±0.000 ^{o}C) whereas oxygenated and hydrogenated limonene derivatives have the highest (-5.000±0.000 ^{o}C). Limonene has the lowest cloud point (-10.000±0.000 ^{o}C) and hydrogenated limonene derivatives have the highest (-7.000 ± 0.000 ^{o}C). Low temperature properties are dependent on degree of

unsaturation and formation of crystals (Cao *et al*., 2014). The high low temperature properties of oxygenated and hydrogenated limonene derivatives are attributed to presence of epoxides in oxygenated limonene derivatives and allylic intermediates in hydrogenated limonene derivatives that may have encouraged early crystal formation.

4.4 Physicochemical and Fuel Properties of FAEE from *J. curcas* oil from dehusked seeds and *R. grande* Oil

4.4.1 Husked and Dehusked *J. curcas* Seeds

Table 4.16 shows % Mass of Dehusked Seeds per Sampling Farm Sites SFA,SFB,SFC,SFD and SFE. Measurements are presented as mean ± standard deviation.

Table 4.16: % Mass of Dehusked Seeds per Sampling Farm Site in Shimba Hills

Sample farm site	Mass of Whole seed (g) Mean±SD	Mass of Dehusked seed (g) Mean ±SD	% mass of Dehusked seed Mean ± SD
SFA	0.7312±0.097	0.442±0.104	59.59±7.915
SFB	0.7555±0.101	0.4882±0.071	64.544±2.199
SFC	0.7495±0.132	0.4715±0.111	62.328±4.300
SFD	0.6885±0.142	0.4082±0.100	58.679±6.183
SFE	0.7530±0.131	0.4740±0.100	62.479±4.755

SFA, SFB, SFC,SFD and SFE - Sampling farm sites in Shimba hills Kwale County

From Table 4.16 the % mean mass of *J. curcas* dehusked seeds from different contracted farmers in an out grower scheme Energy Africa in Shimba hills, Kwale County ranged from 58.679% to 64.544%. This can be attributed to difference in soil texture, fertility and pH. For economic returns from *J. curcas*, a soil with moderate fertility is preferred (Raheman, 2012).

4.4.2 Yield of Jatropha Oil from Dehusked *Jatropha curcas* Seeds

Table 4.17 shows the volume of Jatropha oil extracted from *Jatropha curcas* dehusked seeds using hexane after cold pressing and grinding by blender from five sampling fields in Shimba Hills.

Table 4.17: %yield of Jatropha oil per gram of biomass from each sampling site

Sampling field	Jatropha biomass (g)	Jatropha oil produced (ml) (mean±SD)	%v/w yield of Jatropha oil per gram biomass (mean±SD)
JOFA[a]	750	330±1.00	44±0.130
JOFA[b]	750	390±2.00	52±0.267
JOFB[b]	750	400±1.00	53±0.135
JOFC[b]	750	380±2.00	51±0.267
JOFD[b]	750	390±5.00	52±0.667
JOFE[b]	750	385±4.36	51±0.581

[a]Sample obtained by cold press followed by hexane; [b]Sample obtained by blender followed by hexane

From Table 4.17 the amount of *J. curcas* oil obtained by cold press followed by hexane extraction was lower 330± 1.00 mL (44 %) than that obtained by blender followed by hexane extraction (51-53 %). This may be attributed to loss during pressing by evaporation and wetting of the cold press. According to Xiaohu and Burton (2009), the kernels have about 50% oil. The oil recovery in mechanical expeller is about 85%, while more than 95% recovery of oil could be achieved when extracted by solvent method. The mean yields using blender and hexane solvent were similar to those reported 40-60% (Ginwal *et al*., 2004; Pant *et al*., 2006; Kumar and Sharma, 2008; Nzikou *et al*., 2009).

4.4.3 Physicochemical and Thermodynamic Properties of *R. grande* and *J. curcas* Oil

Table 4.18 and 4.19 show results of analysis for physicochemical and thermodynamic properties using AOCS, AOAC and ASTM standard test methods which include: density kg/dm^3 ASTM D1298 at 20^{o}C, kinematic viscosity at 40^{o}C (cSt) ASTM D445, refractive index (AOAC method 920.212), acid value (ISO method 660:2009), iodine value (AOAC method 920.159) and saponification value (AOAC method 920.160) of oils extracted from *R. grande* and *J. curcas.*

Table 4.18: Physicochemical and Thermodynamic Properties of Algae Oil

Algae oil Sample	Physicochemical and Thermodynamic oil Properties (mean ±SD)					
	Density kg/m^3	Refractive index	Kinematic Viscosity at 40^{o}C (cSt)	Acid Value mg KOH/g	Iodine Value mg/g	Sapon. Value mg/g
AO 1	889.3± 1.4	1.478± 0.305	4.4± 0.3	34.4± 1.6	75.2± 2.0	170.3± 2.0
AO 2	878.7± 1.6	1.476± 0.251	4.3± 0.2	34.5± 1.9	76.9± 1.1	168.3± 1.8
AO 3	890.1± 1.1	1.476± 0.247	4.4± 0.2	35.5± 1.4	75.9± 1.2	168.5± 1.7
AO 4	886.2± 1.3	1.480± 0.312	4.3± 0.1	34.6± 1.8	75.0± 2.1	168.0± 1.8

AO1 Tudor creek, AO2 Shimoni shores, AO3 Shelly beach and AO4 Jamvi la wageni samples

Table 4.19: Physicochemical and Thermodynamic Properties of Jatropha oil

Jatropha oil Sample	Physicochemical and Thermodynamic oil Properties (mean±SD)					
	Density kg/m^3	Refractive index	Kinematic Viscosity at 40^{o}C (cSt)	Acid Value mg KOH/g	Iodine Value mg/g	Sapon. Value mg/g
JOFA[a]	917±1.12	1.497± 0.012	34.12±0.16	36.58±0.12	106±1.0	194.5±0.1
JOFB[b]	916±1.03	1.496± 0.010	33.96±0.13	36.57±0.16	106±1.0	195.2±0.3
JOFC[b]	916±0.19	1.496± 0.011	34.10±0.09	36.40±0.13	107±0.0	195.6±0.6
JOFD[b]	916±1.10	1.496± 0.012	34.09±0.12	36.46±0.18	108±0.0	195.8±0.2
JOFE[b]	916±1.02	1.496± 0.015	35.20±0.11	36.49±0.15	106±1.0	194.9±0.1

[a]Sample obtained by cold press followed by hexane; [b]Sample obtained by blender followed by hexane

From Table 4.18 and 4.19 the density of the algal oil (AO) is less than the *Jatropha curcas* oil (JO). The kinematic viscosity of algal oil (AO) is more than that of JO. The high density, refractive index and kinematic viscosity may be due to the difference molecular weight of fatty acids in both oils. The high kinematic viscosity confirms that the two oils require transesterification to reduce the viscosity. It also indicates the relative ease of pumping the oils. The flash point is lower than that of *JO*. From the flash point values it implies that the oils (AO and JO) have no storage or handling problem without serious fire hazards. The heating value and cetane number is almost similar. These properties are mainly dependent on the elements present in the oils namely carbon, hydrogen and oxygen.

Iodine value is more in Jatropha oil than algae oil. However both are lower than 120 hence can readily be used as biofuel feedstock. The use of iodine value of a maximum of 120 can serve to restrict certain vegetable oils as biodiesel feedstocks especially

when oxidative stability specification parameter are not included in the analysis (Knothe, 2006).

4.4.4 Yield of FAEE from *Rhizoclonium grande* Oil

Table 4.20 shows the percentage yield of the ethyl esters from *R. grande* oil.

Table 4.20: % yield of ethyl esters from algae oil sample from *Rhizoclonium grande*

Algae oil sample	Volume of Algae oil (ml)	Mass of Potassium hydroxide (g)	Volume of dry ethanol (ml)	Mean Volume of ethyl esters (ml)	Mean %yield of ethyl esters
AO1	10	0.3	3	5.7	57
AO2	10	0.3	3	5.8	58
AO3	10	0.3	3	5.9	59
AO4	10	0.3	3	6.2	62

AO1 Tudor creek, AO2 Shimoni shores, AO3 Shelly beach and AO4 Jamvi la wageni samples

From Table 4.20 it is observed that % yield of FAEE was highest in algae oil from Jamvi la Wageni (62%) and the least was that from Tudor creek (57%). The values are in agreement with those in literature for macrofilamentous algae of 68% (Grayburn *et al*., 2013). The relatively lower yield values of ethyl esters compared to methyl esters (81.13%) (Nwakaire *et al*., 2016) could be attributed to difficulty experienced in separation and isolation of ethyl esters and glycerol.

4.4.5 Yield of FAEE from *Jatropha curcas* L. Oil

Table 4.21 shows the percentage yield of ethyl esters obtained from *J. curcas* oil.

Table 4.21: %yield of ethylesters from *Jatropha curcas* oil from different sites

Jatropha oil sample	Volume of Jatropha oil (ml)	Mass of Potassium hydroxide (g)	Volume of dry ethanol (ml)	Mean Volume of ethylesters (ml)	Mean %yield of ethylesters
JOFA[a]	100	3	30	65	65
JOFB[b]	100	3	30	67	67
JOFC[b]	100	3	30	70	70
JOFD[b]	100	3	30	64	64
JOFE[b]	100	3	30	63	63

[a]Sample oil obtained by cold press followed by hexane; [b]Sample oil obtained by blender followed by hexane

From Table 4.21 the % yield of FAEE was highest in oil from JOFC (70%) and the least was that from JOFE (63%). The differences could be attributed to errors in control of experimental conditions such as temperature in the process of FAEE production. The values are lower than those in literature for Jatropha oil methylesters of >90% (Aminul *et al*., 2015). The relatively lower yield values of ethyl esters compared to methyl esters could be attributed to difficulty experienced in separation and isolation of ethyl esters and glycerol. The various steps encountered in separation of ethyl esters lead to loss during transfer from one separating funnel to the other.

4.4.6: Composition of Ethyl Esters from *R. grande* Oil

Figure 4.15 shows the composition of ethyl esters from *R.grande*.

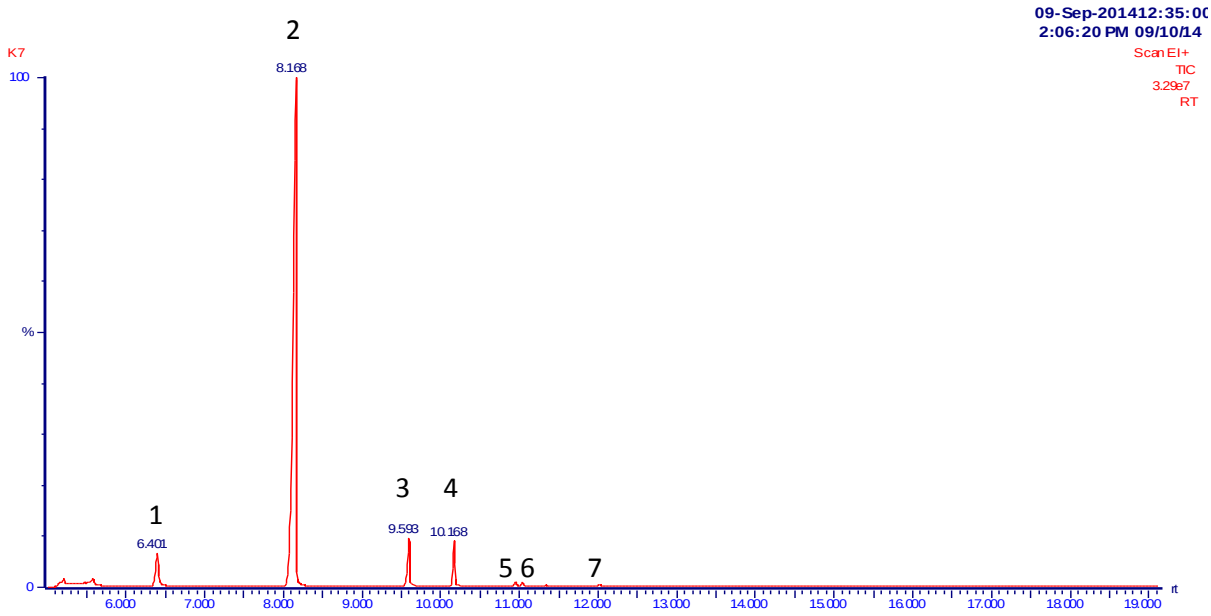

Figure 4.15: GC-MS Spectrum of *R. grande* Ethyl Esters

From Figure 4.15 the composition of the ethyl ester mixture include pentadecanoic acid ethyl ester Rt = 6.376 (1), dodecanoic acid (lauric acid) ethyl ester Rt = 8.168 (2), tetradecanoic acid (myristic acid) ethyl ester Rt = 9.593 (3) and hexadecanoic acid (palmitic acid) ethyl ester Rt =10.168 (4). Others not identified and in low quantities at Rt =10.943 (5), Rt =11.051 (6) and Rt=12.035 (7).

4.4.7 Physicochemical and Fuel Properties of Ethyl Esters from *R. grande* Oil

Table 4.22 shows results of physicochemical and fuel properties of ethyl esters from *R. grande* oil using American Society for Testing and Materials (ASTM) standard test methods which include: density kg/dm^3 ASTM D1298 at 20^{o}C, calorific value (KJ/Kg) ASTM D4809, kinematic viscosity at 40^{o}C (cSt) ASTM D445, flash point (^{o}C) ASTM D93, cetane index ASTM D4737, pour point (^{o}C) ASTM D97, cold filter plugging point (CFPP) (^{o}C) ASTM D6371 and cloud point (^{o}C) ASTM D2500 (ASTM, 2000).

Table 4.22: Physicochemical and Fuel Properties of Ethyl Esters from *R.grande* oil

Algae Ethyl ester (FAEE) Sample	Physicochemical and Fuel Properties (mean values)							
	Density (kg/m^3)	Calorific Value (MJ/Kg)	Kinematic Viscosity at 40°C (cSt)	Flash point (°C)	Cetane Index	Pour Point (°C)	CFPP (°C)	Cloud Point (°C)
FAEE TC[a]	910	33	4.7	153	48	-6	-3	-2
FAEE SS[b]	912	34	4.9	154	50	-5	-2	-1
FAEE SB[c]	909	32	4.7	152	49	-6	-3	0
FAEE JW[d]	913	34	5.1	155	50	-5	-1	1

[a] Tudor creek [b] Shimoni shores [c] Shelly beach [d] Jamvi la wageni samples

From the Table 4.22 the algae ethyl esters from all the sample sites had properties acceptable by ASTM D 6751 (Appendix XXII). The mean values obtained are in agreement with those obtained from different species of algae by Farooq *et al*. (2013). According to the findings on two algae species, *Chlorella vulgaris* and *Rhizoclonium hieroglyphicum* the biodiesel produced was analyzed for kinematic viscosity (4.9 and5.0 mm^2/s), flash point (160 and 156 °C), specific gravity (0.910 and 0.914 g/mL), cetane number (51 and 49) for *C. vulgaris* and *R. hieroglyphicum* respectively. Properties of the biodiesel were compared with ASTM D6751 standard and it was found to be in conformance with quality biodiesel.

4.4.8 Composition of Ethyl Esters from *Jatropha curcas* Oil

Figure 4.16 shows composition of ethyl esters from *J.curcas* oil.

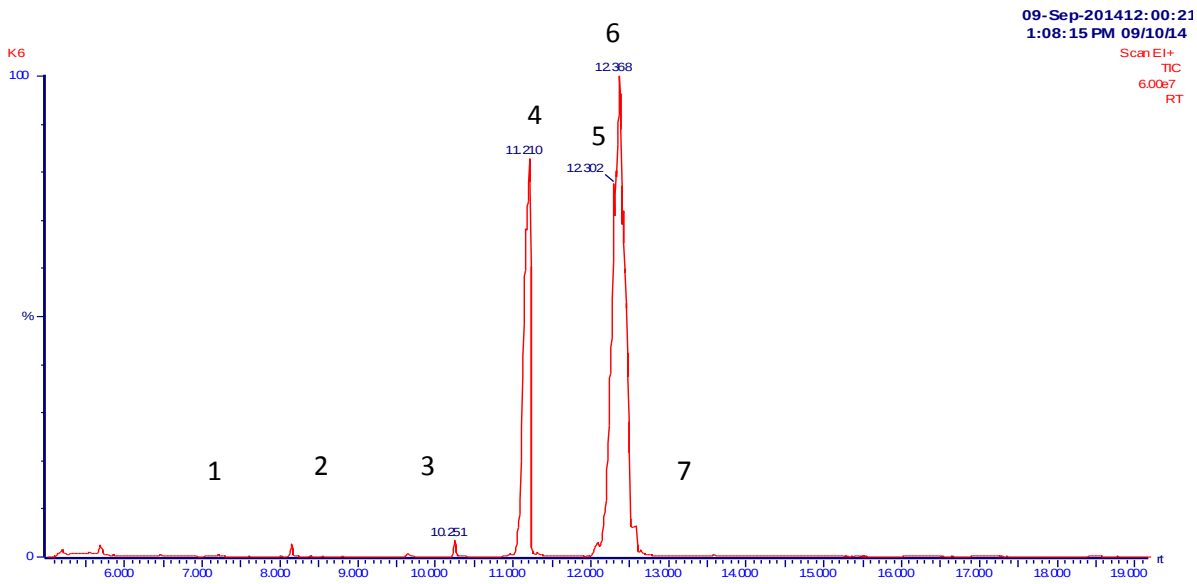

Figure 4.16: GC-MS spectrum of *J. curcas L.* ethyl esters

From Figure 4.16 the main components of *J. curcas* ethyl esters are ethyl hexadecanoate (palmitic acid ethyl ester) (C16:0) Rt 11.21 (4) main m/z 41, 43, 73, 88, 101, 157, 199, 241, 284, ethyl octadecanoate (C18:0) Rt 12.302 (5) and ethyl 9(Z)-octadecenoate (C18:1) Rt 12.368 (6). Others are ethyldecanoate (C10:0) Rt 6.467 (1), ethyl dodecanoate (C11:0) Rt 8.143 (2), ethyl nonadecanoate (C19:0) Rt 9.651 (3) and ethyl eicosanoate (C22:0) Rt 13.619 (7) main m/z 41, 43, 55, 57, 88, 101, 111, 157, 207, 253, 281, 297, 340 in smaller quantities (Appendix XVIIB).

4.4.9 Physicochemical and Fuel Properties of Ethyl Esters from *J. curcas L* Oil

Table 4.23 shows results of physicochemical and fuel properties of ethyl esters from *J.curcas* oil using American Society for Testing and Materials (ASTM) standard test methods which include: density kg/dm^3 ASTM D1298 at 20^{o}C, calorific value (KJ/Kg) ASTM D4809, kinematic viscosity at 40^{o}C (cSt) ASTM D445, flash point (^{o}C) ASTM D93, cetane index ASTM D4737, pour point (^{o}C) ASTM D97, cold filter

plugging point (CFPP) (°C) ASTM D6371 and cloud point (°C) ASTM D2500 (ASTM, 2000).

Table 4.23: Physicochemical and Fuel Properties of Ethyl Esters from *J.curcas* oil

Ethyl ester (FAEE) Sample	Physicochemical and Fuel Properties (mean values)							
	Density (kg/m^3)	Calorific Value (MJ/Kg)	Kinematic Viscosity at 40°C (cSt)	Flash point (°C)	Cetane Index	Pour Point (°C)	CFPP (°C)	Cloud Point (°C)
FAEE1[a]	865.0	41.36	5.350	182	63.3	-10	-2	-4
FAEE2[b]	865.9	40.84	5.405	183	62.4	-9	-2	-3
FAEE3[c]	868.4	40.62	5.426	183	63.2	-9	-2	-4
FAEE4[d]	887.3	41.05	5.432	183	63.4	-8	-1	-2
FAEE5[e]	886.2	40.56	5.430	182	63.2	-8	-2	-3

[A,b,c,d,e] Fatty acid ethyl esters from Shimba Hills farms SFA, SFB, SFC, SFD and SFE respectively

From the Table 4.23 the Jatropha ethyl esters from all the sample sites had properties acceptable by ASTM D 6751 (Appendix XXII). The mean values of physicpchemical and fuel properties such as density 0.8650-0.8873 g/mL, kinematic viscosity 5.350-5.432 mm2/s (cSt), flash point 182-183 °C, calorific value 40.56-41.36 MJ/kg, pour point -10 to -8 °C and cloud point -2 to -4 °C obtained are comparable with those obtained for *J. curcas* methyl esters reported in literature (Tomasevic and Marinkovic, 2003; Anastopoulos *et al*., 2009). According to the findings by Raja *et al.* (2011) FAME biodiesel produced from *J. curcas* has specific gravity 0.84 g/mL, kinematic viscosity 4.82 mm^2/s, flash point 128 °C, calorific value 42.80 MJ/kg, pour point -2 ^{0}C and cloud point 8 ^{0}C (Raja *et al*., 2011). The difference may be attributed to difference in chain length of the fatty acid esters.

4.5 Miscibility, Physicochemical and Fuel Properties of JABLA in Comparison to JAB and Petroleum Fuels

4.5.1 Phase Miscibility and Stability of the Blends of Biodiesel (JAB) with Limonene and Limonene Derivatives (JABLA)

4.5.1.1 Phase Miscibility and Stability of the Blends of Biodiesel (JAB)

Plate 4.2a shows phase miscibility and stability of the blends of biodiesel (JAB) obtained using miscibility ASTM D4682-87 test method (ASTM, 2002c). The blends are 5 % *R.grande* with 95 % *J. curcas* FAEE (JAB5), 10 % *R.grande* with 90 % *J. curcas* FAEE (JAB10), 15 % *R.grande* with 85 % *J. curcas* FAEE (JAB15), 20 % *R.grande* with 80 % *J. curcas* FAEE (JAB20) and 25 % *R.grande* with 75 % *J. curcas* FAEE (JAB25).

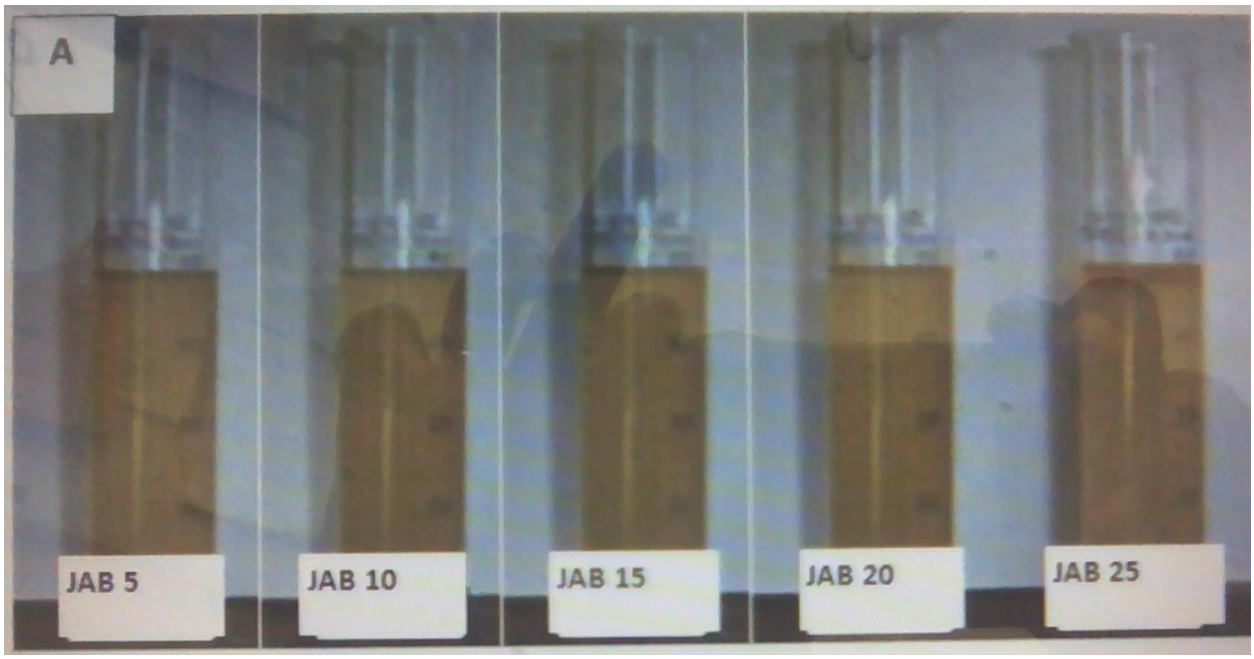

Plate 4.2a: Phase miscibility of *R.grande* FAEE with *J.curcas* FAEE (JAB) blends

From Plate 4.2a it can be observed that the blends of *R.grande* FAEE with *J.curcas* FAEE (JAB) are miscible and were all stable except JAB25 which showed slight phase separation after some time. JAB5 to JAB20 blends maintained phase stability for 72 hours standing while JAB25 started showing slight phase separation. The

separation can be attributed to the effect of hydrophobic mismatch by the components at this concentration bringing about phase separation in the liquid phase (Longo *et al*., 2009). Therefore, JAB20 was taken as the compromise blend to add the limonene and derivatives as additives for the purpose of optimisation. These terpene-based additives have an advantage in that they are totally renewable because they come from plant tissues (Robles-Dutenhefner *et al.,* 2004).

4.5.1.2 Phase Miscibility and Stability of the Blends of Biodiesel (JAB) with *d*-Limonene and *d*-Limonene Derivatives (JABLA)

Plates 4.2b, 4.2c and 4.2d show phase miscibility and stability of the blends JAB20 with *d*-limonene, oxygenated *d*-limonene derivatives and hydrogenated *d*-limonene derivatives respectively as additives (JABLA) obtained using miscibility ASTM D4682-87 test method. The blends are 2 % additives with 98 % JAB20 FAEE (JABLA2), 4 % additives with 96 % JAB20 FAEE (JABLA4), 6 % additives with 94 % JAB20 FAEE (JABLA6), 8 % additives with 92 % JAB20 FAEE (JABLA8) and 10 % additives with 90 % JAB20 FAEE (JABLA10).

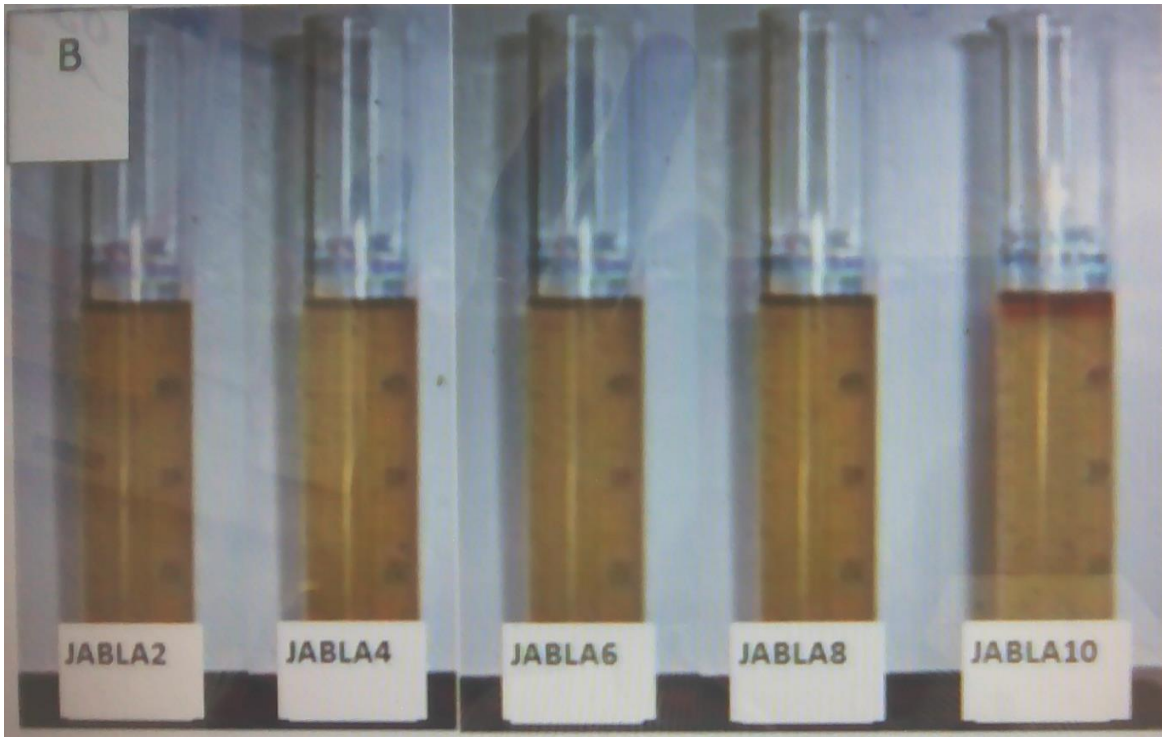

Plate 4.2b: Phase miscibility of JAB20 blend with *d*-limonene

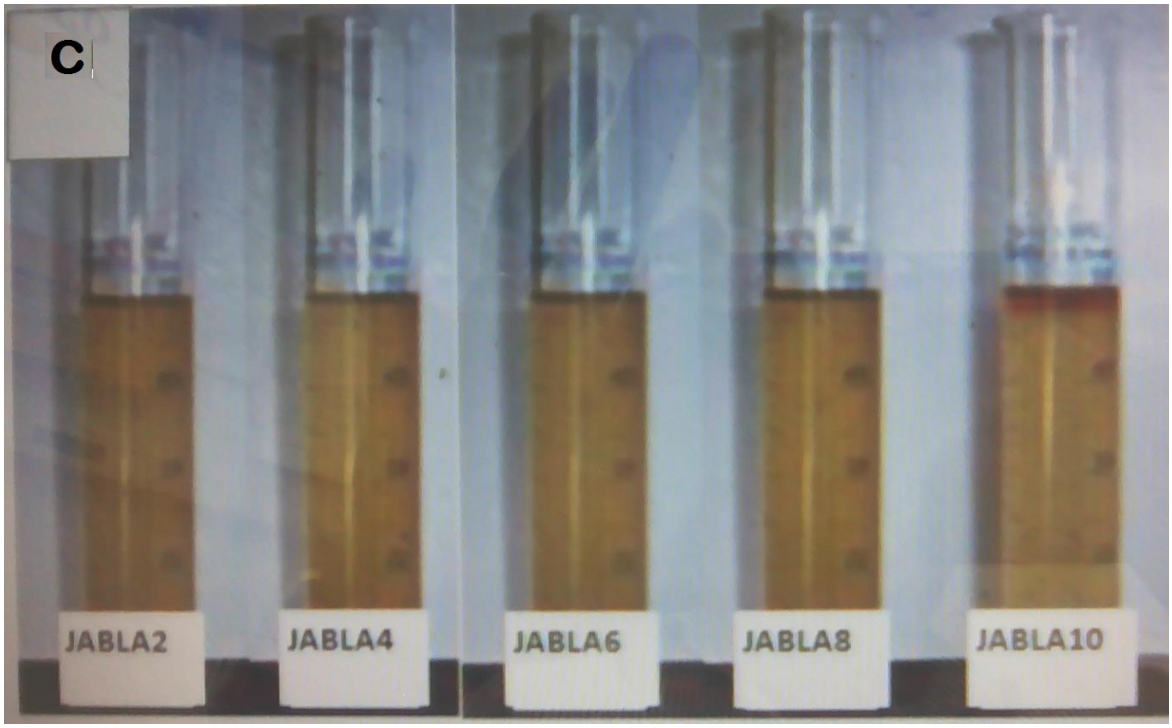

Plate 4.2c: Phase miscibility of JAB20 blend with oxygenated *d*-limonene

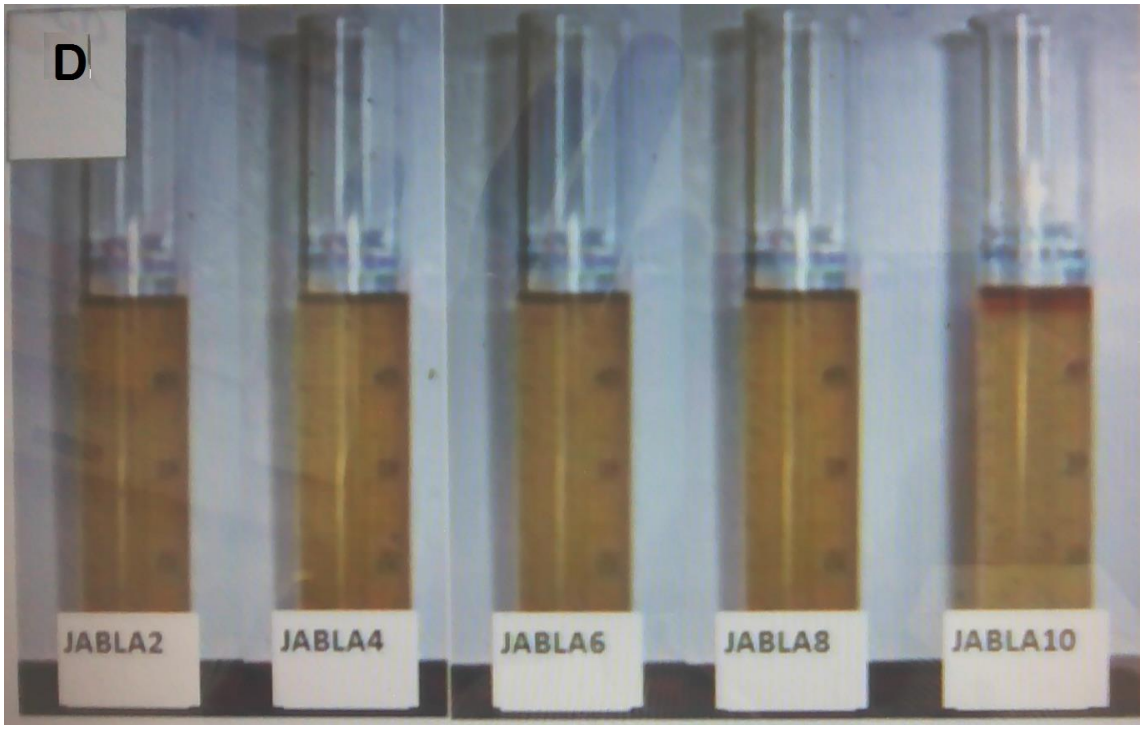

Plate 4.2d: Phase miscibility of JAB20 blend with hydrogenated *d*-limonene

From Plates 4.2b, 4.2c and 4.2d it is observed that all of the additives with JAB20 blend formed homogeneous mixtures before separation started to appear at 10% of additives after 10 days. This may be attributed to gelling caused by presence of some highly polar and unsaturated species (Longo *et al*., 2009) added to the JAB20 biodiesel which may have persisted even after the hydrogenation and oxidation processes. The blends that showed the best stability with very little separation were JABLA2 to JABLA8 for all the three types of additives.

4.5.2 Physicochemical and Fuel properties of the *R. grande* and *J. curcas* FAEE Blends (JAB)

Table 4.24 shows the physicochemical and fuel properties of *R. grande* and *J. curcas* fatty acid ethyl ester blends (JAB) using American Society for Testing and Materials (ASTM) standard test methods which include: density kg/dm^3 ASTM D1298 at 20^{o}C, calorific value (KJ/Kg) ASTM D4809, kinematic viscosity at 40^{o}C (cSt) ASTM D445, flash point (^{o}C) ASTM D93, cetane index ASTM D4737, pour point (^{o}C)

ASTM D97, cold filter plugging point (CFPP) (°C) ASTM D6371 and cloud point (°C) ASTM D2500 (ASTM, 2000).

Table 4.24: Physicochemical and Fuel Properties of *R. grande* and *J. curcas* fatty acid ethyl ester Blends (JAB)

JAB Sample	Physicochemical and Fuel Properties (mean values)							
	Density (kg/m^3)	Calorific Value (MJ/Kg)	Kinematic Viscosity at 40°C (cSt)	Flash point (°C)	Cetane Index	CFPP (°C)	Pour Point (°C)	Cloud Point (°C)
JAB 5[a]	864.5	41.38	4.760	181	63.0	-2	-6	1
JAB 10[b]	865.0	41.35	4.765	182	63.3	-2	-6	1
JAB 15[c]	865.1	41.35	4.780	182	63.2	-1	-6	2
JAB 20[d]	865.2	41.34	4.783	183	63.3	-1	-6	1
JAB 25[e]	865.9	41.34	4.795	183	63.3	-1	-5	2

[a] 5 % *R.grande* with 95 % *J. curcas* FAEE, [b] 10 % *R.grande* with 90 % *J. curcas* FAEE, [c] 15 % *R.grande* with 85 % *J. curcas* FAEE, [d] 20 % *R.grande* with 80 % *J. curcas* FAEE and [e] 25 % *R.grande* with 75 % *J. curcas* FAEE.

4.5.2.1 Density

From Table 4.24 the fuel density expressed in kilograms per cubic meter (Kgm^{-3}), is necessary for the conversion of measured volumes to volumes or volumes to masses at the standard reference temperatures during custody and transfer of fuel. The greater the fuel density that a fuel has, the greater the mass that can be stored in a given tank and the greater the mass of fuel that can be pumped (ASTM, 2006). The density tends to increase with increase in the amount of *R. grande* FAEE added. JAB25 with 5% algae FAEE is the lowest (864.5 kg/m^3) and JAB25 with the highest (865.9 kg/m^3). Fuel density generally increases with increasing molecular weight of the fuel molecules. *R. grande* FAEE adds heavier molecules than in *J.curcas* FAEE. Fuel density is used to calculate fuel volume ratio, which is in turn used to calculate the tank mass for fuels in transit. JAB blends would be slightly heavier for the same

volume transported. Due to the slight phase separation (Fernando *et al.*, 2004) of JAB25 then JAB20 with 20% algae FAEE is the appropriate blend.

4.5.2.2 Calorific Value

From Table 4.24 there is a variation in calorific value of 0.04MJ/kg between the lowest loaded blend JAB5 and the highest loaded JAB25. Calorific value is a measure of the energy available from a fuel. The mass heat of combustion is the heat of combustion per unit mass of fuel measured by the calorific value. Its magnitude is particularly important to weight-limited vehicles such as airplanes, surface effect vehicles, and hydrofoils as the distance such craft can travel on a given weight of fuel is a direct function of the fuel's mass heat of combustion and its density. The volumetric heat of combustion, that is, the heat of combustion per unit volume of fuel, can be calculated by multiplying the mass heat of combustion by the density of the fuel (mass per unit volume). The volumetric heat of combustion, rather than the mass heat of combustion, is important to volume-limited craft such as automobiles and ships, as it is directly related to the distance travelled between re-fuelling (ASTM, 2013). Therefore JAB20 with 41.34 MJ/Kg has almost the same distance between refuelling as JAB5 (41.38 MJ/Kg) with advantage of improving the sustainability of the biofuel due to high composition of *R.grande* FAEE in JAB20.

4.5.2.3 Kinematic viscosity

From Table 4.24 kinematic viscosity of the blends increases from JAB5 (4.76 cSt) to JAB25 (4.795 cSt). This may be attributed to the higher molecular mass components in *Rhizoclonium grande* FAEE. These values are within the allowable limits of 1.9-6.0 cSt (Leung, 2010). These viscosity limits help maintain uniform fuel flow to appliances with gravity flow or pumped satisfactorily and provide satisfactory atomization with constant flow rate. Therefore JAB5 to JAB20 blends are likely to

pose no problems to flow from the tank to the vehicles as well as atomization in the engine.

4.5.2.4 Flash Point

From the results obtained in Table 4.24 JAB blends flash points are above the minimum allowable level of 130 ^{o}C ASTM D 6751 (Leung *et al*., 2010). JAB5 (181 ^{o}C) and JAB20 (183 ^{o}C). The flash point measures the temperature at which the test specimen forms a flammable mixture with air under controlled laboratory conditions. It is thus one of the properties which must be considered in assessing the overall flammability hazard of a fuel. Therefore the blends JAB5 to JAB20 are safe to use in diesel engines.

4.5.2.5 Cetane Index

From Table 4.24 cetane index of the JAB blends is almost constant JAB5 (63.0) and JAB25 (63.3). Cetane index is a reflection of the cetane number. Higher cetane numbers tend to raise soot emission but to a lesser extent than viscosity (Zannis *et al*., 2007) in this case the values are almost constant so blending has little effect on the performance of the biofuel. However addition of oxygenated compounds may reduce soot emission because they supply more oxygen to the system.

4.5.2.6 Low temperature characteristics

4.5.2.6.1 Pour Point

From Table 4.24 JAB blends pour point is found to be constant at -6^{0}C from JAB5 to JAB25. Pour point (PP) (ASTM, 2005), measures the lowest temperature at which the 45mls sample oil is observed to flow. It is important because this defines the lowest temperature at which the fuel can still be moved, before it has gelled. Fuels with high pour points are more difficult to use in areas with lower temperatures because the fuel must be kept warm by some method, such as installation of electric heaters

with insulated tanks. Distributors and blenders use pour point as an indicator of whether the fuel can be pumped, even if it would not be suitable for use without heating or taking other steps (ASTM, 2005). Therefore the JAB blends from JAB5 to JAB25 can be used with ease in relatively cold climates without the need of electrical heater installations in the fuel tank and pipes.

4.5.2.6 .2 Cloud Point

From Table 4.24 the cloud point which is used to determine the point where wax becomes visible in the fuel sample ranges from 1 in JAB5 to 2 in JAB25. This shows that the first indicator of cold weather operability temperature is just above the freezing point of water. Below these cloud point values, wax crystals form and might plug filters or could drop to the bottom of a storage tank so an additive is needed to prevent it. At temperatures below CP values the blends JAB5 to JAB25 can still be pumped.

4.5.2.6 .3 Cold Filter Plugging Point

From Table 4.24 the CFPP of JAB5 is -2 while that of JAB25 is -1. The cold filter plugging point CFPP test employs rapid cooling conditions. The CFPP is therefore considered to be a more reliable indicator of low-temperature operability than CP or PP, since the fuels contain solids of sufficient size to render the engine inoperable due to fuel filter plugging once the CFPP is reached (Park *et al.*, 2008). From Table 4.26 the CFPP of JAB5 is -2 ^{o}C while that of JAB25 is -1 ^{o}C which shows that the blends can give trouble free flow in fuel system just below the freezing point of water. In certain regions this may require an additive such as *d*-limonene and derivatives to help improve low temperature operability.

4.5.3 Physicochemical and Fuel Properties of JAB Blend with *d*-limonene Additive

Table 4.25 shows the physicochemical and fuel properties of JAB20 blend with 2-10% *d*-limonene as the additives (JABLA) using American Society for Testing and Materials (ASTM) standard test methods as indicated in section 4.5.2.

Table 4.25: Physicochemical and Fuel Properties of Ethyl Esters from Algae and Jatropha fatty acids with *d*-limonene additive

JABLA Samples	Physicochemical and Fuel Properties (mean values)							
	Density (kg/m^3)	Calorific Value (MJ/Kg)	Kinematic Viscosity at 40oC (cSt)	Flash point (°C)	Cetane Index	Pour Point (°C)	CFPP (°C)	Cloud Point (°C)
JABLA 2[b]	864.9	40.33	4.339	183	63.2	-3	-1	0
JABLA 4[b]	864.5	40.35	4.219	182	63.2	-3	-1	0
JABLA 6[b]	864.7	40.33	4.204	181	63.3	-4	-1	-1
JABLA 8[b]	864.5	40.34	4.200	181	63.4	-4	-1	-1
JABLA 10[b]	864.4	40.34	4.193	180	63.4	-4	-1	-1

JABLA 2[b] - 2 % *d*-limonene additives with 98 % JAB20 FAEE, JABLA 4[b] - 4 % *d*-limonene additives with 96 % JAB20 FAEE, JABLA 6[b] - 6 % *d*-limonene additives with 94 % JAB20 FAEE, JABLA 8[b] - 8 % *d*-limonene additives with 92 % JAB20 FAEE and JABLA 10[b] - 10 % *d*-limonene additives with 90 % JAB20 FAEE.

Generally JABLA with d-limonene as additives are more suitable for a diesel engine compared to JAB blends without additives in Table 4.26.

4.5.3.1 Density

From Tables 4.25 it is observed that there is a general decrease in density with the addition of *d*-limonene as additives. The density values are lower than that of JAB20 blends. *d*-Limonene as an additive improved the quality of the biofuel because it is relates to a lower kinematic viscosity. Lower density of JABLA than JAB20 allow a larger volume of JABLA biofuel to be transported for a given mass.

4.5.3.2 Calorific value

From Tables 4.25 it is observed that there is a general increase in calorific value with the addition of 2 % and 10 % *d*-limonene as additives. The calorific values are lower than that of JAB20 blend albeit with a value of 1.

4.5.3.3 Kinematic Viscosity

From Tables 4.25 it is observed that there is a general increase in kinematic viscosity values with the addition of 2 % to 10 % *d*-limonene as additives. The kinematic viscosity values are lower than that of JAB20 blend which makes JABLA with *d*-limonene as additive better biofuel. JABLA8 which shows no phase separation has kinematic viscosity of 4.2 cSt. It has the ability to maintain uniform fuel flow to appliances with gravity flow, pumped satisfactorily and provide satisfactory atomization in the diesel engine with constant flow rate.

4.5.3.4 Flash Point

From Tables 4.25 it is observed that there is a general decrease in flash point values with the addition of 2 % to 10 % *d*-limonene as additives. The decrease may be attributed to the low flash point (73.333±0.5773 ^{o}C) of *d*-limonene (Table 4.15) and has a negative effect to JABLA with *d*-limonene as additive because it make the fuel more susceptible to catch fire when exposed to naked flame. However the flash point value of JABLA8 which shows no phase separation was 181 ^{o}C which is within the allowable values of a minimum of 130 ^{o}C (Leung *et al*., 2010).

4.5.3.5 Cetane Index

From Tables 4.25 it is observed that there is a slight increase in cetane index values with the addition of 2 % to 10 % *d*-limonene as additives from 63.2 to 63.4. The cetane index values are slightly higher than that of JAB20 blends (63.3). Cetane index is a reflection of the cetane number. Higher cetane numbers tend to raise soot emission

but to a lesser extent than viscosity (Zannis *et al*., 2007) in this case the values are almost constant so *d*-limonene additive has little effect on the performance of the biofuel JAB blend withrespect to cetane index.

4.5.3.6 Low Temperature Characteristics

4.5.3.6.1 Pour Point

From Tables 4.25 it is observed that there is a slight decrease in pour point values with the addition of 2 % to 10 % *d*-limonene as additives from -3 to -4 ^{o}C respectively. The pour point values are slightly higher that those of JAB blends (-6 to -5 ^{o}C). Therefore the JABLA blends with *d*-limonene as additive from JABLA2 to JABLA8 can be used with ease in relatively cold climates without the need of electrical heater installations in the fuel tank and pipes since JABLA10 may show phase separation.

4.5.3.6.2 Cloud Point

From Tables 4.25 it is observed that there is a slight decrease in cloud point values with the addition of 2 % to 10 % *d*-limonene as additives from 0 to -1 ^{o}C respectively. The cloud point values are slightly lower that those of JAB blends (1 to 2 ^{o}C). Therefore the JABLA blends with *d*-limonene as additive from JABLA2 to JABLA10 have indicated an improvement in cold weather operability though JABLA10 show slight immiscibility and phase separation. Below 1 ^{o}C temperature, wax crystals form and might plug filters or could drop to the bottom of a storage tank in JAB so the *d*-limonene additive is needed to prevent it.

4.5.3.6.3 Cold Filter Plugging Point

From Tables 4.25 it is observed that cold filter plugging point values with the addition of 2 % to 10 % *d*-limonene as additives remains constant at -1 ^{o}C. The cold filter plugging point values are slightly lower that those of JAB5 and JAB10 blends (-2 ^{o}C) and same as for JAB15 to JAB25 (-1 ^{o}C). Therefore the JABLA blends with *d*-limonene as additive from JABLA2 to JABLA10 have no much effect in cold weather operability of JAB. This shows that the blends can give trouble free flow in fuel system just below the freezing point of water except JABLA10 which show phase separation.

4.5.4 Physicochemical and Fuel Properties of JAB Blend with Oxygenated *d*- Limonene Additives

Table 4.26 shows the physicochemical and fuel properties of JAB20 blend with 2-10% oxygenated *d*-limonene as the additive (JABLA) using American Society for Testing and Materials (ASTM) standard test methods as indicated in section 4.5.2.

Table 4.26: Physicochemical and Fuel Properties of Ethyl Esters Blend from Algae and Jatropha Fatty Acids with Oxygenated *d*-limonene Additives

JABLA Samples	Physicochemical and Fuel Properties (mean values)							
	Density (kg/m^3)	Calorific Value (MJ/Kg)	Kinematic Viscosity at 40^{o}C (cSt)	Flash point (^{o}C)	Cetane Index	Pour Point (^{o}C)	CFPP (^{o}C)	Cloud Point (^{o}C)
JABLA 2^{c}	864.8	40.39	5.450	181	63.3	-5	-2	4
JABLA 4^{c}	865.0	40.40	5.451	181	63.4	-5	-2	3
JABLA 6^{c}	865.2	40.40	5.450	182	63.4	-6	-3	3
JABLA 8^{c}	865.3	40.41	5.454	182	63.5	-6	-3	4
JABLA 10^{c}	865.9	40.52	5.443	182	63.5	-7	-3	3

JABLA 2^{c} - 2 % oxygenated *d*-limonene additives with 98 % JAB20 FAEE, JABLA 4^{c} - 4 % oxygenated *d*-limonene additives with 96 % JAB20 FAEE, JABLA 6^{c} - 6 % oxygenated *d*-limonene additives with 94 % JAB20 FAEE, JABLA 8^{c} - 8 % oxygenated *d*-limonene additives with 92 % JAB20 FAEE and JABLA 10^{c} - 10 % oxygenated *d*-limonene additives with 90 % JAB20 FAEE.

Generally JABLA with oxygenated *d*-limonene as additives are more suitable for a diesel engine compared to JAB blends without additives in Table 4.24.

4.5.4.1 Density

From Tables 4.26 it is observed that there is a general increase in density with the addition of 2-10 % oxygenated *d*-limonene as additives. This may be attributed to addition of compounds with oxygen such as the 1,2- limonene epoxide, 8,9-limonene epoxide, 1,2,8,9- limonene epoxide, carvone, carveol and trans- carveyl ethanoate which add to the mass of the components in the blend. The density values are generally lower than that of JAB20 blends. Oxygenated *d*-Limonene as additives improved the quality of the biofuel because it is related to a lower kinematic viscosity. Lower density of JABLA than JAB20 allow a larger volume of JABLA biofuel to be transported for a given mass.

4.5.4.2 Calorific value

From Tables 4.26 it is observed that there is a general increase in calorific value with the addition of 2 % to 10 % oxygenated *d*-limonene as additives from 40.39 to 40.52 MJ/Kg respectively. The calorific values are lower than that of JAB20 blend which may be attributed to replacement of some FAEE with shorter molecular compounds with reduction of the number of carbon and hydrogen. However the presence of oxygenated compounds reduce the amount of soot emitted making JABLA more environmentally friendly than JAB20 because there are less unburnt fuel that get exhausted into the crankcase (Núbia *et al.*, 2007).

4.5.4.3 Kinematic Viscosity

From Tables 4.26 it is observed that kinematic viscosity values with the addition of 2 % to 10 % oxygenated *d*-limonene as additives remain almost constant. The kinematic viscosity values are higher than that of JAB20 blend which makes JABLA

with oxygenated *d*-limonene as additive become a more viscous biofuel. JABLA8 which shows no phase separation has kinematic viscosity of 5.454 cSt. It has the ability to maintain uniform fuel flow to appliances with gravity flow, pumped satisfactorily and provide satisfactory atomization in the diesel engine with constant flow rate because it is within the limits of ASTM D6751 standard of 1.9-6.0 cSt (Leung *et al*., 2010).

4.5.4.4 Flash Point

From Tables 4.26 it is observed that there is a general increase in flash point values with the addition of 2 % to 10 % oxygenated *d*-limonene as additives. The increase may be attributed to the higher flash point (76.333±1.1547 ^{o}C) of oxygenated *d*-limonene (Table 4.15) and has a positive effect to JABLA with oxygenated *d*-limonene as additive because it make the fuel less susceptible to catch fire when exposed to naked flame. However the flash point value of JABLA8 which shows no phase separation was 182 ^{o}C which is within the allowable values of a minimum of 130 ^{o}C (Leung *et al*., 2010).

4.5.4.5 Cetane Index

From Tables 4.26 it was observed that there is a slight increase in cetane index values with the addition of 2 % to 10 % oxygenated *d*-limonene as additives from 63.3 to 63.5. The cetane index values are slightly higher than that of JAB20 blends (63.3). Cetane index is a reflection of the cetane number. Higher cetane numbers tend to raise soot emission but to a lesser extent than viscosity (Zannis *et al*., 2007) in this case the values show that oxygenated *d*-limonene additive has some positive effect on the performance of the biofuel JAB blend with respect to cetane index.

4.5.4.6 Low Temperature Characteristics

4.5.4.6.1 Pour Point

From Tables 4.26 it was observed that there is a slight decrease in pour point values with the addition of 2 % to 10 % oxygenated *d*-limonene as additives from -5 to -7 ^{o}C respectively. The pour point values are slightly higher that those of JAB blends (-6 to -5 ^{o}C). Therefore the JABLA blends with oxygenated *d*-limonene as additive from JABLA2 to JABLA8 can be used with ease in relatively cold climates without the need of electrical heater installations in the fuel tank and pipes since JABLA10 may show slight immiscibility and phase separation and may be of little use (Fernando and Hanna, 2004).

4.5.4.6.2 Cloud Point

From Tables 4.26 it was observed that there is a slight decrease in cloud point values with the addition of 2 % to 10 % oxygenated *d*-limonene as additives from 4 to 3 ^{o}C respectively. The cloud point values are slightly higher that that of JAB 20 blend (1 ^{o}C). Therefore the JABLA blends with oxygenated *d*-limonene as additive from JABLA2 to JABLA10 have indicated a decline in cold weather operability. JABLA10 show slight immiscibility and phase separation. Below 1 ^{o}C temperature, wax crystals form and might plug filters or could drop to the bottom of a storage tank in JAB so the oxygenated *d*-limonene additive though needed for other improvement of other parameters should be used in low quantities.

4.5.4.6.3 Cold Filter Plugging Point

From Tables 4.26 it was observed that cold filter plugging point values with the addition of 2 % to 10 % oxygenated *d*-limonene as additives decrease from -2 to -3 ^{o}C. The cold filter plugging point values are slightly lower than that of JAB20 blend (-1 ^{o}C). Therefore the JABLA blends with *d*-limonene as additive from JABLA2 to

JABLA10 have some effect in cold weather operability of JAB. This shows that the blends can give trouble free flow in fuel system just below the freezing point of water except JABLA10 which show slight immiscibility and phase separation.

4.5.5 Physicochemical and Fuel properties of JAB Blend with hydrogenated *d*-limonene additives

Table 4.27 shows the physicochemical and fuel properties of JAB20 blend with 2-10% hydrogenated *d*-limonene as the additive (JABLA) using American Society for Testing and Materials (ASTM) standard test methods as indicated in section 4.5.2.

Table 4.27: Physicochemical and Fuel Properties of Ethyl Esters from Algae and Jatropha fatty acids and hydrogenated *d*-limonene derivatives

JABLA Samples	Physicochemical and Fuel Properties (mean values)							
	Density (kg/m^3)	Calorific Value (MJ/Mol)	Kinematic Viscosity at 40°C (cSt)	Flash point (°C)	Cetane Index	Pour Point (°C)	CFPP (°C)	Cloud Point (°C)
JABLA 2^d	864.9	41.37	4.782	183	63.3	-6	-2	3
JABLA 4^d	864.8	41.34	4.820	182	63.2	-5	-1	2
JABLA 6^d	864.8	41.30	4.968	182	64.1	-5	-1	2
JABLA 8^d	864.7	41.28	5.146	181	64.1	-4	0	2
JABLA 10^d	864.6	41.25	5.149	181	64.1	-4	-1	1

JABLA 2^d - 2 % hydrogenated *d*-limonene additives with 98 % JAB20 FAEE, JABLA 4^d - 4 % hydrogenated *d*-limonene additives with 96 % JAB20 FAEE, JABLA 6^d - 6 % hydrogenated *d*-limonene additives with 94 % JAB20 FAEE, JABLA 8^d - 8 % hydrogenated *d*-limonene additives with 92 % JAB20 FAEE and JABLA 10^d - 10 % hydrogenated *d*-limonene additives with 90 % JAB20 FAEE.

Generally JABLA with hydrogenated *d*-limonene as additives are more suitable for a diesel engine compared to JAB blends without additives in Table 4.24.

4.5.5.1 Density

From Tables 4.27 it was observed that there is a general decrease in density with the addition of 2-10 % hydrogenated *d*-limonene as additives from 864.9 to 864.6 kg/m^3. This may be attributed to addition of saturated compounds such as (S)-1-methyl -4-(1-

methylethyl)cyclohexane (22), (R)-1-methyl-4-(1-methylethyl)cyclohexane (23), (S)-1-methylene-4-(1-methylethyl) cyclohexane (24), (R)-1-methylene -4-(1-methylethyl)cyclohexane (25) which tend to reduce the mass of the components in the blend. The density values are generally lower than that of JAB20 blends (865.2 kg/m^3). Hydrogenated *d*-Limonene as additives improved the quality of the biofuel because lower density of JABLA than JAB20 allow a larger volume of JABLA biofuel to be transported for a given mass (ASTM, 2006).

4.5.5.2 Calorific value

From Tables 4.27 it was observed that there is a general decrease in calorific value with the addition of 2 % to 10 % hydrogenated *d*-limonene as additives from 41.37 to 41.25 MJ/Kg respectively. The calorific values are almost the same as that of JAB20 blend (41.34 MJ/Kg) which may be attributed to replacement of some bulky FAEE with shorter molecular compounds with carbon and hydrogen atoms. In addition the presence of saturated hydrogenated compounds reduce the amount of soot emitted making JABLA more environmentally friendly than JAB20 because there are less unburnt fuel that get exhausted into the crankcase (Núbia *et al.*, 2007).

4.5.5.3 Kinematic Viscosity

From Tables 4.27 it was observed that kinematic viscosity values with the addition of 2 % to 10 % hydrogenated *d*-limonene as additives increases from 4.782 to 5.149 cSt respectively. The kinematic viscosity values are higher than that of JAB20 blend (4.783 cSt) which make JABLA with hydrogenated *d*-limonene as additive become a more viscous biofuel. JABLA8 which shows no phase separation has kinematic viscosity of 5.146 cSt. It has the ability to maintain uniform fuel flow to appliances with gravity flow, pumped satisfactorily and provide satisfactory atomization in the

diesel engine with constant flow rate because it is within the limits of ASTM D6751 standard of 1.9-6.0 cSt (Leung *et al*., 2010).

4.5.5.4 Flash Point

From Tables 4.27 it was observed that there is a general decrease in flash point values with the addition of 2 % to 10 % hydrogenated *d*-limonene as additives from 183 to 181 ^{o}C. The decrease may be attributed to the lower flash point (74.333±0.4714 ^{o}C) of hydrogenated *d*-limonene (Table 4.17) and has a negative effect to JABLA with hydogenated *d*-limonene as additive because it make the fuel more susceptible to catch fire when exposed to naked flame. However the flash point value of JABLA8 which shows no phase separation was 181 ^{o}C which is within the allowable values of a minimum of 130 ^{o}C (Leung *et al*., 2010).

4.5.5.5 Cetane Index

From Tables 4.27 it was observed that there is a slight increase in cetane index values with the addition of 2 % to 10 % hydrogenated *d*-limonene as additives from 63.3 to 64.1. The cetane index values are slightly higher than that of JAB20 blends which is 63.3. Cetane index is a reflection of the cetane number. Higher cetane numbers tend to raise soot emission but the advantage is that it helps cold engines start quicker, significantly improves combustion efficiency, and reduces harmful emissions. In this case the values show that hydrogenated *d*-limonene additive has some positive effect on the performance of the biofuel JAB blend with respect to cetane index.

4.5.5.6 Low Temperature Characteristics

4.5.5.6.1 Pour Point

From Tables 4.27 it was observed that there is a slight increase in pour point values with the addition of 2 % to 10 % hydrogenated *d*-limonene as additives from -6 to -4 ^{o}C respectively. The pour point values are slightly higher that those of JAB 20 blend

which is -6 ^{o}C except for JABLA2. JABLA blends with hydrogenated *d*-limonene as additive from JABLA2 to JABLA8 though with higher pour point values can be used with ease in relatively cold climates without the need of electrical heater installation in the fuel tank and pipes. JABLA10 may show immiscibility and phase separation and may be of little use (Fernando and Hanna, 2004).

4.5.5.6.2 Cloud Point

From Tables 4.27 it was observed that there is a slight decrease in cloud point values with the addition of 2 % to 10 % hydrogenated *d*-limonene as additives from 3 to 1 ^{o}C respectively. The cloud point values are slightly higher that that of JAB 20 blend (1 ^{o}C) except JABLA10 which has same value. This may be attributed to presence of exocyclic double bonds in (S)-1-methylene-4-(1-methylethyl) cyclohexane (24), (R)-1-methylene -4-(1-methylethyl) cyclohexane (25) which tend to be readily autoxidised and polymerised to form waxes (Monteiro and Veloso, 2004). Therefore the JABLA blends with hydrogenated *d*-limonene as additive from JABLA2 to JABLA8 have indicated a decline in cold weather operability. JABLA10 show immiscibility and phase separation. Below 1 ^{o}C temperature, wax crystals form and might plug filters or could drop to the bottom of a storage tank in JAB so the hydrogenated *d*-limonene additive though needed for other improvement of other parameters should be used in low quantities.

4.5.5.6.3 Cold Filter Plugging Point

From Tables 4.27 it was observed that cold filter plugging point values with the addition of 2 % to 10 % hydrogenated *d*-limonene as additives increase from -2 to 0 ^{o}C. The cold filter plugging point values are slightly lower than that of JAB20 blend (-1 ^{o}C) except for JABLA8. Therefore the JABLA blends with hydrogenated *d*-limonene as additive have no much effect in cold weather operability of JAB except

JABLA2. This shows that the blends can give trouble free flow in fuel system just below the freezing point of water (Park *et al*., 2008) except JABLA8 with a value of 0 ^{o}C and JABLA10 which show immiscibility and phase separation.

4.5.6 GC-MS Spectrum of Petroleum diesel

Figure 4.17 shows the GC spectrum of petroleum diesel sample from Jomvu Total Petrol Station.

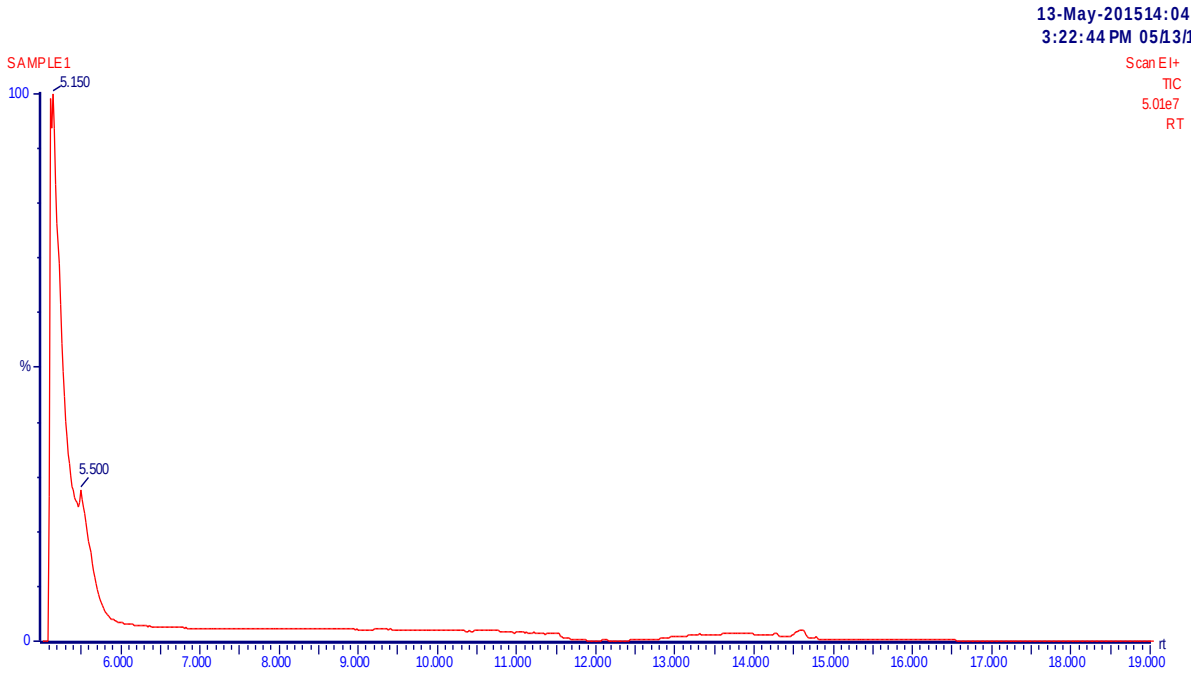

Figure 4.17: GC-MS spectrum of petrodiesel

From Figure 4.17 two main peaks at RT 5.150 and 5.500 min were obtained for dodecane with mass spectra major peaks m/z 41,43,57,71,85,170 and tetradecane with mass spectra major peaks m/z 29,41,43,55,57,71,85,198 respectively. This spectrum is characteristic to long aliphatic and cyclic alkanes with carbon numbers in the range C_{10} – C_{20}. A common phenomenon in GC-MS of fuels is that two or more GC peaks have very similar or even identical mass spectra although different retention times and different chemical nature (Song *et al*., 2011).

4.5.7 FTIR Spectrum of Petroleum diesel

Figure 4.18 shows FTIR spectrum of petroleum diesel sample from Jomvu Total Petrol Station.

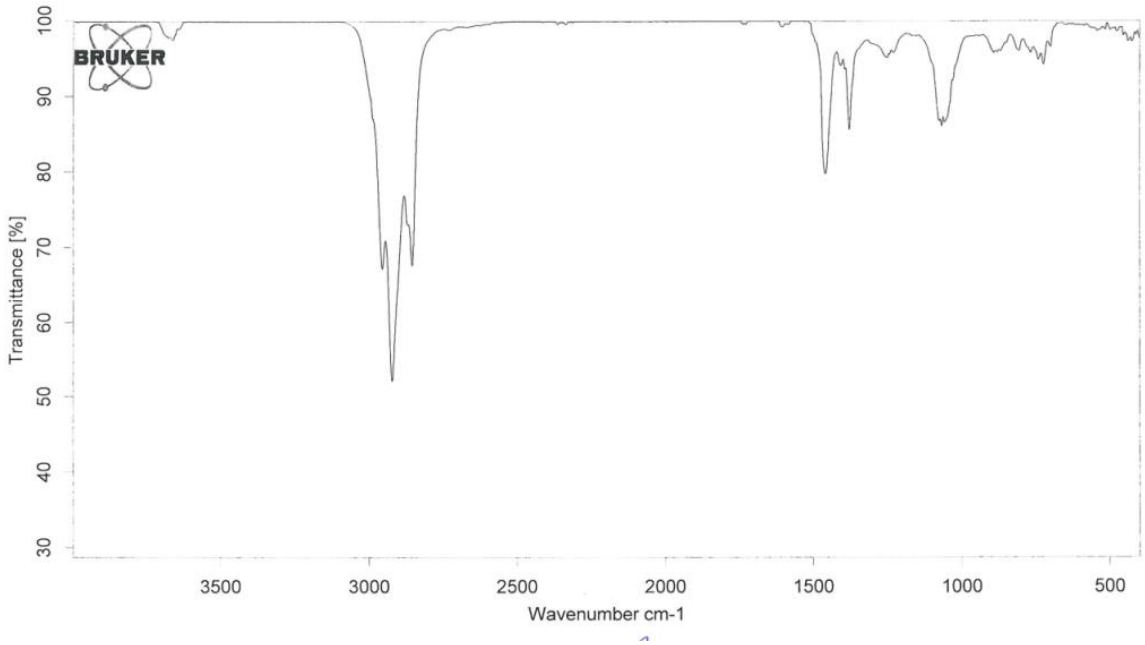

Figure 4.20: FTIR spectrum of petrodiesel

From Figure 4.18 major peaks detected were 3000-2850cm^{-1} from CH_3, CH_2 and CH stretching, 3100-3000 cm^{-1} from =CH_2 and =C-H or C-H of arenes, 1470-1450 cm^{-1} from CH_3 deformations and 725-720 cm^{-1} for CH_2 bending. This shows that the petrodiesel contained a mixture of hydrocarbon compounds though may have contained additives.

4.5.8 Physicochemical and Fuel Properties of Petroleum Diesel

Table 4.28 shows the physicochemical and fuel properties of petroleum diesel obtained from Jomvu Total Petrol Station, Likoni Shell Local Dealer, Bamburi National Oil Local Dealer, Kisauni Engen Local Dealer and Mombasa CBD National Oil Petroleum station using American Society for Testing and Materials (ASTM) standard test methods as indicated in section 4.5.2. In addition Table 4.30 includes

standard allowable values for quality petroleum diesel using ASTM D975 (ASTM, 2007b).

Table 4.28: Physicochemical and Fuel Properties of Petroleum Diesel

Fossil diesel sample	Density at 20° c (Kg/m^3)	Calorific Value (MJ/Kg)	Flashpoint (°c)	Kinematic Viscosity (cSt)	Cetane index	Pour Point (oC)	CFPP (°C)	Cloud Point (°C)
FD1	839±0.001	43.378±0	76.0±0.100	3.024±0.001	52±0	-15±0	-6±0	-8±0
FD2	837±0.001	43.109±0	71.0±0.000	3.097±0.001	54±0	-14±0	-5±0	-8±0
FD3	835±0.000	43.213±0	70.0±0.000	3.095±0.001	53±0	-14±0	-5±0	-7±0
FD4	839±0.000	43.377±0	76.0±0.058	2.938±0.001	51±0	-15±0	-6±0	-8±0
FD5	840±0.001	43.305±0	63.0±0.635	2.911±0.001	50±0	-14±0	-5±0	-7±0
ASTM D975	760-850	43.1	52 Min	1.9 Min 4.1 Max	40 min	Varies	Varies	8.9 max

FD1, Jomvu Total Petrol Station FD2 - Likoni Shell Local Dealer, FD3 - Bamburi National Oil Local Dealer, FD4, Kisauni Engen Local Dealer, FD5 - CBD National Oil Petroleum station

From Table 4.28 the physicochemical and fuel properties of petroleum diesel shows that all the quality parameters agree with the standard quality petrodiesel. The ASTM D975 standard (ASTM, 2007b) requires that the cold temperature characteristics though varies should be stated in order to show the cold weatherability of the fuel.

4.5.9 Petroleum Diesel Boiling Points and % Distillate

4.5.9.1 Petroleum Diesel Boiling Points and % Distillate Curves

Figure 4.19 to Figure 4.23 shows the boiling points and % distillate curves of petroleum diesel samples FD1 from Jomvu Total Petrol Station, FD2 from Likoni Shell Local Dealer, FD3 from Bamburi National Oil Local Dealer, FD4 from Kisauni Engen Local Dealer and FD5 from CBD National Oil Petroleum station.

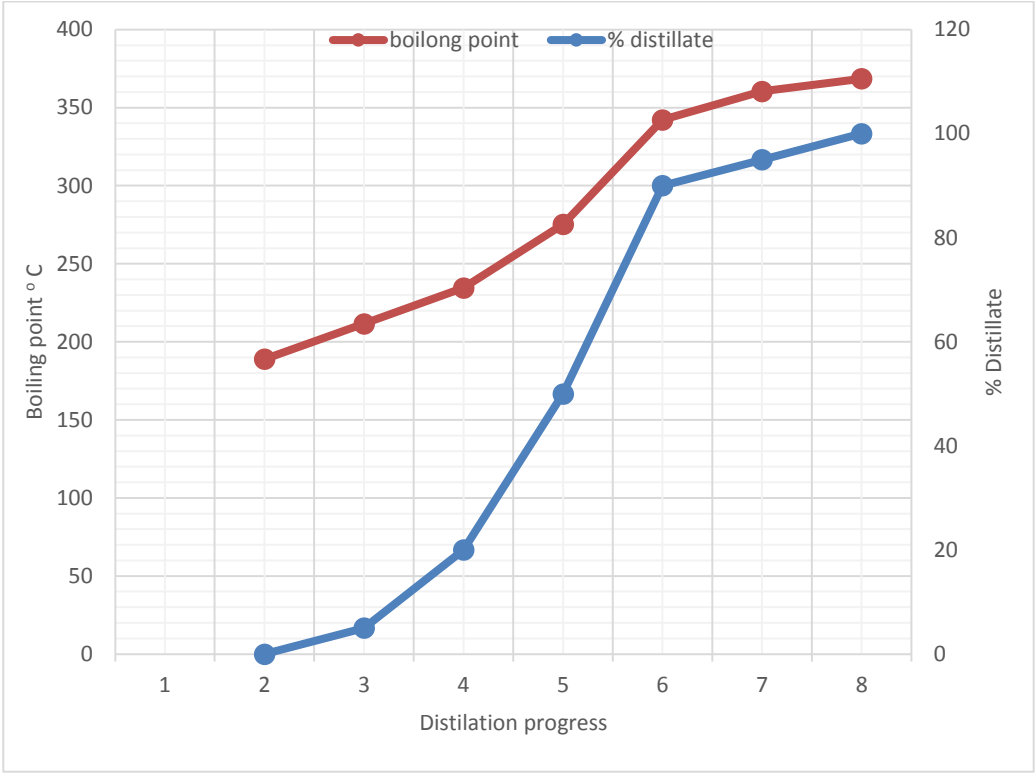

.

Figure 4.19: Sample FD1 distillation chart ASTM D 86

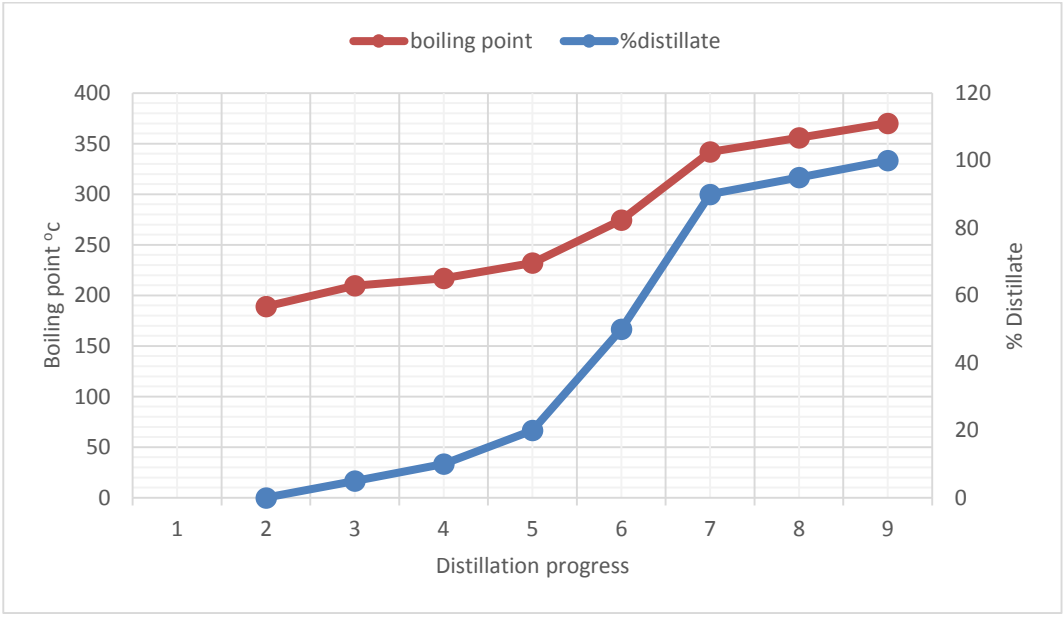

Figure 4.20: Sample FD2 distillation chart ASTM D86

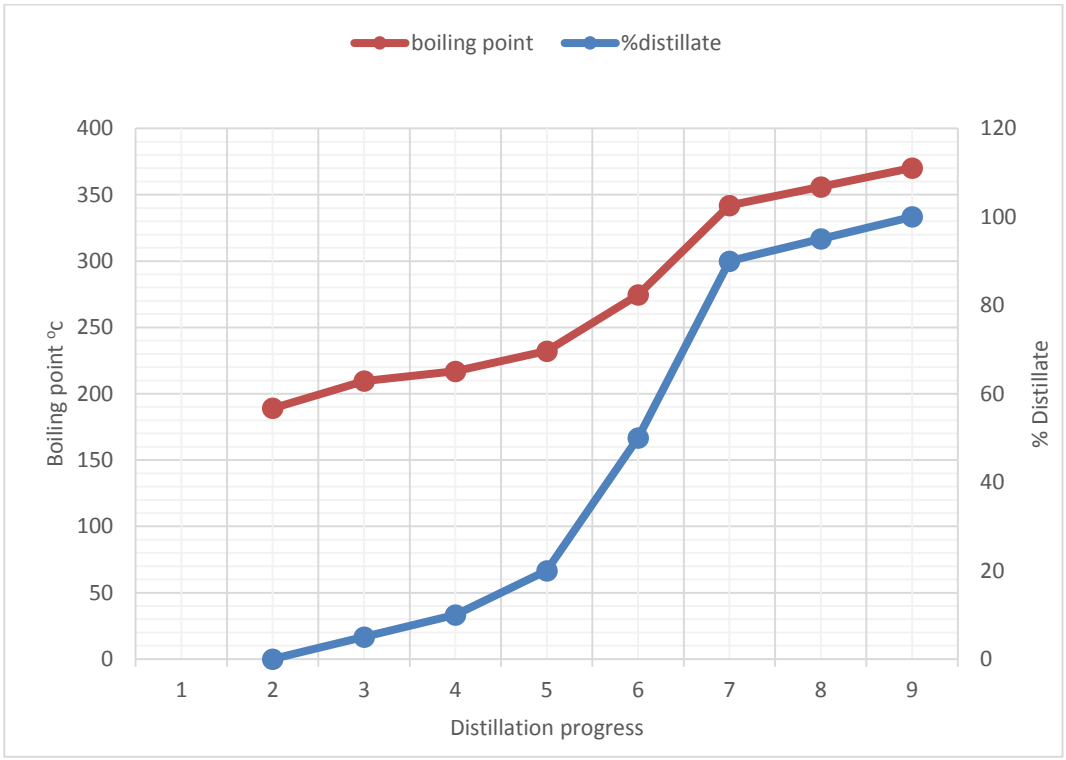

Figure 4.21: Sample FD3 distillation chart ASTM D86

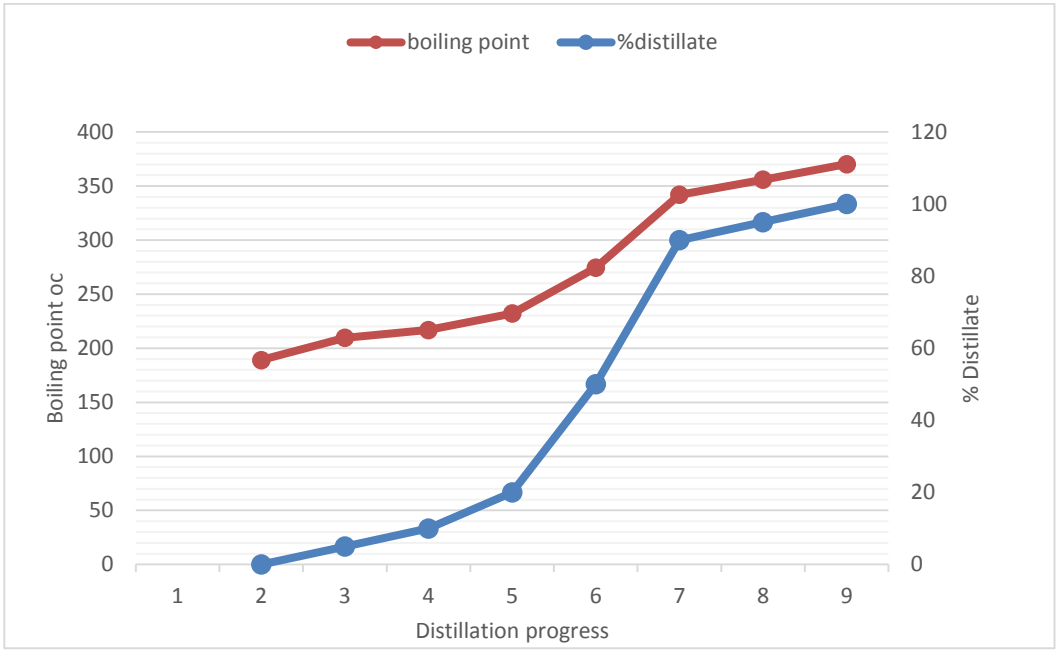

Figure 4.22: Sample FD4 distillation chart ASTM D86

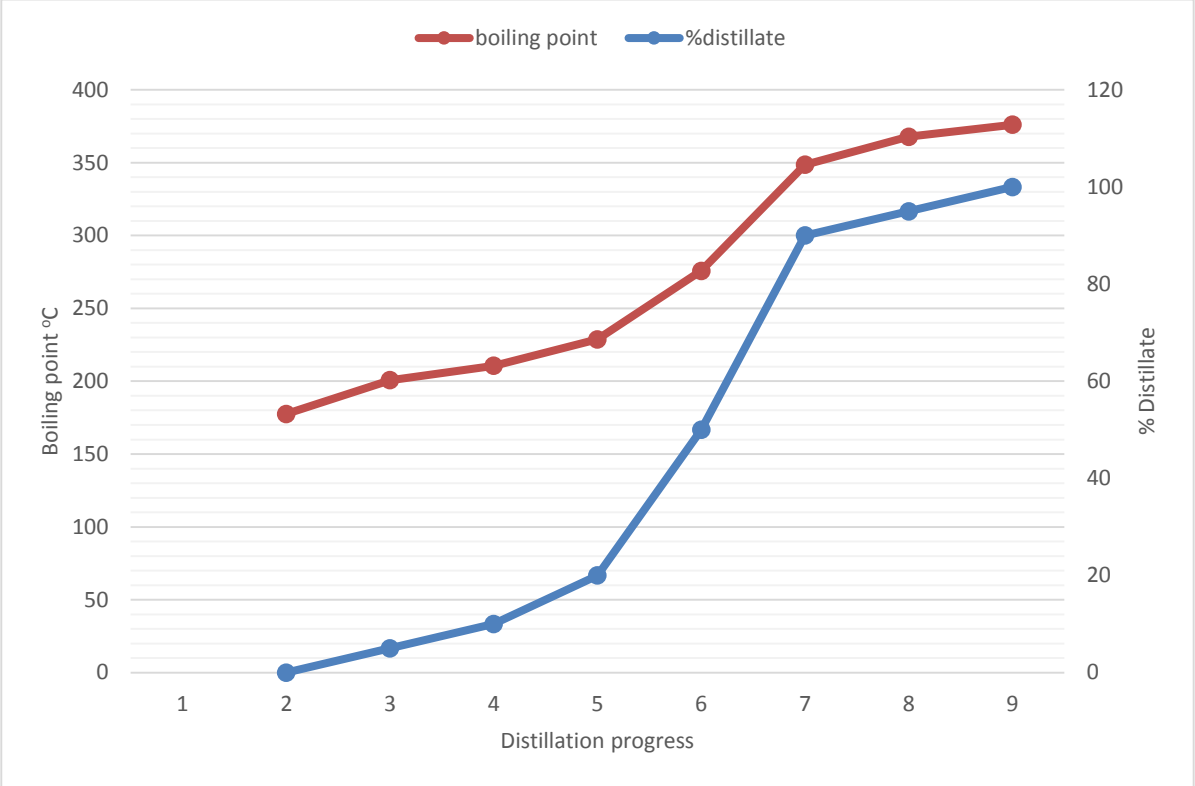

Figure 4.23: Sample from FD5 distillation chart ASTM D86

According to ASTM D975 (ASTM, 2007b) Distillation temperature, at 90% minimum 282°C and maximum 338°C. Figure 4.21 showed that the distillation temperature at 90% was 342.2°C which suggests adulteration. Figure 4.20, Figure 4.21 and Figure 4.22 showed that the distillation temperature at 90% was 342°C which also suggest adulteration. Figure 4.23 showed that the distillation temperature at 90% was 348.6°C which also suggest adulteration or tail-end volatility adjustment for fuel economy and minimisation of volatile organic compound (VOC) exhausts emission. The distillation characteristics of hydrocarbons have an important effect on their safety and performance. The various ranges of a distillation profile have been correlated with specific aspect of diesel performance. Front-end volatility is adjusted to provide easy cold starting, easy hot starting, freedom from vapour lock, and low evaporation and running-loss emissions. Mid-range volatility is adjusted to provide

rapid warm-up and smooth running, good short-trip fuel economy, good power and acceleration, and protection against carburettor icing and hot stalling. Tail-end volatility is adjusted to provide good fuel economy after engine warm-up, freedom from engine deposits, minimal fuel dilution of crankcase oil, and minimal volatile organic compound (VOC) exhausts emission (Al-Ghouti *et al*., 2008).

4.5.9.2 Biofuel Boiling Points and % Distillate

Table 4.29 and Table 4.30 show boiling points and % distillates of biofuels JAB and JABLA respectively.

Table 4.29: Distillation Temperature of JAB

Tests	1st run	2nd run	3rd run	Means ± SE	ASTM D 6751
Initial Distillation BP °C (I.B.P)	268.2	269.8	270.4	269.5±1.1	268.5±3.2
10% Distillation BP °C	316.3	314.7	315.2	315.4±0.8	315.0±1.2
50% Distillation BP °C	337.8	338.2	339.6	338.5±0.9	337.0±0.8
90% Distillation BP °C	355.0	354.7	355.2	355.0±0.3	360 max
Final Distillation BP °C (F.B.P)	369.7	369.2	368.8	369.2±0.5	-

Table 4.30: Distillation Temperatures of JABLA

Tests	JAB + *d*-limonene	JAB + oxygenated *d*-limonene	JAB + hydrogenated *d*-limonene	ASTM D 6751
Initial Distillation BP °C (I.B.P)	175.2±0.6	174.9±1.1	174.8±1.4	268.5±3.2
10% Distillation BP °C	220.1±0.8	219.7±1.0	220.8±0.9	315.0±1.2
50% Distillation BP °C	280.9±0.4	281.2±0.6	280.3±0.7	337.0±0.8
90% Distillation BP °C	345.0±0.2	345.3±0.8	345.7±1.1	360 max
Final Distillation BP °C (F.B.P)	365.1±0.1	365.2±0.5	365.5±0.9	-

According to ASTM D 6751 standard for biofuel the distillation temperatures at initial, 10 %, 50 % should be reported and that the distillation temperature at 90 % should be a maximum 360 ^{o}C. Table 4.29 and Table 4.30 showed distillation temperature at 90% as 355.0±0.3 ^{o}C for JAB and 345.0±0.2 ^{o}C, 345.3±0.8 ^{o}C and 345.7±1.1 ^{o}C for JABLA with *d*-limonene, oxygenated *d*-limonene and hydrogenated *d*-limonene respectively. These distillation temperatures are within the expected standard values at 90 % according to ASTM D 6751 of maximum 360 ^{o}C (Leung *et al*., 2010). This shows that the additives have an effect in distillation characteristics of JAB20 in that they reduce the distillation boiling point temperatures. JABLA8 containing 8% additives from *d*-limonene, oxygenated *d*-limonene and hydrogenated *d*-limonene can be used in the market directly without any engine modifications.

4.5.10 Microbial Analysis

4.5.10.1 Inoculation of the test isolates

Test strains of bacteria *Pseudomonas aeroginosa* was separately inoculated in Nutrient Broth then incubated at 37 ^{o}C for 24 hours aerobically in the Astra incubator. The nutrient broth turned turbid. *Candida albicans* isolates were inoculated on Sabouroud dextrose agar at 25 ^{o}C for 48 hours with growth observation done after every 24 hours. Creamy white colonies with smooth surface and characteristic yeast odour were observed.

4.5.10.2 Antimicrobial assay

Table 4.27 shows the results of antimicrobial assay done on JAB20 and JABLA samples using paper disc-diffusion method, expressed by diameter mean±SD (mm) of inhibition zone which include the disc diameter of 6 mm (Mith *et al*., 2014). All tests were performed in triplicates.

Table 4.31: Antimicrobial activity of JAB and JABLA

	Sample Inhibition zone in diameter (mm)			
Microorganism	JAB20	JABLA8[b]	JABLA8[c]	JABLA8[d]
Pseudomonas aeroginosa (ATCC 25923)	6.03 ± 0.52 [x]	6.20 ± 0.40 [y]	23.20 ± 0.80 [z]	8.56±0.94 [w]
Candida albicans (ATCC 70231)	6.05± 0.20 [x]	7.05± 0.20 [y]	25.30± 0.30 [z]	8.20± 0.60 [w]

JABLA8[b] JAB20 with 8% *d*-limonene, JABLA8[c] JAB20 with 8% oxygenated *d*-limonene and JABLA8[d] JAB20 with 8% hydrogenated *d*-limonene

From Table 4.31 values followed by the different letter (x, y, z and w) under the same row are significantly different ($p < 0.05$). JABLA8[c] with 8% oxygenated limonene derivatives showed the largest zone of inhibition and JAB20 the least zone of inhibition as shown in plate 4.3 and plate 4.4 below. This shows that JABLA with 8 % oxygenated limonene derivatives is best suited for longer storage life of JAB20 from reduced microbial attack. Some biofuels are degraded by microorganisms at a rate comparable to that of sugar (Blin *et al.*, 2007). Such degradation might lead to undesired fuel properties such as acid formation, and particle formation in the biofuel which in turn may affect cold temperature characteristics.

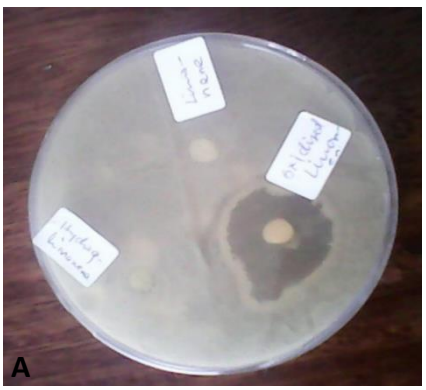

Plate 4.3: Zones of inhibition by crude *d*-limonene, hydrogenated and oxygenated *d*-limonene derivatives

Plate 4.4: Zones of inhibition by JABLA with 8 % *d*-limonene, hydrogenated and oxygenated *d*-limonene derivatives

4.6 Statistical Comparison of JOFAEE, JAB, JABLA and Petrodiesel Properties

The variations in the physicochemical and fuel properties with the % amount of various additives added to *J. curcas* and *R. grande* biofuel blends is followed using general linear model techniques, t tests (Paired sample t-tests, Independent sample t-tests), one-way analysis of variance (ANOVA) and post-hoc comparisons . In this research differences between groups % algae JAB, % *d*-limonene JABLA[b], % oxygenated *d*-limonene JABLA[c] and % hydrogenated *d*-limonene JABLA[d] are of much interest , as well as the strength of the relationship between variables.

4.6.1 JOFAEE Control and JAB Experimental t-Tests

Table 4.32 and Table 4.33 show a comparison of physicochemical and fuel properties between control 0% algae JOFAEE mean values (Table 4.25) and experimental = 5, 10, 15, 20 and 25% algae JAB (Table 4.26).

Table 4.32: Physicochemical and fuel properties of JOFAEE Control and JAB Experimental

Sample	Percent. algae	density	Cal. value	Kin. Visc	Flash point	Cet. index	Pour point	Cloud point	CFPP
JOFAEE	0	874.56	40.89	5.41	182.6	64.1	-9	-3	-2
JAB 5	5	864.5	41.38	4.76	181.0	63.0	-6	1	-2
JAB 10	10	865.0	41.35	4.77	182.0	63.3	-6	1	-2
JAB 15	15	865.1	41.35	4.78	182.0	63.2	-6	2	-1
JAB 20	20	865.2	41.34	4.78	183.0	63.3	-6	1	-1
JAB 25	25	865.9	41.34	4.80	183.0	63.3	-5	2	-1

Table 4.33: One sample t- test values of Physicochemical and fuel properties of JOFAEE Control and JAB Experimental

Property	One-Sample t-Test				
	Test Value = 874.56				
	t	Sig. (2-tailed)	Mean Difference	95% Confidence Interval of the Difference	
				Lower	Upper
Density	-41.877	0.001	-9.42000	-10.0445	-8.7955
Calorific value	62.870	0.001	0.46200	0.4416	0.4824
Kinematic viscosity	-100.074	0.001	-0.63340	0-.6510	-0.6158
Flash point	-1.069	0.345	-0.40000	-1.4389	0.6389
Cetane index	2.058	0.109	0.12000	-0.0419	0.2819
Pour point	16.000	0.001	3.20000	2.6447	3.7553
Cloud point	17.963	0.001	4.40000	3.7199	5.0801
CFPP	2.449	0.070	0.60000	-0.0801	1.2801

4.6.1.1 Density

From Table 4.32 and Table 4.33 the density values of JAB show significant difference with the JOFAEE density at 95% confidence ($p = 0.001$). The composition and profile of algae fatty acid ethyl esters biodiesel have lower densities which when blended with JOFAEE cause an overall lowering of density. The density of vegetable oils which are the source of the fatty acid ethyl esters is related to the fatty acid

composition most of which are saturated and respective critical properties for each of the oils (Pratas *et al*., 2011).

4.6.1.2 Calorific value

From Table 4.32 and Table 4.33 the calorific value of JAB is significantly different from that of JOFAE at 95% confidence level (p = 0.001). The energy content of JAB is closer to that of diesel fuel than that of JOFAEE to diesel fuel.

4.6.1.3 Kinematic viscosity

From Table 4.32 and Table 4.33 the Kinematic viscosity of JAB is significantly different from that of JOFAEE at 95% confidence level (p = 0.001). This was brought about by the lower kinematic viscosity of AOFAEE than that of JOFAEE.

4.6.1.4 Flash point

From Table 4.32 and Table 4.33 the Flash point of JAB is not significantly different from that of JOFAEE at 95% confidence level (p = 0.345). JAB fuel which has a higher flash point than JOFAEE can prevent auto ignition and fire hazard at high temperature during transportation and storage periods. Hence, the higher the safety during handling, transportation, and storage.

4.6.1.5 Cetane index

From Table 4.32 and Table 4.33 the cetane index of JAB is not significantly different from that of JOFAE at 95% confidence level (p = 0.109). There is a decreasing cetane response with increasing unsaturation for biofuels, algae FAEE contain more of the saturated fatty acids that add to those of JOFAEE though the change is not significant. JAB 20 has a higher cetane index than JAB 5.

4.6.1.6 Pour point

From Table 4.32 and Table 4.33 the Pour point of JAB is significantly different from that of JOFAE at 95% confidence level (p = 0.001). The pour point of biofuel is the

lowest temperature at which it loses its fuel properties and semi-solidifies. This semi solidification is attributed to the occurrence of high unsaturated compounds content such as C18:2 and C18:3 even in low quantities. AOFAEE contained FAEE at Rt=10.943, Rt=11.051 and Rt=12.035 high unsaturated fatty acid moieties (Figure 4.15).

4.6.1.7 Cloud point

From Table 4.32 and Table 4.33 the Cloud point of JAB is significantly different from that of JOFAEE at 95% confidence level ($p = 0.001$). CP is a measure of cold weather operability which are higher in JAB than in JOFAEE. This could have been caused by presence of wax crystals in algae FAEE resulting from auto-oxidation of small quantities of unsaturated fatty acid moeities.

4.6.1.8 Cold filter plug point

From Table 4.32 and Table 4.33 the Cold filter plug point of JAB is not significantly different from that of JOFAEE at 95% confidence level ($p = 0.070$). The blending of AOFAEE with JOFAEE does not affect the cold filter plug point. For significant difference at 95% confidence level $p < 0.05$.

4.6.2 Paired Samples t-Test Experimental JAB and Control JOFAEE

Table 4.34 shows the results of paired samples t-test of experimental JAB and the control JOFAEE. Experimental JAB contains 5, 10, 15, 20 and 25 % AOFAEE in 95, 90, 85, 80 and 75 % JOFAEE while the control contains 0 % AOFAEE in 100 % JOFAEE.

Table 4.34: Paired samples t-test of experimental JAB and the control JOFAEE

Parameter	Paired Differences					t	Sig. (2-tailed)
	Mean	Std. Dev.	Std. Error Mean	95% Confidence Interval of the Difference Lower	Upper		
Density 1 - Density2	-9.420	10.826	4.841	-22.862	4.022	-1.946	0.124
Cal. value 1 – Cal. value 2	0.466	0.316	0.141	0.073	0.859	3.295	0.030
Kinematic 1 – kinematic 2	-0.632	0.024	0.011	-0.662	-0.602	-58.654	0.001
Flash point 1 – Flash point 2	-0.400	0.894	0.400	-1.511	0.711	-1.000	0.374
Cet. index 1 – Cet. index 2	0.120	0.460	0.206	-0.452	0.692	0.583	0.591
Pour point 1 - Pour point 2	3.000	0.707	0.316	2.122	3.878	9.487	0.001
Cloud 1 - Cloud 2	2.800	0.447	0.200	2.245	3.355	14.000	0.001
CFPP 1 – CFPP 2	0.400	0.548	0.245	-0.280	1.080	1.633	0.178

1 = Experimental 2 = Control

The paired sample t-test, sometimes called the dependent sample t-test, is a statistical procedure used to determine whether the mean difference between two sets of observations is zero the null hypothesis. From Table 4.34 this test shows that there is a confirmation that the % AO FAEE added to JOFAEE has a significant influence in physicochemical and fuel properties of the biofuel such as calorific value $p = 0.030$, kinematic viscosity $p = 0.001$, pour point $p = 0.001$ and cloud point $p = 0.001$.

4.6.3 JAB20 Control and JABLA Experimental t – Test

Table 4.35 shows a comparison of physicochemical and fuel properties between control JAB20 and experimental JABLA mean values. Control JAB20 contains 20 % AOFAEE and 80 % JOFAEE (Table 4.26) and experimental JABLA contains 2, 4, 6, 8 and 10 % *d*-limonene, oxygenated *d*-limonene and hydrogenated *d*-limonene additives to 98, 96, 94, 92 and 90 % JAB20 (Tables 4.27, 4.28 and 4.29)

Table 4.35: One sample t- test values of Physicochemical and fuel properties of JAB20 Control and JABLA experimental

	Parameters *P* values (2-tailed)							
Samples	density	Cal value	Kin. Visc	Fls point	Cet. index	CFPP	Pour point	Cloud point
JABLA[b]	0.003	<0.001	<0.001	0.035	0.969	0.374	<0.001	0.003
JABLA[c]	0.840	<0.001	<0.001	0.005	0.033	0.003	0.621	<0.001
JABLA[d]	0.001	0.208	0.071	0.033	0.092	0.969	0.033	0.034

JABLA[b] JAB20 with *d*-limonene, JABLA[c] JAB20 with oxygenated *d*-limonene and JABLA[d] JAB20 with hydrogenated *d*-limonene

4.6.3.1 Density

From Table 4.35 the density p-values of JABLA[b] ($p = 0.003$) and JABLA[d] ($p = 0.001$) show significant difference with JAB20 at 95% confidence ($p < 0.05$). The composition and profile of *d*-limonene and hydrogenated *d*-limonene derivatives have lower molecular weights which when blended with JAB cause an overall lowering of density. JABLA[c] show no significant difference ($p = 0.840$) this may be attributed to presence of oxygen with higher mass than hydrogen.

4.6.3.2 Calorific value

From Table 4.35 the calorific *p*-values of JABLA[b] ($p < 0.001$) and JABLA[c] ($p < 0.001$) show significant difference with the JAB20 at 95% confidence ($p < 0.05$). The composition and profile of *d*-limonene and oxygenated *d*-limonene derivatives have

fewer atoms that contribute to calorific value causing a slight decrease in overall calorific value when blended with JAB20. Presence of more saturated hydrogenated *d*-limonene though show no significant difference ($p = 0.028$) with JAB20 produces less soot.

4.6.3.3 Kinematic viscosity

From Table 4.35 the kinematic viscosity *p*-values of $JABLA^b$ ($p < 0.001$) and $JABLA^c$ ($p < 0.001$) show significant difference with the JAB20 at 95% confidence ($p < 0.05$). However the kinematic viscosity *p*-values of $JABLA^d$ ($p = 0.071$) shown no significant difference with the JAB20 at 95% confidence ($p < 0.05$). *d*-Limonene when blended with JAB20 cause a decrease in kinetic viscosity value which may be attributed to lower viscosity of *d*-limonene. Oxygenated *d*-limonene derivatives have higher molecular weights than *d*-limonene which may also hydrogen bond so when blended with JAB20 cause an increase in overall kinetic viscosity value. Presence of more saturated and hydrogenated compounds in $JABLA^d$ however produces more viscous biofuels than for *d*-limonene additive the reason the percentage added were kept low.

4.6.3.4 Flash point

From Table 4.35 the flash point *p*-values of $JABLA^b$ ($p = 0.035$), $JABLA^c$ ($p = 0.005$) and $JABLA^d$ ($p = 0.033$) show significant difference with the JAB20 at 95% confidence ($p < 0.05$). The composition and profile of d-limonene, oxygenated *d*-limonene and hydrogenated *d*-limonene derivatives have more volatile compounds which when blended with JAB20 also cause some lowering of flash point values. Presence of more saturated and more oxygenated compounds however produce better ignition characteristics of biofuels.

4.6.3.5 Cetane index

From Table 4.35 the cetane index *p*-values of JABLA^{c} (p = 0.033) and JABLA^{d} (p =0.092) show significant difference with the JAB20 at 95% confidence ($p < 0.05$). However *p*-values of JABLA^{b} (p = 0.969) show no significant difference with the JAB20 at 95% confidence ($p < 0.05$). The composition and profile of oxygenated *d*-limonene and hydrogenated *d*-limonene derivatives have lower molecular weight and more volatile compounds than AOFAEE and JOFAEE so when blended with JAB20 cause some lowering of density and distillation temperatures affecting cetane index values. Presence of more saturated and more oxygenated compounds than *d*-limonene needed which increase cetane index therefore producing smoother combustible JABLA biofuels than JAB20.

4.6.3.6 Pour point

From Table 4.35 the pour point *p*-values of of JABLA^{b} ($p < 0.001$) and JABLA^{d} (p =0.033) show significant difference with the JAB20 at 95% confidence ($p < 0.05$). However the pour point *p*-values of JABLA^{c} (p = 0.621) show no significant difference with the JAB20 at 95% confidence ($p < 0.05$). *d*-Limonene is unsaturated and subject to form auto-oxidation products (Monteiro and Veloso, 2004) which when blended with JAB20 cause some increase in pour point values. The composition and profile of hydrogenated *d*-limonene derivatives have saturated and unsaturated compounds. Therefore when blended with JAB20 hydrogenated *d*-limonene derivatives cause some increase in pour point values than in oxygenated *d*-limonene derivatives which show no much change in pour point values. The biofuel may require more additives to lower the pour point especially if it is to be used in countries with severe winters. However JABLA is within the limits of good flowability of biofuels from storage tanks.

4.6.3.7Cloud point

From Table 4.35 the cloud point *p*-values of JABLA^{b} (p = 0.003), JABLA^{c} (p< 0.001) and JABLA^{d} (p =0.034) show significant difference with the JAB20 at 95% confidence (p < 0.05). The composition and profile of oxygenated *d*-limonene and hydrogenated *d*-limonene derivatives have unsaturated compounds and may turn waxy on exposure to air which when blended with JAB20 cause some increase in cloud point values. However *d*-limonene cause a slight decrease in cloud point value of JAB20 that may be attributed to absence of hydrogen bonding and low cloud point value of *d*-limonene (Table 4.15). Below these cloud point values, wax crystals form and might plug filters or could drop to the bottom of a storage tank so an additive is needed to prevent it. At temperatures below CP values the blend can still be pumped because it is within the limits of good flowability of biofuels from storage tanks.

4.6.3.8 Cold filter plugging point

From Table 4.35 the cold filter plugging point *p*-values of JABLA^{b} (p = 0.374) and JABLA^{d} (p =0.969) show no significant difference with the JAB20 at 95% confidence (p < 0.05). However *p*-values of JABLA^{c} (p = 0.969) show significant difference with the JAB20 at 95% confidence (p < 0.05). *d*-Limonene cause no much change in CFPP values due to absence of hydrogen bonding and relatively similar values of CFPP values of d-limonene and JAB20 blend. The composition and profile of hydrogenated *d*-limonene derivatives have more of saturated than unsaturated compounds which when blended with JAB20 cause no significant change in cloud filter plugging point values. The CFPP test emplows rapid cooling conditions therefore generally considered to be a more reliable indicator of low temperature operability than CP or PP (Park *et al*., 2008). JABLA^{c} biofuel contain oxygenated *d*-limonene compounds which cause a decrease in CFPP to JAB20 and is within the limits of good operability

from storage tanks and through the fuel filter because it is below the freezing point of water.

4.6.4 Effect of Percentage Increase in Algae FAEE on Physicochemical and Fuel properties of JOFAEE

Table 4.36 shows test results between % AOFAEE (independent variable) and several physicochemical and fuel properties **(**dependent variables) of JOFAEE with AOFAEE blend using glm multivariate regression (Afifi *et al*., 2004). This is used to explain the effect of % increase in AOFAEE on the JOFAEE physicochemical and fuel properties.

Table 4.36: Effect of Variation in % AOFAEE on physicochemical and fuel properties of JOFAEE

Source	Dependent Variable	F	Sig.
% AOFAEE	Density	24.107	.016
	Calorific value	9.000	.058
	Kinematic viscosity	86.687	.003
	Flash point	25.000	.015
	Cetane index	3.375	.164
	Pour point	3.000	.182
	Cloud	1.500	.308
	CFPP	9.000	.058

From Table 4.36 there are significant differences in physicochemical and fuel properties as the percentage of AOFAEE added to JOFAEE increases. The properties affected are density (p = 0.016), kinematic viscosity (p = 0.003) which increases due to presence of high molecular weight FAEE in AOFAEE added to JOFAEE and flash point (p = 0.015) which reduces due to presence of more volatile compounds in AOFAEE (Figure 4.13) than in JOFAEE (Figure 4.14).

4.6.5 Effect of Percentage Increase in *d*-Limonene and Derivatives as additives on Physicochemical and Fuel Properties of 20% JAB

4.6.5.1 Test Results of % *d*-Limonene effect on Physicochemical and Fuel Properties of 20% JAB

Table 4.37 shows test results between % *d*-limonene (independent variable) and several physicochemical and fuel properties **(**dependent variables) of JABLA using glm multivariate regression. This is used to explain the effect of % increase in *d*-limonene on the JAB20 physicochemical and fuel properties.

Table 4.37: Effect of variation in % d-limonene on physicochemical and fuel properties of JAB20

Source	Dependent Variable	F	Sig. (*p* value)
% *d*-Limonene	Density	49.000	.006
	Calorific value	337.500	.001
	Kinematic viscosity	39.844	.008
	Flash point	25.000	.015
	Cetane index	10.714	.047
	Pour point	25.000	.015
	cloud	12.000	.041
	CFPP	2.455	.215

From Table 4.37 the tests for the overall mode shown under source, indicate that the model is statistically significant, regardless of the type of multivariate criteria that is used because all of the p-values are less than 0.05 except for CFPP.This confirms that % *d*-limonene additive has some effect on the physicochemical and fuel properties of JAB20.

4.6.5.2 Test Results of % Oxygenated *d*-Limonene effect on Physicochemical and Fuel Properties of 20% JAB

Table 4.38 shows test results between % oxygenated *d*-limonene (independent variable) and several physicochemical and fuel properties **(**dependent variables) of JABLA using glm multivariate regression. This is used to explain the effect of %

increase in oxygenated *d*-limonene on the JAB20 physicochemical and fuel properties.

Table 4.38: Effect of variation in % oxygenated *d*-limonene on physicochemical and fuel properties of JAB20

Source	Dependent Variable	F	Sig. (*p* value)
% Oxygenated *d*-Limonene	Density	27.985	.013
	Calorific value	4.937	.113
	Kinematic viscosity	.684	.469
	Flash point	9.000	.058
	Cetane index	25.000	.015
	Pour point	25.000	.015
	cloud	.273	.638
	CFPP	9.000	.058

From Table 4.38 the tests for the overall mode shown under source, indicate that the model is statistically significant, regardless of the type of multivariate criteria that is used because all of the p-values are less than 0.05 except for calorific value (p – 0.113), kinematic viscosity (p – 0.469), flash point (p – 0.058), cloud point (p – 0.638) and CFPP (p – 0.058).This confirms that % oxygenated *d*-limonene additives have some effect on the physicochemical and fuel properties of JAB20.

4.6.5.3 Test Results of % Hydrogenated *d*-Limonene effect on Physicochemical and Fuel Properties of 20% JAB

Table 4.39 shows test results between % hydrogenated *d*-limonene (independent variable) and several physicochemical and fuel properties **(**dependent variables) of JABLA using glm multivariate regression. This is used to explain the effect of % increase in hydrogenated *d*-limonene on the JAB20 physicochemical and fuel properties.

Table 4.39: Effect of variation in % hydrogenated *d*-limonene on physicochemical and fuel properties of JAB20

Source	Dependent Variable	F	Sig. (*p* value)
% Hydrogenated *d*-Limonene	Density	49.000	.006
	Calorific value	337.500	.001
	Kinematic viscosity	39.844	.008
	Flash point	25.000	.015
	Cetane index	10.714	.047
	Pour point	25.000	.015
	cloud	12.000	.041
	CFPP	2.455	.215

From Table 4.39 the tests for the overall mode shown under source, indicate that the model is statistically significant, regardless of the type of multivariate criteria that is used because all of the p-values are less than 0.05 except CFPP (*p* – 0.215).This confirms that % hydrogenated *d*-limonene additives have some effect on the physicochemical and fuel properties of JAB20.

4.6.6 Anova Test Results of a Comparison of Physicochemical and Fuel Properties of JABLA8 , B100 and Petrodiesel

Table 4.40 shows Anova test results of physicochemical and fuel properties of JABLA[b], JABLA[c], JABLA[d], ASTM D6751 (B100) and petroleum diesel ASTM D975 which comprise the rows.

Table 4.40: Anova Test Results of a Comparison of Physicochemical and Fuel Properties of JABLA8 , B100 and Petrodiesel

Source of Variation	SS	df	MS	F	P-value	F crit
Rows	20549.29	19	1081.541	1.459	0.110	1.665

From Table 4.40 the calculated F value is less than the F critical value and p=0.110, showing no significant difference between 8% JABLA blends and the biodiesel specifications B100 ASTM D6751 and petroleum diesel standard specifications ASTM D975. Therefore the additives can be used without engine modification.

CHAPTER FIVE

5 CONCLUSIONS AND RECOMMENDATIONS

5.1 Conclusions

From the results obtained in this research work the following conclusions are made:

5.1.1 Conclusions from Objective i

There is large amount of citrus peelings per *Citrus senensis* fruit which range from a mean of 26.821g (12.811%) in Malindi to 26.285g (13.152%) in Muheza. This usually goes to waste and can be useful in extraction of citrus oil containing *d*-limonene and release large amount of biomass.

Citrus lemoni though has larger amount of peelings per fruit which range from 56.178g (34.951%) in Muheza to 60.886g (35.330%) in Malindi than in *Citrus senensis* may require further processing because the citrus oil contain *l*-limonene in addition to d-limonene.

Citrus tangerine have the lowest amount of peelings per fruit from a mean 16.743g (22.970%) in Shimba hills to 20.851g (23.174%) in Muheza. This low amount of peelings together with presence of *l*-limonene in the citrus oil may not favour cost effective extraction of *d*-limonene.

Bioethanol from *Citrus senensis* peels and *Rhizoclonium grande* can be prepared from the biomass through saccharification using *A. niger* and fermentation by *S. cerevisiae.* The mean yield of bioethanol from *Citrus senensis* biomass (9.42 % v/w) is higher than that from *Rhizoclonium grande* biomass (5.36%).

Each 150g biomass from *Citrus senensis* peels and *Rhizoclonium grande* together produce cumulatively large quantities of bioethanol which is a mean of 22.17mL/g of biomass useful for transesterification of *Rhizoclonium grande* algae oil and *Jatropha curcas* oil.

5.1.2 Conclusions from Objective ii

There is large quantity of citrus oil per gram of peelings from *Citrus senensis* which range from a mean of 5.748% w/w in Muheza to 6.683% w/w in Malindi. This usually goes to waste and can be useful in obtaining 95% *d*-limonene.

Citrus lemoni and *Citrus tangerine* peelings yield moderate amounts of citrus oil per gram of peelings which range from a maximum mean of 3.281 % w/w Malindi to 4.500% from Shimba hills. These may require further processing to obtain *d*-limonene because the citrus oil contain *l*-limonene in addition to *d*-limonene.

Catalytic hydrogenation of *d*-limonene using 5% Palladium supported on alumina produce mainly (S)-1-methyl-4-isopropyl-cyclohexane or *cis*-p-menthane (**22**), (*R)*-1-methyl-4-isopropyl-cyclohexane or *trans*-p-menthane (**23**), (S)-1-methylene -4-(1-methylethyl)cyclohexane (**24**), (R)-1-methylene -4-(1-methylethyl)cyclohexane (**25)** which represent 60 % of the whole amount of hydrogenated products formed. Other products of hydrogenation include tricyclic and bicyclic compounds such as Octahydro-7-methyl-3-methylene-4-(1-methylethyl)-1H-cyclopenta[1.3]cyclopropa[1.2] benzene (**26**), R- 1,2,3,5,6,7,8,8a-octahydro-1,8a-dimethyl-7-(1-methylethenyl)naphthalene or valencene (**27)** and R- 1,2,3,4,4a,5-hexahydro-1,6-dimethyl-4-(1-methylethyl)naphthalene (**28**).

Catalytic oxidation of *d*-limonene using 4.74% palladium supported on hydrotalcite derived from copper magnesium aluminium oxide system produce mainly 1,2-limonene epoxide (2), 8,9-limonene epoxides (**3**), 1,2,8,9- diepoxylimonene (**4**), carveol (**5**) and carvone (**6**) which represent 78.402 % of the whole amount of oxidation products. Other minor products are *cis*-p-menth-2,8-dienol (**29**) and *trans* – carveyl ethanoate (**30**).

5.1.3 Conclusions from Objective iii

Rhizoclonium grande algae oil FAEE and *Jatropha curcas* oil FAEE have similar processing characteristics and yields. In the transesterification process the oil to bioethanol mixture ratio was 3:10 respectively heated at 65 ^{o}C with stirring at 200rpm for two hours. The bioethanol mixture containing the ethoxide ions required dry potassium hydroxide and bioethanol in a ratio of 1:10. The highest yield of fatty acid ethyl esters from *Rhizoclonium grande* and *Jatropha curcas* oils was a mean of 62% and 70% respectively.

Rhizoclonium grande algae oil FAEE can be used to blend with Jatropha oil FAEE for sustainability. Both have good miscibility and no phase separation at 5-20 % algal FAEE. Further the physicochemical and fuel characteristics of the 5-20 %Algae FAEE blends showed that there is significant influence on the *Jatropha curcas* FAEE especially calorific value p = 0.030, kinematic viscosity p = 0.001, pour point p = 0.001 and cloud point p = 0.001.

5.1.4 Conclusions from Objective iv

d-Limonene from *Citrus senensis* peel oil, oxygenated *d*-limonene and hydrogenated *d*-limonene can be used as additives to *R. grande* and *J. curcas* biofuel blend JAB20 since they have good miscibility and no phase separation at 2-8 % level of addition. They improve critical physicochemical and fuel characteristic parameters of JAB20.

The 2-8 % *d*-limonene additive has some effect on the physicochemical and fuel properties of JAB20. All of the p-values for density, calorific value, kinematic viscosity, flash point, cetane index, pour point and cloud point are less than 0.05 except for CFPP with a p value 0.215.

The 2-8 % hydrogenated *d*-limonene additive has some effect on the physicochemical and fuel properties of JAB20 all of the p-values for density, calorific value, kinematic

viscosity, flash point, cetane index, pour point and cloud point are less than 0.05 except for CFPP with a p value 0.215.

The 2-8 % oxygenated *d*-limonene additive has some effect on the physicochemical and fuel properties of JAB20 all of the p-values for density, cetane index and pour point are less than 0.05 except for calorific value p=0.113, kinematic viscosity p=0.469, flash point p=0.058, cloud point p=0.638 and CFPP p=0.058.

They can also improve the shelf life of the 20% JAB blend especially the 8% oxygenated d-limonene which shows *Pseudomonas aeroginosa* growth inhibition of 23.20 ± 0.80 mm and *Candida albicans* growth inhibition of 25.30± 0.30 mm.

The use of *d*-limonene multifunctional derivatives as additives have more benefits compared to the downside. The source of the raw materials, orange peel waste are in plenty around the country. Bioethanol in large production of biofuel can be recovered and re-used.

From the data analysis the calculated F and p-values are less than the critical values, showing no significant difference between 8% JABLA blends and the biodiesel specifications B100 ASTM D6751 and petroleum diesel standard specifications ASTM D975. Therefore JABLA8 containing 8% additives from *d*-limonene, oxygenated *d*-limonene and hydrogenated *d*-limonene can be used in the market directly without any engine modifications.

5.2 Recommendations

5.2.1 Recommendations from This Research

From this research, the following are the recommendations:

i. Preparation of bioethanol from *C. senensis* and *R. grande* biomass where 150 g biomass produce upto 9.42% v/w yield of bioethanol.

ii. Trans-esterification of *Rhizoclonium grande* and *Jatropha curcas* oil blend with ratio of dry KOH to bioethanol of 1:10 and ethoxide ion mixture to oil of 3:10 preheated at 65 ^{o}C for a period of two hours to produce 70 % yield of FAEE.

iii. Addition of 2-8 % hydrogenated and oxygenated d-limonene as additives to 5 - 20 % JAB to obtain JABLA biofuel with similar physicochemical and fuel parameters to those of petroleum diesel standard specifications and longer shelf life than B100.

5.2.2 Recommendations for Further Research

i. Further research to be done on the factors affecting the process of trans-esterification of *Rhizoclonium grande* and *Jatropha curcas* oil blend including mode of reaction, molar ratio of ethanol to oil, type and amount of catalysts, reaction time, temperature and purity of reactants.

ii. Diesel engine test to be done on JABLA and JAB, from the analytical results it showed that both have similar physicochemical and fuel parameters to those of petroleum diesel standard specifications.

iii. Isolation and physicochemical characterization of the different multifunctional *d*-limonene derivatives from different citrus peel oil to determine which has the best quality as additive to biodiesel.

iv. Further research to be done on shelf-life of JAB and JABLA with isolated oxygenated multifunctional *d*-limonene derivatives as additives.

v. Glycerol is a by-product from trans-esterification of *Jatropha curcas* and *Rhizoclonium grande* oil. Further research can be done to catalytically or otherwise convert the trihydric alcohol to a monohydric alcohol and use it in subsequent reactions to reduce production cost. This would require first to carry out esterification and trans-esterification of the oils using propanol as the alcohol

followed by analysis of fuel and physicochemical properties of the biodiesel that is produced.

vi. The by-product glycerol can be purified and used in pharmaceutical and soap industry which can further reduce production cost of biofuel blends.

vii. From the results obtained citrus oil from *Citrus sinensis* peels contain mainly *d*-limonene and analysis of JAB with crude *d*-limonene as additive show similar parameters to petroleum diesel standard specification. Further research can be done to ascertain the results using isolated and purified *d*-limonene.

viii. Though JABLA with 8 % oxygenated limonene derivatives is best suited for longer storage life of JAB20 from reduced microbial attack further test is required for long-term fuel storage stability. .

ix. Further research to be done on life cycle assessment of biofuel JAB and JABLA with *d*-limonene, oxygenated *d*-limonene and hydrogenated *d*-limonene.

REFERENCES

Afifi, A., Clark, V. and May, S. (2004). *Computer-Aided Multivariate Analysis*. 4th ed., Fl: Chapman & Hall/CRC, Boca Raton

Ahmad M. M., Rehman S. U., Anjum F.A. and Bajwa E. E. (2006). Comparative physical examination of various citrus peel essential oils. *International Journal of Agriculture and Biology*, 8 (2): 186-190

Ahmad M. M., Rehman S., Qureshi T. M., Nadeem M. and Asghar M. (2016). Variability in peel composition and quality evaluation of peel oils of citrus varieties. *Journal of Agricultural Research* 54(4):747-756.

Al-Ghouti M. A., Al-Degs Y. S. and Amer M. (2008). Determination of motor gasoline adulteration using FTIR spectroscopy and multivariate calibration, *Talanta*, 76: 1105–1112

Amazon.com. "Seaweed Biofuels: Production of Biogas and Bioethanol from Brown Macroalgae". http://www.amazon.com/dp/3639153073. Retrieved 2010-07-14.

Ambadas, B. R., Keunwoo, C., Young-Wun, K. and In Seok Hong. (2010). Synthesis and cetane-improving performance of 1,2,4,5-Tetraoxane and 1,2,4,5,7,8-Hexaoxonane derivatives, *Energy Fuels*, 24: 1636–1639.

Aminul Islam A. K. M., Yaakob Z., Anuar N., Osman M. and Primandari S. R. P., (2015). Preparation of Biodiesel from Jatropha Hybrid Seed Oil through Two-step Transesterification. *Energy Sources, Part A: Recovery, Utilization, and Environmental Effects,* 37(14): 1550-1559

Anastopoulos G., Zannikou Y., Stournas S. and Kalligeros S. (2009). Transesterification of Vegetable Oils with Ethanol and Characterization of the Key Fuel Properties of Ethyl Esters. *Energies,* 2: 362-376

Andres P., Natalia M., Santiago V., Dellacassa E., Sapelli M., Marquez V. and Bussi J. (2012). Limonene oxidation by molecular oxygen under solvent-free conditions: the influence of peroxides and catalysts on the reaction rate. *Reaction Kinetics Mechanisms and Catalysis,* 107:263–275

Aransiola E.F., Ojumu T.V., Oyekola O.O., Madzimbamuto T.F. and Ikhu-Omoregbe D.I.O. (2014). A review of current technology for biodiesel production: State of the art. *Biomass and bioenergy,* 61: 276-297

Association of Official Analytical Chemists (A.O.A.C), (2000). Official Methods of Analysis of AOAC International, 17th Edition, AOAC International, Gaithersburg, MD.

Association of Official Analytical Chemists (A.O.A.C), (2001). Official Methods of Analysis of AOAC International, 18th Edition, AOAC International, Gaithersburg, MD.

ASTM International, (1994). ASTM D130-12 Standard Test Method for Corrosiveness to Copper from Petroleum Products by Copper Strip Test , Annual Book of Standards, West Conshohocken, PA.

ASTM International, (1999a). ASTM D6371 Standard Test Method for Cold Filter Plugging Point of Diesel and Heating Fuels , Annual Book of Standards, West Conshohocken, PA.

ASTM International, (1999b). ASTM D95 Standard Test Method for water in Petroleum Products and Bituminous Materials by Distillation, Annual Book of Standards, West Conshohocken, PA.

ASTM International, (2000a). ASTM D482 Standard Test Method for Ash from Petroleum Products, Annual Book of Standards, West Conshohocken, PA.

ASTM International, (2000b). ASTM D86 Standard Test Method for Distillation of Petroleum Products at Atmospheric Pressure, Annual Book of Standards, West Conshohocken, PA.

ASTM International, (2002a). ASTM D1500-2 Standard Test Method for ASTM Color of Petroleum Products, Annual Book of Standards, West Conshohocken, PA.

ASTM International, (2002b). ASTM D2500-2 Standard Test Method for Cloud Point of Petroleum Products, Annual Book of Standards, West Conshohocken, PA.

ASTM International, (2002c). ASTM D4682-87 Standard Specification For Miscibility With Gasoline and Fluidity of Two-Stroke-Cycle Gasoline Engine Lubricants, Annual Book of Standards, West Conshohocken, PA.

ASTM International, (2004a). ASTM D445-04 Standard Test Method for Kinematic Viscosity of Transparent and Opaque Liquids, Annual Book of Standards, West Conshohocken, PA.

ASTM International, (2004b). ASTM D86-04b Standard Test Method for Distillation of Petroleum Products at Atmospheric Pressure, Annual Book of Standards, West Conshohocken, PA.

ASTM International, (2005). ASTM D97-05 Standard Test Method for Pour Point of Petroleum Products, Annual Book of Standards, West Conshohocken, PA.

ASTM International, (2006). ASTM D1298 Standard Test Method for Density, relative density or API gravity of crude petroleum products by hydrometer method, Annual Book of Standards, West Conshohocken, PA.

ASTM International, (2007a). ASTM D93 Standard Test Method for Flash Point by Pensky-Martens Closed Cup Tester, Annual Book of Standards, West Conshohocken, PA.

ASTM International, (2007b). ASTM D975 Standard Specification for Diesel Fuel Oils, Annual Book of Standards, West Conshohocken, PA.

ASTM International, (2008). ASTM D7371 Standard Test Method for Determination of Biodiesel (Fatty Acid Methyl Esters) Content in Diesel Fuel Oil Using Mid Infrared Spectroscopy (FTIR-ATR-PLS Method), Annual Book of Standards, West Conshohocken, PA.

ASTM International, (2009). ASTM D4737 Standard Test Method for Calculated Cetane Index by Four Variable Equation , Annual Book of Standards, West Conshohocken, PA.

ASTM International, (2013). ASTM D4809 – 13 Standard Test Method for Heat of Combustion of Liquid Hydrocarbon Fuels by Bomb Calorimeter (Precision Method), Annual Book of Standards, West Conshohocken, PA.

Barnwal B.K. and Sharma M.P. (2005). Prospects of biodiesel production from vegetable oils in India. *Renewable and Sustainable Energy Reviews*, 9(4): 363–378.

Bart J.C.J., Gucciardi E. and Cavallaro S. (2013). Chemical transformations of renewable lubricant feedstocks. *Biolubricants*, woodhead publishing pp. 249-350

Beatriz, A.B., Andrea de Leon, A., Natalia, B., Alejandro, L., Daniel, P., Natalia, M., Daniel, L., Eduardo, D. and Juan, B. (2007). A clean process for the production of oxygenated limonene derivatives starting from orange oil. *Journal of Chemical Technology & Biotechnology*, 82:532–538.

Beckman, E.J. (2002). Using CO_2 to produce chemical products sustainably. *Environmental Science & Technology*, 36: 347A–353A.

Beckman, E.J. (2003). Green chemical processing using CO_2. *Industrial & Engineering Chemistry Research*, 42: 1598–1602.

Bello E. I., Out F. and Osasona A. (2012). Cetane number of three vegetable oils, their biodiesels and blends with diesel fuel. *Journal of Petroleum Technology and Alternative Fuels*, 3(5): 52-57.

Birdlife International, (2012). A study to analyse the status of production and impacts of biofuels on food security and environment in Kenya, Tanzania and Ethiopia: A summary of key recommendations for policy makers.

Blin, J., Volle, G., Girard, P., Bridgwater, T. and Meier, D. (2007). Biodegradability of biomass pyrolysis oil: Comparison to conventional fuels and alternative fuels in current use. *Fuel*, *86*: 2670–2686.

B.P. (2012). Statistical Review of World Energy, London, United Kingdom. Available from: www.bp.com/statisticalreview, June 2012 (Last accessed: 08.10.13).

Bussi J., Lopez A., Pena F., Timbal P., Paz D., Lorenzo D. and Dellacasa E. (2003). Liquid phase oxidation of limonene catalyzed by palladium supported on hydrotalcites. *Applied Catalysis A General*, 253(1):177-189

Cao L., Wang J., Liu C., Chen Y., Liu K. and Han S. (2014). Ethylene vinyl acetate copolymer: A bio-based cold flow improver for waste cooking oil derived biodiesel blends. *Applied Energy*, 132(1): 163-167.

Chafer, A., Berna, A., Monton, J.B. and Mulet, A. (2001). High pressure solubility data of the system limonene linalool CO_2. *Journal of Chemical & Engineering Data*, 46: 1145–1148.

Cheng-Yu F. W., Kuangnan Q. and Larry A. G. (2005). GC-MS of Diesel: A Two-Dimensional Separation Approach. *Analytical Chemistry*, 7: 2777 - 2785

Chesneau, H. (2008). *Overcoming Microbiological Contamination, Material Compatibility*. Retrieved February 12, 2014, from www.biodieselmagazine.com: http://www.biodieselmagazine.com/articles/2391/overcoming-microbiological-contamination-material-compatibility/

DeMello J. A., Carmichael C. A., Peacock E. E., Nelson R. K., Arey J. S. and Reddy C. M. (2007). Biodegradation and environmental behavior of biodiesel mixtures in the sea: An initial study; *Marine Pollution Bulletin*, *54*: 894–904

Demirbas A. and Demirbas M.F. (2011). Importance of algae oil as a source of biodiesel. *Energy Conversation Management*, 52:163–170.

Devendra P. S. and Rakesh K. T. (2013). Production of biofuel from algae: An economic and eco-friendly resource, *International Journal of Science and Research*, 2(11):352-357.

Divakaran, R. and Sivasankara, P.V. N. (2002). Flocculation of algae using chitosan. *Journal of Applied Phycology*, 14(5): 419-422.

Dugo G. and Mondello L. (2010). Citrus Oils: Composition, Advanced Analytical Techniques, Contaminants, and Biological Activity. CRC Press, Boca Raton U.S.A. ISBN 9781439800287.

Ehimen E.A., Sun Z.F. and Carrington C.G. (2010). Variables affecting the in situ transesterification of microalgae lipids. *Fuel*, 98:677–684.

Ejikeme P. M., Anyaogu I. D., Ejikeme C. L., Nwafor N. P., Egbuonu C. A. C., Ukogu K., and Ibemesi J. A. (2010). Catalysis in Biodiesel Production by Transesterification Processes-An Insight. *Journal of Chemistry*, 7(4): 1120-1132

Enferadi T. S., Rabiei Z. and Vannozzi G.P. (2006) Protection of Biodiesel Based on Sunflower Oil from Oxidative Degradation by Natural Antioxidants, *Helia*, 29: 25-32.

Evans, G. (2008).*"Liquid Transport Biofuels-Technology status report"*, National non-food crops centre.

Eviana, H. (2008). *"A Promising Oil Alternative: Algae Energy"*. WashingtonPost.http://www.washingtonpost.com/wpdyn/content/article/2008/01/03/AR2008010303907.html.

Farooq, A., Amin, U. K. and Yasar, A. (2013). Transesterification of oil extracted from different species of algae for biodiesel production. *African Journal of Environmental Science and Technology*, 7(6): 358-364.

Fernando, S. and Hanna, M. (2004). Development of a novel biofuel blend using ethanol - biodiesel - diesel microemulsions: EB-Diesel. *Energy & Fuels*, 18:1695-1703.

Fingas M. (2011). Introduction to Oil Chemistry and Properties. *Oil Spill Science and Technology*, Gulf professional publishing, Houston pp. 51-59

Finn, M.G. and Sharpless, K.B. (1991). Mechanism of asymmetric epoxidation. 2. Catalyst structure. *Journal of the American Chemical Society*, 113:113-126.

Frizzo C. D., Lorenzo D., Dellacassa E. (2004). Composition and seasonal variation of the essential oils from two mandarin cultivars of Southern Brazil. *Journal of Agricultural and Food Chemistry*, 52: 3036-3041.

Ginwal, H., Rawat, P. and Srivastava, R. (2004) Seed Source Variation in Growth Performance and Oil Yield of *Jatropha curcas* Linn. in Central India. *Silvae Genetica*, 53: 186-191.

Glass D. (February 2, 2010). EUEC 2010 conference "Prospects for the use of genetic engineering in biofuel production."

Grau R.J., Zgolicz P.D., Guiterrez C. and Taher H.A. (1999). Liquid phase hydrogenation, isomerization and dehydrogenation of limonene and derivatives with supported palladium catalysts, *Journal of Molecular Catalysis A: Chemical*, 148: 203–214.

Grayburn W. S., Tatara R. A., Rosentrater K. A., Holbrook G. P. (2013). Harvesting, oil extraction, and conversion of local filamentous algae growing in wastewater into biodiesel, *International Journal of Energy and Environment*, 4(2): 185-190

Green Car Congress. (September 20, 2007). Cyclone power showcase external combustion engine at SAE event.

Gryglewiez S. (2000). Alkaline-earth metal compounds as alcoholysis catalysts for ester oils synthesis. *Applied Catalysis A: General*, 192: 23-28.

Gunstone F. D.; Harwood J. L. (2007). Occurrence and characterization of oils and fats‘. In: Gunstone F. D.; Harwood J. L.; Dijkstra A. J. (eds) The lipid handbook. 3rd ed. CRC, Boca Raton, 37-142.

Gusakov A. V. , Kondratyeva E. G. and Sinitsyn A. P. 2011. Comparison of Two Methods for Assaying Reducing Sugars in the Determination of Carbohydrase Activities. *International Journal of Analytical Chemistry*. 2011: 283658. Published online 2011 May 26. doi: 10.1155/2011/283658

Gusevskaya E.V., dos Santos E.N., Augusti R., de Dias A O. and Foca C.M. (2000). Platinum/tin catalyzed hydroformylation of naturally occurring monoterpenes, *Journal of Molecular Catalysis A: Chemical*, 152: 15–24.

Han J., Lian J., Tian X., Zhou S., Zhen X. and Liu S. (2014). Total Synthesis of Micromide: a Marine Natural Product. *European Journal of Organic Chemistry*, 2014 (32): 7232–7238. DOI: 10.1002/ejoc.201402977

Harwood L. M., Moody C. J. and Percy J. M.. (1999). Experimental organic chemistry: Standard and microscale. 2nd Edition, Wiley-Blackwell Publishing London U.K.

Háznagy-Radnal E., Czigle S and Máthé I. (2007). TLC and GC analysis of the essential oils of Stachys species *Journal of Planar Chromatography*, 20: 189-196.

Hirano T.I and Tsuto K., United States Patent No. 6090959, Methods of Producing Fatty Acid and Lower Alkyl Ester from Fats and Oils, July, 2000, 18.

Hydrogensolar.com. "Hydrogen Solar home". http://www.hydrogensolar.com/. Retrieved 2010-07-14.

Jobard, H. (2010). 'Determination of the relative density of the substance d-limonene', Les Dérivés Résiniques et Terpéniques (DRT), Laboratoire Contrôle, Route de Linxe, 40560 Vieille Saint Girons, France.

Jones D.S.J. and Pujado P.R., Eds. (2006). Petroleum products and a refinery configuration. *Handbook of petroleum processing*, Springer, Netherlands, 47–110.

Jumat, S. and Rozaini, A. (2008). Physicochemical properties of Malaysian *Jatropha curcas* seed oil. *Sains Malaysiana*, 37: 379-382.

Katleen V. M , Smekens A. , Behets M., Kazandjian P., and Grieken R.V. (2007). Determination of Platinum, Palladium, and Rhodium in Automotive Catalysts

Using High-Energy Secondary Target X-ray Fluorescence Spectrometry. *Analytical Chemistry*, 79 (16): 6383–6389

Kazinform (Kazakhstan National Information Agency). (2008, April 11). "Biofuels major cause of global food riots".

Keith A. (2007). Biodiesel and your vehicle quality testing. (http://journeytoforever.org/biodiesel vehicle.html quality; Accessed on 14th May 2010 at 3.25PM).

Knothe G. (1999). Rapid monitoring of transesterification and assessing biodiesel fuel quality by NIR spectroscopy using a Fiber – optic probe. *Journal of the American Oil Chemists' Society*,76(7): 795 –800.

Knothe G. (2000). Monitoring the turnover of a progressing transesterification reaction by fiber – optic NIR spectroscopy with correlation to ^{1}H – NMR spectroscopy. *Journal of the American Oil Chemists' Society*, 77(5): 489 – 493.

Knothe G., Matheaus A.C., Ryan T.W. (2003). Cetane numbers of branched and straight chain fatty esters determined in an ignition quality tester. *Fuel*, 82: 971-975.

Knothe G., Gerpen J.V. and Krahl J. (2005). The Biodiesel Handbook. AOCS Press, Champaign, Illinois.

Knothe, G. (2006). Analyzing Biodiesel: Standards and Other Methods. *Journal of the American Oil Chemists' Society*, 83 (10): 823-833

Kumar, A. and Sharma, S. (2008). An Evaluation of Multipurpose Oil Seed Crop for Industrial Uses (*Jatropha curcas* L.): A Review. *Industrial Crops and Products*, 28: 1-10.

Kurnia J. C., Jangam S. V., Akhtar S., Sasmito A. P., Mujumdar A. S. (2016). Advances in Biofuel Production from Oil Palm and Palm Oil Processing Wastes: A Review. *Biofuel Resource. Journal* 3, 332-346.

Lange, B.M. (2015). Biosynthesis and biotechnology of high-value p-menthane monoterpenes, including menthol, carvone, and limonene. *Advances in Biochemical Engineering - Biotechnology* 148:319–353.

Leadbeater N. E. and Stencel L. M. (2006). Fast, easy preparation of biodiesel using microwave heating, *Energy* and *Fuels*, 20: 2281-2283.

Lehmann N., Finger R., Tommy Klein T., and Calanca P. (2013). Sample Size Requirements for Assessing Statistical Moments of Simulated Crop Yield Distributions, *Agriculture*, 3: 210-220.

Leung D. Y.C., Xuan W.u and Leung M.K.H. (2010). A review on biodiesel production using catalyzed transesterification. *Applied Energy*, 87 (4): 1083-1095.

Longo G. S., Schick M., and Szleifer I. (2009). Stability and Liquid-Liquid Phase Separation in Mixed Saturated Lipid Bilayers. *Biophysical Journal*, 96: 3977–3986.

Ma F. and Hanna M. (1999). Biodiesel production: A review. *Bioresource Technology*, 70: 1–15.

Mahamuni N.N. and. Adewuyi Y. G. (2009). Fourier Transform infrared Spectroscopy (FTIR) Method to Monitor Soy Biodiesel and Soybean Oil in Transesterification Reactions, Petrodiesel-Biodiesel Blends, and Blend Adulteration with Soy Oil, *Energy & Fuels*, 23: 3773-3782.

Mathers R.T., McMahon K.C., Damodaran K., Retarides C.J. and Kelley D.J. (2006). Ring-opening metathesis polymerization in D-limonene: a renewable polymerization solvent and chain transfer agent for the synthesis of alkene macromolecules, *Macromolecules*, 39: 8982–8986.

McCormick R.L. (2009). Biodiesel handling and use guide 4th edition, National Renewable Energy, Oakridge US.

McKenzie L. C., Thompson J, E., Sullivan R. and Hutchison J. E. (2004). Liquid CO2 extraction of natural products. *Green Chemistry*, 6: 355–358.

Meher L.C., Sagar D.V. and Naik S.N. (2006). Technical aspects of biodiesel production by transesterification a review, *Renewable & Sustainable Energy Reviews*,10: 248-268.

Meng X., Yang J., Xu X., Zhang L., Nie Q. and Xian M. (2009). Biodiesel production from oleaginous microorganisms, *Renewable Energy*, 34(1):1–5.

Milewska A., Banet Osuna, A., Fonseca I. M. and Nunes da Ponte, M. (2005). Biphasic hydrogenation of α-pinene in high-pressure carbon dioxide. *Green Chem*istry, 7(10): 726-732.

Mith H., Duré R., Delcenserie V., Zhiri A., Daube G. and Clinquart A. (2014). Antimicrobial activities of commercial essential oils and their components against food-borne pathogens and food spoilage bacteria. *Food Science and Nutrition*. 2(4):403-416.

Mittelbach, M., Roth G., and Bergmann A. (1996). Simultaneous gas chromatographic determination of methanol and free glycerol in biodiesel. *Chromatographia*, 42(7/8): 431–434.

Monteiro J.L.F and Veloso C.O. (2004). Catalytic conversion of terpenes into fine chemicals. *Topics in Catalysis*, 27:169–180.

Moussa A. A. and Hamed S.F. (2007). Application of FTIR Spectroscopy in the Assessment of Olive Oil Adulteration. *Journal of Applied Sciences Research,* 3 (2): 102-108

Mukhopadhyay M. (2000). *Natural Extracts Using Supercritical Carbon Dioxide*; CRC Press, Washington, DC.

Núbia, M.R., Angelo, C.P., Cristina, M.Q., Gisele, O. da R., Leonardo, S.G., Teixeira, L., Guarieiro, L.N., Maria do Carmo, R., Márcia, C.C.V., Michelle, J.C.R., Rosenira, S. da C., Ana, M. de O., Ednildo, A.T., and Jailson, B.A. (2007). The Role of Additives for diesel and diesel blended (Ethanol or Biodiesel) fuels: A Review *Energy Fuels*, 21 (4): 2433–2445.

Nwakaire J. N., Akubuo C.O., Ohagwu C.J., and Ugwuishiwu B. O. (2016). Pressure effect on the yield of methyl ester biodiesel for application in low income countries. *Sylwan*, 160(3): 203-212.

Nzikou, J., Matos, L., Mbemba, F., Ndangui, C., Pambou-Tobi, N., Kimbonguila, A., *et al.* (2009) Characteristics and Composition of *Jatropha curcas* Oils, Variety Congo-Brazzaville. *Research Journal of Applied Sciences, Engineering and Technology*, 1: 154-159.

Pagés O., Legendre B., Odlyha M. and Craig D. (1996). Phase miscibility in oil/resin mixtures: a study by FTIR and thermomechanical analysis. *Thermochimica Acta*, 287(1): 53-70.

Pant, K., Khosla, V., Kumar, D. and Gairola, S. (2006). Seed Oil Content Variation in *Jatropha curcas* Linn. in Different Altitudinal Ranges and Site Conditions in HP India. *Lyonia*,11:31-34.

Park J.Y., Kim D. K., Lee J. P., Park S. C., Kim Y. J. and Lee J. S. (2008). Blending effects of biodiesels on oxidation stability and low temperature flow properties. *Bioresource Technology*, 99: 1196-1203.

Pena, A., Veiga, S., Sapelli, M., Martínez N., Márquez V. , Dellacassa E. and Bussi J. (2012). Limonene oxidation by molecular oxygen under solvent-free conditions: the influence of peroxides and catalysts on the reaction rate. *Reaction Kinetics, Mechanism and Catalysis,* 107: 263-275.

Pienkos P.T. and Darzins A. (2009). The promise and challenges of microalgal-derived biofuels. *Biofuels Bioproduction and Biorefining,* 3:431–440.

Pokoo-Aikins, G., Nadim A., El-Halwagi M. M. and Mahalec V. (2009). Design and analysis of biodiesel production from algae grown through carbon sequestration. *Clean Technologies and Environmental Policy,* 12(3): 239 - 254.

Polak, J. T., Balaban, M., Peplow, A. and Phlips, A. J. (1989). Supercritical fluid science and technology, *ACS Symposium Series*, 406 Chapter 28, 449–467.

Prankl, H. and Schindlbauer, H. (1998). Oxidation stability of fatty acid methyl esters. 10th European Conference on Biomass for Energy and Industry, Wurburg, Germany.

Pratas M. J., Freitas S., Oliveira M. B., Monteiro S. C., Lima A. S., and Coutinho J.A.P. (2011). Densities and Viscosities of Minority Fatty Acid Methyl and Ethyl Esters Present in Biodiesel, *Journal of Chemical Engineering Data*, 56: 2175–2180.

Qui, Huanguang, Jikun Huang, Michiel Keyzer and Wim van Veen. (2008). *Policy options for China's bio-ethanol development and the implications for its agricultural economy. China & World Economy*, 16(6): 112-124.

Raja, S. A., Smart, D. S. R., and Lee, C. L. R. (2011). Biodiesel production from jatropha oil and its characterization. Research Journal of Chemical Sciences, 1:81–87.

Raheman, H. (2012). Jatropha: chapter 14. In: Chittaranjan K., Joshi, C. P. and Shonnard, D. R. (Eds). Handbook of bioenergy crop plants. CRC Press, Taylord & Francis Group

Robert, S., Ireland, E. and Bey, P. (1988). Homogeneous catalytic hydrogenation: Dihydrocarvone, *Organic Syntheses Collections*, 6: 459.

Robles-Dutenhefner P. A., da Silva M. J., Sales L. S., Sousa E.M.B., and Gusevskaya E.V. (2004). Solvent-free liquid-phase autoxidation of monoterpenes catalyzed by sol-gel Co/SiO2, *Journal of Molecular Catalysis A: Chemical*, 217:139–144.

Robles-Dutenhefner P.A., Speziali M.G., Sousa E.M.B., dos Santos E.N. and Gusevskaya E.V. (2005). Selective hydrogenation of myrcene catalyzed by sol–gel Pd/SiO_2, *Applied Catalysis A: General*, 295: 52–58.

Sahoo P.K and Das L. M. (2009). Combustion analysis of Jatropha, Karanja and Polanga based biodiesel as fuel in a diesel engine. *Fuel*, 88: 994-999.

Sanford S. D., White J. M., Shah P. S., Wee C., Valverde M. A., and Meier G. R. (2009). "Feed stock and Biodiesel Characteristics Report," Renewable Energy Group, Inc., www.regfuel.com.

Sheteni P. (2016). Smallholder farmers' awareness of biofuel crops in the Eastern Cape Province, South Africa. *Environmental Economics*, 7 (3): 75-80.

Shihui W., Chaoyang L., Yun L., Zhicheng S., Jenasia J. and Wensheng Q. (2016). Characterization of a starch-hydrolyzing α-amylase produced by Aspergillus niger WLB42 mutated by ethyl methanesulfonate treatment. *International Journal of Biochemistry and Molecular Biology* 7(1):1-10.

Smith D. C., Forland S., Bachanos E., Matejka M. and Barrett V. (2001). Qualitative analysis of citrus fruit extracts by GC/MS. *Journal of Chemical Education*, 6: 28–31.

Song C., Lai W. Reddy K. M., and Wei B. (2011). Temperature-Programmed Retention Indices for GC and GC-MS of Hydrocarbon Fuels and Simulated Distillation GC of Heavy Oils, In: Hsu C.S. (eds) *Analytical Advances for Hydrocarbon Research* , Modern Analytical Chemistry. Springer, Boston, MA. Chapter 7 pp 147-210

Spangenberg B., Poole C.F. and Weins C. (2010) Preparing and Applying Samples. In: *Quantitative Thin-Layer Chromatography*. Springer, Berlin, Heidelberg. Chapter 5 pp105-118.

Speziali M.G., Moura F.C.C., Robles-Dutenhefner P.A., Araujo M.H., Gusecskaya E.V. and dos Santos E.N. (2005). Selective hydrogenation of myrcene catalyzed by complexes of ruthenium, chromium, iridium and rhodium. *Journal of Molecular Catalysis A: Chemical*, 239: 10–14.

Sridevi A., Narasimha G., Rajasekhar B.R. (2008). Production of Cellulase by *Aspergillus niger* on natural and pretreated lignocellulosic wastes. *The Internet Journal of Microbiology* 7(1): 1-8.

Stashenko E., Jaramillo B. E. and Martinez J. R. (2004). Comparison of different extraction methods for the analysis of volatile secondary metabolites of Lippia alba (Mill.) N.E. Brown, grown in Colombia, and evaluation of its in vitro antioxidant activity. *Journal of Chromatography A*, 1025(1): 93-103.

Stloukal R., Komers, K. and Machek, J. (1997). Ternary phase diagram biodiesel fuel-methanol-water. *Journal fuer praktische Chemie - Chemiker Zeitung*, 339 (5): 485-487.

Suppes G. J., Goff M., Burkhart M. L., Bockwinkel K., Mason M. H., Botts J.B., and Heppert J. A. (2001). Multifunctional diesel fuel additives from triglycerides. *Energy Fuels*, 15: 151–157.

Svein J.H. (2009). Seaweed Biofuels: Production of Biogas and Bioethanol from Brown Macroalgae , Verlag.

Swift K.A.D. (2004). Catalytic transformations of the major terpene feedstocks. *Topics in Catalysis*, 27: 143–155.

Tanchoux N. and Leitner W. (2002). *Handbook of Green Chemistry and Technology*, eds. Clark J. and Macquarrie D., Blackwell Science, Oxford, pp. 482–501.

Thangarasu V. and Anand R., (2019). Physicochemical fuel properties and tribological behavior of aegle marmelos correa biodiesel. *Advances in Eco-Fuels for a Sustainable Environment*, Woodhead publishing, Cambridge, pp. 309-336.

Tomasevic A. V. and Marinkovic S. S. (2003) Methanolysis of used frying oil. *Fuel Processing Technology*, 81: 1–6.

Tracy N. I., Daichuan C., Crunkleton D. W. and Price G. L. (2009). Hydrogenated monoterpenes as diesel fuel additives. *Fuel*, 88 (11): 2238-2240.

Umarah M., Wajahat H., Ikram-ul-Haq and Kauser A. M. 2011. Study of Native Algal Species for Growth Potential and Lipid Yield, *Current Research Journal of Biological Sciences,* 3(3): 240-245.

Varjani Sunita J., Rana Dolly P., Bateja S. and Upasani Vivek N. (2013). Isolation and Screening for Hydrocarbon Utilizing Bacteria (HUB). *International Journal of Current Microbiology and Applied Sciences*, 2(4): 48-60.

Van Gerpen, J., Shanks, B., Pruszko, R., Clements, D. and Knothe, G. (2004). Biodiesel Production Technology, National Renewable Energy Laboratory, 1617 Cole Boulevard, Golden, Colorado 80401-3393.

Vashist H., Rathor D. S. and Sigh G. (2014). A comparative report on the percentage yield of volatile oil from citrus fruits by hydrodistilation. *Singapore Journal of scientific research,* 4: 15-18.

Waynick J.A. (2005). Characterization of Biodiesel Oxidation and Oxidation Products, SwRI Project No. 08-10721.

Wroblewska A. (2014). The epoxidation of limonene over the TS-1 and Ti-SBA-15 catalysts. *Molecules* 19: 19907-19922.

Xiaohu F. and Burton R. (2009). Recent Development of Biodiesel Feedstocks and the Applications of Glycerol: A Review. *The Open Fuels & Energy Science Journal*, 2: 100-109

Xin J., Imahara H. and Saka S. (2008). Oxidation Stability of Biodiesel Fuel as Prepared by
Supercritical Methanol, *Fuel,* 87: 1807-1813.

Younis M. N., Saeed M. S., Khan S., Furqan M. U., Khan R. U., and Saleem M. (2009). Production and characterization of biodiesel, from waste and vegetable oils. *Journal of Quality and Technology Management,* 5(1): 111-121.

Yuan W., Hansen A. and Zhang Q. (2005). Vapor pressure and normal boiling point predictions for pure methyl esters and biodiesel Fuels. *Fuel*, 84: 943-950.

Zagonel G., Peralta-Zamora P. and Ramos L. (2004). Multivariate monitoring of soybean oil ethanolysis by FTIR, *Talanta*, 63: 1021–1025.

Zannis T.C., Hountalas D.T. and Papagiannakis R.G. (2007). Experimental study of diesel fuel effects on direct injection diesel engine performance and pollutant emissions. *Energy Fuel*, 21: 2642–2654.

Zhang, Y., Dube, M. A., McLean and D. D., Kates, M. (2003a). Biodiesel Production from Waste Cooking Oil: Process Design and Technological Assessment. *Bioresource. Technology*, 89: 1-16.

Zhang, Y., Dube, M. A., McLean D. D. and Kates, M. (2003b). Biodiesel production from waste cooking oil: Economic assessment and sensitivity analysis. *Bioresource Technology*, 90: 229–240.

Zhou, W., Konar, S.K. and Boocock, D.G.V. (2003). Ethyl esters from the single-phase base-catalyzed ethanolysis of vegetable oils. *Journal of American Oil Chemists' Society*, 80: 367-371.

Zimmer A., Cazarolli J., Teixeira R.M., Viscardi S.L.C., Cavalcanti E.S.H., Gerbase A.E., Ferrão M.F., Piatnicki C.M.S. and Bento F.M. (2013). Monitoring of efficacy of antimicrobial products during 60 days storage simulation of diesel (B0), biodiesel (B100) and blends (B7 and B10). *Fuel* 112:153–162.

APPENDICES

APPENDIX I: **Algae samples from Shimoni and Shelly beach after cleaning and before drying**

APPENDIX II: **Slides used in investigating Lipid distribution in ten algae species using sudan IV dye**

APPENDIX III: **Jatropha curcas perennial shrubs in Shimba Hills Kwale County**

APPENDIX IV: ***Jatropha curcas*** **sample from Shimba Hills**

APPENDIX V: **Fabricated Jatropha dehusker**

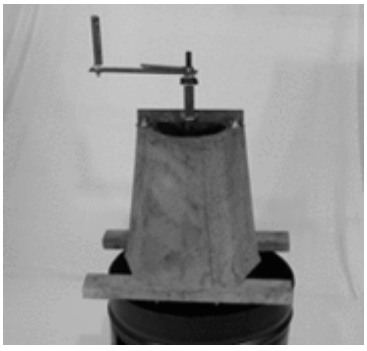

APPENDIX VI: **Citrus oil containing Limonene extracted from citrus peelings samples**

APPENDIX VII: Apparatus used for oil extraction using liquid and supercritical carbon dioxide

APPENDIX VIII: Recovering hexane by vacuum evaporator

APPENDIX IX: Fabricated oil press extractor

APPENDIX X: Jatropha oil sample extracted using hexane

APPENDIX XI: Saccharification of algae and citrus biomass using A.niger

APPENDIX XII: Fractional Distillation and drying of bioethanol

APPENDIX XIII: Synthesis Reactor (A), Synthesized hydrogenated *d*-limonene derivatives and Pd/Al_2O_3 Catalyst in sample bottles (B)

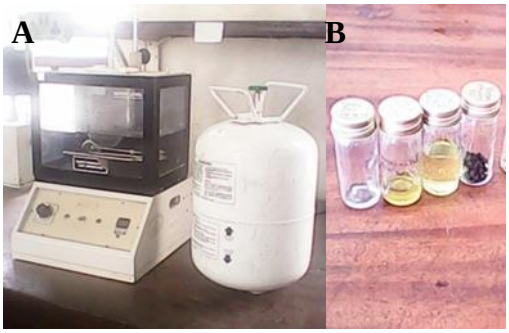

APPENDIX XIV: Mass Spectra of *d*-Limonene and Multifunctional Derivatives

(A) Mass Spectrum of *d*-Limonene in Orange oil

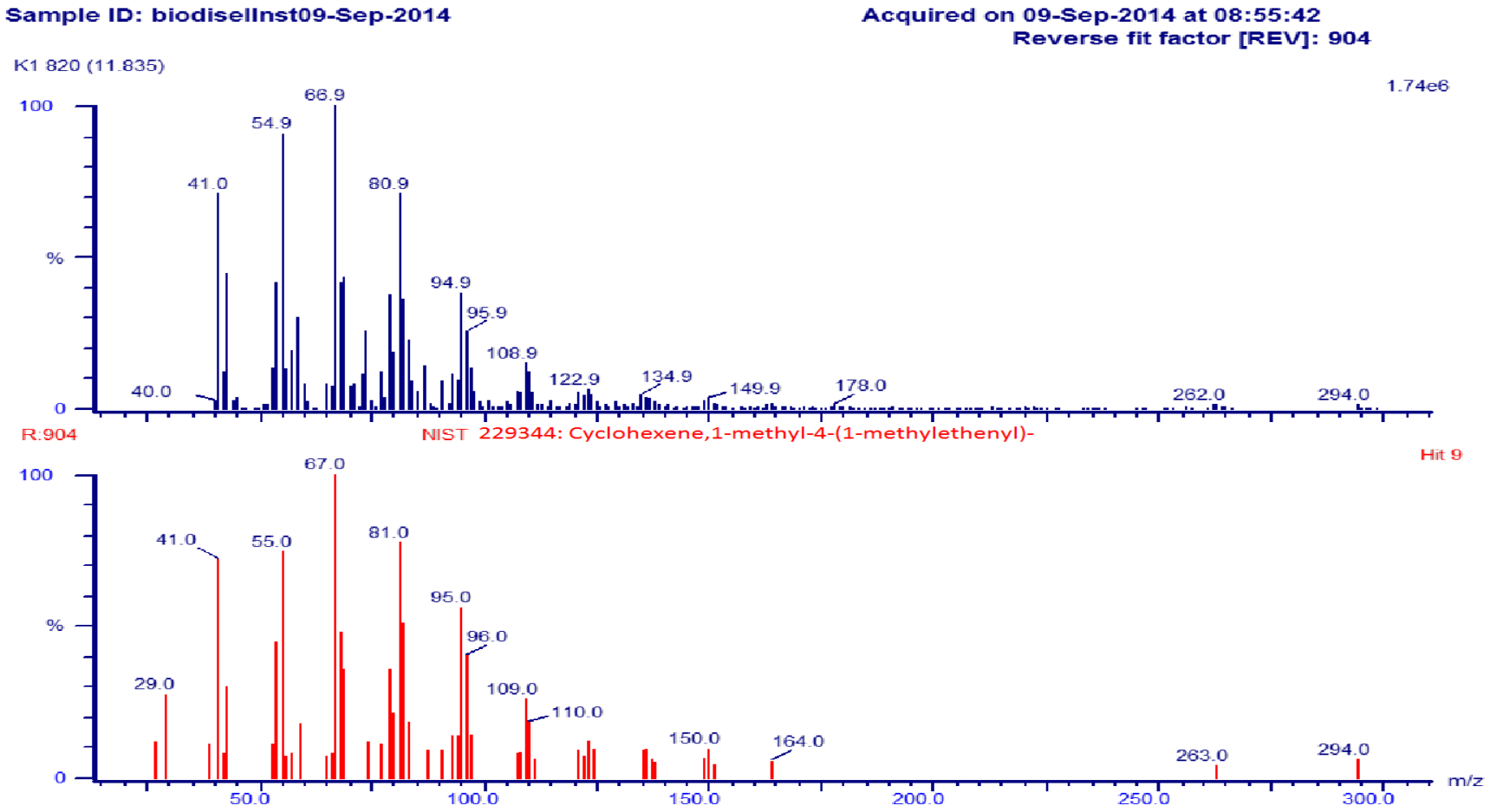

(B) Mass Spectra of Hydrogenated *d*-limonene derivatives in Orange Oil

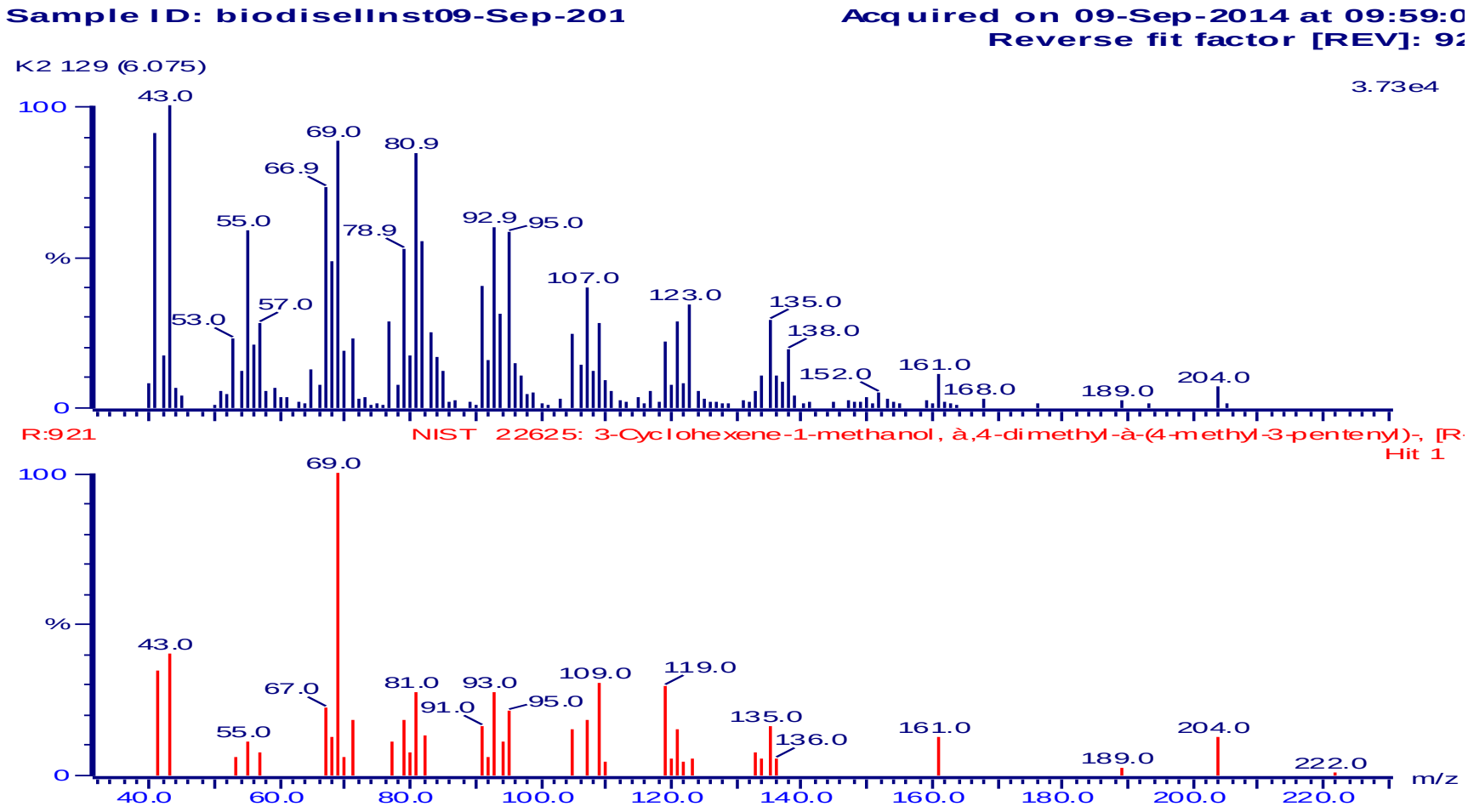

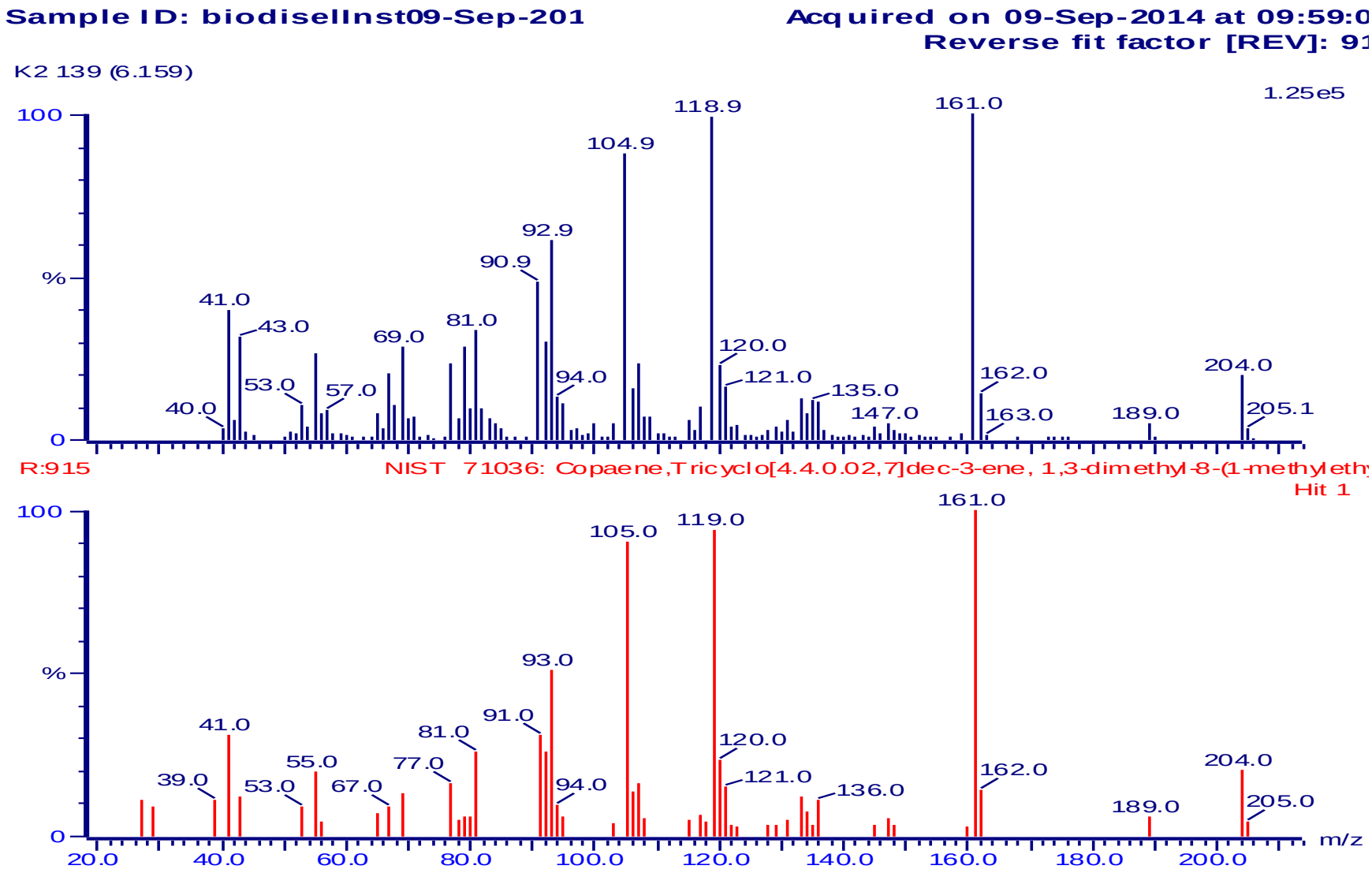
Sample ID: biodiselInst09-Sep-201
Acquired on 09-Sep-2014 at 09:59:0
Reverse fit factor [REV]: 91
K2 139 (6.159)
1.25e5
100
%
0
41.0
43.0
40.0
53.0
57.0
69.0
81.0
90.9
92.9
94.0
104.9
118.9
120.0
121.0
135.0
147.0
161.0
162.0
163.0
189.0
204.0
205.1
R:915
NIST 71036: Copaene,Tricyclo[4.4.0.02,7]dec-3-ene, 1,3-dimethyl-8-(1-methyleth
Hit 1
100
%
0
39.0
41.0
53.0
55.0
67.0
77.0
81.0
91.0
93.0
94.0
105.0
119.0
120.0
121.0
136.0
161.0
162.0
189.0
204.0
205.0
20.0
40.0
60.0
80.0
100.0
120.0
140.0
160.0
180.0
200.0
m/z

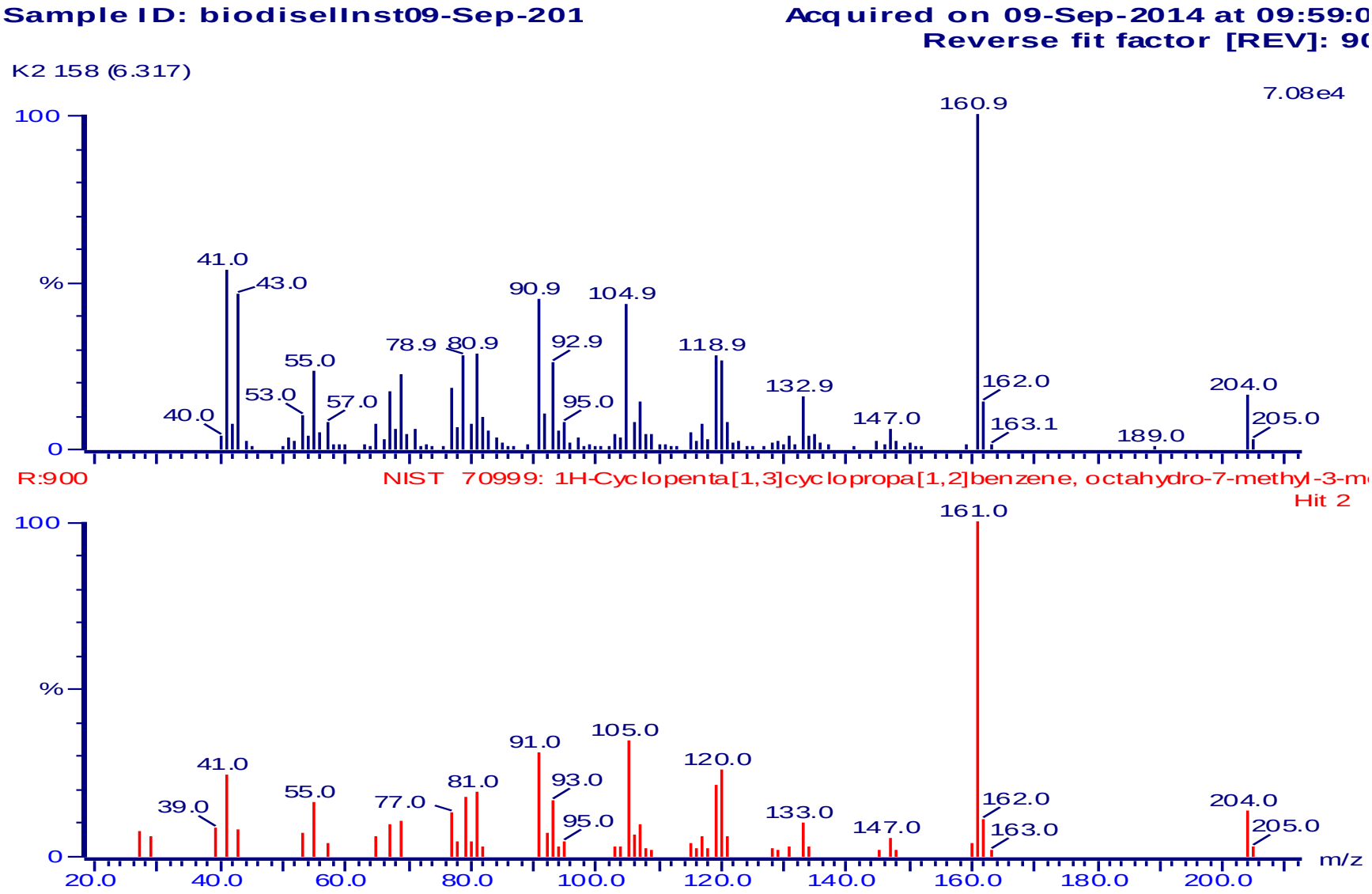
Sample ID: biodiselInst09-Sep-201
Acquired on 09-Sep-2014 at 09:59:0
Reverse fit factor [REV]: 9(
K2 158 (6.317)
7.08e4
100
%
0
160.9
41.0
43.0
90.9
104.9
78.9
80.9
92.9
118.9
55.0
53.0
57.0
132.9
162.0
204.0
40.0
95.0
147.0
163.1
205.0
189.0
R:900
NIST 70999: 1H-Cyclopenta[1,3]cyclopropa[1,2]benzene, octahydro-7-methyl-3-m
Hit 2
100
%
0
161.0
91.0
105.0
41.0
120.0
93.0
81.0
55.0
39.0
77.0
133.0
162.0
204.0
95.0
147.0
163.0
205.0
m/z
20.0
40.0
60.0
80.0
100.0
120.0
140.0
160.0
180.0
200.0

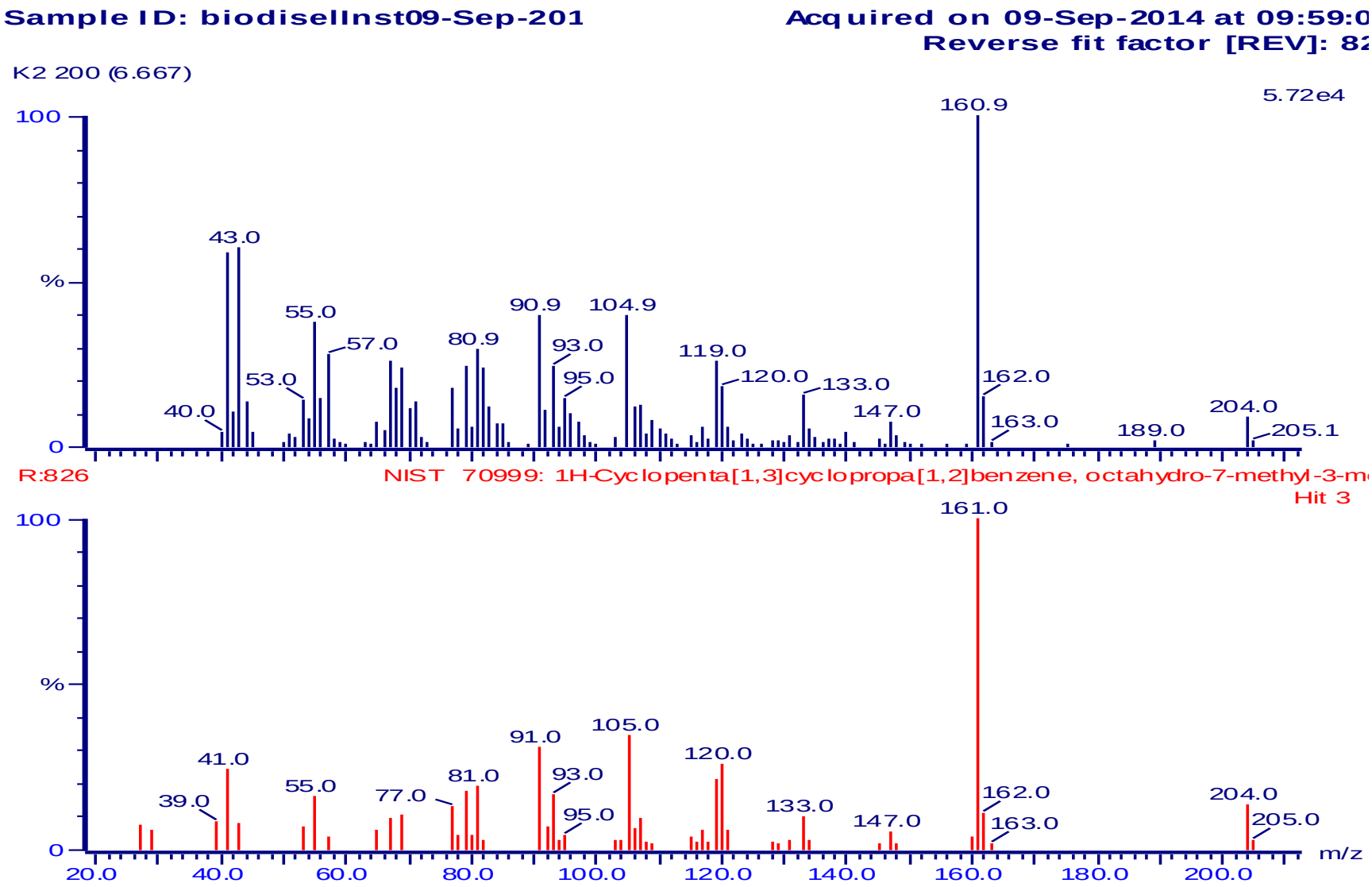
Sample ID: biodiselInst09-Sep-201
Acquired on 09-Sep-2014 at 09:59:0
Reverse fit factor [REV]: 82
K2 200 (6.667)
5.72e4
100
%
0
160.9
43.0
55.0
57.0
53.0
40.0
80.9
90.9
104.9
93.0
95.0
119.0
120.0
133.0
147.0
162.0
163.0
189.0
204.0
205.1
R:826
NIST 70999: 1H-Cyclopenta[1,3]cyclopropa[1,2]benzene, octahydro-7-methyl-3-m
Hit 3
100
%
0
161.0
91.0
105.0
120.0
41.0
39.0
55.0
77.0
81.0
93.0
95.0
133.0
147.0
162.0
163.0
204.0
205.0
20.0
40.0
60.0
80.0
100.0
120.0
140.0
160.0
180.0
200.0
m/z

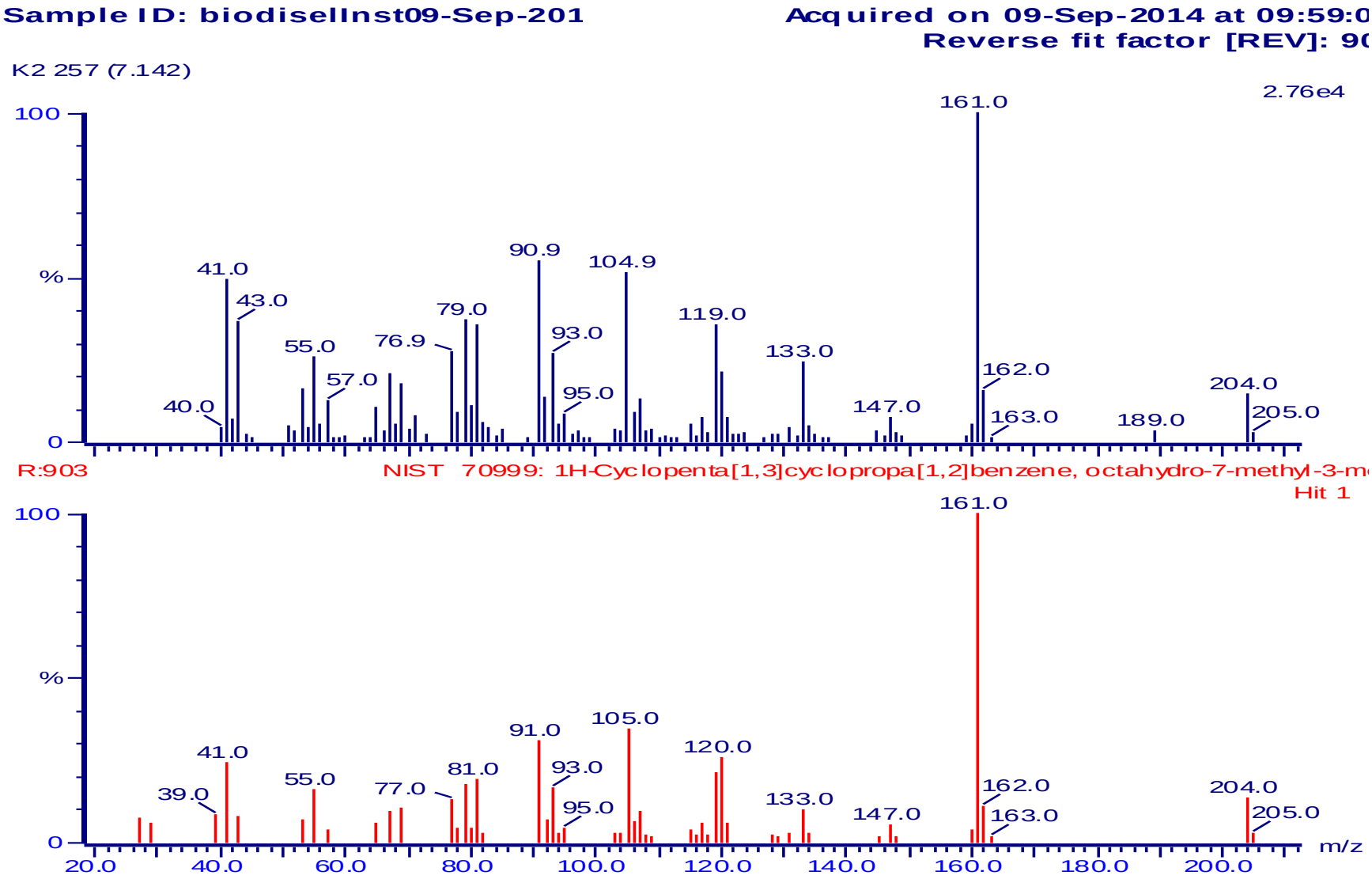
Sample ID: biodiselInst09-Sep-201
Acquired on 09-Sep-2014 at 09:59:0
Reverse fit factor [REV]: 9(
K2 257 (7.142)
2.76e4
100
%
0
41.0
43.0
40.0
55.0
57.0
76.9
79.0
90.9
93.0
95.0
104.9
119.0
133.0
147.0
161.0
162.0
163.0
189.0
204.0
205.0
R:903
NIST 70999: 1H-Cyclopenta[1,3]cyclopropa[1,2]benzene, octahydro-7-methyl-3-m
Hit 1
100
%
0
39.0
41.0
55.0
77.0
81.0
91.0
93.0
95.0
105.0
120.0
133.0
147.0
161.0
162.0
163.0
204.0
205.0
20.0
40.0
60.0
80.0
100.0
120.0
140.0
160.0
180.0
200.0
m/z

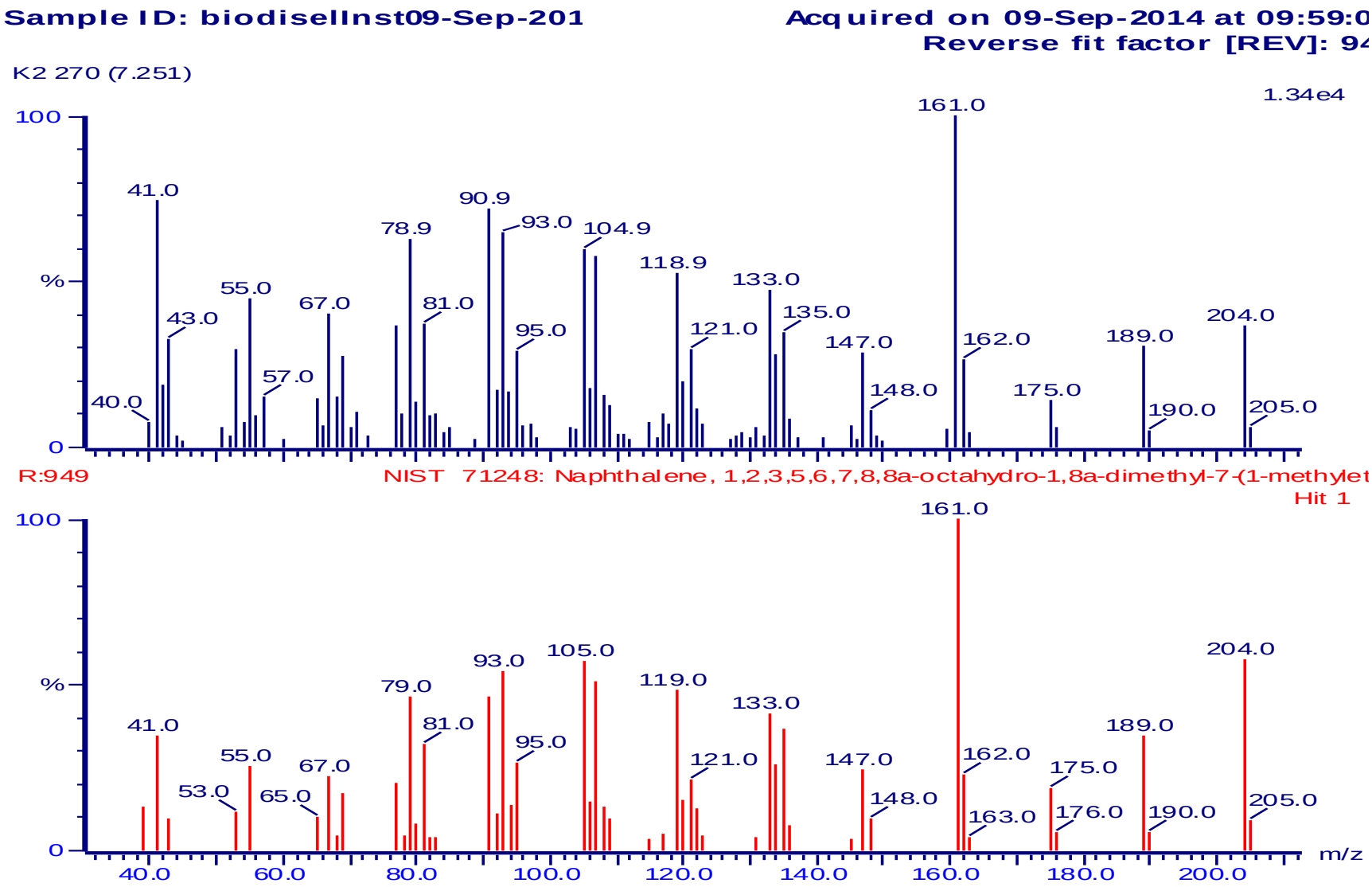
Sample ID: biodiselInst09-Sep-201
Acquired on 09-Sep-2014 at 09:59:0
Reverse fit factor [REV]: 94
K2 270 (7.251)
1.34e4
100
%
0
41.0
43.0
55.0
57.0
67.0
78.9
81.0
90.9
93.0
95.0
104.9
118.9
121.0
133.0
135.0
147.0
148.0
161.0
162.0
175.0
189.0
190.0
204.0
205.0
40.0
R:949
NIST 71248: Naphthalene, 1,2,3,5,6,7,8,8a-octahydro-1,8a-dimethyl-7-(1-methylet
Hit 1
100
%
0
41.0
53.0
55.0
65.0
67.0
79.0
81.0
93.0
95.0
105.0
119.0
121.0
133.0
147.0
148.0
161.0
162.0
163.0
175.0
176.0
189.0
190.0
204.0
205.0
m/z
40.0
60.0
80.0
100.0
120.0
140.0
160.0
180.0
200.0

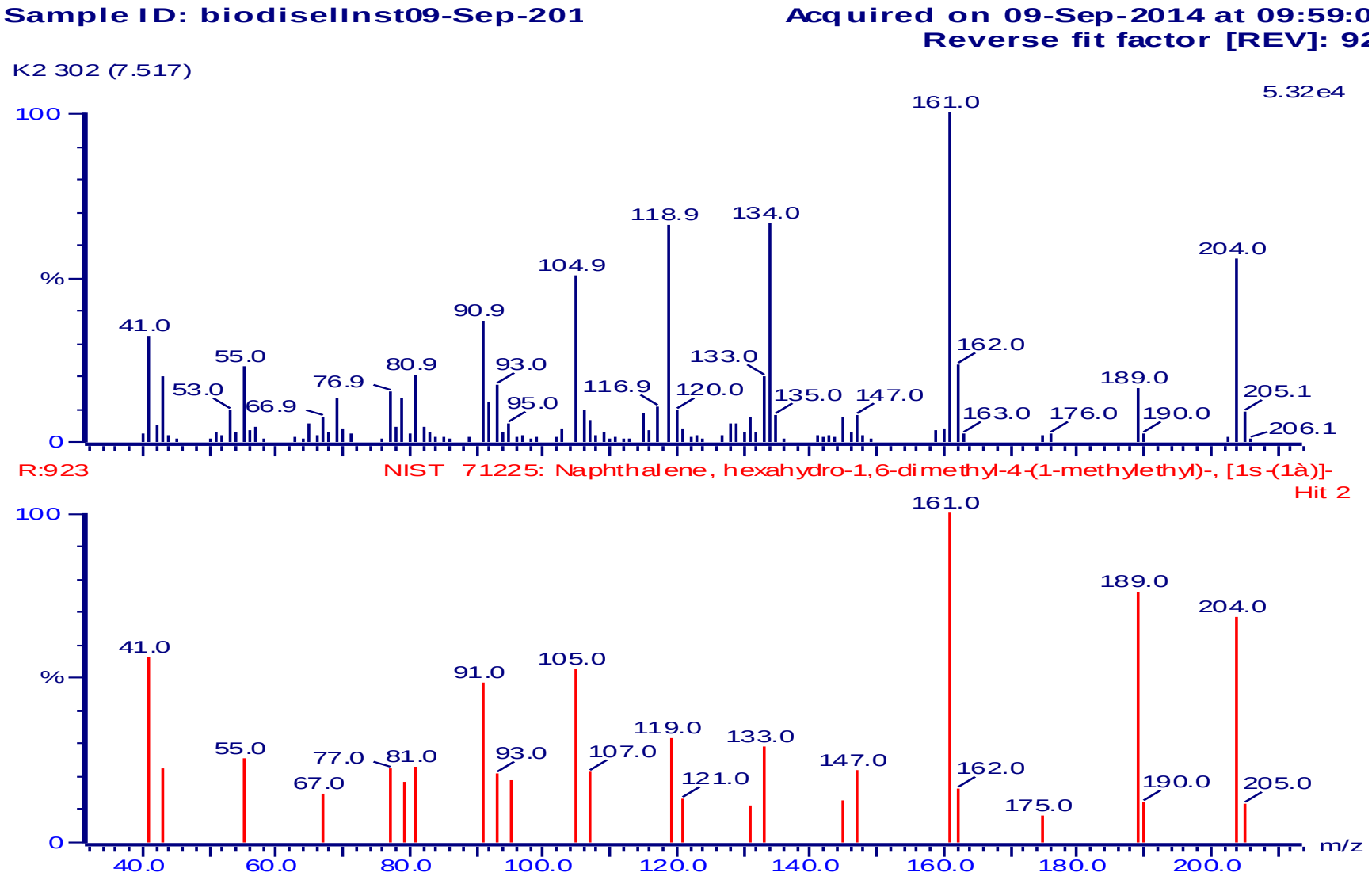
Sample ID: biodiselInst09-Sep-201
Acquired on 09-Sep-2014 at 09:59:0
Reverse fit factor [REV]: 92
K2 302 (7.517)
5.32e4
100
%
0
41.0
53.0
55.0
66.9
76.9
80.9
90.9
93.0
95.0
104.9
116.9
118.9
120.0
133.0
134.0
135.0
147.0
161.0
162.0
163.0
176.0
189.0
190.0
204.0
205.1
206.1
R:923
NIST 71225: Naphthalene, hexahydro-1,6-dimethyl-4-(1-methylethyl)-, [1s-(1à)]-
Hit 2
100
%
0
41.0
55.0
67.0
77.0
81.0
91.0
93.0
105.0
107.0
119.0
121.0
133.0
147.0
161.0
162.0
175.0
189.0
190.0
204.0
205.0
m/z
40.0
60.0
80.0
100.0
120.0
140.0
160.0
180.0
200.0

(B) Mass spectra of Oxygenated Orange Oil

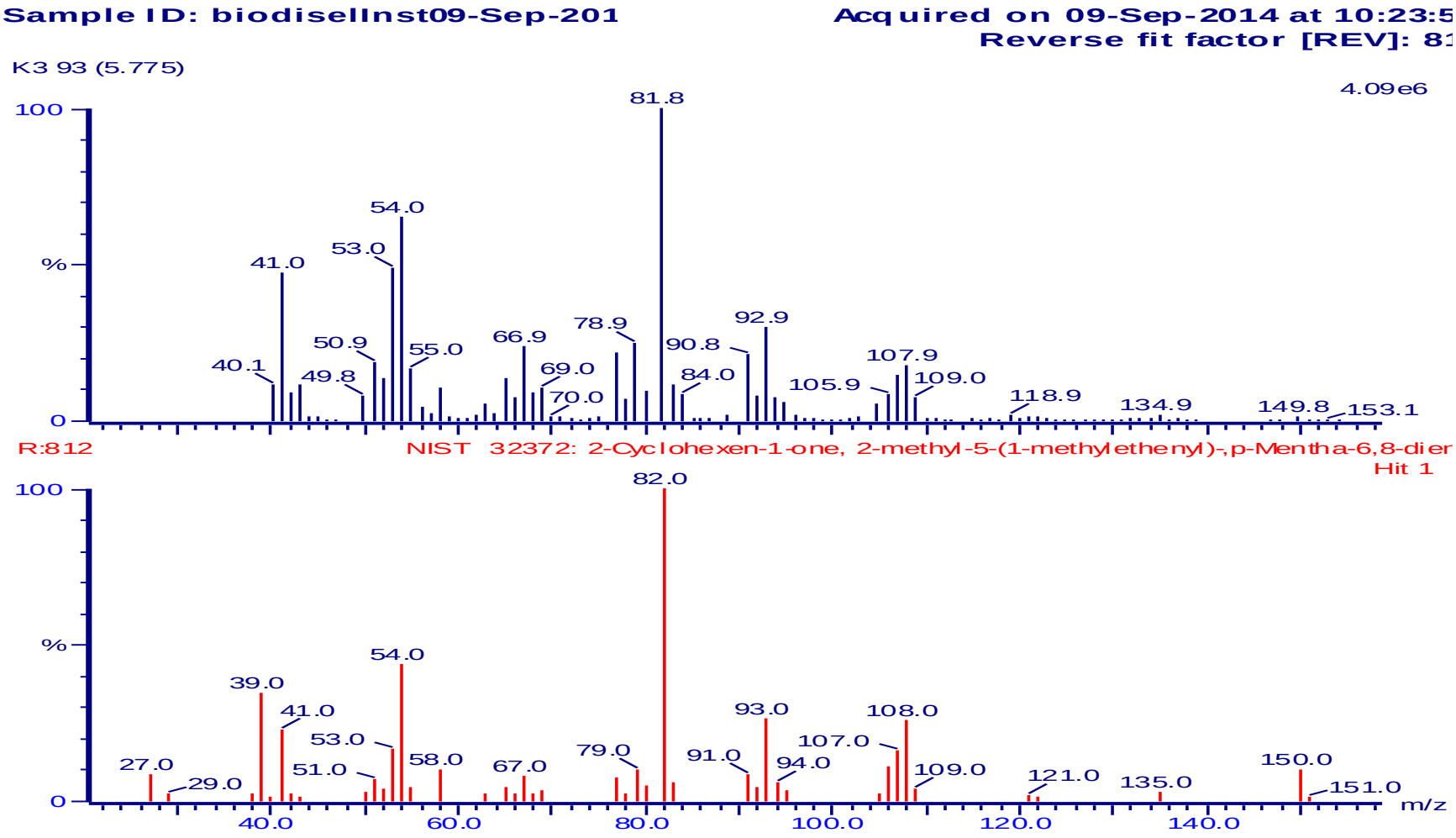

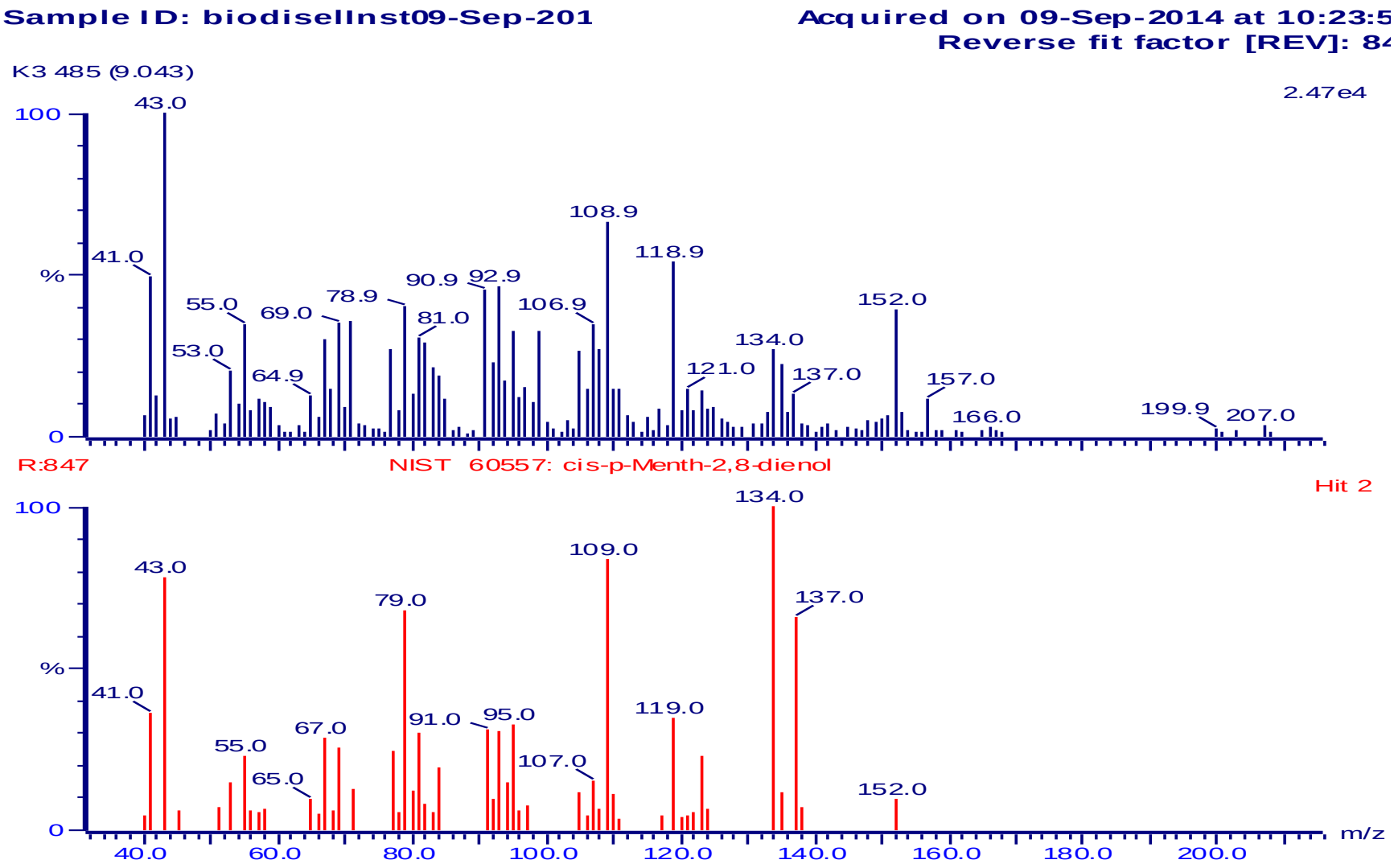
Sample ID: biodiselInst09-Sep-201
Acquired on 09-Sep-2014 at 10:23:5
Reverse fit factor [REV]: 84
K3 485 (9.043)
2.47e4
100
%
0
43.0
41.0
55.0
53.0
69.0
64.9
78.9
90.9
92.9
81.0
108.9
106.9
118.9
121.0
134.0
137.0
152.0
157.0
166.0
199.9
207.0
R:847
NIST 60557: cis-p-Menth-2,8-dienol
Hit 2
100
%
0
134.0
109.0
43.0
79.0
137.0
41.0
91.0
95.0
67.0
55.0
119.0
107.0
65.0
152.0
40.0
60.0
80.0
100.0
120.0
140.0
160.0
180.0
200.0
m/z

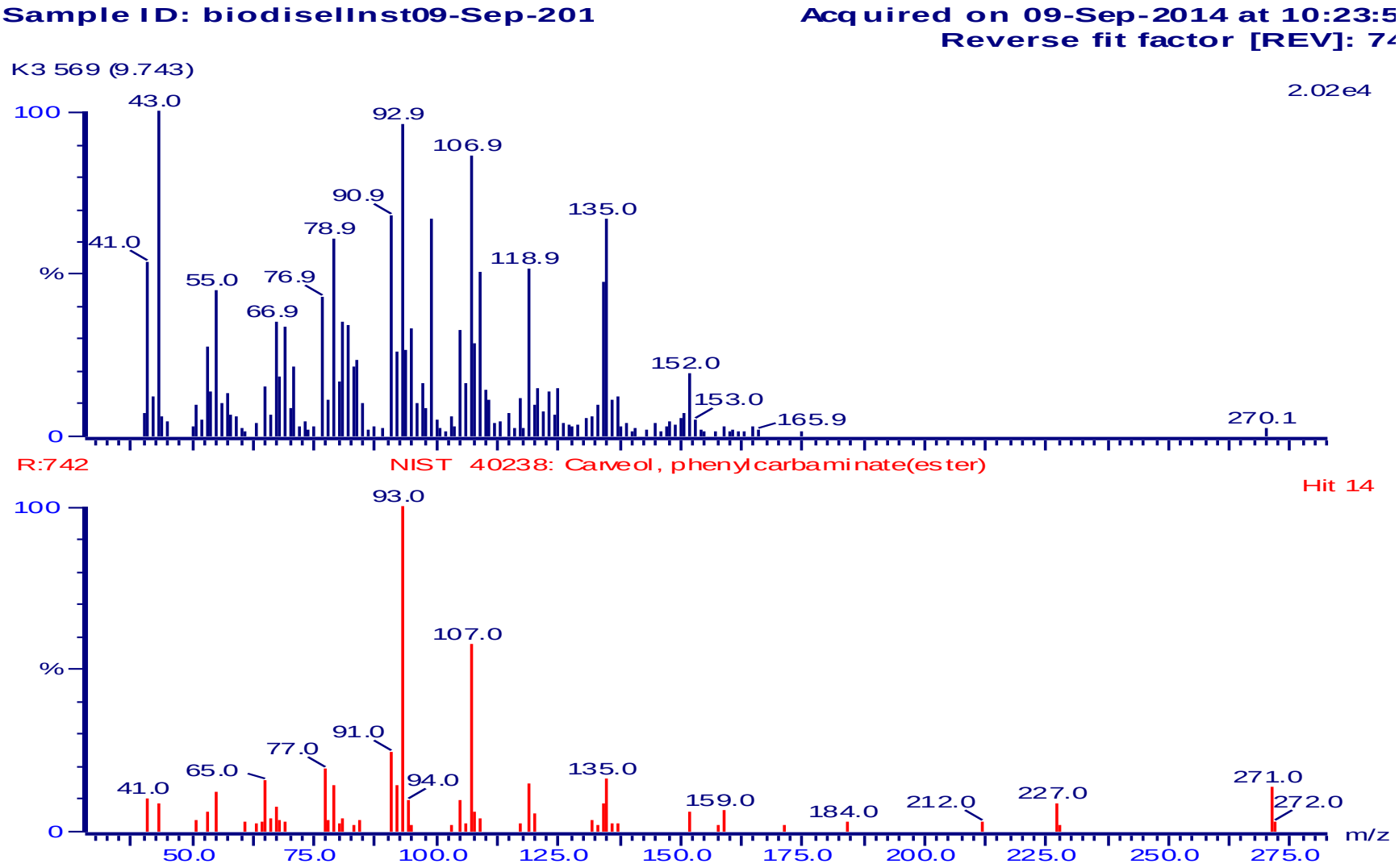
Sample ID: biodiselInst09-Sep-201
Acquired on 09-Sep-2014 at 10:23:5
Reverse fit factor [REV]: 74
K3 569 (9.743)
2.02e4
100
%
0
43.0
92.9
106.9
90.9
135.0
78.9
41.0
118.9
55.0
76.9
66.9
152.0
153.0
165.9
270.1
R:742
NIST 40238: Carveol, phenylcarbaminate(ester)
Hit 14
93.0
107.0
91.0
77.0
65.0
41.0
94.0
135.0
159.0
184.0
212.0
227.0
271.0
272.0
m/z
50.0
75.0
100.0
125.0
150.0
175.0
200.0
225.0
250.0
275.0

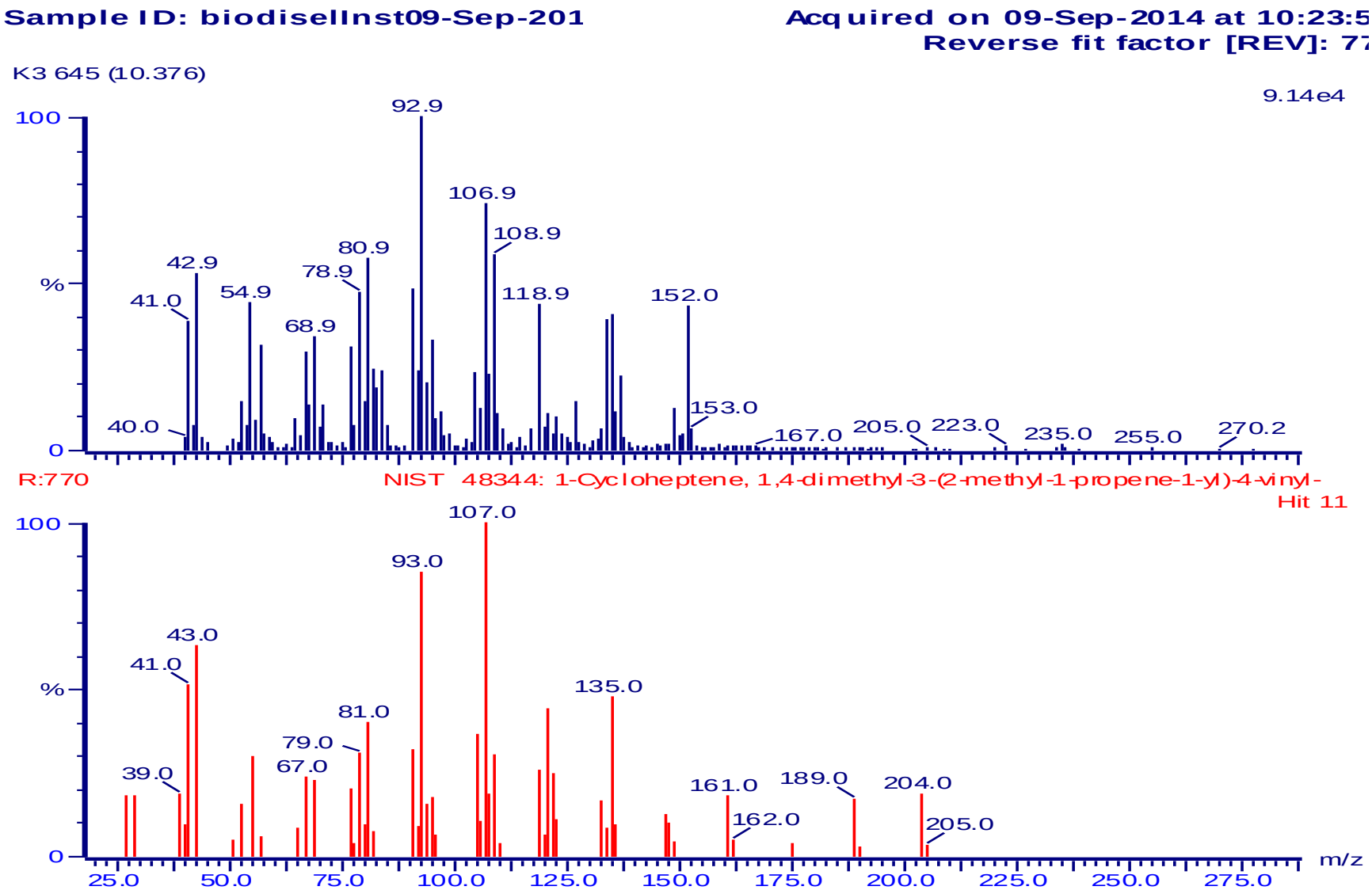
Sample ID: biodiselInst09-Sep-201
Acquired on 09-Sep-2014 at 10:23:5
Reverse fit factor [REV]: 77
K3 645 (10.376)
9.14e4
100
%
0
92.9
106.9
108.9
80.9
42.9
78.9
54.9
41.0
118.9
152.0
68.9
153.0
40.0
167.0
205.0
223.0
235.0
255.0
270.2
R:770
NIST 48344: 1-Cycloheptene, 1,4-dimethyl-3-(2-methyl-1-propene-1-yl)-4-vinyl-
Hit 11
100
%
0
107.0
93.0
43.0
41.0
135.0
81.0
79.0
67.0
39.0
161.0
189.0
204.0
162.0
205.0
m/z
25.0
50.0
75.0
100.0
125.0
150.0
175.0
200.0
225.0
250.0
275.0

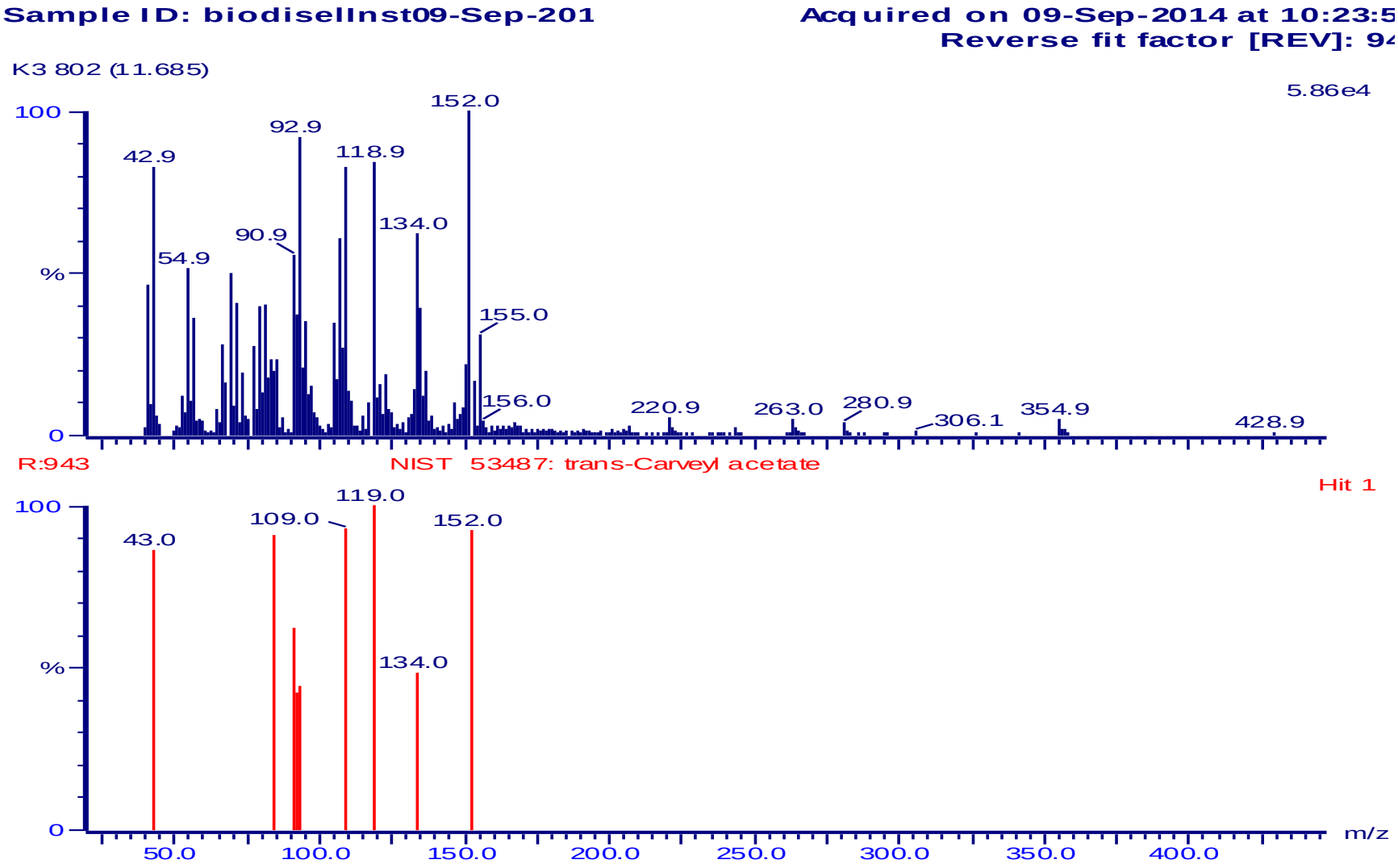
Sample ID: biodiselInst09-Sep-201
Acquired on 09-Sep-2014 at 10:23:5
Reverse fit factor [REV]: 94
K3 802 (11.685)
5.86e4
100
%
0
42.9
54.9
90.9
92.9
118.9
134.0
152.0
155.0
156.0
220.9
263.0
280.9
306.1
354.9
428.9
R:943
NIST 53487: trans-Carveyl acetate
Hit 1
100
%
0
43.0
109.0
119.0
134.0
152.0
50.0
100.0
150.0
200.0
250.0
300.0
350.0
400.0
m/z

APPENDIX XV: FTIR Spectra of *d*-Limonene and Derivatives

(A) FTIR Spectrum of *d*-Limonene

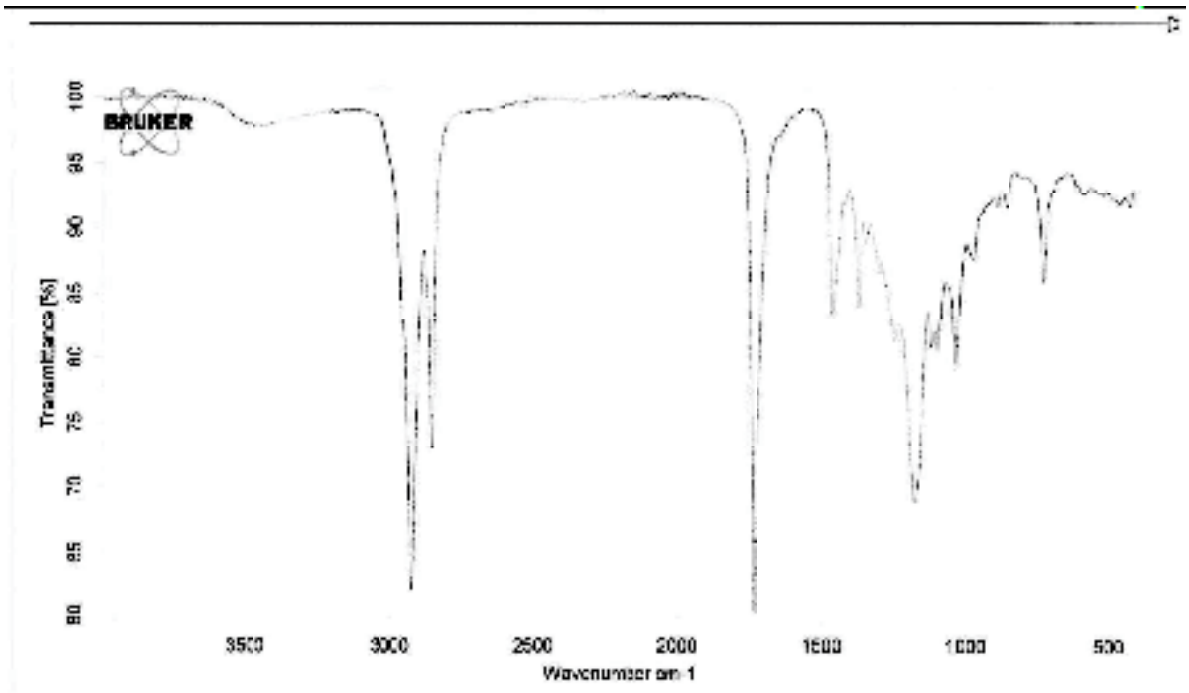

(B) FTIR Spectrum of Oxygenated *d*-Limonene derivatives

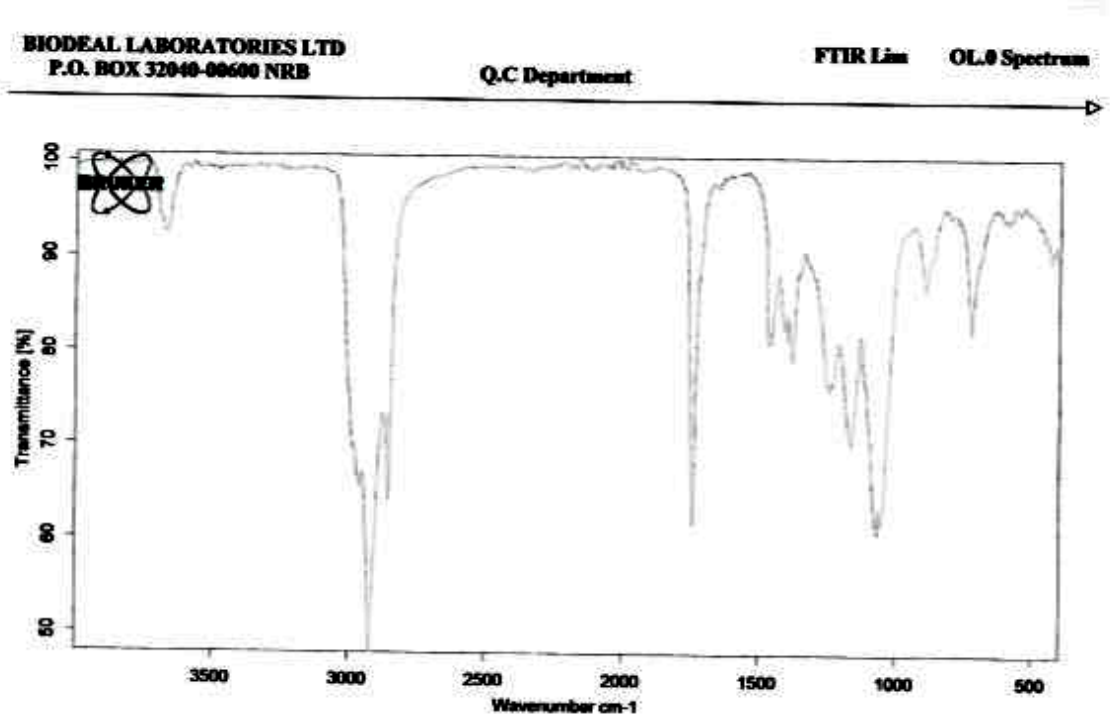

(C) FTIR Spectrum of Hydrogenated *d*-Limonene derivatives

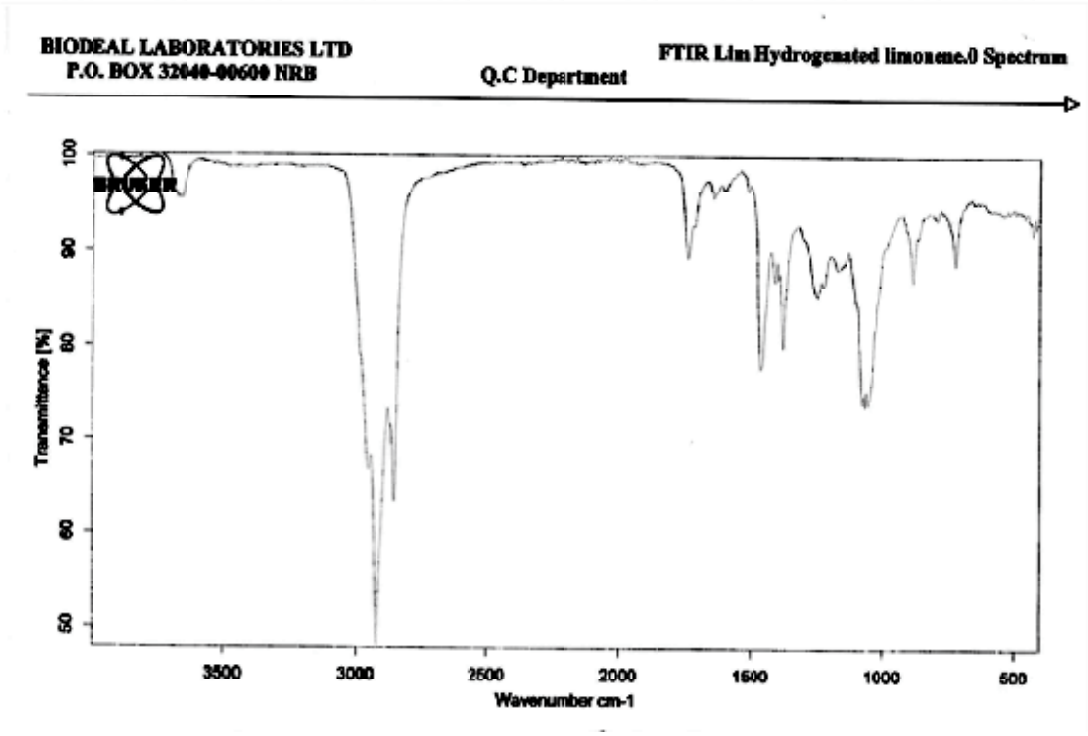

APPENDIX XVI: Transesterification to Obtain Ethyl Esters (A) Separation (B) Cleaning (C) and Drying (D)

APPENDIX XVII: Mass Spectra of Fatty Acid Ethyl Esters

(A) Mass spectra of *Rhizoclonium grande* ethyl esters

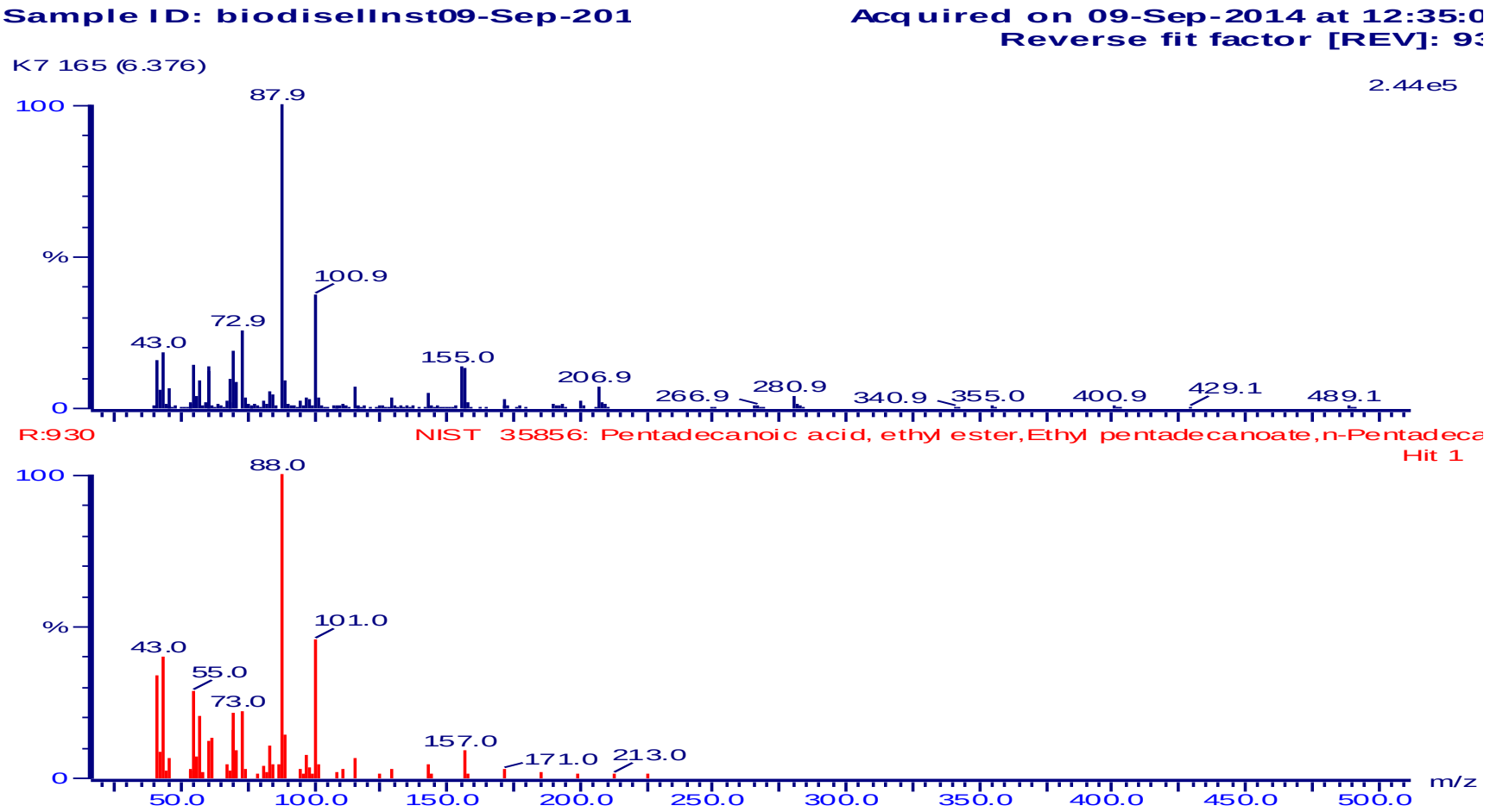

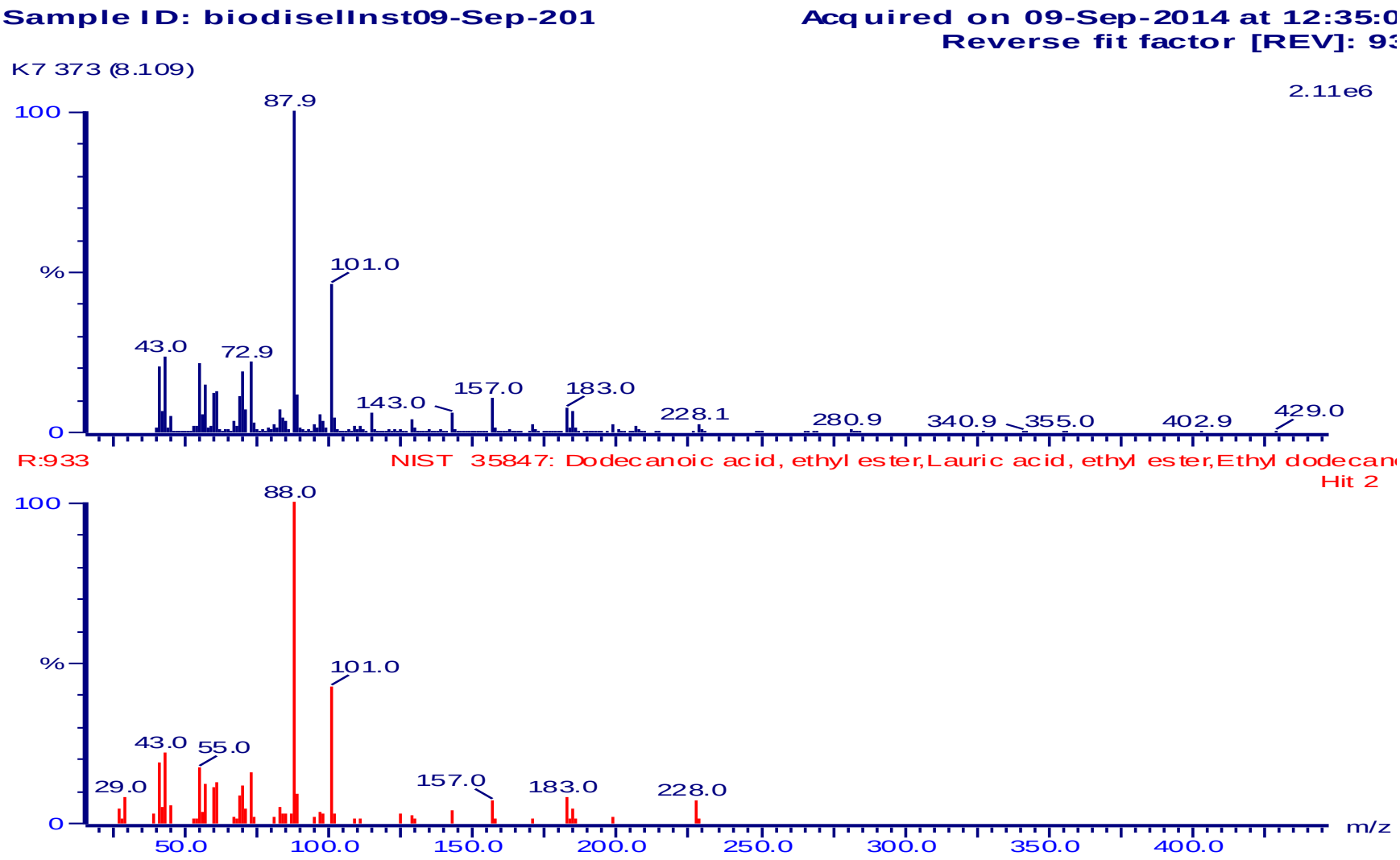
Sample ID: biodiselInst09-Sep-201
Acquired on 09-Sep-2014 at 12:35:0
Reverse fit factor [REV]: 93
K7 373 (8.109)
2.11e6
100
%
0
87.9
101.0
43.0
72.9
143.0
157.0
183.0
228.1
280.9
340.9
355.0
402.9
429.0
R:933
NIST 35847: Dodecanoic acid, ethyl ester,Lauric acid, ethyl ester,Ethyl dodecan
Hit 2
100
%
0
88.0
101.0
43.0
55.0
29.0
157.0
183.0
228.0
m/z
50.0
100.0
150.0
200.0
250.0
300.0
350.0
400.0

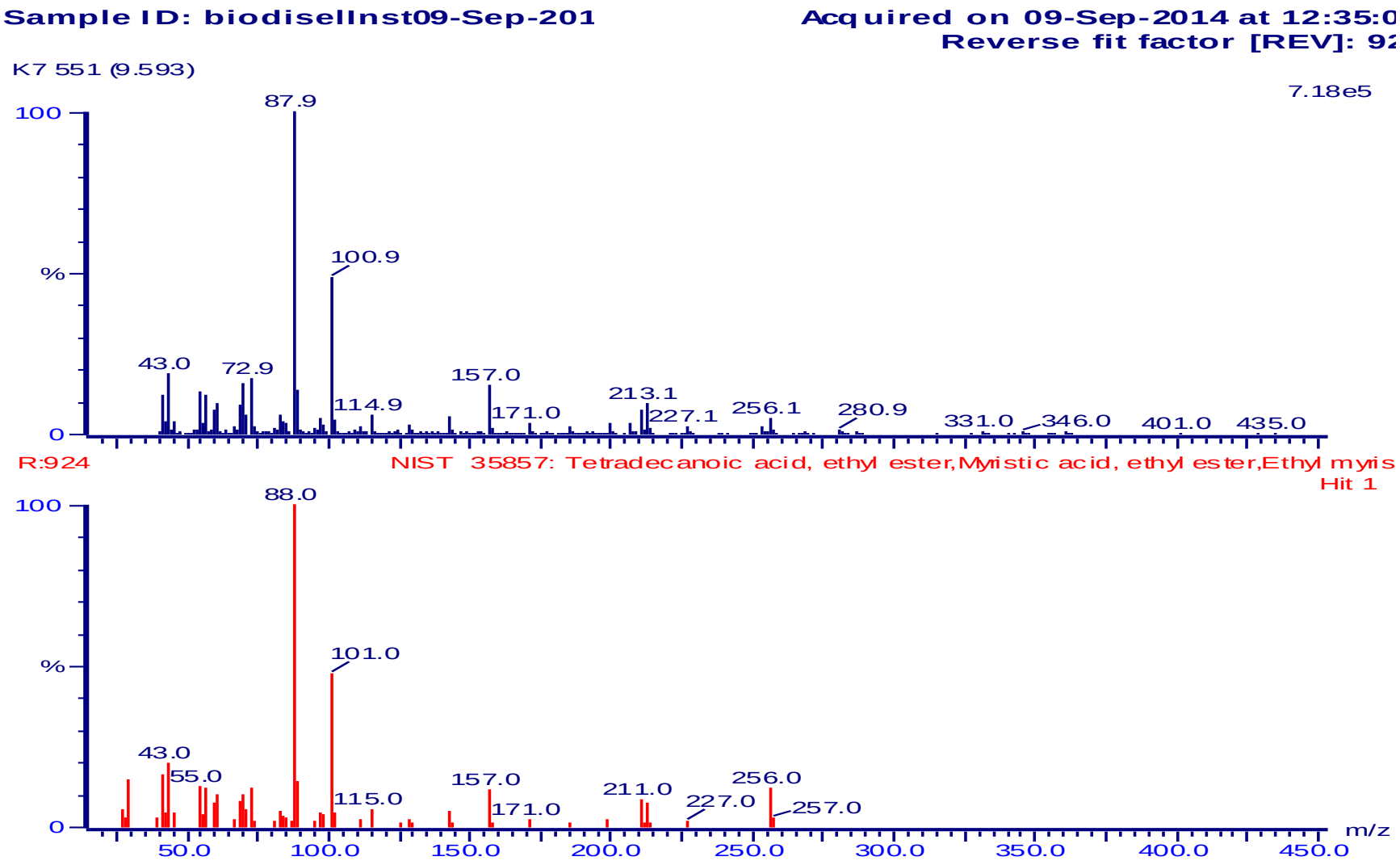
Sample ID: biodiselInst09-Sep-201
Acquired on 09-Sep-2014 at 12:35:0
Reverse fit factor [REV]: 92
K7 551 (9.593)
7.18e5
100
%
0
87.9
100.9
43.0
72.9
157.0
213.1
114.9
171.0
227.1
256.1
280.9
331.0
346.0
401.0
435.0
R:924
NIST 35857: Tetradecanoic acid, ethyl ester,Myristic acid, ethyl ester,Ethyl myris
Hit 1
100
%
0
88.0
101.0
43.0
55.0
115.0
157.0
171.0
211.0
227.0
256.0
257.0
m/z
50.0
100.0
150.0
200.0
250.0
300.0
350.0
400.0
450.0

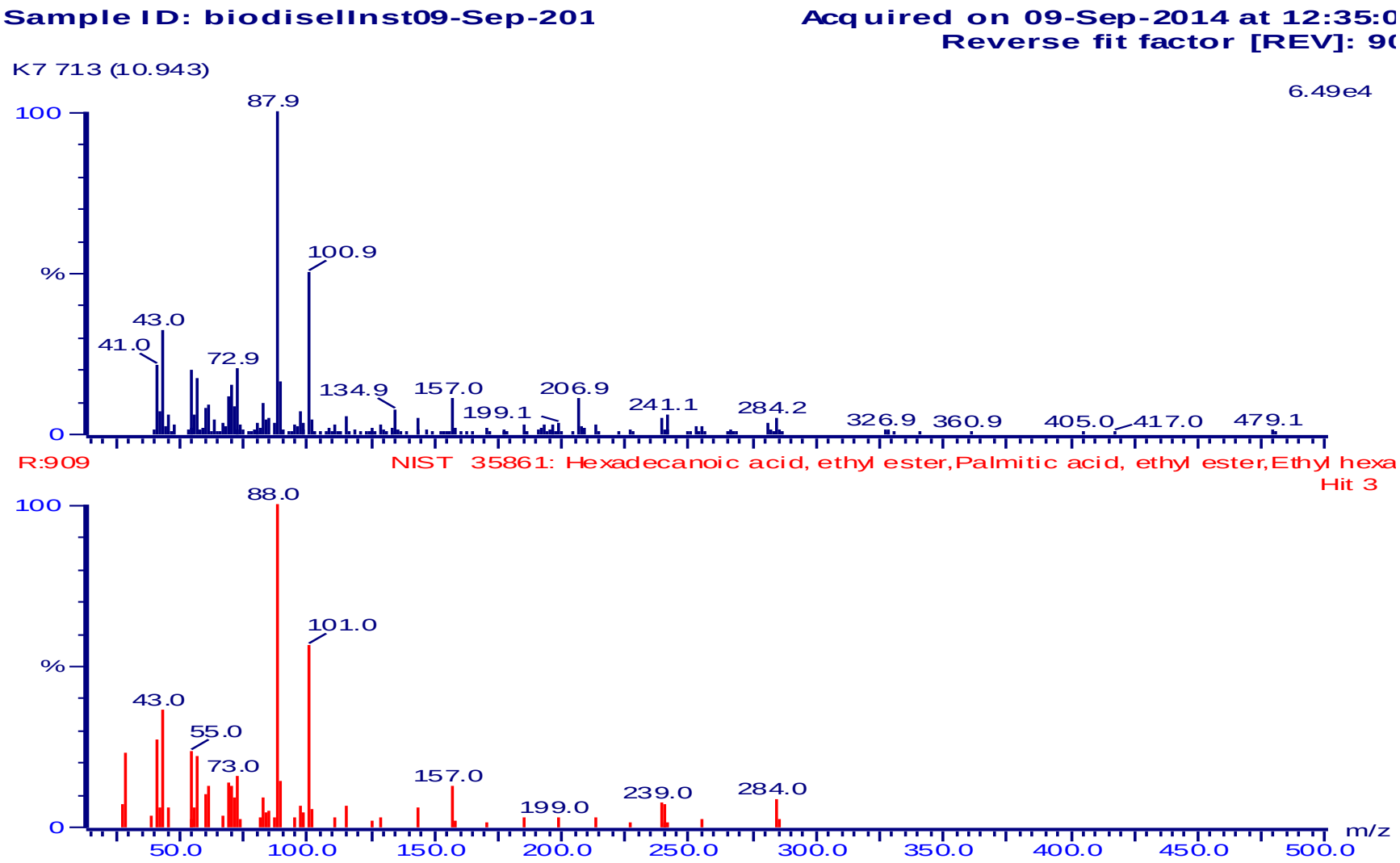
Sample ID: biodiselInst09-Sep-201
Acquired on 09-Sep-2014 at 12:35:0
Reverse fit factor [REV]: 9(
K7 713 (10.943)
6.49e4
100
%
0
87.9
100.9
43.0
41.0
72.9
134.9
157.0
199.1
206.9
241.1
284.2
326.9
360.9
405.0
417.0
479.1
R:909
NIST 35861: Hexadecanoic acid, ethyl ester,Palmitic acid, ethyl ester,Ethyl hexa
Hit 3
100
%
0
88.0
101.0
43.0
55.0
73.0
157.0
199.0
239.0
284.0
m/z
50.0
100.0
150.0
200.0
250.0
300.0
350.0
400.0
450.0
500.0

(B) Mass spectra of *Jatropha curcas* ethyl esters

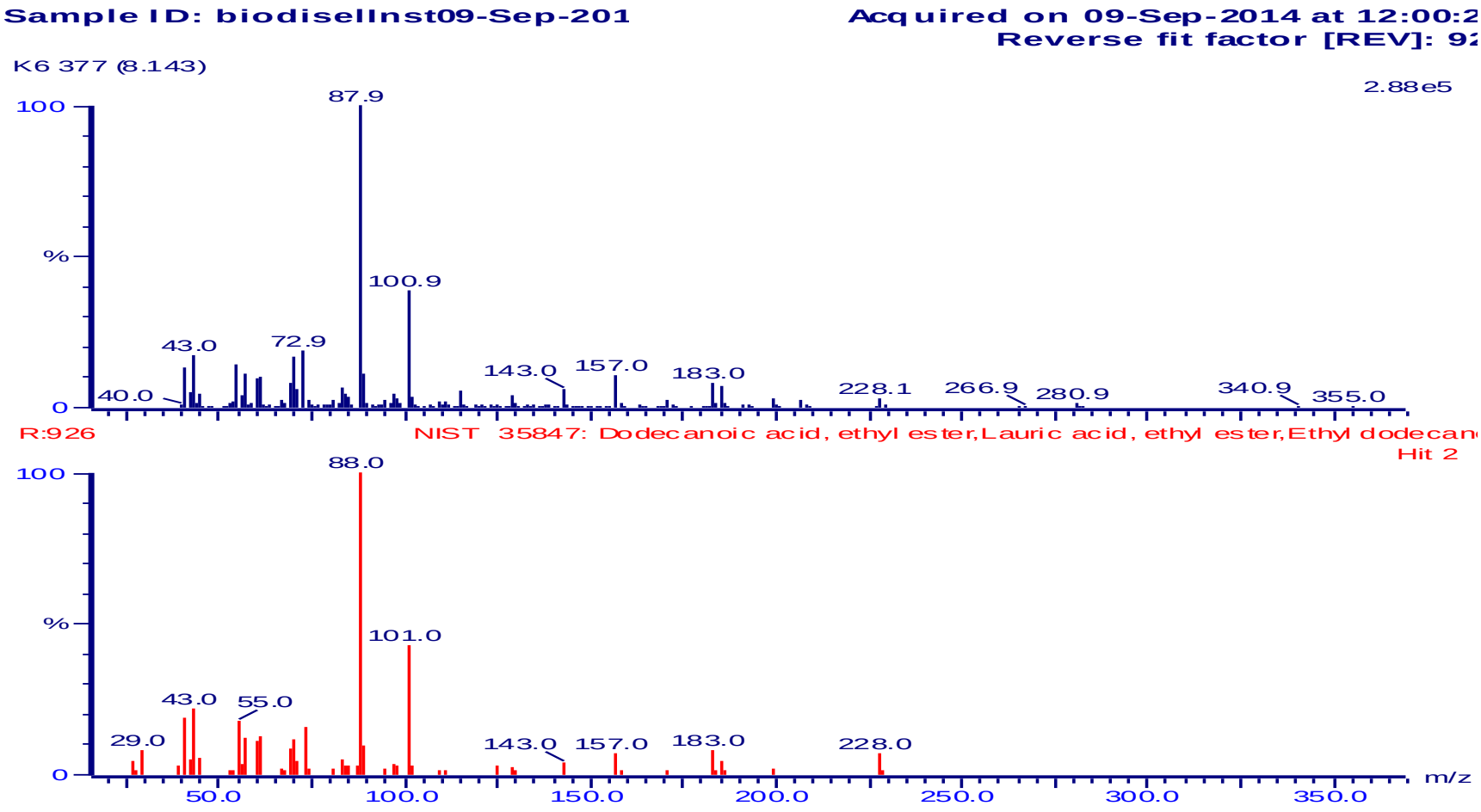

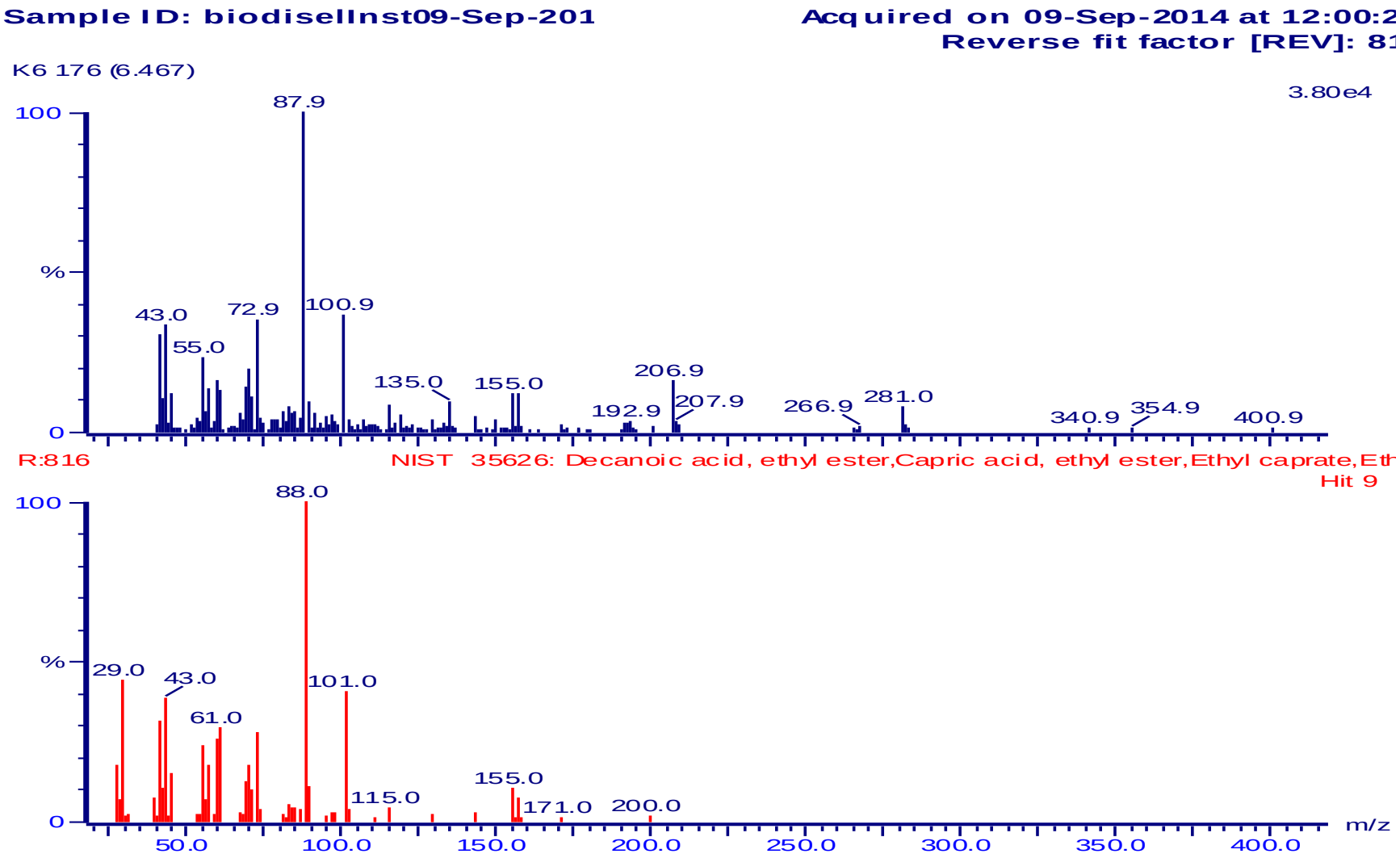
Sample ID: biodiselInst09-Sep-201
Acquired on 09-Sep-2014 at 12:00:2
Reverse fit factor [REV]: 81
K6 176 (6.467)
3.80e4
100
%
0
87.9
43.0
72.9
100.9
55.0
135.0
155.0
206.9
192.9
207.9
266.9
281.0
340.9
354.9
400.9
R:816
NIST 35626: Decanoic acid, ethyl ester,Capric acid, ethyl ester,Ethyl caprate,Eth
Hit 9
100
%
0
88.0
29.0
43.0
101.0
61.0
155.0
115.0
171.0
200.0
m/z
50.0
100.0
150.0
200.0
250.0
300.0
350.0
400.0

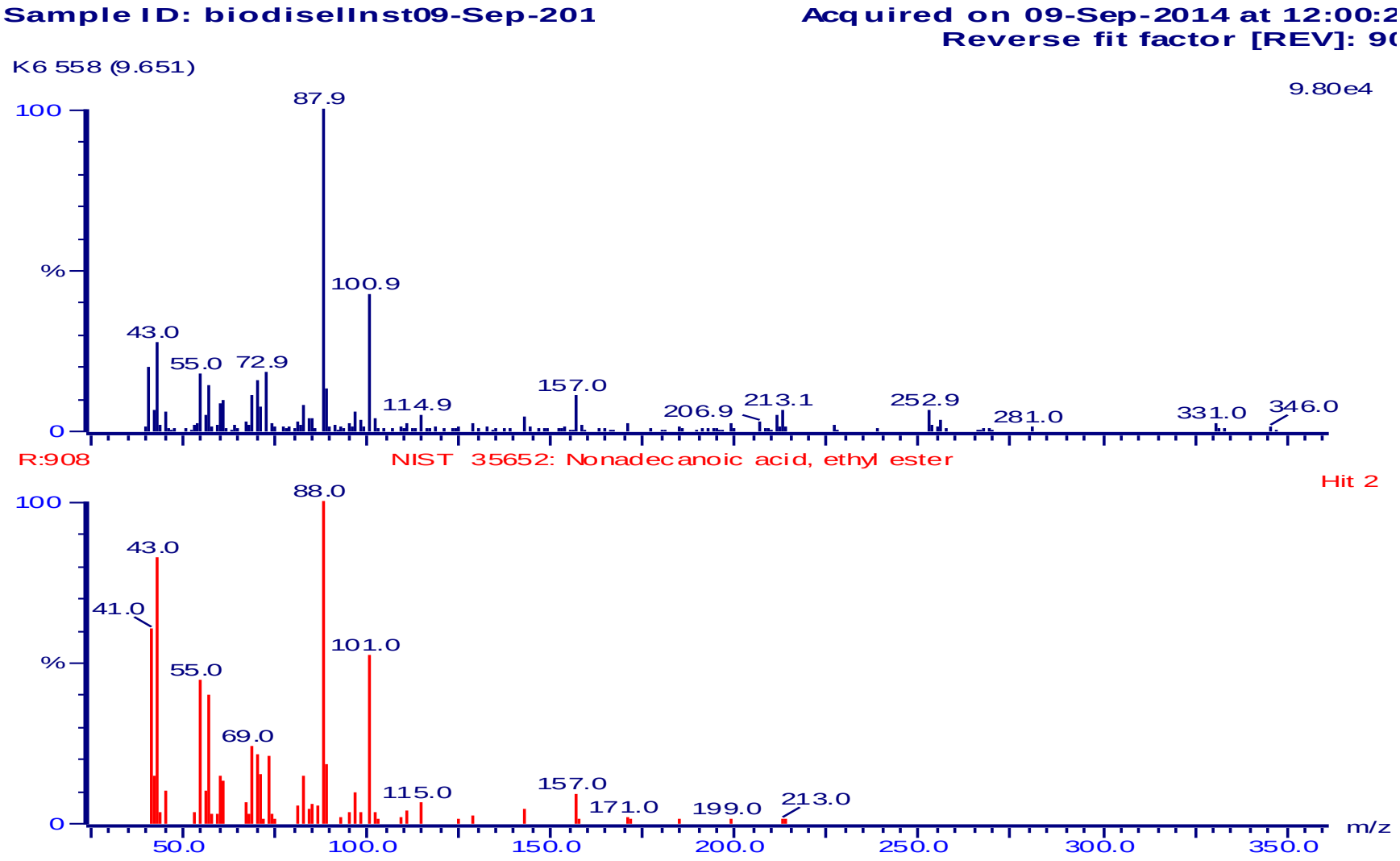
Sample ID: biodiselInst09-Sep-201
Acquired on 09-Sep-2014 at 12:00:2
Reverse fit factor [REV]: 9(
K6 558 (9.651)
9.80e4
100
%
0
87.9
100.9
43.0
55.0
72.9
114.9
157.0
206.9
213.1
252.9
281.0
331.0
346.0
R:908
NIST 35652: Nonadecanoic acid, ethyl ester
Hit 2
88.0
43.0
41.0
101.0
55.0
69.0
115.0
157.0
171.0
199.0
213.0
m/z
50.0
100.0
150.0
200.0
250.0
300.0
350.0

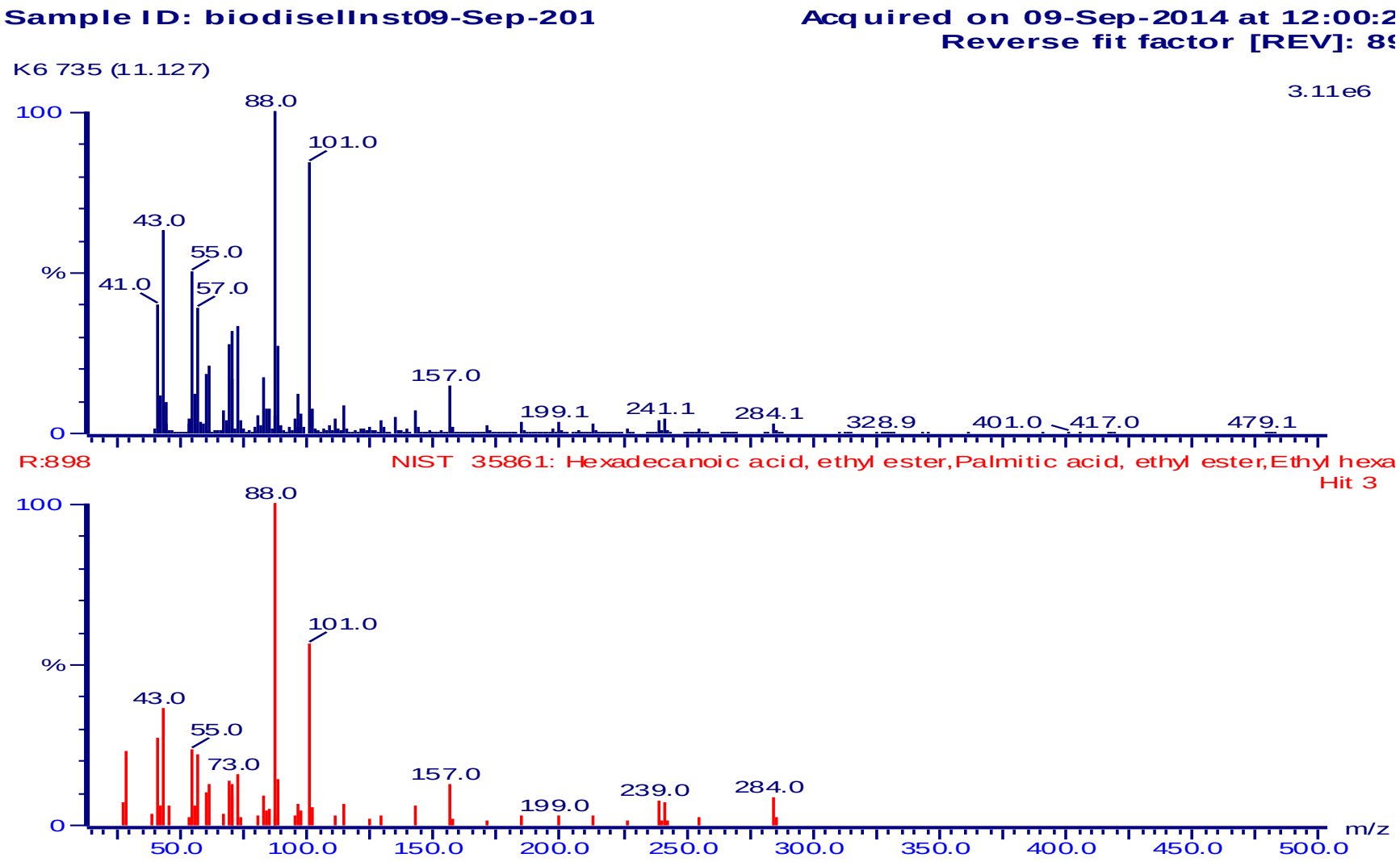
Sample ID: biodiselInst09-Sep-201
Acquired on 09-Sep-2014 at 12:00:2
Reverse fit factor [REV]: 8
K6 735 (11.127)
3.11e6
100
%
0
88.0
101.0
43.0
55.0
41.0
57.0
157.0
199.1
241.1
284.1
328.9
401.0
417.0
479.1
R:898
NIST 35861: Hexadecanoic acid, ethyl ester,Palmitic acid, ethyl ester,Ethyl hexa
Hit 3
100
%
0
88.0
101.0
43.0
55.0
73.0
157.0
199.0
239.0
284.0
m/z
50.0
100.0
150.0
200.0
250.0
300.0
350.0
400.0
450.0
500.0

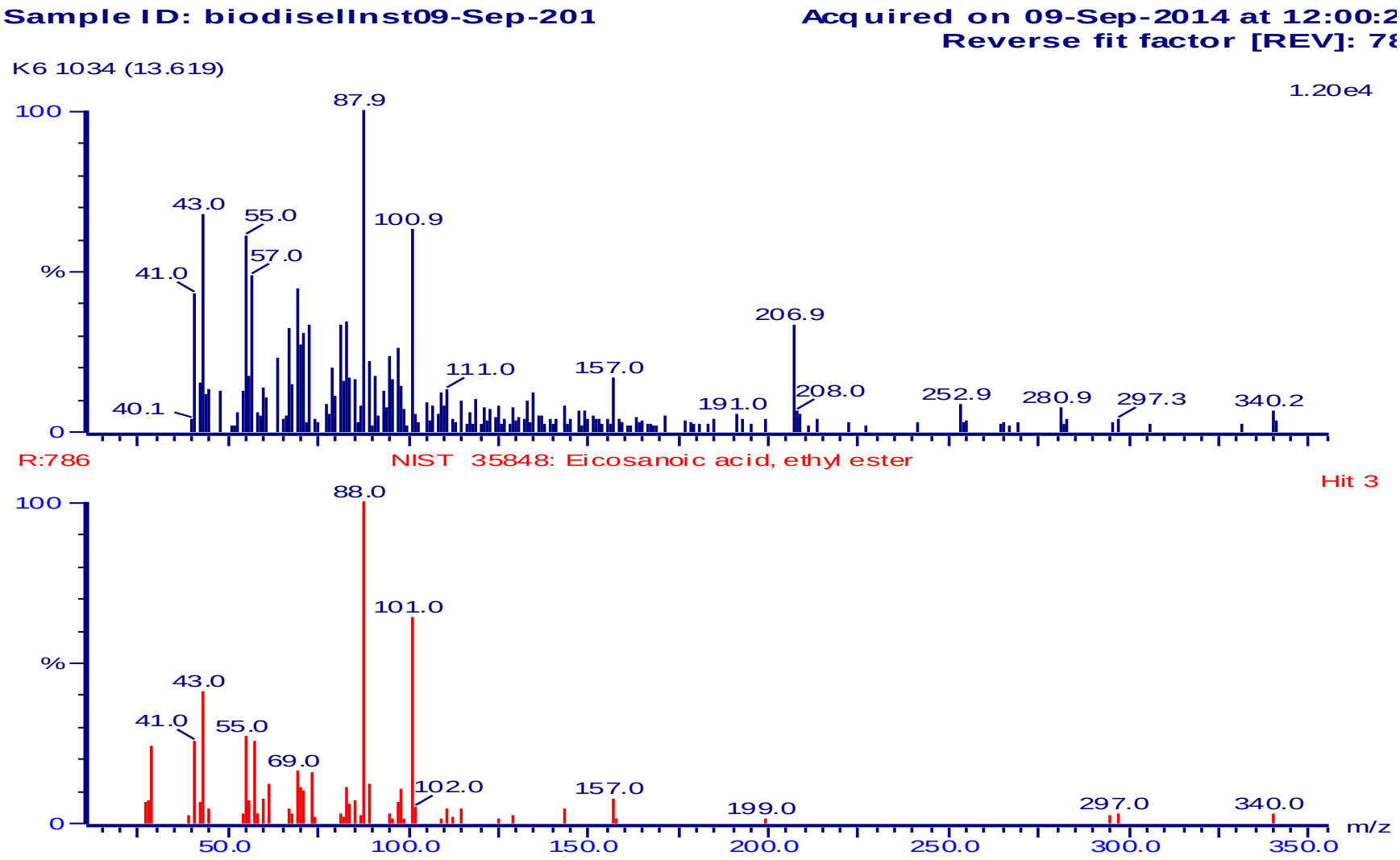
Sample ID: biodiselInst09-Sep-201
Acquired on 09-Sep-2014 at 12:00:2
Reverse fit factor [REV]: 78
K6 1034 (13.619)
1.20e4
100
%
0
87.9
43.0
55.0
100.9
57.0
41.0
206.9
111.0
157.0
40.1
191.0
208.0
252.9
280.9
297.3
340.2
R:786
NIST 35848: Eicosanoic acid, ethyl ester
Hit 3
88.0
101.0
43.0
41.0
55.0
69.0
102.0
157.0
199.0
297.0
340.0
m/z
50.0
100.0
150.0
200.0
250.0
300.0
350.0

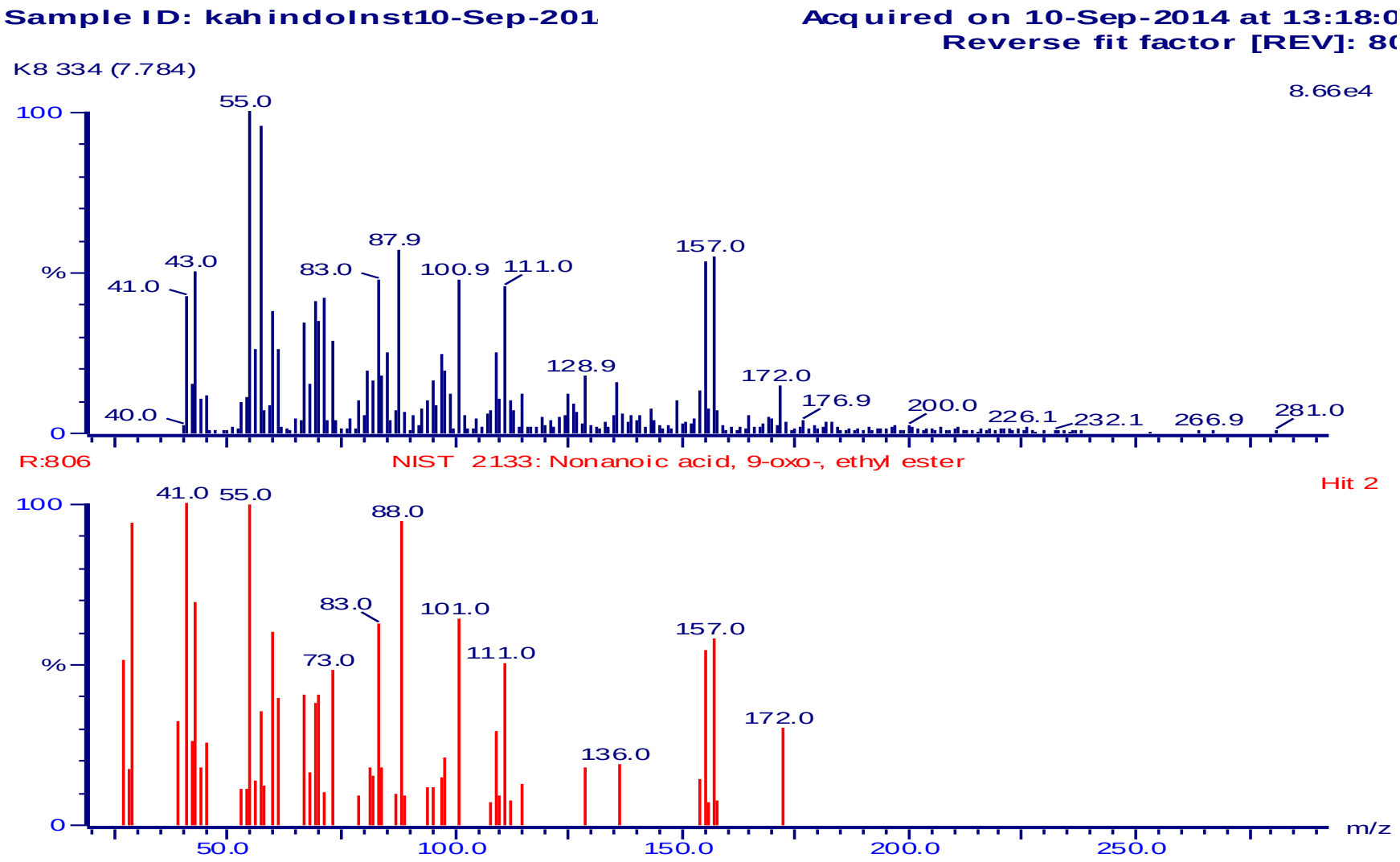
Sample ID: kahindoInst10-Sep-201
Acquired on 10-Sep-2014 at 13:18:0
Reverse fit factor [REV]: 8(
K8 334 (7.784)
8.66e4
100
%
0
55.0
43.0
41.0
87.9
83.0
100.9
111.0
157.0
128.9
172.0
176.9
200.0
226.1
232.1
266.9
281.0
40.0
R:806
NIST 2133: Nonanoic acid, 9-oxo-, ethyl ester
Hit 2
41.0
55.0
88.0
83.0
101.0
157.0
73.0
111.0
172.0
136.0
50.0
100.0
150.0
200.0
250.0
m/z

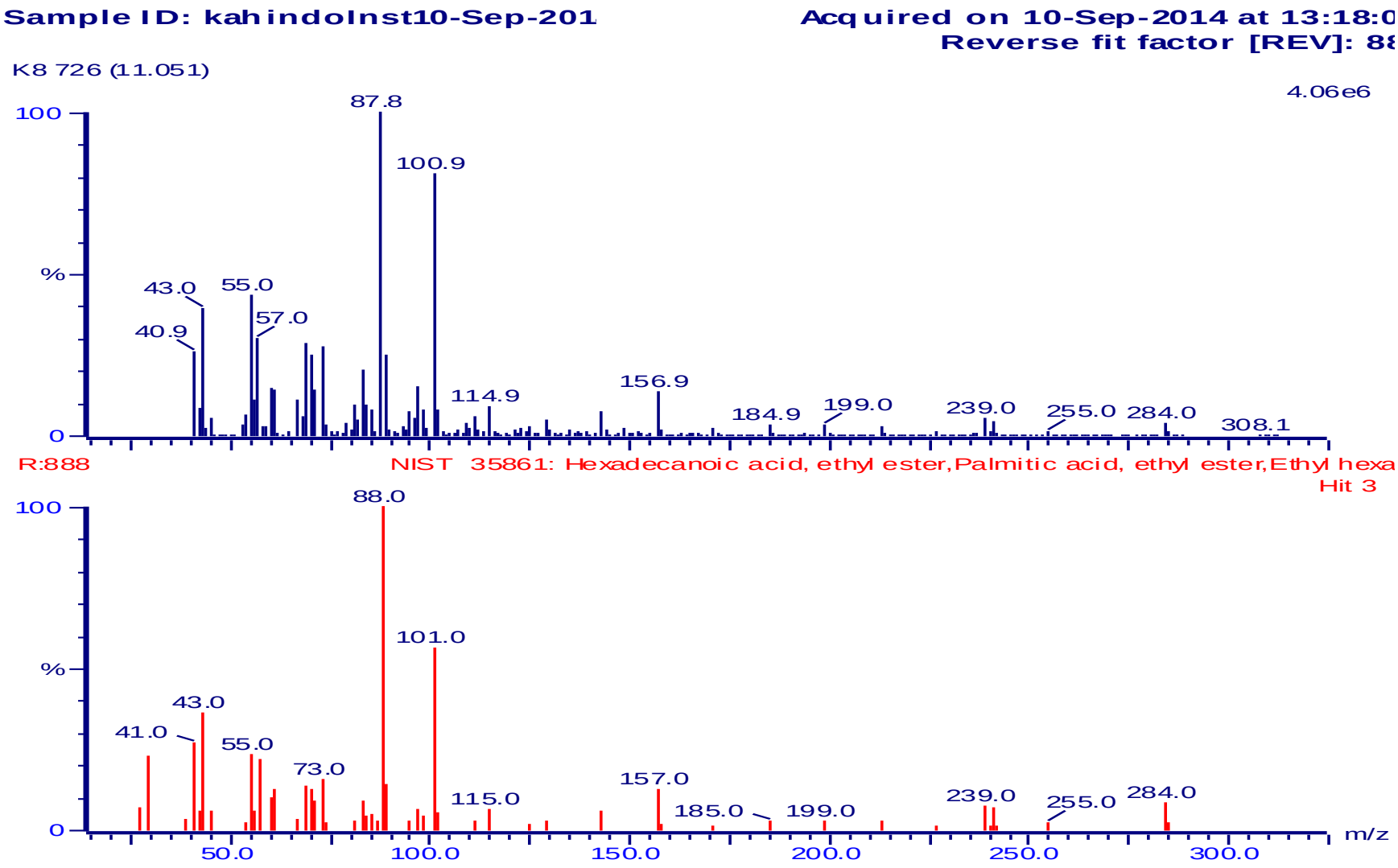
Sample ID: kahindoInst10-Sep-201
Acquired on 10-Sep-2014 at 13:18:0
Reverse fit factor [REV]: 8
K8 726 (11.051)
4.06e6
100
%
0
87.8
100.9
43.0
55.0
57.0
40.9
114.9
156.9
184.9
199.0
239.0
255.0
284.0
308.1
R:888
NIST 35861: Hexadecanoic acid, ethyl ester,Palmitic acid, ethyl ester,Ethyl hexa
Hit 3
100
%
0
88.0
101.0
43.0
41.0
55.0
73.0
115.0
157.0
185.0
199.0
239.0
255.0
284.0
m/z
50.0
100.0
150.0
200.0
250.0
300.0

APPENDIX XVIII: FTIR Spectra of Fatty Acid Ethyl Esters

(A) FTIR spectra of JOFAEE

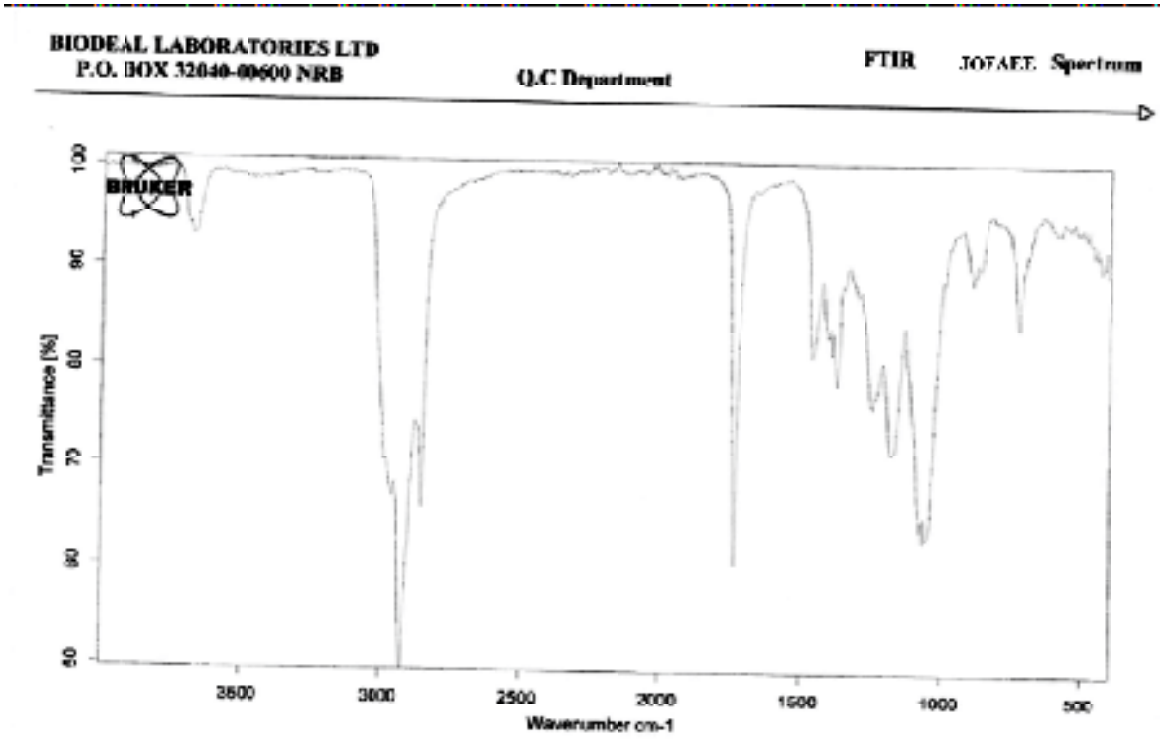

(B) FTIR spectra of JOFAEE

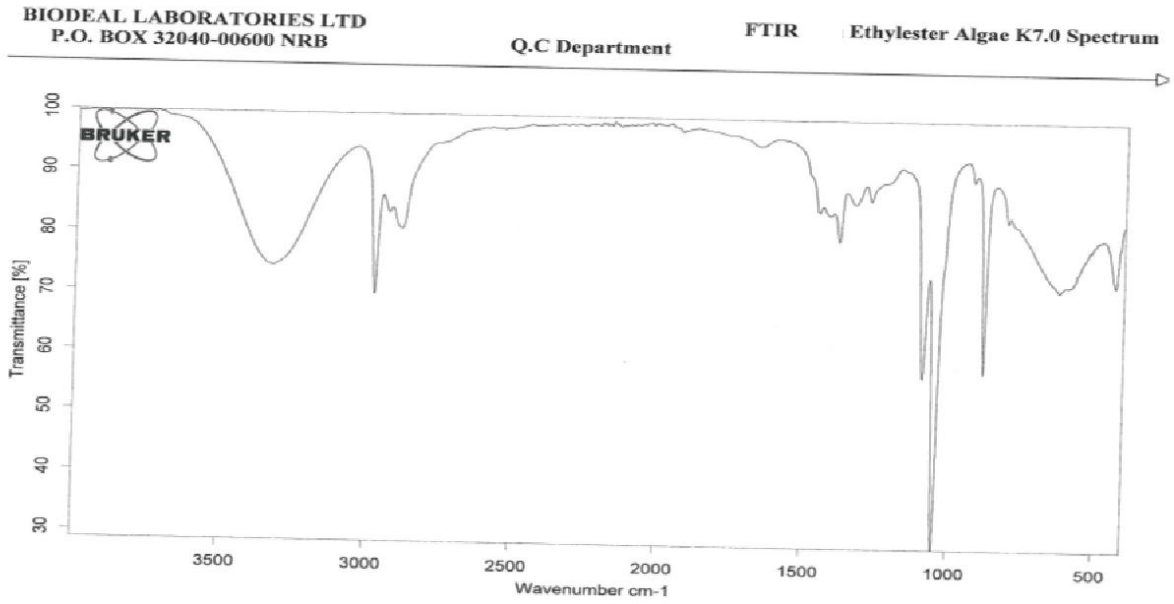

APPENDIX XIX: Auto distiller Model AD865G2 (A), Pensky – Martens closed cup apparatus (B) and Cloud point equipment (C)

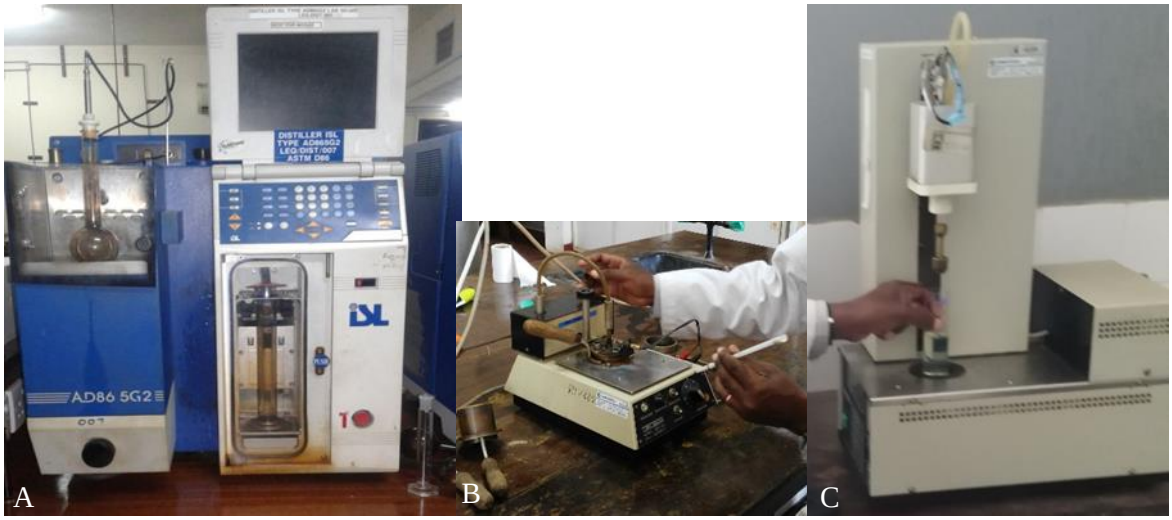

APPENDIX XX: Mass of Peelings Obtained from Citrus senensis Fruits

Sample No.	Sample Site/ Source	Mass of Whole Fruit (Grams±SD)	Mass of Peelings Per fruit (Grams±SD)	% Peelings per fruit
OS01	Malindi	237.016± 0.649	25.060± 0.247	10.573
OS02	Malindi	207.694± 0.556	28.859± 0.225	13.895
0S03	Malindi	254.402± 0.307	32.173± 0.312	12.646
OS04	Malindi	197.736± 0.638	25.510± 0.216	12.901
OS05	Malindi	186.650± 1.020	23.894± 0.338	12.802
OS06	Malindi	200.019± 0.634	27.633± 0.242	13.815
OS07	Malindi	172.100± 1.038	23.700± 0.423	13.771
OS08	Malindi	208.595± 0.653	27.659± 0.287	13.260
OS09	Malindi	244.423± 0.535	30.182± 0.245	12.348
OS10	Malindi	194.545± 0.668	23.539± 0.299	12.100
OS11	Muheza	252.113± 0.540	34.421± 0.232	13.653
OS12	Muheza	203.807± 0.560	26.118± 0.243	12.815
0S13	Muheza	187.030± 0.831	23.800± 0.256	12.725
OS14	Muheza	196.280± 0.654	28.606± 0.230	14.574
OS15	Muheza	188.026± 0.932	24.469± 0.415	13.013
OS16	Muheza	197.854± 0.712	23.716± 0.318	11.987
OS17	Muheza	199.054± 0.668	24.056± 0.256	12.085
OS18	Muheza	186.232± 0.738	23.724± 0.218	12.739
OS19	Muheza	197.271± 0.697	29.006± 0.241	14.704
OS20	Muheza	188.527± 0.554	24.938± 0.320	13.228

Sample No.	Sample Site/ Source	Mass of Whole Fruit (Grams±SD)	Mass of Peelings Per fruit (Grams±SD)	% Peelings per fruit
OS21	Shimba hills	192.068± 0.442	23.937± 0.213	12.463
OS22	Shimba hills	204.062± 0.685	29.338± 0.202	14.377
0S23	Shimba hills	203.871± 0.622	26.745± 0.334	13.119
OS24	Shimba hills	186.062± 0.716	23.493± 0.235	12.627
OS25	Shimba hills	190.275± 0.653	25.532± 0.221	13.419
OS26	Shimba hills	234.511± 0.718	32.414± 0.250	13.822
OS27	Shimba hills	244.670± 0.512	29.519± 0.247	12.065
OS28	Shimba hills	214.062± 0.664	28.998± 0.203	13.546
OS29	Shimba hills	205.341± 0.687	26.745± 0.311	13.024
OS30	Shimba hills	189.231± 0.723	23.897± 0.334	12.629

APPENDIX XXI: Mass of Orange Oil Extracted from the *Citrus senensis* Fruit Peelings Using Hexane

Sample No.	Sample Site/ Source	Mass of Peelings Per fruit (Grams±SD)	Mass of Orange Oil Extracted (g)	% w/w of Orange Oil Per Gram of Peelings
OS01	Malindi	25.060± 0.247	1.920± 0.088	7.66
OS02	Malindi	28.859± 0.225	1.952± 0.053	6.76
0S03	Malindi	32.173± 0.312	1.824± 0.033	5.67
OS04	Malindi	25.510± 0.216	2.304± 0.040	9.03
OS05	Malindi	23.894± 0.338	2.048± 0.057	8.57
OS06	Malindi	27.633± 0.242	1.760± 0.083	6.37
OS07	Malindi	23.700± 0.423	1.664± 0.056	7.02
OS08	Malindi	27.659± 0.287	1.700± 0.064	6.15
OS09	Malindi	30.182± 0.245	1.718± 0.055	5.69
OS10	Malindi	23.539± 0.299	0.920± 0.042	3.91
OS11	Muheza	34.421± 0.232	1.600± 0.051	4.65
OS12	Muheza	26.118± 0.243	1.728± 0.032	6.62
0S13	Muheza	23.800± 0.256	1.312± 0.035	5.52
OS14	Muheza	28.606± 0.230	1.856± 0.042	6.49
OS15	Muheza	24.469± 0.415	1.472± 0.039	6.02
OS16	Muheza	23.716± 0.318	1.632± 0.040	6.88
OS17	Muheza	24.056± 0.256	1.280± 0.036	5.32
OS18	Muheza	23.724± 0.218	1.244± 0.061	5.24
OS19	Muheza	29.006± 0.241	1.570± 0.055	5.41
OS20	Muheza	24.938± 0.320	1.328± 0.047	5.33
OS21	Shimba hills	23.937± 0.213	1.344± 0.039	5.61
OS22	Shimba hills	29.338± 0.202	1.504± 0.028	5.13
0S23	Shimba hills	26.745± 0.334	1.604± 0.052	6.00
OS24	Shimba hills	23.493± 0.235	1.888± 0.054	8.04

Sample No.	Sample Site/ Source	Mass of Peelings Per fruit (Grams±SD)	Mass of Orange Oil Extracted (g)	% w/w of Orange Oil Per Gram of Peelings
OS25	Shimba hills	25.532± 0.221	1.503± 0.029	5.89
OS26	Shimba hills	32.414± 0.250	1.632± 0.037	5.03
OS27	Shimba hills	29.519± 0.247	1.696± 0.044	5.75
OS28	Shimba hills	28.998± 0.203	1.942± 0.043	6.70
OS29	Shimba hills	26.745± 0.311	1.596± 0.051	5.97
OS30	Shimba hills	23.897± 0.334	1.332± 0.028	5.57

APPENDIX XXII: Biodiesel parameters specification for test methods of ASTM D6751 and EN 14214 standards

Property	Unit	Limits		Test method	
		ASTM D6751	EN 14214	ASTM D6751	EN 14214
Flash point	°C	130.0 min	101.0 min	D93	ISO CD3679e
Kinematic viscosity at 40 °C	mm^2/s	1.9–6.0	3.5–5.0	D445	EN ISO 3104
Cetane number	–	47 min	51 min	D613	EN ISO 5165
Sulphated ash content	% (m/m)	0.020 max		D874	ISO 3987
Copper strip corrosion	–	No. 3 max	Class 1	D130	EN ISO 2160
Acid value	mg KOH/g	0.80 max	0.5 max	D664	pr EN 14104
Free glycerol	% (m/m)	0.020 max		D6584	pr EN 14105m pr EN 14106
Total glycerol	% (m/m)	0.240 max	0.25 max	D6584	pr EN 14105m
Phosphorous content	% (m/m)	0.001 max	0.01 max	D4951	pr EN 141101
Carbon residue					
ASTM D6751 (100% sample)	% (m/m)	0.050 max	–	D4530	–
EN 14214 (10% bottoms)		–	0.3 max	–	EN ISO 10370
Cloud point	°C	Report customer	–	D2500	–
Density at 15 °C	kg/m^3	–	860–900	–	EN SIO 3675 EN SIO 12185
Distillation T90 AET	°C	360 max	–	D1160	–
Sulfur (S 15 Grade)	ppm	0.0015 max	–	D5453	–
Sulfur (S 500 Grade)	ppm	0.05 max	–	D5453	–
Sulfur content	mg/kg	–	10 max	–	–
Water and sediment	%vol.	0.050 max	–	D2709	–
Water content	mg/kg	–	500 max	–	EN ISO 12937
Total contamination	mg/kg	–	24 max	–	EN 12662
Oxidation stability at 110 °C	h	–	6 min	–	pr EN 14112
Iodine value	–	–	120 max	–	pr EN 14111
Linolenic acid methyl ester	% (m/m)	–	12 max	–	pr EN 14103d
Polyunsaturated (≥4 double bonds) methyl esters	% (m/m)	–	1 max	–	pr EN 14103
Ester content	% (m/m)	–	96.5 min	–	pr EN 14103d
Methanol content	% (m/m)	–	0.2 max	–	pr EN 141101

*(*Leung *et al.*, 2010*)*

PUBLICATIONS LIST FROM THE RESEARCH

Kahindo J. M., Chhabra, S., Musau, R., Odalo, J. O. and Thoruwa, T. (2019) Physico-chemical and Fuel Properties of Fatty Acid Ethyl Esters from *Jatropha curcas* Oil Transesterified Using *Rhizoclonium grande* and *Citrus senensis* Bioethanol. Kenyatta University Biennial Research and Innovation Conference 2019 from 23rd – 25th October 2019.

Kahindo J.M., Chhabra S. C., Musau R., Odalo J.O. and Thoruwa T.F. (2018). *Rhizoclonium grande* bioethanol in biofuel production by transesterification of *Jatropha curcas* oil. *Green and Sustainable Chemistry*, 8, 62-73.

Kahindo J.M., Chhabra S. C., Musau R., Odalo J.O. and Thoruwa T.F. (2018). Effect of *Rhizoclonium grande* Saturated Fatty Acid Ethyl Esters on Physico-Chemical and Fuel Properties of *Jatropha curcas* Biofuel. *Chemical Science International Journal*, 23(1): 1-9.

Kahindo J.M., Chhabra S. C., Musau R., Odalo J.O. and Thoruwa T.F. (2017). The potential of sustainable macroalgae bioethanol in biofuel production by transesterification of *Jatropha curcas* oil. In Abstracts of the Kenya Chemical Society International Conference; The role of chemistry in inventing a sustainable future. pg 79.